CDOT-UCD-R-93-21

UNIVERSITY

OF COLORADO

AT DENVER

Investigating Performance of Geosynthetic-Reinforced Soil Walls

by

Nelson N.S. Chou and Jonathan T.H. Wu

Prepared in cooperation with the
U.S. Department of Transportation
Federal Highway Administration

COLLEGE OF ENGINEERING

AND APPLIED SCIENCE

The contents of this report reflect the views of authors who are responsible for the facts and the accuracy of the data presented herein. The contents do not necessarily reflect the official views of the Colorado Department of Transportation or the Federal Highway Administration. This report does not constitute a standard, specification, or regulation.

Technical Report Documentation Page

1. Report No.	2. Government Accession No.	3. Recipient's Catalog No.
CDOT-UCD-R-93-21		

4. Title and Subtitle	5. Report Date
Investigating Performance of Geosynthetic-Reinforced Soil Walls	October 1993
	6. Performing Organization Code 76.98
7. Author(s)	8. Performing Organization Rpt.No.
Nelson N. S. Chou and Jonathan T. H. Wu	CDOT-UCD-R-93-21
9. Performing Organization Name and Address	10. Work Unit No. (TRAIS)
University of Colorado at Denver College of Engineering and Applied Science Denver, Colorado 80204	11. Contract or Grant No.
12. Sponsoring Agency Name and Address	13. Type of Rpt. and Period Covered
Colorado Department of Transportation 4201 E. Arkansas Ave. Denver, Colorado 80222	Final Report 14. Sponsoring Agency Code

15. Supplementary Notes

Prepared in Cooperation with the U.S. Department of Transportation Federal Highway Administration

16. Abstract

The comparative study of four finite element programs (SSCOMP, CRISP, CON2D86, and DACSAR), led to selecting DACSAR for this research. This program was then modified and validated for analyzing the performance of Geosynthetic-Reinforced Soil (GRS). The validation was conducted by comparing the analytical results with a laboratory "element test" of soil, reinforcement, and facing; with another validated FEM program (SSCOMP); and with measurements from two full-scale test walls. Using the analytical model, a parametric study was conducted to investigate the effects of various factors on the performance of GRS walls: wall height, wall shape, backfill type, facing rigidity, reinforcement tensile stiffness/strength, and K of the backfill. The parametric study gave valuable insight into the performance of GRS walls. Some highlights of the findings are: (1) When kept near optimum moisture, cohesive backfill walls can perform at least as well as those with granular backfill, provided that wetting of backfill is prevented; (2) Foundation soil has a significant influence on the wall performance; and (3) Wall facing affects lateral movement of GRS walls even under a service load of 5 psi.

Implementation:

From the results, a preliminary design procedure is proposed. The procedure overcomes three major drawbacks of current design methods: (1) It accommodates the interaction among soil, reinforcement, and facing; (2) It does not use arbitrarily assigned safety factors to ensure satisfactory performance of a GRS wall; and (3) It accounts for the effects of foundation stiffness and facing rigidity and permits judicious use of cohesive soil as backfill.

17. Key Words		18. Distribution Statement
Finite element	Cohesive backfill	No Restrictions: This report is available to the public through the National Technical Info. Service, Springfield, VA 22161
Facing rigidity	Lateral deformation	

19.Security Classif. (report)	20.Security Classif. (page)	21. No. of Pages	22. Price
Unclassified	Unclassified	341	

Final Report
to
Colorado Department of Transportation

Investigating Performance of Geosynthetic-Reinforced Soil Walls

by

Nelson N.S. Chou and Jonathan T.H. Wu

Abstract

A study was undertaken to investigate the performance of Geosynthetic-Reinforced Soil (GRS) retaining walls. The objectives of this research study were: (1) to establish a reliable analytical model capable of simulating the performance of GRS walls; (2) to investigate the effects of various factors on the performance of GRS walls; and (3) to propose a preliminary design procedure and design and construction guidelines for GRS walls.

A comparative study of four finite element programs (SSCOMP, CRISP, CON2D86 and DACSAR) led to selecting DACSAR for this research. The program DACSAR was modified and validated for analyzing the performance of GRS walls. The validation was conducted by comparing the analytical results with laboratory "element tests" of soil, reinforcement and facing; with another validated FEM program (SSCOMP); and with measurements from two full-scale test walls.

Using the analytical model, a parametric study was conducted to investigate the effects of various factors on the performance of GRS walls. The factors investigated were: wall height, wall shape, backfill type, foundation stiffness, facing rigidity,

reinforcement tensile stiffness/strength and K_o of backfill (due to compaction). The parametric study gave valuable insight into the performance of GRS walls. Some highlights of the findings are:

- When kept near optimum moisture, cohesive backfill walls can perform at least as well as those with granular backfill, provided that wetting of backfill is prevented.

- Foundation soil has a significant influence on the wall performance.

- Wall facing affects lateral movement of GRS walls even under a service load of 5 psi.

From the results of the parametric study, a preliminary design procedure was proposed. The design procedure was based on an allowable lateral wall deformation and limited reinforcement strain. The proposed design procedure overcomes three major drawbacks of the current design methods; namely:

(1) The proposed design procedure accommodates the interaction among soil, reinforcement and facing.

(2) The proposed design method does not use arbitrarily assigned safety factors to ensure satisfactory performance of a GRS wall.

(3) The proposed design method accounts for the effects of foundation stiffness and facing rigidity, and permits judicious use of cohesive soil as backfill.

TABLE OF CONTENTS

CHAPTER

CHAPTER

CHAPTER

CHAPTER

CHAPTER

List of Tables

List of Figures

FIGURE

FIGURE

FIGURE

FIGURE

FIGURE

FIGURE

FIGURE

CHAPTER I

INTRODUCTION

1.1 General

The development of Mechanically Stabilized Earth (MSE) walls represents a major advance in geotechnical engineering practices in the last two decades. The MSE wall is a generic name for a retaining wall with linearly or planarly distributed inclusions, such as steel strips, polymeric grids, geotextile sheets, steel nails, or anchors. The inclusions typically serve to reinforce the backfill in a manner that provides tensile resistance to soil weight and loadings. A Geosynthetic-Reinforced Soil (GRS) wall, using either geogrid or geotextile sheets as the inclusion, is a member of the MSE wall family. "Geosynthetic wall" and "geosynthetic reinforced soil wall" (GRS wall) are used interchangeably in this dissertation. Also, "geotextile" is interchangeable with "geofabric" or "fabric".

Figure 1.1 shows the typical configuration of a GRS wall. The GRS wall comprises five major components: backfill, reinforcement (geosynthetic), facing, foundation, and retained soil.

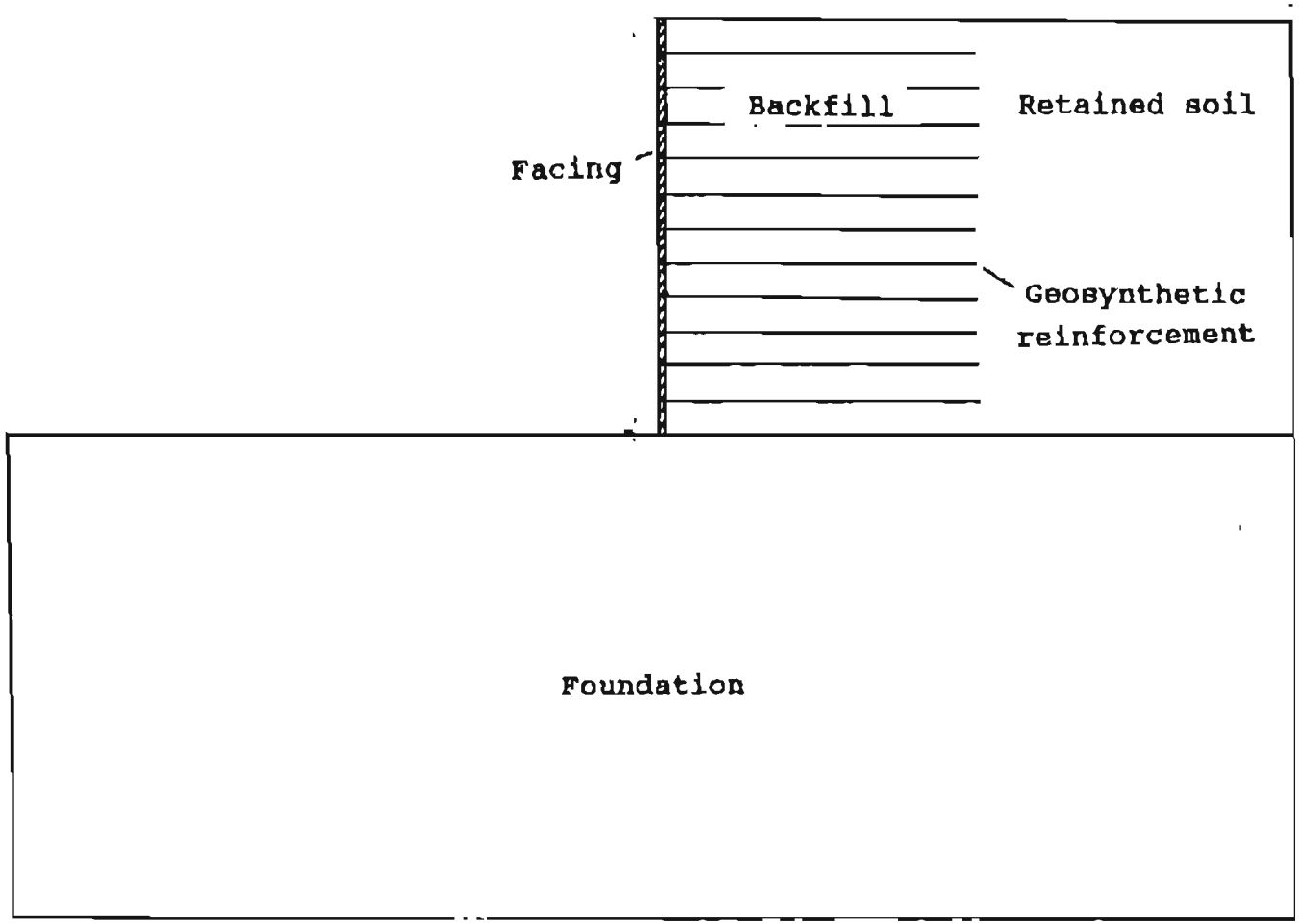

Figure 1.1: Components of a Geosynthetic Reinforced Soil Retaining Wall

1.2 Overview of Geotextile and Geogrid

Geotextiles are porous fabric manufactured from such synthetic materials as polypropylene, polyester, polyamide (Nylon), polyethylene, and other polymers (Koerner, 1986). Geotextiles can be manufactured in a variety of ways; the most common methods are woven, non-woven and knit, although knit fabrics are seldom used in geotechnical engineering applications. Woven geotextiles are usually made from continuous monofilament fibers or from continuous slit-film fibers. Non-woven fabrics are usually made from continuous or staple fibers laid down in a random pattern, then jointed together by various mechanical, thermal or chemical processes. Depending on the process used, non-woven geotextiles can be classified as spun-bonded (including heat, mechanical or chemical bondings), melt-bonded, resin-bonded, and needle-punched (Koerner,1986).

Geogrids are high strength synthetic materials manufactured from high-density polyethylene or polypropylene. They are made from a sheet of polymer that is punched with closely spaced holes in a uniform pattern, then elongated uniaxially or biaxially.

The behaviors of geotextiles and geogrids are similar, except in the stress transfer mechanism between the soil and reinforcement; geotextiles typically bond with soil through adhesion, whereas

geogrids typically bond with soil through both adhesion and passive resistance (i.e., interlocking forces between the grid and the soil in the grid). Geogrids generally exhibit higher strength, higher stiffness, and lower creep than geotextiles; however, the cost of geogrids is usually higher.

1.3 Development of GRS Walls

The first GRS wall was built in Rouen, France, in 1971 (Puig, 1977). It was an experimental wall constructed by using a non-woven geotextile (Bidim) and a low quality backfill (wet, clayey and sensitive soil). This 13-foot high, 66-foot long vertical wall, situated on a very compressible peat, was built with a wrapped fabric facing.

The first geotextile wall built in the U.S. was initiated by the U.S. Forest Service in 1974 and was built at the Oregon State University. They first conducted small-scale model tests to verify that the design method developed for Reinforced Earth Walls (Lee, Adams & Vagneron, 1973) could be adopted for geotextile walls. Based on these model tests, geotextile walls were constructed in Siskiyou National Forest in Oregon in 1974 and Olympic National Forest in Shelton, Washington, in 1975 (Steward & Mohney, 1982).

The excellent performance and low cost of these two "Forest Service walls" provided the impetus for other geotextile walls to be constructed by the Forest

Service, as well as state highway agencies and the Federal Highway Administration (FHWA). Highway departments in New York (Douglas, 1981) and Colorado (Bell, Barrett & Ruckman, 1983) constructed geotextile walls in 1980 and 1982, respectively. Along I-70 at Glenwood Canyon, Colorado, the behavior of a full-scale geotextile reinforced test wall, together with other proprietary reinforced walls, was instrumented and monitored (see Section 2.4.1 for details).

Since its development in early 1980s, geogrid has become rapidly accepted in a wide range of soil reinforcement applications, including embankment reinforcement and retaining walls. Geogrid-reinforced embankments and walls have been constructed in England and Continental Europe for several years before being introduced in the United States in 1983. Between 1983 and 1990, over 300 walls and slopes were constructed in the U.S. (Mitchell and Christopher, 1990). The Colorado Department of Transportation has used geogrids to stabilize I-76 embankments over sanitary landfills and cement wash deposits in Denver (Wu, Siel, Chou and Helwany, 1992).

Over the past 10 years, both geogrid and geotextile walls have been widely used around the world. Numerous case histories of geosynthetic walls have been reported in Canada (Bathurst and Benjamin, 1990; Burwash and Frost, 1991), Japan (Tatsuoka and

Yamauchi, 1986), France (Wichter, Risseeuw and Gay, 1986; Gourc and Matichard, 1992), Netherlands (Brakel, Coppens, Maagdenberg and Risseeuw, 1982), Hong Kong (Ng and Mak, 1988), China (Ouyang, 1988), Taiwan (Chang, Chen and Su), Australia (Fabian and Fourie, 1988), just to name a few.

1.4 Advantages and Limitations of GRS Walls

GRS walls have demonstrated numerous characteristics that are preferable to conventional concrete retaining walls (and, to a lesser extent, over other MSE walls), including:

(1) GRS walls are inherently flexible; therefore, they are capable of withstanding large foundation settlements or differential settlement (Wu and Lin, 1991). In the Glenwood Canyon geotextile test wall, for instance, only hairline cracks were detected, although more than two feet of settlement occurred. This superior feature makes GRS walls suitable for soft foundation, especially if the staged construction technique is adopted;

(2) GRS walls are comparatively low in cost. In Colorado, a permanent geotextile wall with timber facing costs ranging from $12 to $20 per square foot in 1991, about half of the cost of a cantilever concrete wall (CDOT, 1991). Geogrid walls with precast panels cost slightly more ($20 to $25). In general, GRS walls are very cost-effective when compared with cantilever

concrete walls, especially when the average wall height is more than 15 feet, and/or when a deep foundation is required for conventional concrete walls.

(3) Construction requires neither heavy equipment nor skilled labor (Bell, Barrett and Ruckman, 1983);

(4) Foundation excavation and preparation can be minimized. This is especially beneficial if hazardous material is encountered in the excavation;

(5) Geosynthetic reinforcements have strong resistance to corrosion and bacterial action, compared to metallic reinforcements;

(6) Since the geosynthetic/soil contact areas are larger compared to some other MSE walls, the requirement of high quality backfill may be less stringent (Tatsuoka, et. al., 1986).

However, GRS walls also have several limitations; namely (Wu and Lin, 1991):

(1) There may be a drastic reduction in geosynthetic strength when it is exposed to ultraviolet (UV) light; the UV effects are generally more severe for geotextiles;

(2) GRS walls are susceptible to damage during construction and vandalism after construction;

(3) The long-term durability of the GRS walls is uncertain; and

(4) There is a lack of a rational design approach that is based on sound engineering research.

The first two limitations can be alleviated by good construction practice and utilization of appropriate wall facings. A comprehensive research project on the durability of geosynthetic materials, sponsored by the FHWA, is presently being conducted. The last limitation is the focus of this research.

1.5 Problem Statement

The present design and construction practices of GRS walls are faced with the following three major problems:

(1) Most of the currently available design methods fail to accommodate the interaction among soil, reinforcement and facing in a GRS wall. Most of the methods are based on the limiting equilibrium approach and use arbitrarily assigned safety factors. An inherent problem of the limiting equilibrium approach is its inability to estimate the deformation under service loads. The lateral wall deformations are of particular interest in the design of GRS walls because:
(a) Most geosynthetics are relatively low in stiffness, which may result in larger lateral deformations. The performance of the structures situated on top of the wall (i.e., pavement, guardrail, sign structures, high mast light post) may be significantly influenced by the deformations.
(b) Geosynthetics of similar ultimate strengths may have very different tensile stiffness.

Claybourn (1989), Claybourn & Wu (1991) compared six existing design methods. They revealed that, while there are significant differences in the design concept of these methods, the greatest discrepancies among the various design methods relate to the safety factors. In a typical wall examined in their study, the combined factor of safety (in terms of the quantity of reinforcement needed) ranged from 3 to 23, depending on the method used. Apparently, the safety factors assigned in these design methods are somewhat arbitrary and are not based on sound engineering research or field experience.

(2) As previously indicated, one of the advantages of GRS walls is that they are capable of withstanding large deformations due to foundation settlement. However, none of the existing design methods addresses the effects of foundation settlement. These design methods simply assume that the wall will be constructed over a rigid foundation. The effects of foundation settlement on the wall performance have not been elucidated. In addition, facing rigidity, which is also known to have a significant effect on the wall performance, is not addressed in any of the existing design methods.

(3) Conventional design methods for GRS walls require granular soil as backfill. Since the backfill cost plays a major role (Richardson and Bove, 1988) in

the total cost of a GRS wall (see Figure 1.2), it would be highly cost-effective to use on site soil, including cohesive soil, as backfill. Due to the large contact areas between the geosynthetic reinforcement and the backfill, it is conceivable that a cohesive soil with a low-friction angle may be acceptable as backfill, provided that proper precautions are taken. In fact, sometimes, it is more cost-effective to increase the amount of reinforcement and install proper drainage than to use granular backfill from borrow sites.

1.6 Objectives of Research

The objectives of this research are three-fold:

(1) To establish a reliable finite element analytical model that is capable of analyzing the performance of GRS walls under various conditions, including walls constructed over soft foundations and walls with cohesive backfills;

(2) To investigate the effects of various factors on the performance of GRS walls. The factors include: wall height, wall shape, backfill, foundation, facing, reinforcement, and compaction effect. Emphasis is placed on studying the feasibility of using cohesive backfill for GRS wall construction and studying the effects of soft foundation soils on the wall performance.

(3) To establish design and construction guidelines for GRS walls. Using the results obtained

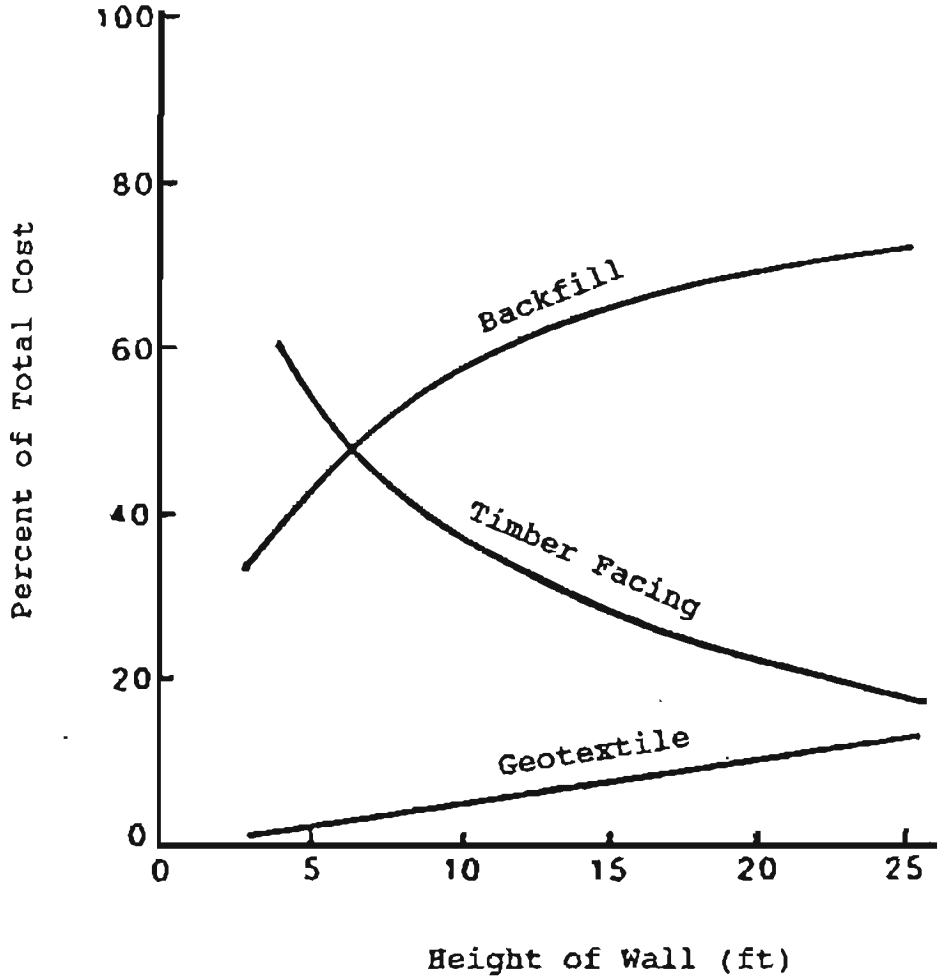

Figure 1.2: Relative Costs of Components of a Geotextile Reinforced Soil Retaning Wall (After Richardson & Bove, 1988)

from the parametric study, a preliminary design procedure based on an allowable lateral wall deformation is to be developed. It is to be noted that the performance of GRS walls under service loads is the main focus of this research. The behavior of walls under ultimate loads, and the creep and durability of GRS walls is not included in this research study.

1.7 Method of Research

To achieve the objectives outlined above, the research plan is organized into the following tasks:

Task 1: Conduct a literature review, to examine the prevailing analytical and design methods for GRS walls.

Task 2: Investigate the features that need to be simulated in the analysis of a GRS wall, and select a finite element program which can successfully simulate these features.

Task 3: Validate the selected FEM program by comparing the analytical results with close-form solutions, results of laboratory tests and results of full-scale test walls; and modify the analytical model, if necessary.

Task 4: Perform a parametric study using the validated analytical model. Investigate the factors affecting the wall performance, including wall height,

wall shape, backfill, foundation, facing, reinforcement and compaction effect.

Task 5: Recommend a preliminary design procedure and construction guidelines, and establish preliminary deformation-controlled design tables.

A flow chart showing an overview of this research program is depicted in Table 1.1.

Table 1.1 Flow Chart for the Research Program

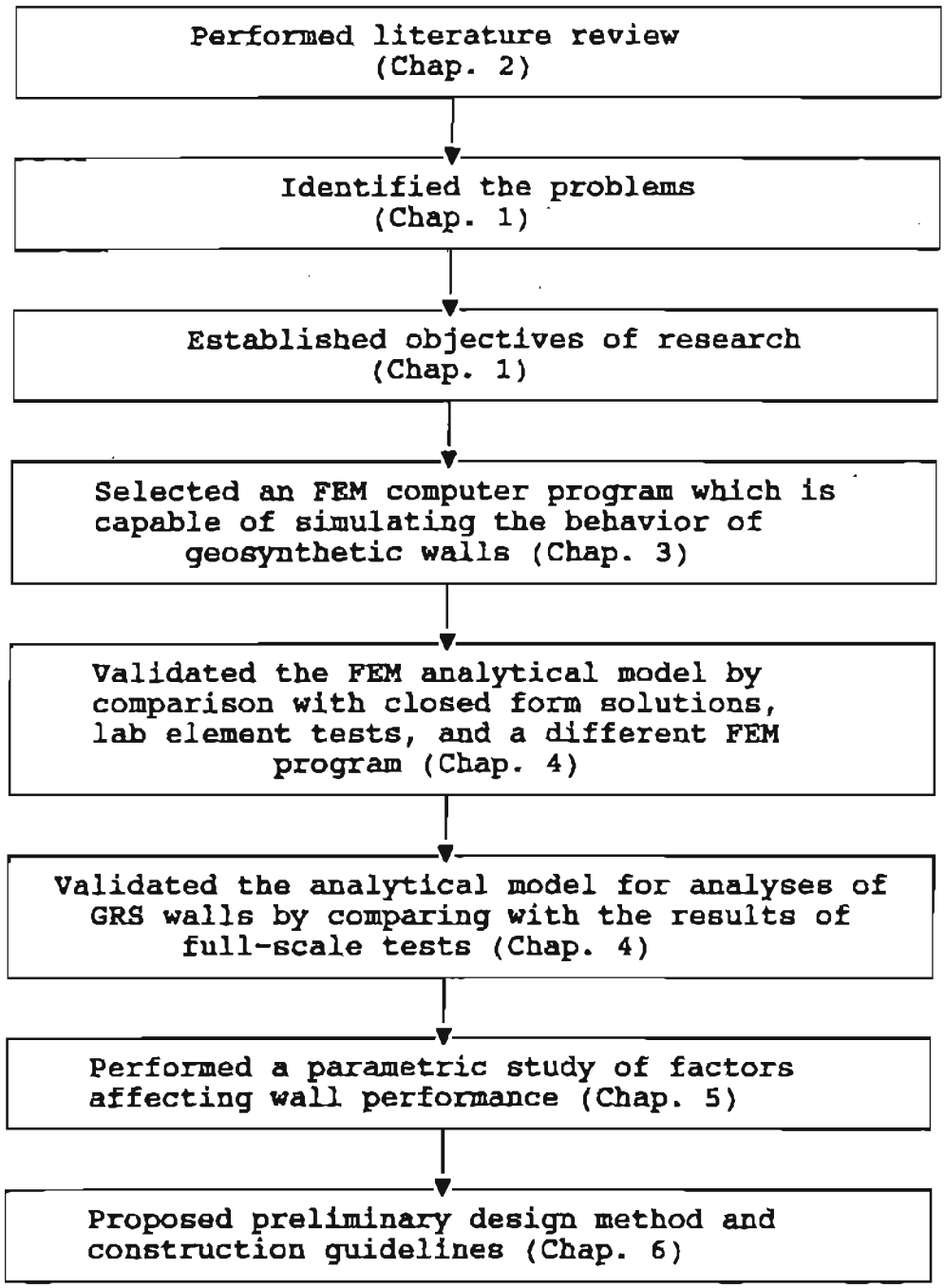

CHAPTER II

A LITERATURE REVIEW

2.1 Introduction

In designing a geosynthetic reinforced soil wall (GRS wall), one must consider both internal and external stabilities. The internal stability criteria for GRS walls requires an evaluation of adequate stability against (a) tensile rupture failure, (b) pullout failure, and (c) long-term failure, such as creep failure, chemical and biological deteriorations (Mitchell and Villet, 1987). External stability refers to stability against failures outside the reinforced zone. The external failure modes include overturning, sliding, overall slope stability and bearing capacity. Classical soil mechanics methods have been used for evaluating external stability of GRS walls.

The following literature review is focused on the internal stability analysis of GRS walls. This review includes the current design methods for GRS walls, state-of-art analyses of GRS walls, and full-scale, instrumented GRS walls.

2.2 Review of Current Design Methods

Two design approaches are used for GRS walls:

(1) The safety factor approach, which considers limiting equilibrium state of stress for evaluating the stability of a GRS wall; and

(2) The deformation-limit approach, which considers allowable lateral wall deformations of a GRS wall.

2.2.1 Safety Factor Design

A comprehensive evaluation and comparison of six design methods for the safety factor approach has been conducted by Claybourn and Wu (1991). The six design methods are:

(1) Forest Service Method (Steward, Williamson and Mohney, 1977, revised 1983);

(2) Broms Method (Broms, 1978);

(3) Bonaparte, et. al. Method (Bonaparte, Holtz and Giroud, 1985);

(4) Collin Method (Collin, 1986);

(5) Leshchinsky and Perry Method (Leshchinsky and Perry, 1987); and

(6) Schmertmann, et. al. Method (Schmertmann, Chourey-Curtis, Johnson and Bonaparte, 1987).

Methods 1 through 4 are based on the earth pressure analysis; i.e., the horizontal forces due to lateral earth pressure are equated with the stabilizing tensile forces in the horizonal reinforcement. The stresses considered are vertical and lateral earth pressures, the horizontal tensile stresses in the

reinforcement, and the horizontal resistance to pullout of the reinforcement from behind a failure surface. Two independent safety factors are required for each layer of reinforcement: (1) the safety factor for reinforcement rupture, which is the ratio of reinforcement strength to the induced tensile force in the geosynthetic reinforcement, and (2) the safety factor for pullout, which is the ratio of pullout resistance to the lateral earth pressure thrust for that layer. Pullout resistance is provided by horizontal shear stresses resulting from the soil/reinforcement interface friction under the vertical confining stress on the portion of the layer behind the failure surface.

These methods typically presume a failure surface through the reinforced mass described by a Rankine active failure condition. The stresses on the failure plane are not analyzed. The reinforcements extended beyond the assumed failure surface are considered to be tension-resistant tiebacks for the assumed failure wedge. As a result, these are frequently referred to as tied-back wedge methods. Although the tied-back wedge methods have many similarities, they assume different lateral earth pressure distributions to be resisted (Claybourn and Wu, 1991).

Methods 5 and 6 employ the approach commonly used in conventional slope stability analysis, which

involves analyzing the stresses on the failure plane. Leshchinsky and Perry used a limiting equilibrium analysis of rotational (log-spiral) and translational (planar) failure surfaces based on extremization using variational calculus to develop design charts. The Schmertmann, et. al. method is based on the limiting equilibrium method using wedge failure models. Straight line and bi-linear wedges were used for different aspects of the analysis. Extended versions of Bishop's modified and Spencer's method of slope stability analysis were used to modify the results of the wedge analysis.

Claybourn and Wu indicated that while there are significant differences in the design concepts, the more prominent discrepancies among the design methods relate to the significant disparity in defining allowable reinforcement strength and safety factors. They pointed out that the various safety factors used in the design methods are somewhat arbitrary and are not based on empiricism.

To demonstrate the differences of various methods, in terms of reinforcement quantity requirements, Claybourn (1990) used a 30-foot high vertical wall with all safety factors set equal to one. The combined factor of safety (in terms of the quantity of geotextile needed) ranged from 3.0 to 23.1.

The limiting equilibrium approach also has the following drawbacks:

(1) The approach does not account for the interaction between the soil, reinforcement, and facing;

(2) The lateral wall deformation and settlement cannot be obtained explicitly;

(3) The effects of facing rigidity and construction sequence are not accommodated. The lateral earth pressure is assumed to be resisted by the reinforcement alone. However, the global bending rigidity of facing (if available) and the reactions at the bottom of the facing may also provide significant resistance to the lateral earth pressure.

(4) The effects due to foundation settlement are not addressed; and

(5) The backfill is limited to granular materials.

2.2.2 Deformation-Limit Design

A number of researchers have proposed design methods that calculate lateral deformation of a GRS wall (Jewell, 1988; Jewell & Milligan, 1989; FHWA,1989; Christopher, 1988; Gourc, et. al., 1986; Gourc, et. al., 1988). This section reviews three of those methods: Jewell's method, GeoService method, and Christopher, et. al. method. It is to be noted that

the GeoService method combines both the safety factor approach and deformation-limit approach.

Jewell's Method

Jewell (1988), Jewell & Milligan (1989) proposed a method for calculating wall deformation. They made the following assumptions:

(1) Rankine failure plane is valid for the reinforced soil mass; and

(2) Within the zone of Rankine failure, tensile force is constant along each reinforcement. This assumption implies that a GRS wall is considered to behave similar to a multiple anchor wall, in which the entire active thrust is applied to the facing.

Using the limiting equilibrium analysis concept, Jewell and Milligan (1989) divided a MSE wall into three zones, as shown in Figure 2.1.a. Large reinforcement forces are required in Zone 1 to maintain stability across a series of critically inclined planes such as AB. In Zone 2, the required reinforcement forces decrease progressively as the inclination of a plane, such as OC, gets smaller, until the line OD is reached, beyond which no reinforcement force is needed for stability in Zone 3.

The minimum provision of reinforcement is that needed to maintain equilibrium at all points within Zone 1. The required horizontal stresses for stability in this zone are the active pressure, due to surcharge

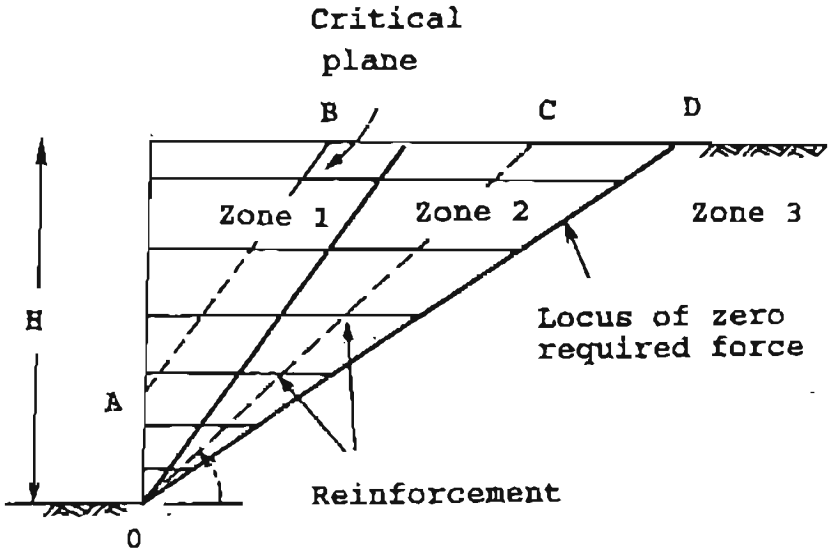

(a) Major Zones of Reinforcement Force in a Wall

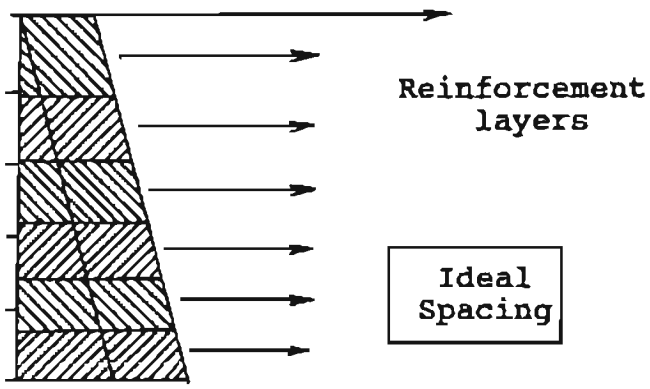

(b) Stress Equilibrium for Ideal Spacing of the Reinforcement

Figure 2.1: Jewell's Method (After Jewell & Milligan, 1989)

and self-weight of the soil (see Figure 2.1.b). Each reinforcement is assumed to resist the horizontal stress in the soil to half the spacing above and below it.

Jewell analyzed two idealized equilibrium stress distributions for MSE walls: the ideal reinforcement length layout and the truncated reinforcement length layout. In Figure 2.1.a, if the reinforcement at each level extends to the back of Zone 2, it is considered as having an ideal length. In the ideal length arrangement, the total reinforcement force is governed by the soil stress in Zone 1. Each reinforcement layer has an allowable force sufficient to maintain equilibrium in this zone, but over the reinforcement length in Zone 2, the mobilized reinforcement force is less than the available force. Better use of the reinforcement forces may be made by truncating the reinforcement length near the top, but increasing the length at the bottom of the wall.

Jewell considered the deformation of an MSE wall stem from the following sources:

(1) Deformation in the reinforced zone;

(2) Deformation caused by the unreinforced soil behind the reinforced zone; and

(3) Apparent deformation caused by incremental construction.

The calculation procedure consists of evaluating the mobilized internal friction angle, which is used to calculate the global horizontal force in the reinforcement. This global force is then distributed between the various layers of reinforcements as a function of the reinforcement density.

Jewell and Milligan presented the results of deformation analyses in the form of charts. The charts provide the value of the wall displacement at different heights of the wall. The charts were furnished for different values of the internal friction angle and for four types of reinforcement configuration. The four types of reinforcement configurations are: uniform spacing and ideal spacing (i.e., equal tensile forces in each layer of reinforcement) for both the ideal length and the truncated length layouts.

Jewell's method provides a systematic approach for wall deformation calculation. However, the validity of those assumptions is questionable.

GeoServices Method

J.P. Giroud of GeoServices, Inc. (1989) presented a comprehensive design method for GRS walls. The method includes evaluation of both external and internal stabilities of a GRS wall. In this method, the following assumptions are made:

(1) Cohesion of backfill soil is zero, i.e., either the soil is cohesionless, or an effective stress analysis is conducted with C'= 0;

(2) The surcharge load on top of the fill is uniformly distributed, and its maximum value is:

$$q_{max} = 0.2\gamma h \qquad (2.2)$$

where γ = unit weight of backfill, and
h = height of wall

(3) The wall face is vertical;

(4) The crest of the wall is horizontal;

(5) There is no pore water pressure within the soil mass and there is no seismic loading;

(6) A triangular tensile strain distribution (see Figure 2.2) is induced over the length of the geosynthetic reinforcement. The maximum horizontal displacement of the wall is given by:

$$\delta = \frac{\varepsilon_{max} \cdot L}{2} \qquad (2.3)$$

where ε_{max} = maximum reinforcement strain, and
L = length of reinforcement

(7) The vertical stresses induced by the thrust of the retained soil are calculated using Meyerhof's recommendation for eccentrically loaded footings (Bonaparte, et. al. 1985);

(8) A Rankine failure plane and the active earth pressure exerted by the retained soil are assumed; and

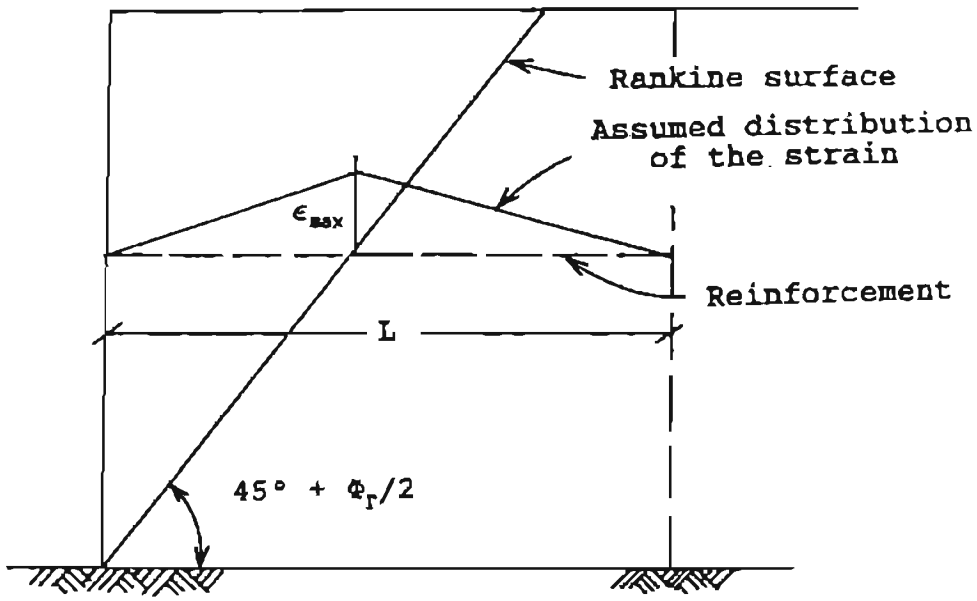

Figure 2.2: Assumed Triangular Strain Distribution Over the Length of the Reinforcement, GeoServices Method (After FHWA, 1989)

(9) All geosynthetic reinforcements have the same length.

The GeoServices method provides a step-by-step approach for selecting a geosynthetic material and a required reinforcement length. An iterative process may be required to obtain the final selections. Performance limits need to be specified; i.e., limiting the maximum allowable horizontal displacement of the wall to, say, two inches; and limiting the allowable strain of reinforcement to, say, two percent. The design procedures can be described by the following steps:

(1) Check if the assumptions made in the design method are satisfied;

(2) Select the design limit strain;

(3) Select the friction angle of the backfill (i.e., peak, residual);

(4) Determine the backfill active earth pressure;

(5) Select a tentative reinforced length that satisfies the safety requirements with respect to sliding, overturning, bearing, eccentricity of the resultant, and adequate anchorage beyond the Rankine failure zone;

(6) Determine the maximum horizontal displacement;

(7) Determine the maximum vertical stress;

(8) Determine the maximum horizontal stress;

(9) Determine the required design reinforcement tension;

(10) Select the reinforcement and check creep limit tension;

(11) Determine the tentative anchored reinforcement length;

(12) Check the pullout resistance; and

(13) Select the final reinforcement length.

The design procedure has been coded in a computer program by Lin, Macklin, Chou and Wu (1991). Using the computer program, computational errors can be eliminated and computation time is minimized.

Christopher, et. al., Method

In the report "Reinforced Soil Structures" prepared for the FHWA, Christopher, et. al. (1988) recommended a simple empirical chart for calculation of reinforced soil wall deflection. They suggested that the total lateral displacement of an MSE wall resting on a firm foundation can be estimated from Figure 2.3. This is based on the length of reinforcement (L) to height of the wall (H) ratio and the extensibility (tensile modulus) of the reinforcement. Figure 2.3 is said to be empirically developed using data from actual structures and computer simulation models. However, the details on how the empirical curve was obtained were not presented in their report.

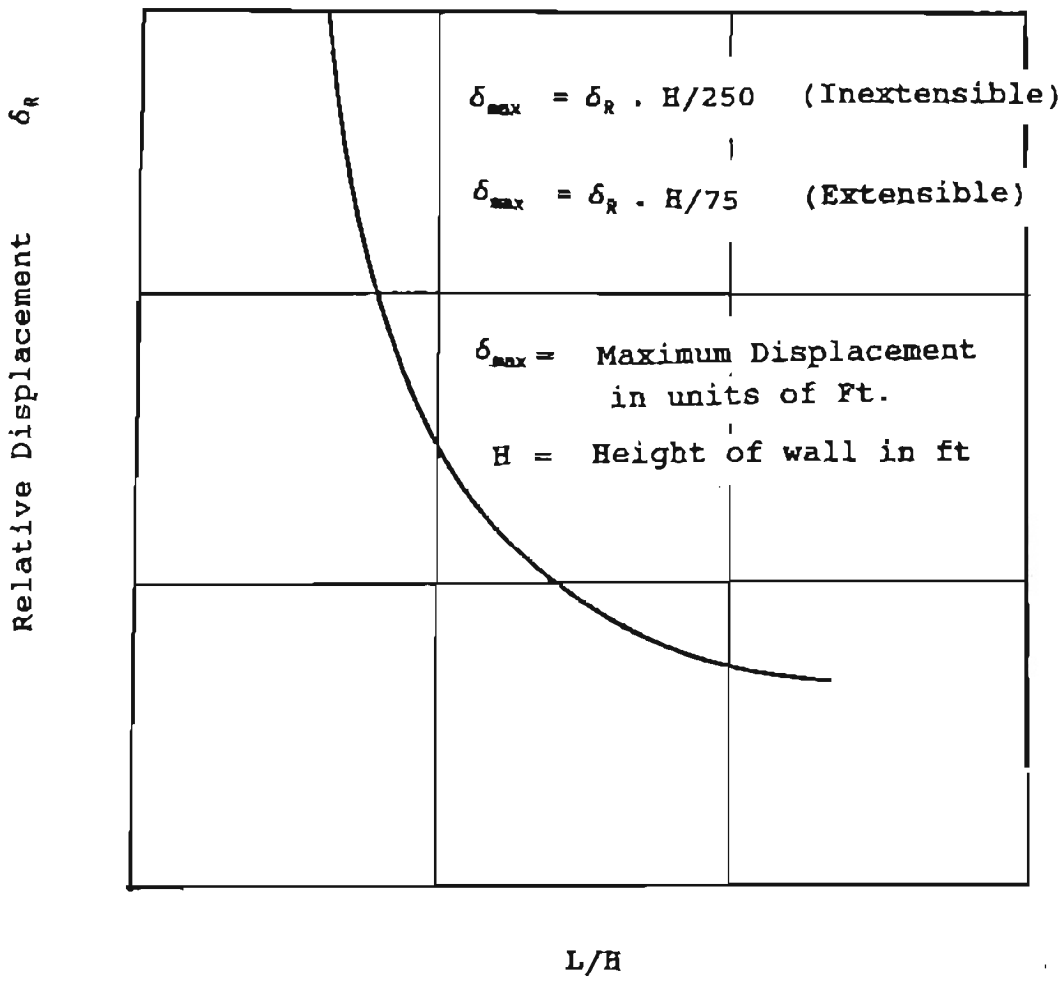

Note: Increase Relative Displacement 25% for every 400 psf of surcharge.

Figure 2.3: Empirical Curve for Estimating Anticipated Lateral Wall Displacement (After FHWA, 1988)

Christopher, et. al. recommended using the following equation to calculate the lateral displacement of GRS walls:

$$\delta_{max} = \delta_R H/75 \qquad (2.4)$$

where δ_{max} = maximum displacement (in feet)
H = height of wall (in feet)
δ_R = empirically derived relative displacement coefficient (see Figure 2.3).

2.3 Review of State-of-the-Art Analyses for Geosynthetic Walls

The topics included in this review are GRS wall behavior (i.e., soil reinforcing mechanisms, maximum tension and failure surfaces, lateral earth pressure) and the analytical methods (i.e., the strain-compatibility analysis and the finite element analysis).

2.3.1 GRS Wall Behavior Mechanisms of Soil Reinforcement

It has been suggested by Vidal (1978) and Yang (1972) that reinforcement acts to increase the effective confining pressure acting on the soil. As shown in Figure 2.4, the addition of reinforcement to a soil restrains the soil from expanding horizontally. This is equivalent to an increase in confining stress in the direction of reinforcement. If the particles of

soil at points A and B (Figure 2.4.a) are rigidly connected to the reinforcement by the action of friction, the soil between A and B is confined (Figure 2.4.b). Therefore, the strength of a reinforced soil mass may be increased due to this confining effect.

The effect of confining pressure can also be viewed as adding an apparent or pseudo cohesion to the soil (Schlosser and Long,1972; Yang, 1972). The reinforced soil may be considered as equivalent homogeneous but anisotropic soil. Figure 2.5.c showed the Mohr circles for this case. Mohr's circles (a) and (b) represent the failure condition for the unreinforced and reinforced soil samples, respectively. The additional confinement provided by the reinforcement is shown as Figure 2.5.b. Considering the reinforced soil as an equivalent homogeneous soil, the confining pressure remains unchanged. Circle (c), with the same diameter as circle (b), represents the circle for the reinforced soil and Cr is the pseudo cohesion induced in the reinforced soil.

Schlosser and Long (1972) study the behavior of sand reinforced by aluminum foil disks by triaxial tests (Figure 2.6.a). The reinforcement gives the sand an apparent cohesion, which is mobilized more rapidly than the internal friction angle of the soil (Figure 2.6.c).

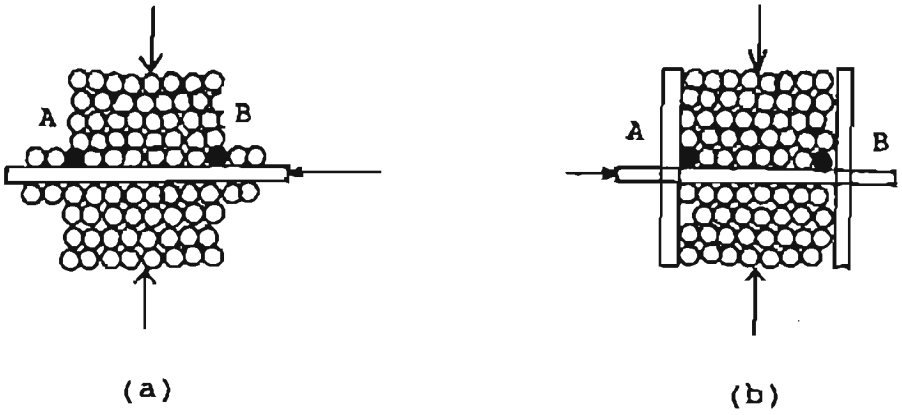

Figure 2.4: Concept of Added Confinement Reinforcement

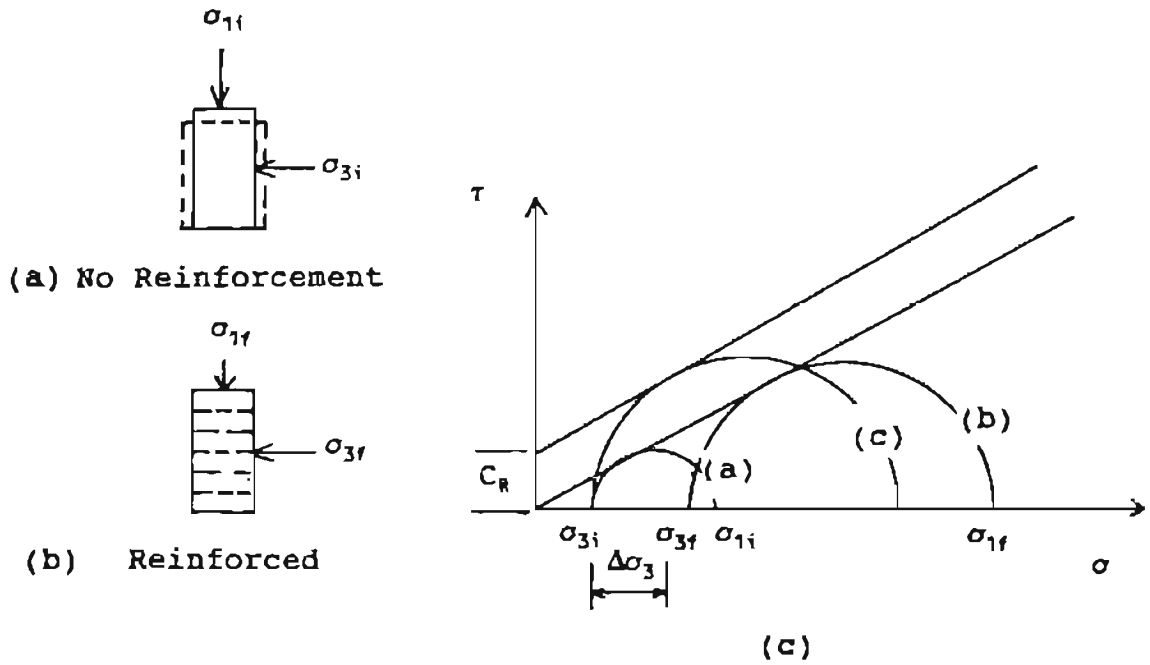

Figure 2.5: Concept of Pseudo Cohesion and its Effects on the Mohr-Coulomb Failure Envelope (After Schlosser & Long, 1972; Yang, 1972; Collin, 1986)

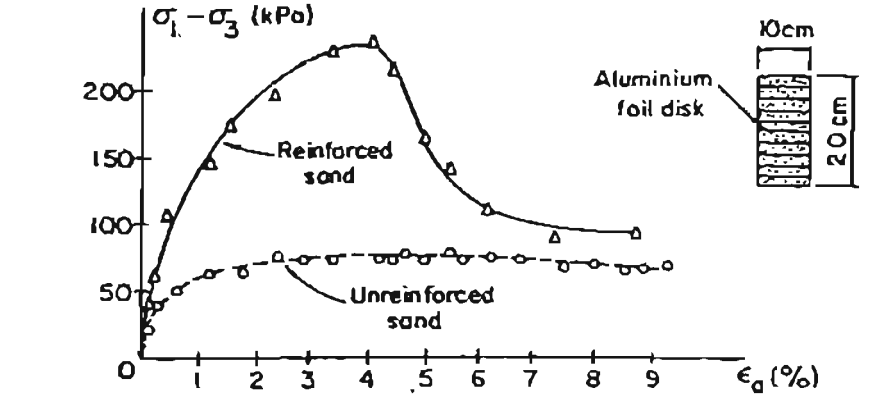

a - INEXTENSIBLE REINFORCEMENT (Aluminium foil)

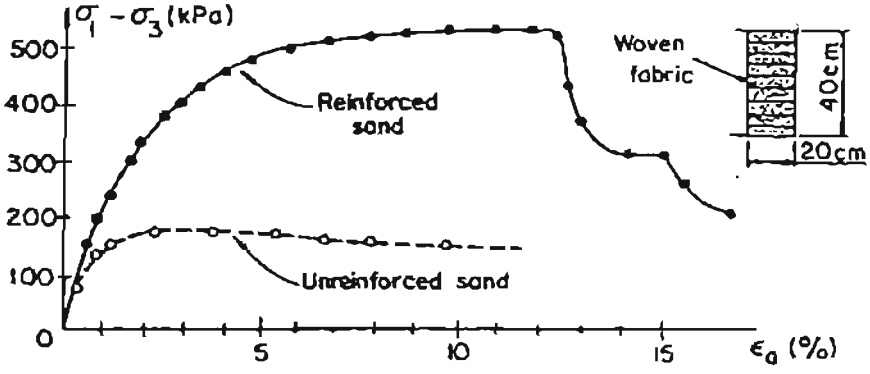

b - EXTENSIBLE REINFORCEMENT (Woven Fabric)

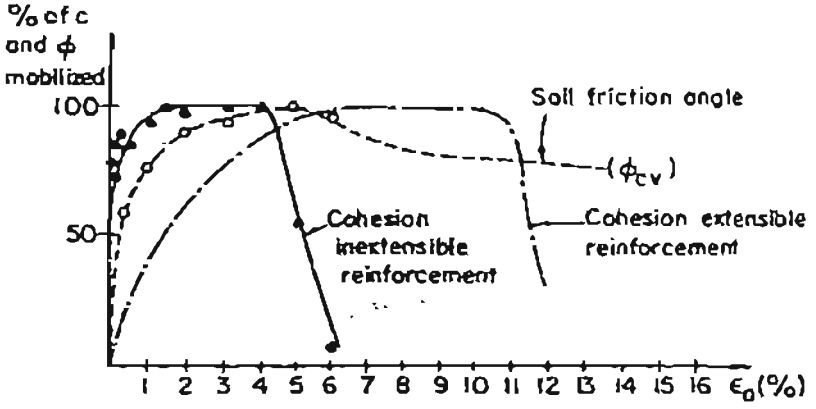

c - RESPECTIVE MOBILIZATIONS OF COHESION AND FRICTION ANGLE DUE TO THE REINFORCEMENT

Figure 2.6: Mobilization of the Shear Characteristics (c, ϕ) for reinforced sand samples. (After Schlosser & Buhan, 1990)

Chandrasekaran (1988) performed triaxial tests on samples of sand reinforced with a woven geotextile (Figure 2.6.b). The main difference between quasi-inextensible reinforcements (such as aluminum foil disks) and extensible reinforcements (such as geotextile) is the amount of deformation necessary to mobilize the peak resistance. Chandrasekaran's study suggested that the total tensile resistance of extensible reinforcements could not be mobilized simultaneously with the shear strength of the soil. This behavior of composite materials has been discussed by Jewell (1985) and gave rise to the concept of strain compatibility (Jewell, 1988; McGown, 1989; Juran, Ider and Farrag, 1990) in the limiting equilibrium analysis. Considering strain compatibility, these researchers have suggested that the limiting state design of geosynthetic walls should be performed using the critical state friction angle instead of the peak internal friction angle of the soil (Schlosser and Buhan, 1990).

The frictional interaction between reinforcement and soil induces shear stresses on horizontal planes; and consequently, changes the stress and strain distribution in the soil (Schlosser and Buhan, 1990). This effect was theoretically established by Bassett and Last (1978) and has resulted in one of the major contributions to the understanding of the at-failure

behavior of reinforced soil. Bassett and Last indicated that for quasi-inextensible reinforcements, the stress characteristic lines in the reinforced soil wall are vertical rather than inclined at $45^\circ + \phi/2$, as in the case of a conventional retaining wall without reinforcements (Figure 2.7). They also demonstrated that the optimum directions for placement of reinforcements coincide with the principal strain directions induced in the soil.

In dense granular backfill, soil dilatancy plays an important role in the mobilization of the interface friction, especially when the overburden pressure is small. The restrained dilantancy effect due to the presence of the reinforcement was proposed by Schlosser and Elias (1978), and led to the definition of an apparent friction coefficient, which is related to the initial normal stress acting on the reinforcement. Geogrid exhibits higher dilation effects than geotextile, due to larger interlocking forces between the soils and reinforcements (Schlosser, 1990).

Maximum Tension Line and Failure Surface

Bassett and Last (1978) have demonstrated that the failure surface of a retaining wall reinforced with inextensible inclusions is vertical in the upper part of the wall and does not correspond to the Mohr-Coulomb failure surface. The potential slip surface is assumed to coincide with the maximum tensile force line

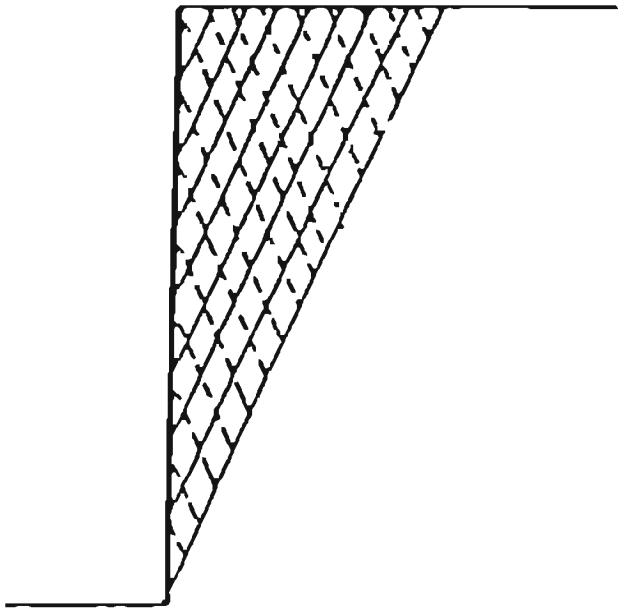

(a) Without reinforcement

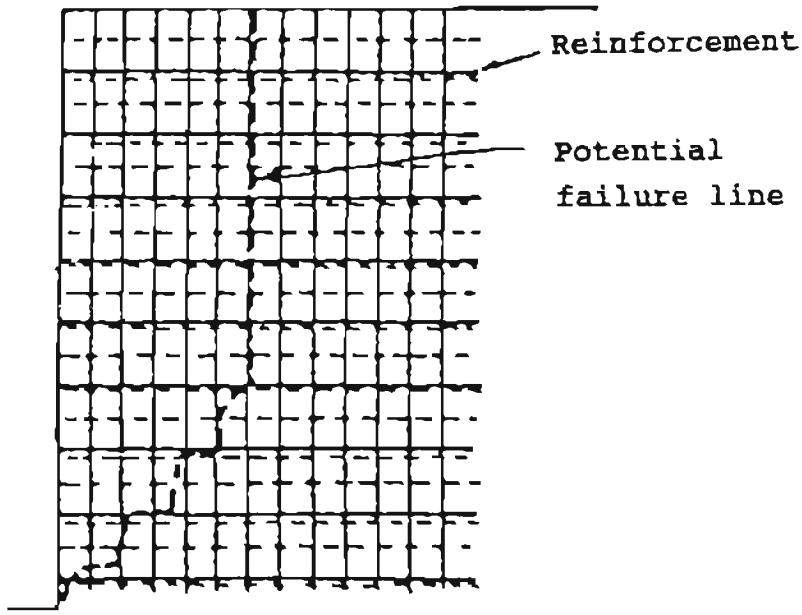

(b) With Reinforcement

Figure 2.7: Influence of Reinforcement on the Potential Failure Lines (After Bassett and Last, 1978).

(Billiard and Wu, 1991, Christopher, et. al., 1989). This maximum tensile force line is assumed to be bilinear in the case of inextensible reinforcements, linear in the case of extensible reinforcements (Figure 2.8), and passes through the toe of the wall in both cases (Christopher, et. al., 1989).

Soil Pressures

Full-scale experiments on MSE walls, utilizing both inextensible and extensible reinforcements, demonstrate the differences in their structural behavior (Gray, 1981). Extensible reinforcements allow lateral displacements, which may lead to the mobilization of the active state of stress (K_a). On the other hand, inextensible reinforcements usually develop an at-rest (K_o) state of stress in the upper part of the structure, related to small lateral displacements of the facing (Schlosser, 1990).

The K_o state of stress observed in the upper part of a wall constructed with inextensible reinforcements is probably a result of overstress induced by compaction. Compaction affects the tensile forces in the reinforcement by generating additional lateral stresses in the soil, which induces additional tensile forces in the reinforcement. This effect is less significant in the lower reinforcement layers, since there is a relief of the overstress in these layers resulting from the lateral displacements due to

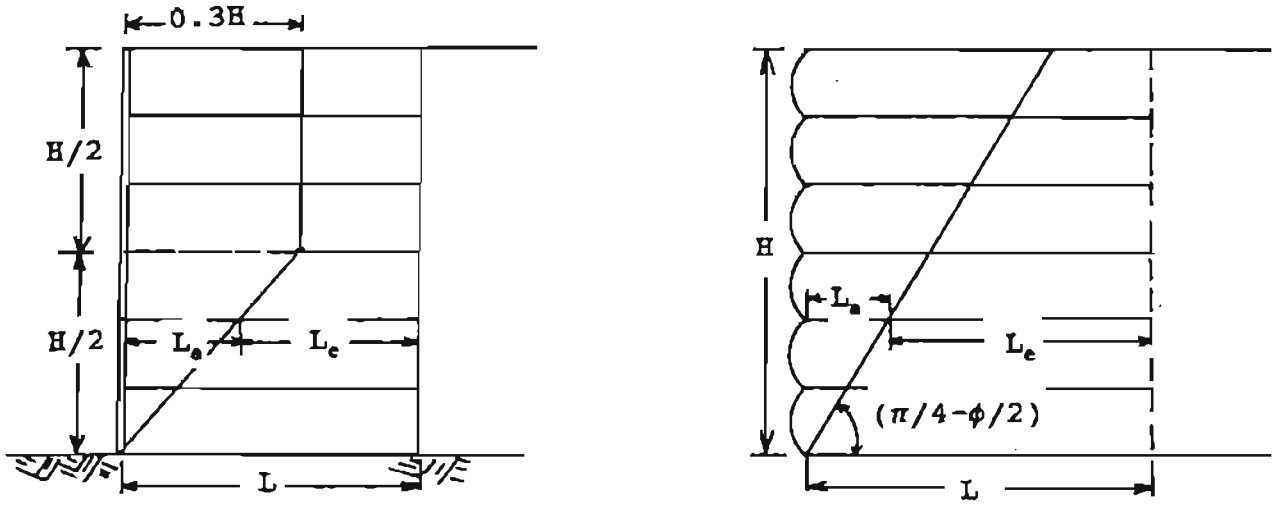

(a) inextensible reinforcements

(b) extensible reinforcements

Figure 2.8: Tensile Forces in the Reinforcements and Schematic Maximum Tensile Force Line (After Christopher, et. al., 1989)

increase of overburden. For geotextile walls, because of the relatively low stiffness of geotextiles, the amount of overstress is relatively small (Schlosser, 1990).

In the lower part of the wall, tensile forces in the reinforcement correspond to a state of stress below K_a. This is attributed to the arching effect developed between the foundation soil and the upper section of the wall (Schlosser, 1990).

2.3.2 Analytical Methods

The analytical approaches include the limiting equilibrium method and the finite element methods. The limiting equilibrium methods were discussed in Section 2.2.1. Only the limiting equilibrium method that considers the strain compatibility analysis is presented in this section.

Strain Compatibility Analysis for GRS Walls

Juran, Ider and Farrag (1990) presented a strain compatibility analytical method for reinforced soil walls with extensible geosynthetic reinforcements. A soil-reinforcement load transfer model (Juran, et. al., 1988) was used to calculate the tension force generated in the reinforcements. This load transfer model allows for an evaluation of the effects of reinforcement extensibility and soil dilatancy on the tension forces.

Juran, et. al. made the following assumptions in their model:

(1) Constitutive models for the soil. Two soil models were used. The first is an elasto-plastic strain hardening soil model; the second is a Mohr-Coulomb type rigid-plastic material with a nonassociated flow rule;

(2) Stress-strain relationship for the reinforcement. The reinforcement is assumed to be an elastic-perfectly plastic material;

(3) Soil-reinforcement interaction. Perfect adherence is assumed to prevail at the soil-reinforcement interface;

(4) Strain path. It is assumed that during construction, the progressive rigid body translation of the active zone causes a continuous distortion of the limit reinforced soil layer along the potential sliding surface;

(5) Effect of construction process. Juran et. al. uses the finite difference method to incrementally simulate the construction process. The construction process (including compaction) may induce an initial soil distortion.

This strain compatibility analytical method has been used to predict the maximum tension forces mobilized in the reinforcement and the location of the potential failure plane. It also has been used to evaluate the local structure stability at each reinforcement level with respect to a potential failure due to either breakage or sliding of the reinforcement.

This analytical method has a major advantage over the conventional limiting equilibrium method in meeting the requirement of strain compatibility. In addition, it considers the effect of soil dilatancy and the extensibility of the reinforcement on the mobilized tension forces and structure stability. However, boundary conditions as well as stress equilibrium at each point within the mass and along the slip plane are not included in the formulation (Leshchinsky, 1992).

2.3.3 Finite Element Analyses

The complicated soil/reinforcement interaction and its effects on the behavior of GRS walls can best be analyzed by the finite element methods (FEM). Two different finite element modelling approaches have been used for analyzing MSE walls (i.e., composite approach and discrete approach). In the composite approach, the reinforced soil is idealized as a homogeneous composite structure (Herrmann & Al Yassin, 1978; Romstod, et. al., 1976; Chou, et. al., 1991; Wu, et. al., 1991). The properties of the composite material are obtained by testing the soil-reinforcement composites. In the discrete approach, the reinforced soil is considered to be a heterogeneous system in which the soil and the reinforcement are separately represented by different material properties. Wu (1989) discussed the trade-offs of the two approaches for analysis of geosynthetic reinforced soil structures.

Numerous finite element analyses on GRS walls have been conducted over the past 10 years. Most analyses employed the discrete approach. Three finite element analyses of GRS walls are briefly reviewed in the following:

Collin (1986)

Collin used an FEM program, SSCOMP, to analyze various types of MSE walls, including GRS walls. The Duncan-Chang model was adopted, and an hysteretic soil model was used to model loading-unloading of the soil due to compaction process. Other features of SSCOMP are described in Section 3.2.1.

Soil-reinforcement interface was modelled by hyperbolic interface elements, and compaction of backfill was represented by a peak lateral compaction-induced stress profile. The analysis indicates that the tension force in each layer of reinforcement steadily decreases from the wall face to the free end of the reinforcement. It should be pointed out that Collin used the maximum force for each layer of reinforcement to determine the lateral earth pressure within the wall. By doing so, the earth pressure within the reinforced soil mass is nearly uniform with depth and is very small in value (see Figure 2.9).

Collin compared the FEM analysis results with field measurements of MSE walls with inextensible reinforcement, and concluded that an analysis without

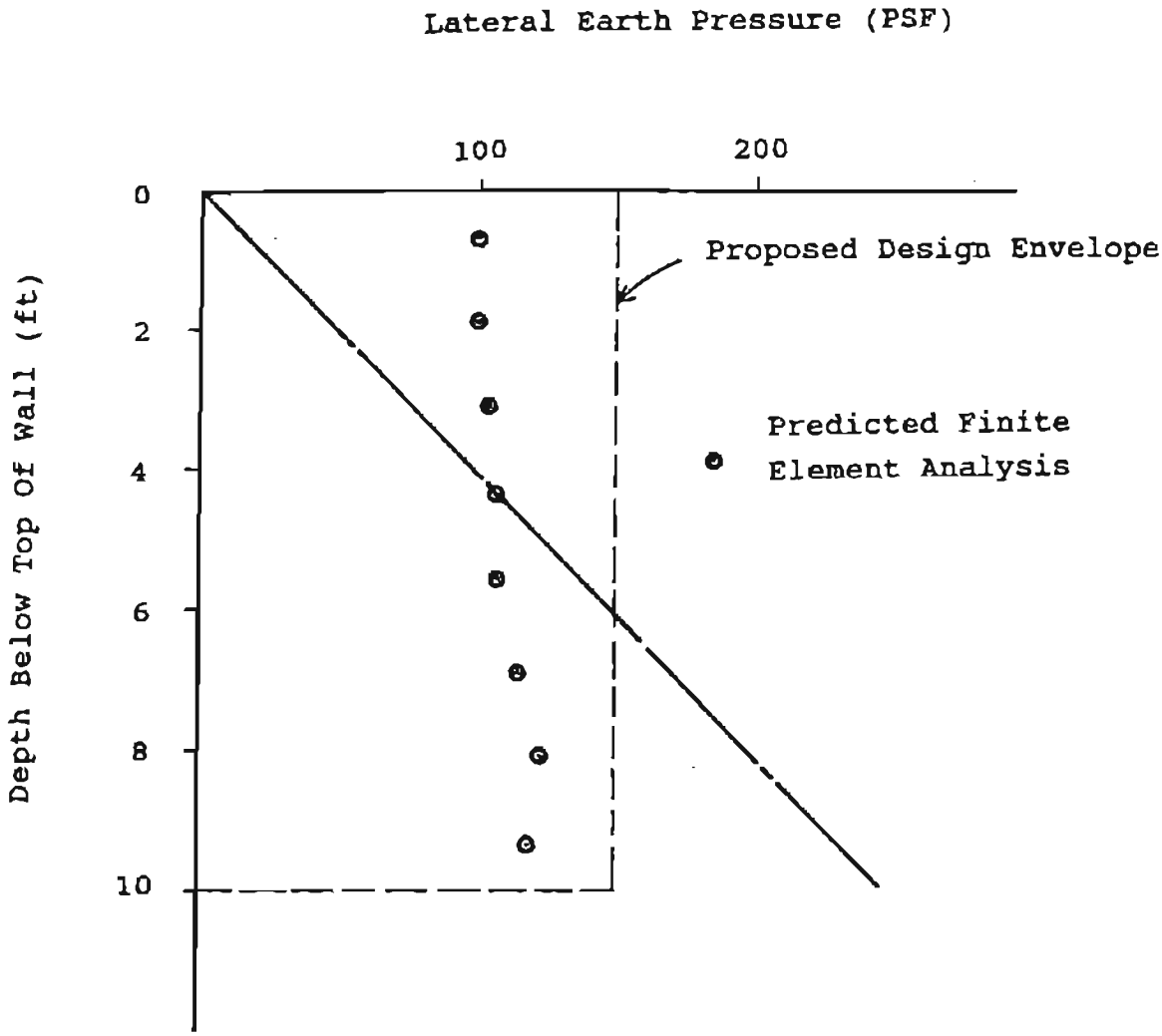

Figure 2.9: Predicted Lateral Earth Pressure for a Geotextile Wall by Collin Method (After Collin, 1986)

considering compaction effects would underestimate the tensile stresses in the reinforcement. However, the author suspects that the compaction effect is less significant in GRS walls since the flexible and extensible reinforcement allows the reinforced soil mass to deform more freely, thus relieving some lateral stresses during the placement and compaction of the backfill.

Adib (1988)

Using SSCOMP program, Adib (1988) and Adib, et. al. (1990), performed finite element analyses and compared the results with the measured field behavior of five reinforced soil walls and four reinforced embankments. These walls and embankments were constructed as part of a FHWA sponsored study on the behavior of reinforced soil structures.

The comparisons of field measurements with the FEM analysis results were made in the following aspects:

(a) Location of maximum tension in the reinforcement;

(b) Distribution of tension along the reinforcement;

(c) Lateral earth pressures and their distribution with depth; and

(d) Lateral movement of the facing during and after construction.

One of the walls investigated was a geotextile wall with gravelly sand backfill. The wall was designed to fail when reaching the full height. To avoid injuries to workers, a pond was built in front of the wall to increase stability near the toe. The wall was then built to its design height of 20 feet, and the water was subsequently drained from the pond to induce wall failure.

Adib made the following two observations about the failure of the wall:

(1) The failed elements are largely concentrated in the reinforced zone, instead of the retained soil or foundation; and

(2) No definite failure pattern is noticed.

Wu & Lin (1991)

A parametric study has been undertaken by Wu & Lin (1991) to investigate the factors influencing the performance of GRS walls. The parametric study was conducted by using SSCOMP program. The effects of the following parameters on the performance of geosynthetic walls were investigated:

- the backfill stiffness and strength
- the geosynthetic stiffness
- the geosynthetic length
- the geosynthetic layer spacing
- the foundation stiffness and strength
- the foundation depth

- the surcharge pressure

- the facing rigidity

Two 12-foot high "control walls" were selected for the FEM analysis, one on a rigid foundation and the other on a flexible foundation. Lateral deformations, tension force in the geosynthetics and lateral earth pressures against the facing were studied for each case.

2.4 Review of Full-Scale Instrumented Geosynthetic Walls

Several full-scale instrumented GRS walls have been monitored and reported in the literature (Holtz & Broms, 1977; Bell, Barrett & Ruckman, 1983; Tatsuoka & Yamauchi, 1986; Wichter, Risseeuw & Gay, 1986; Fukuda, Yamanouchi & Miura, 1986; Fabian & Fourie, 1988; Juran & Christopher, 1989; Bathurst & Benjamin, 1990; Christopher, Holtz & Allen, 1990; Burwash & Frost, 1991 ; Allen, Christopher & Holtz, 1992).

Three of these full-scale test walls are reviewed:

(1) Glenwood Canyon Test Wall: The first instrumented, geosynthetic test wall in the USA; constructed over a soft foundation, and the facing unprotected.

(2) Seattle Geotextile Wall: The tallest geotextile wall built in the USA to date.

(3) Calgary Geogrid Wall: The first well-documented failure case of GRS walls; constructed using cohesive backfills and a temporary facing.

These three case histories echo the problems stated in Chapter I (Section 1.5):

Problem Statement

Case History	Design Based on Limit Analysis	Cohesive Backfill	Soft Foundation	Facing Rigidity
Glenwood	x		x	x
Seattle	x			
Calgary	x	x		x

2.4.1 Glenwood Canyon Test Walls

In 1982, the Colorado Department of Highways (CDOH) designed and constructed a 10-section geotextile wall on Interstate-70 through Glenwood Canyon. Design, construction, and measurement data of the test wall have been reported by Bell, Barrett, and Ruckmann (1983).

The soils at the site consisted of very deep lacustrine deposits of highly compressible silt and clay layers. Settlements up to 40 in. were predicted to occur within 15 years after construction. This led to the consideration of flexible earth retaining systems.

The test wall was designed according to the U.S. Forest Service design method (Steward, et. al., 1977).

This method is based on the tie-back wedge analysis, using the at-rest earth pressure conditions, which was believed to be conservative. Portions of the wall were designed at or near equilibrium conditions and were, therefore, expected to exhibit significant strains or possibly failure.

Geometry:

The wall was 15-ft high, 12-ft wide, and 300-ft long, and was divided into ten 30-foot segments. A typical cross section of the wall is shown in Figure 2.10.

Four non-woven geotextiles, each in two different weights, were used as the reinforcement. Segments 1 through 8 were reinforced with a different geotextile or geotextile strength combination, extending 12 ft into the fill. Segments 9 and 10 were identical to segments 1 and 2, respectively; except the lower layers were shorter. All segments incorporated a stronger geotextile (Trevira 115) for the lower three layers. The length of fabric overlap for the folded portion was three feet for all layers.

Soil and Reinforcement Properties:

Foundation Soil: The foundation consisted of 10 to 60 feet of compressible silt and clay. These soils are the result of lake deposition.

Geotextile: Four different brands of nonwoven geotextiles were used as reinforcement. Samples 8

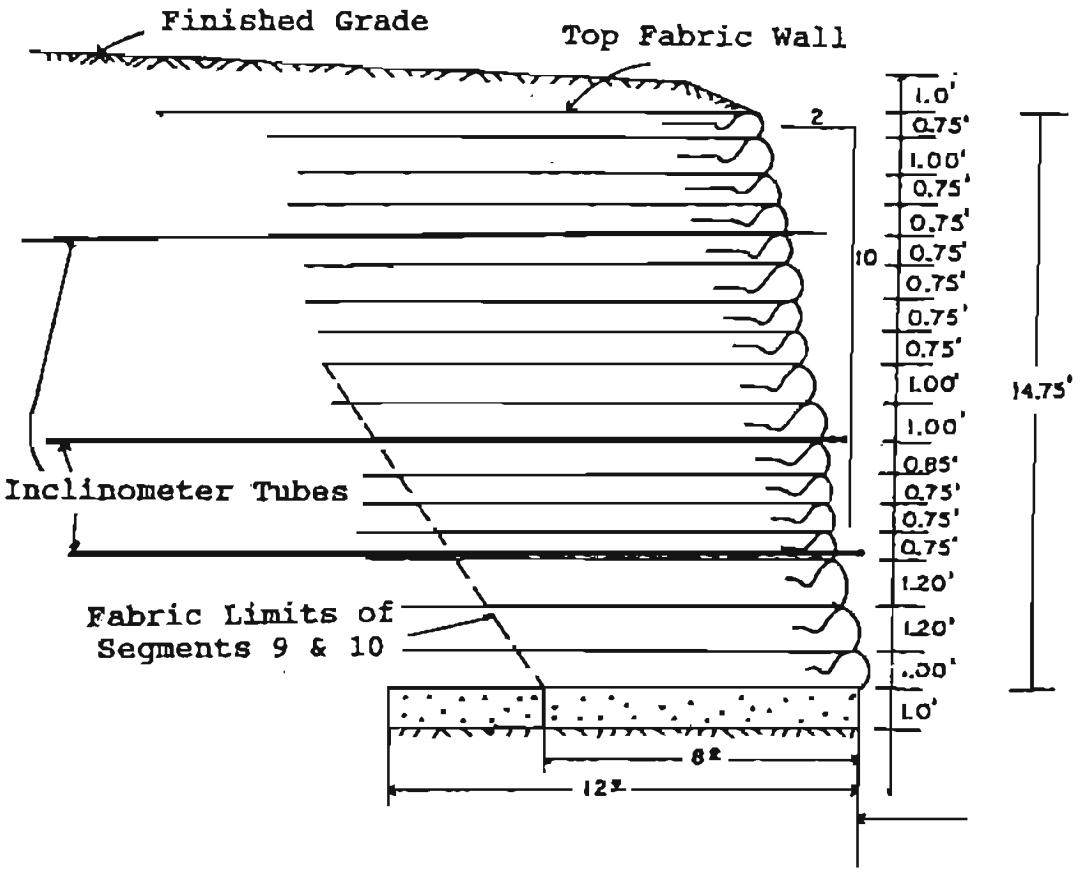

Figure 2.10: A Section of the Glenwood Canyon Geotextile Test Wall.
(After Bell, Barrett & Ruckmann, 1983)

inches wide by 4 inches long were soaked in water and tested in a series of wide-strip tensile tests at a constant strain rate to determine their tensile strengths.

Backfill Materials: The backfill material was free draining pit-run, rounded, well-graded, clean, sandy gravel. Compaction of backfill was carried to 95% of AASHTO T-180.

Instrumentation:

The instrumentation consists of the following:

(1) Foundation soil instrumentation:
   (a) Vertical inclinometer/Sondex System
   (b) Soil pressure cells
   (c) Piezometer
   (d) Manometers

(2) Geotextile Wall Instrumentation:
   (a) Horizontal inclinometers
   (b) Laser targets

A surcharge load up to 15 feet high of uncompacted fill was placed directly on top of the wall four months after its completion. Although portions of the wall had very low safety factors and were expected to be highly stressed or fail, the wall withstood 1.4 ft of settlement one year after construction, and no major distress has been observed since then.

To investigate long-term behavior, and to obtain samples for durability testing, a portion of the test

wall was excavated in 1985 and has remained unprotected ever since (see Figure 2.11). Surprisingly, the integrity of the wall has been maintained for the past seven years despite the fact that the backfill is essentially cohesionless and the unprotected facings are in southern exposure. The geotextile reinforcement is obviously very effective in stabilizing the near vertical wall even without a facing.

The cost of the test wall ranged from $11.00 to $12.50 per square foot of wall face. This is one of the lowest cost walls ever constructed.

Conclusions

The following conclusions can be drawn from the experience learned from the Glenwood Canyon test walls:

(1) Geotextile walls are very economical and can be built by a general contractor rather than a specialized contractor;

(2) Geotextile walls can tolerate very large settlement and differential settlement without distress;

(3) Conventional designs based on the Forest Service method are much too conservative;

(4) The test walls did not exhibit measurable creep although stress levels in some portions of the reinforcement could be high; and

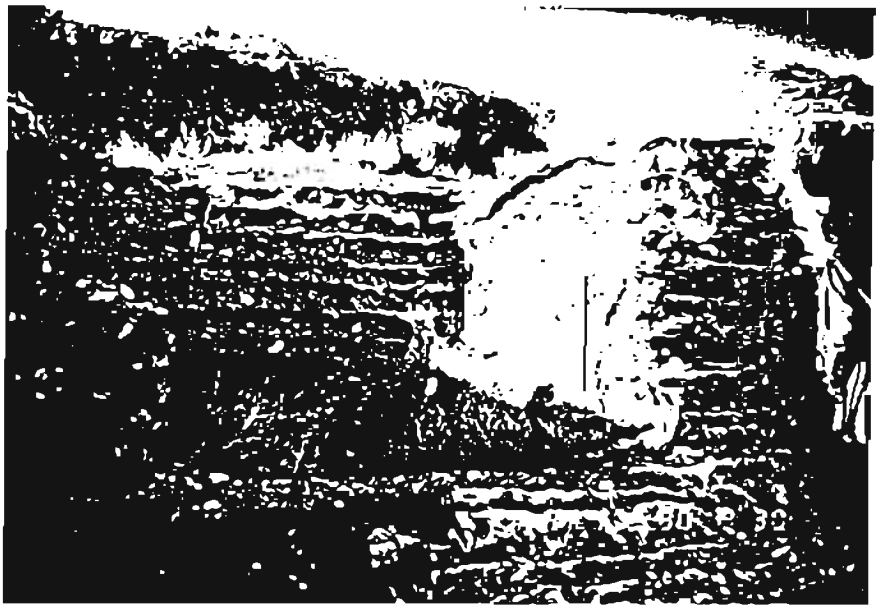

Figure 2.11: Unprotected Geotextile Wall Facing, Glenwood Canyon Wall

(5) The reinforcement can effectively induce an apparent cohesion of cohesionless backfill to assume a vertical slope even without a facing.

2.4.2 Calgary Geogrid Wall

The following is based on a documented case history reported by Burwash & Frost (1991), which describes the failure of a 9 m-high geogrid wall backfilled with a cohesive soil. This is the first well-documented case history of failure of GRS walls.

General

In the fall of 1983, a commercial development in Calgary, Alberta, called for constructing a retaining wall to support an asphalt surfaced parking lot. The wall was up to 9 m in height and consisted of vertical steel H-piles, timber laggings and deadman anchors. An alternative design using high strength geogrids (Tensar SR2) to replace the deadman anchors, and continuing to incorporate the H-pile and timber lagging facade was accepted by the owner on the basis of lower cost.

As part of the alternative design, a low plasticity clay till was used as backfill. Drainage was provided by a 600 mm-wide zone of granular fill adjacent to the timber lagging. A 75 mm void was constructed between the geogrid facing and the H-pile with timber lagging to allow for possible post-construction movement. Foundation soil was a deep

deposit of very stiff low plasticity clay till. The groundwater table was well below the ground surface.

The wall was constructed in the spring of 1984 and performed satisfactorily until September, 1985, when signs of settlement were first observed. Conditions gradually deteriorated, and in January, 1986, a slope indicator was placed on the face of the wall to monitor the outward movement. The measurement showed that the wall facing was rotating about its base, and after 17 months, the deflection at the top of the wall was 310 mm. Settlement of the parking lot behind the retaining wall was observed to continue over the same period and was estimated to be up to 0.9 m by June, 1987. At that time, the upper 6 m of the wall was replaced with a free standing 2(H):1(V) slope.

The geogrid reinforced wall consisted of two segments, called the north and northwest walls. The segments were oriented at an angle of 142° between them, with a total length of 59.4 m and a maximum height of 9.0 m.

The H-piles, consisting of W250 x 49 steel sections, were placed in 600 mm diameter augured holes; the holes (about 3 m deep) were then backfilled with concrete. The H-piles were positioned at 2.2 m centers. The pressure treated timber lagging was 75-mm thick and 150-mm wide and positioned on the inside of

pile flanges and held in place by wooden blocks wedged into the opposite flange.

The reinforcement was Tensar SR2, a high strength oriented polymer grid. The wall was reinforced by up to 10 layers of the geogrid with lengths up to 6.8 m. The geogrids were incorporated into the wall design using the "wrap around" method shown in Figure 2.12. A temporary spacer was placed between the H-piles and the geogrids to produce a 75 mm wide void which was used to accommodate creep of the geogrid. The length of geogrid (L) to height of wall (H) ratio was at least 0.7.

The outer 600 mm of soil contained by the geogrids was a granular fill which provided drainage. The backfill consisted of low plasticity clay till, which is similar to the foundation soil. Typical index properties of the clay till were: liquid limit 30 and plastic limit 15, and average gradation of 25% sand, 50% silt and 25% clay sizes. The backfill was compacted to a minimum of 95% of the standard Proctor dry density. The earthwork operations were observed by a full-time inspector who conducted 105 in-situ density tests. Areas of failing density tests were reworked until they met the compaction specification.

A second wall, termed the south wall, was constructed at the same time as the north-northwest wall, using nearly the same method. However, the

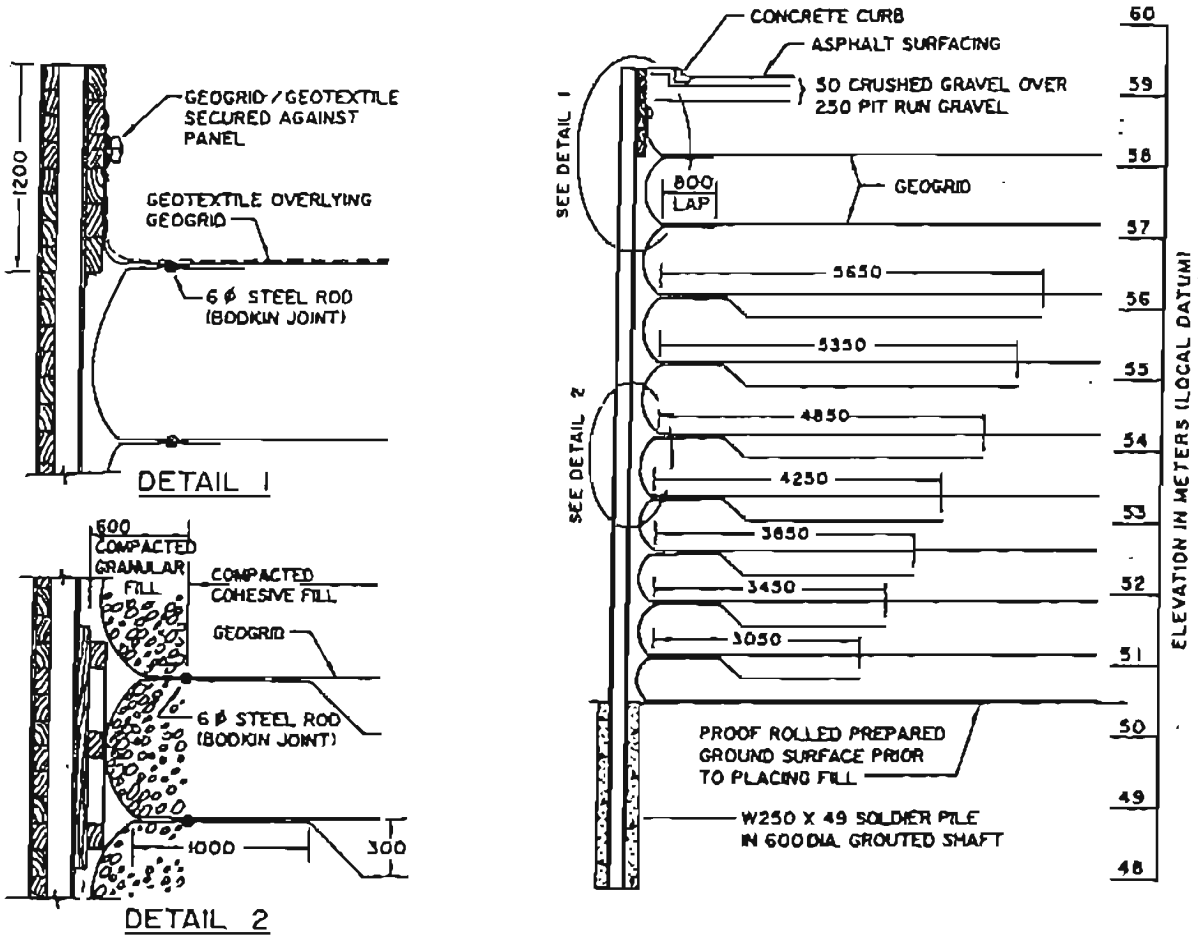

Figure 2.12: Typical Section of the Calgary wall (After Burwash & Frost, 1991)

maximum wall height was 5.4 m (compared to 9.0 m) and the embedded depth of H-piles was 8.0 m (compared to 3.0 m). The south wall suffered no distress.

External Stability

The length of the reinforcement was selected, so a factor of safety of at least 1.5 was obtained, to prevent external instability. The lateral earth pressure was calculated using the Rankine theory with an angle of internal frictions of 30°.

For a L/H ratio of 0.7, the overturning requirement was achieved. Conventional stability analyses showed that the factor of safety with respect to global or deep seated shear failure exceeded the conventional minimum safety factor of 1.5.

Internal Stability

The geogrid reinforcement has a peak tensile strength of 79 kN/m. However, a long-term design load of 29.2 kN/m was used in permanent structures to ensure that deformation of the structures remain within acceptable limits over its entire service life. A safety factor of 1.5 was applied to the long-term design load to give an allowable design strength. The geogrids were spaced, so the tension induced in the geogrids was less than the allowable strength. The top geogrid was placed 1.2 m below the finished grade and the bottom layer at the level of the ground surface

outside the toe of the wall. The lower geogrid layers were spaced as close as 300 mm apart.

Readings from inclinometers were taken, and the results indicated that the facing was rotating about the toe but the rate of rotation was not accelerating. After 17 months, the facing had moved 310 mm, which was 3.4% of the wall height or 2.0° rotation about the toe. It was noted that these measurements were initiated some 21 months after the end of construction and 5 months after the first evidence of distress; thus, actual displacements were larger. By August of 1986, it was apparent that the distress showed no sign of abating and the wall was designated as unsafe. The parking lot near the wall was then cordoned off.

In November, 1986, three bore holes were drilled behind the juncture of the north and northwest walls. The results showed that the clay backfill had softened to a depth of about 3 m. Construction records showed that the average moisture content of the clay backfill at placement was 10.5%, which was 4.0% dry of the optimum value of 14.5%. However, the moisture content of samples taken from the boreholes, which were drilled 30 months after completion of construction, showed a noticeable increase. This was particularly evident in the upper 3 m where the moisture contents were typically 1.5% to 3.0% above optimum and 5.5% to 7.0% above the placement moisture content. This increase

was less apparent both at increasing depth and increasing distances from the wall.

In June, 1987, the upper 6 m of the wall was removed and replaced with a free standing 2(H) : 1(V) slope. The lower 3 m of the wall was left in place. A site survey conducted just before reconstruction showed a maximum settlement of about 0.9 m (approximately 10% of the height of the fill). The maximum settlement at the back of the reinforced zone was about 0.5 m or about 5.5 % of the height of the fill.

Reasons of Failure

A post-construction site investigation showed that the moisture content of the clay backfill had increased significantly from that measured during construction of the wall. The upper 3 m of the fill appeared to be saturated and was much softer than the as-compacted condition.

The parking lot was graded to a catch basin located 21 m from the wall. The area surrounding the catch basin was designed to act as a holding pond and extended up to the wall. Water would pond in this area after heavy rainfalls and would in time flow through the storm sewer system. The difference in elevation between the paved surface at the wall and at the catch basin was 200 mm. This difference in elevation eventually was reversed by subsidence. Burwash and Frost suspected that the subsidence caused failure of

the storm sewer leading from the catch basin. Runoff water then seeped through the cracks in the asphalt into the clay backfill. These series of events were consistent with the saturated condition of the clay backfill.

Burwash and Frost noted that a heavy rainfall (40 mm in 24 hrs) preceded observation of the first sign of distress in September, 1985. The rainfall could have caused ponding which would allow a source of free water to seep into the clayey backfill.

Subsequently, a series of laboratory tests were conducted on samples of clay backfill recovered during the reconstruction. The samples were compacted to 95% standard Proctor dry density at the placement moisture content (10.5%) and consolidated in an odometer under a pressure of 100 kPa to simulate the loading at mid-height of the wall. At completion of consolidation, the samples were inundated and settlement of 0.7% to 0.8% of the sample height occurred immediately. The dry state of the backfill (about 4% dry of optimum) contributed to the observed collapse type of compression. However, the compression, even when combined with foundation and backfill settlement, still did not explain the magnitude of the observed settlement. The behavior of the clay at low confining pressures (e.g. within 3 m of finished grade) was expected to be different from that observed in the

odometer tests. The clay may swell in this upper zone. The loss of lateral support of the soil resulting from swelling and strength loss could lead to rotation of the wall, which was not modeled in the odometer tests, and may explain some of the discrepancies between the predicted and observed settlements.

A unconsolidated undrained (UU) triaxial test conducted on a sample of the clay compacted to 93% of the standard Proctor dry density at a moisture content of 10.5% gave a compressive strength of 375 Kpa. A similar sample when saturated gave a compressive strength of only 49 Kpa, and the moisture content had increased to 18.7%. These test results were consistent with the observation in the field, e.g., the clay gained moisture and lost considerable strength.

Author's View on Reasons of Failure

The author agrees with Burwash & Frost that saturation of the cohesive backfill, which caused the loss of shear strength, was the major reason for the failure. However, the author believes that the following factors also may have contributed to the failure:

(1) The moisture content during compaction was too low (4% below the OMC). If the placement moistures were above optimum, the loss of shear strength and increase in settlement, due to wetting, would have been significantly reduced (Hilf, 1975). The adverse

effects due to wetting of the cohesive backfill will be further discussed in Section 5.3; and

(2) The H-piles probably did more harm than good to the wall. The temporary support provided by the H-piles may have prevented tension in the reinforcement from developing during wall construction. After the temporary support is removed, the backfill and the reinforcement in the wrap-around portion move outward a few inches before friction can be fully mobilized. This behavior was evidenced in a large-scale geotextile test wall performed by Billiard (1988). In one of his tests, a temporary support was removed after the wall reached its full height. This led to a pullout failure of the wrap-around geotextile.

In addition, the author believe that the drainage material placed in front of the wall facing was not effective. The geogrid/wood lagging and H-pile system is rather pervious; therefore, it is unnecessary to place the free draining material adjacent to the facing. Instead, it would be more effective to place the free-draining material at the top, bottom and back of the reinforced zone (see Section 6.3).

2.4.3 Seattle Wall

The following case history is based on the paper presented by Christopher, Holtz and Allen (1990). The Seattle wall, a 41-ft high temporary geotextile wall, was constructed by the Washington State Department of

Transportation (WSDOT) to provide a preload fill for a bridge abutment, which is located in an area of limited right-of-way. The project was located at a major motorway interchange in Seattle, Washington. Because the wall supported a surcharge fill more than 15 feet in height and was significantly higher than any previously constructed wall of this type, an extensive program of instrumentation and measurement was instituted. The wall was partially demolished and buried after about one year of temporary service.

Subsurface investigations indicated that an upper layer consisting of 19 feet of dense granular soils overlies up to 49 feet of soft lacustrine silty clays and clayey silts. These soft deposits were expected to result in abutment settlements of up to 1.3 feet; thus, a temporary surcharge fill was deem required.

A conventional tie-back wedge analysis was performed by WSDOT engineers. The analysis assumed an active earth pressure coefficient with a $\phi = 36°$ and $\gamma = 20.4$ KN/m^3 for the backfill. The reinforcing spacing was 0.38 m. The wall was designed with a safety factor of 1.2 against rupture for internal stability plus an additional reduction factor for polymer creep. Geotextile strength was varied with the height of the wall, with the highest strength geotextile near the base of the wall.

Figure 2.13 shows the strain distribution of each layer of geotextile. These measurements were taken at the end of construction and six months after placement of the surcharge. Based on the strain measurements, the maximum strain in the reinforcement was approximately 0.5%. Strains measured by the extensometers ranged from 0.7% to 1.0%. The maximum deflection obtained from the inclinometers was about 6 inches. The creep response of the reinforcement, especially under constant surcharge loading, was rather small (see Allen, et. al., 1992).

This 41 foot-high wall again indicates that the tieback wedge analysis is conservative, and that strains in the reinforcement were much less than anticipated. Although designed with a safety factor of 1.2, the actual safety factor appears to be much higher. This case history also indicates the need of a rational design approach based on an allowable wall displacement.

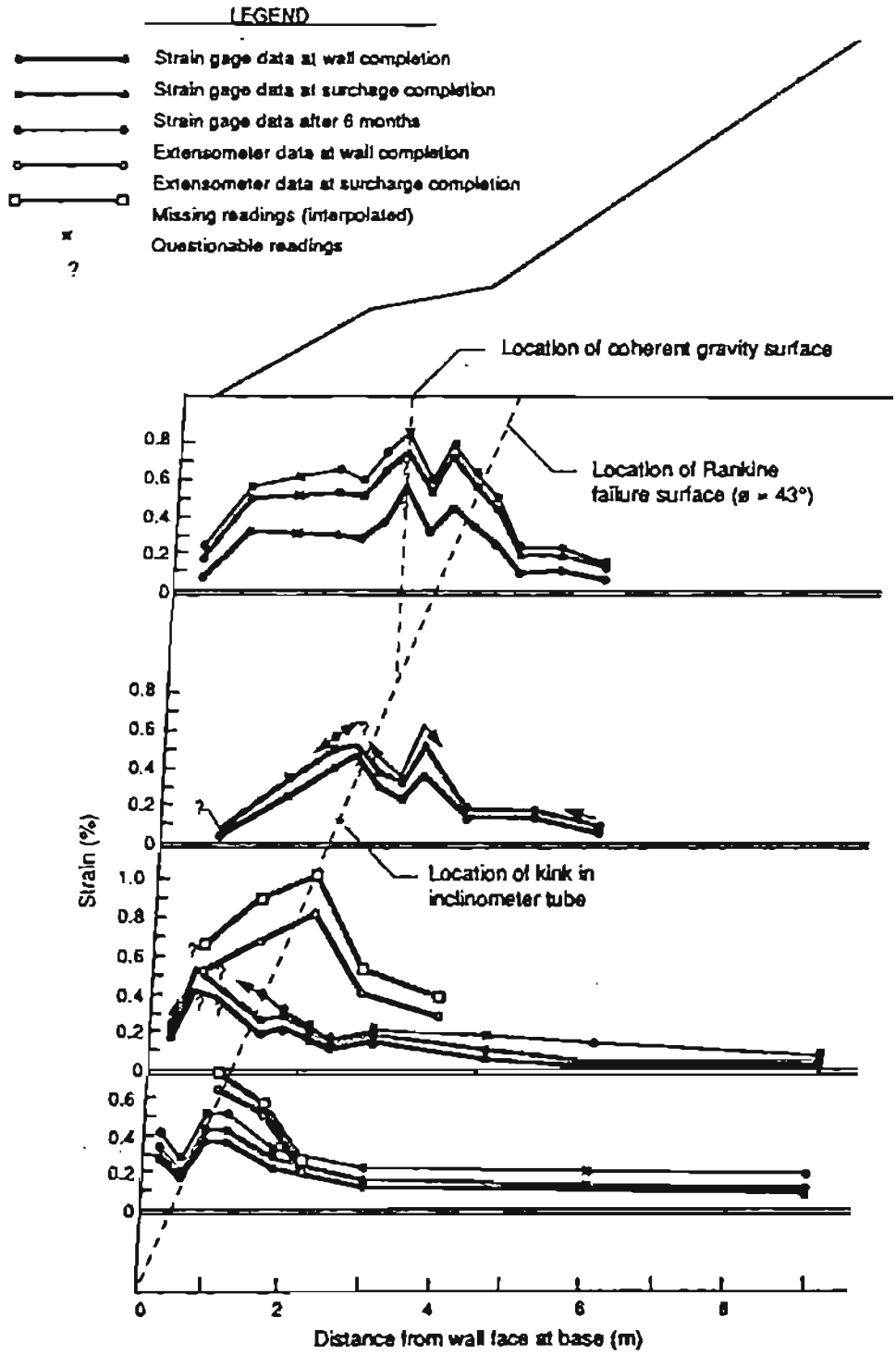

Figure 2.13: Distribution of Strains in Each Instrumented Layer at Various Times, the Seattle Wall (After Christopher, et. al., 1991)

CHAPTER III

FINITE ELEMENT SIMULATION OF GEOSYNTHETIC WALLS

3.1 Analysis of GRS Wall Behavior by FEM

The behavior of a GRS wall is rather complicated. Among various analytical methods, the finite element method is the most versatile analytical tool for analyzing the behavior of GRS walls. This method is capable of accommodating: (a) practically any geometric configurations of GRS walls; (b) material characteristics of the soils (retained soil, backfill, and foundation), the geosynthetic reinforcement and the facing; (c) interactive behavior among the soil, the reinforcement, and the facing; (d) sequential construction and compaction operation of GRS walls; (e) nonhomogeneity of GRS walls; and (f) surcharge loads on GRS walls.

Based on the parametric study results (Wu and Lin,1991), and experiences learned from reduced-scale model tests and actual construction of GRS walls, it is believed that the following are the most important features to be simulated in the finite element analysis of a GRS wall:

- Wall configuration (including wall height, reinforcement length, and reinforcement spacing)

- Stress-strain-volume change relationship of the backfill and the foundation
- Load-deformation relationship of the geosynthetic
- Bending stiffness of the facing
- Consolidation and porewater pressure response of soft foundation (if present)
- Construction sequence, including facing construction
- Compaction operation

3.2 Selection of a FEM Program

The following FEM programs were tested and evaluated, for analyzing the behavior of GRS walls:

(1) SSCOMP (Seed, 1983)

(2) CRISP (Britto & Gunn, 1987)

(3) CON2D86 (Schaefer & Duncan, 1987)

(4) DACSAR (Iizuka & Ohta, 1987)

The following sections briefly describe the development, special features and limitations of each program. Their suitability for analysis of GRS wall behavior also is discussed.

3.2.1 SSCOMP

SSCOMP was developed at the University of California at Berkeley during 1970's & 1980's, through several revisions spanning a period of 10 years. The original program containing only soil analysis was coded by Ozawa in 1973 and was named ISBILD. Dicken

added structural elements in the program and changed its name to SSTIP. In 1980, Wong implemented interface elements and the modified-Duncan soil model, and renamed it SSTIPN.

The program SSCOMP improved on SSTIPN by incorporating a bilinear model to account for compaction induced stresses. The program was modified and coded by Raymond Seed (1983).

SSCOMP employs two soil models. One is a hyperbolic soil model with bulk moduli formulation (Duncan, Byrne, Wang & Mabry, 1980), which is used to calculate soil properties during each load increment. The other soil behavior model is a hysteric loading-unloading model for calculating stresses resulting from compaction. The second soil model is based on the assumption that the soil is under an "at rest" condition. The author suspects that the compaction induced stress is probably over-estimated in the analysis of typical GRS walls, especially near the facing. Due to the relatively low rigidity of the geosynthetic reinforcement, significant lateral deformations may occur during compaction and, therefore, the amount of over stress due to compaction is probably small.

The author has used SSTIP, an early version of SSTIPN, to study the effectiveness of using geogrid to reduce the differential settlement of an I-76

embankment over soft foundation (Chou, Wu & Siel, 1987; Wu, Siel, Chou & Helwany, 1992). In this study, SSTIP gave a very good simulation of the soil/reinforcement interaction problem. Collins (1986) and Adib (1988) used SSCOMP to perform analyses of reinforced soil walls. They concluded that the results of SSCOMP compared reasonably well with field measurements of a number of instrumented test walls.

SSCOMP was not chosen for this research study because it lacks an elasto-plastic soil model, which is considered important for better simulation of soft foundation behavior.

3.2.2 CRISP

CRISP (CRItical State Program) was developed by the researchers at the University of Cambridge, U.K., starting in 1975. The program was revised and published by Britto and Gunn, accompanying a book, entitled Critical State Soil Mechanics Via Finite Elements (Britto & Gunn, 1987).

The program incorporates the original and modified Cam-clay models, as well as anisotropic elasticity and nonhomogeneous elasticity (properties varying with depth) models. There are no structural (bar or beam) elements nor interface elements available in the version tested, CRISP84.

Critical state soil model provides an excellent qualitative representation of soil behavior, especially

for normally consolidated clay. The major contribution of the model to engineering practice lies in its capability of interpreting and predicting soil behavior under various stress paths and drainage conditions. For example, from the results of a series of undrained triaxial tests on a given soil, it is possible to predict how the soil will behave in drained triaxial tests, and vice versa. In addition, the prediction of pore pressure changes is often more accurate by the stress path technique of the critical state model, than with Skempton's pore pressure parameters, which are very sensitive to the stress level.

A well-documented case history was reported by the MIT Foundation Deformation Prediction Symposium held in November, 1974. A full-scale field test of an instrumented embankment, loaded rapidly to failure, was carried out. Prior to the test, ten different groups, drawn from consulting firms and universities, made predictions of the failure loads, excess pore pressure, and deformation at specified points on the ground (Boston blue clay).

Professor Worth of Cambridge University participated in this prediction using the modified Cam-clay model. His predictions were very satisfactory and were closer to the observed field behavior than other predictions.

The critical state soil model was initially developed to model isotropic, normally consolidated clay. Later, it was modified to include over-consolidated clay and sand. However, these modifications were not as good, especially with regard to prediction of deformation. In GRS wall construction, the backfill used is usually compacted granular or cohesive soils, generally with a high over-consolidation ratio (OCR). Therefore, the suitability of using the Cam-clay model for analysis of GRS walls with compacted backfill is questionable.

There was no beam nor bar element available in CRISP when the evaluation was performed, which was considered essential in simulation of wall facing and geosynthetics. Consequently, the CRISP program was not chosen for this study.

3.2.3 CON2D-86

CON2D-86 was originally developed by Chang and Duncan (1977) to analyze consolidation behavior of partially saturated earth structures. During its development, the original Cam-clay model was extended to provide for a better representation of the stress-strain-strength behavior of compacted clay. Further improvements were made by Duncan et. al., (1981). In 1986, the program was extensively rewritten by Schaefer & Duncan (1987), to account for static pore water

pressure and to incorporate structural elements. The program was renamed CON2D-86.

The soil model used in CON2D-86 is an extended version of the Modified Cam-clay model. In the original Cambridge version, the failure surface for the modified Cam-clay model passes through the origin. To represent soils that have a cohesion intercept (such as compacted clay), the failure surface was revised (Chang and Duncan, 1977). Other features, such as yield surface, flow rule, hardening law and elastic behavior were kept the same as those of the Modified Cam-clay model.

Although equipped with an extended Cam-clay model for compacted soil, CON2D86 was not chosen for the following reasons:

(1) Suitability of using the modified Cam-clay model for compacted clay was suspected, because of high OCR and the unsaturated nature of the backfills in typical GRS walls.

(2) Prediction of pore water pressure response was unsatisfactory (Duncan, Schaefer, Franks & Collins, 1989);

(3) At the time of this study (1990), the program did not have beam elements, which are essential in simulation of flexible wall facing;

3.2.4 DACSAR

DACSAR (Deformation Analysis Considering Stress Anisotropy and Reorientation) was developed at the Kyoto University and Kanazawa University, Japan (Ohta and Iizuka, 1986; Iizuka and Ohta, 1987). This program was chosen for this research study because:

(1) This program is well organized and well documented. Incorporation of a new model and/or modification of an existing model can be done with relative ease. During this research study, the Duncan-Chang soil model and a hyperbolic bar model have been successfully incorporated in the original DACSAR code.

This program has been consistently maintained and updated by Dr. Atsushi Iizuka of Kanazawa University since its development. It appears to be "bug" free. It also has been employed to predict the behavior of embankments on soft foundation with and without geosynthetic reinforcement (Ohta, et. al., 1983; Iizuki & Ohta, 1987). The predicted results compared well with the field measurements;

(2) This program includes all the element types (i.e. soil, beam, bar and interface elements) needed to simulate the behavior of GRS walls; and

(3) In this program, the viscid and inviscid versions of the Sekiguchi-Ohta model (Ohta & Sekiguchi, 1979) are implemented. The model, taking anisotropic consolidation of soil into account, is considered an

improvement to the original Cam-clay model. This model also considers the effects of dilatancy (deformation due to shearing), consolidation, creep, shearing rate and stress relaxation.

3.3 Description of the DACSAR Code

3.3.1 Element Types

DACSAR incorporates the following element types:

(1) Soil Elements: Soil elements are four node, quadrilateral, isoparametric elements. Each node has two degrees of freedom, horizontal and vertical displacements;

(2) Bar Elements (called "truss element" in DACSAR): Bar elements are two node elements with axial stiffness only (i.e. can only resist axial forces). This is used to represent the geosynthetic reinforcement;

(3) Beam Elements: The beam elements are two node elements with axial, shear and bending stiffness. This is used to simulate the wall facing; and

(4) Interface Element (called "joint element" in DACSAR): The interface element is made up of two linear elasto-plastic springs (i.e. normal and shear springs) that control the relative displacement between the boundary of two materials, such as soil-reinforcement, soil-facing, or between two layers of different soils.

3.3.2 Material Models

3.3.2.1 Soil

The soil models available in the original DACSAR are the linear elastic and the Ohta & Sekiguchi model. The modified Duncan-Chang model was implemented in DACSAR to better simulate the behavior of compacted clay and sand. The implementation was accomplished with the assistance of the researchers at the University of Massachusetts.

3.3.2.1.1 Linear Elastic Model

The linear elastic model incorporated in DACSAR employs Lame's constant, λ , and shear modulus G:

$$\lambda=\frac{\nu E}{(1+\nu)(1-2\nu)} \tag{3.1}$$

and

$$G=\frac{E}{2(1+\nu)} \tag{3.2}$$

where ν = Poisson's ratio
E = Young's modulus

The linear elastic model can be used to check the basic logic of DACSAR program by comparing the FEM results with closed-form solutions, such as a beam subjected to loading, Terzaghi's consolidation theory, etc.

3.3.2.1.2. Hyperbolic Model

The Duncan-Chang model assumes that the stress-strain curves obtained from triaxial tests can be approximated as hyperbolas. This model has been widely used in finite element analysis of different earth

structures. The values of hyperbolic parameters have been determined for more than one hundred different soils tested under the drained and undrained conditions (Duncan, et. al., 1980). The hyperbolic model accounts for three important characteristics of the stress-strain behavior of soils, namely, nonlinearity, stress dependency and inelasticity. The reasons for implementing the Duncan-Chang model in DACSAR for GRS wall analysis include:

(1) The model has been shown to give satisfactory simulation of soil behavior, provided that the loading is predominantly monotonic and that the shear stress level is not approaching failure. For GRS wall under "working stress" condition, the model should give good representation of the behavior of both granular and cohesive backfills.

(2) The Duncan-Chang model can be used for either total stress or effective stress analysis. For an unsaturated backfill, it is very difficult to determine effective stress soil parameters. Use of the Duncan-Chang model could avoid this difficulty; and

(3) The wide data base available in the literature can be used to estimate the parameters when the available information on the soil is restricted to descriptive classification. The data base is also useful for assessing whether parameter values derived

from laboratory test results are consistent with experience.

Two versions of the hyperbolic model have been published. In the first version, the model employs Young's modulus and Poisson's ratio. In the modified version, bulk modulus, B, is employed in place of Poisson's ratio. The modified version of the Duncan-Chang model was implemented in DACSAR.

The stress-dependent Young's modulus, E, is expressed as a function of the shear stress level, $(\sigma_1-\sigma_3)/(\sigma_1-\sigma_3)_f$, and the confining pressure σ_3, as

$$E_t = \{1-\frac{R_f\ (\sigma_1-\sigma_3)}{(\sigma_1-\sigma_3)_f}\}^2\ \ KP_a\ (\frac{\sigma_3}{P_a})^n \qquad (3.3)$$

in which R_f = failure ratio, i.e., the ratio of failure and ultimate stress difference; K and n are constants, and Pa is the a reference pressure usually chosen as the atmospheric pressure.

The inelastic behavior is represented by different values of E for loading and unloading. The same value of unloading-reloading modulus, E_{ur}, is used for both unloading and reloading. The stress dependent E_{ur} is represented by the following equation:

$$E_{ur} = K_{ur}\ \ P_a\ \ (\frac{\sigma_3}{P_a})^n \qquad (3.4)$$

where K_{ur} is the unloading-reloading modulus number. The value of K_{ur} is always larger than the value of K (for primary loading).

A simple loading-unloading criterion is used in DACSAR, in which a soil element is considered in unloading-reloading when the current value of the stress level $(\sigma_1-\sigma_3)/(\sigma_1-\sigma_3)_f$ is less than the maximum previous value.

The bulk modulus, B, is assumed independent of shear stress level $(\sigma_1-\sigma_3)$, but dependent on the confining pressure, $\sigma 3$, as:

$$B = K_b P_a \left(\frac{\sigma_3}{P_a}\right)^m \qquad (3.5)$$

where K_b and m are material parameters, to be determined from the volumetric strain of triaxial drained tests.

A summary of the Duncan-Chang parameters is shown in Table 3.1. The hyperbolic model, however, has some limitations when it is used to simulate the behavior of GRS walls:

(1) Being based on the generalized Hook's law, the model is most suitable for analyzing stress and movements in the elastic range. Whenever the performance of a wall is controlled to a large extent by the properties artificially assigned to soil elements which have "failed", (i.e., $(\sigma_1-\sigma_3)$ is equal to

Table 3.1: Summary of the Hyperbolic Parameters

Parameter	Name	Function
K, K_{ur}	Modulus number	Relates E_i and E_{ur} to σ_3
n	Modulus exponent	
c	Cohesion intercept	Relates $(\sigma_1-\sigma_3)_f$ to σ_3
ϕ, $\Delta\phi$	Friction angle parameters	
R_f	Failure ratio	Relates $(\sigma_1-\sigma_3)_{ult}$ to $(\sigma_1-\sigma_3)_f$
K_b	Bulk modulus number	Value of B/P_a at $\sigma_3 = P_a$
m	Bulk modulus exponent	Change in B/P_a for ten-fold increase in σ_3

or greater than $(\sigma_1-\sigma_3)_f$, the results will no longer be reliable.

(2) The Duncan-Chang model does not account for shear dilatancy. In GRS wall analyses, the values of the lateral deformations, settlements, earth pressures and axial strains of geosynthetic could be affected by shear dilatancy. This effect may be more pronounced for well compacted dense sand under low confining pressures; and

(3) The parameters are not fundamental soil properties, but only curve fitting coefficients that represent the behavior of the soil under the triaxial test conditions. To ensure that the parameters represent the behavior of the soil in the field, the laboratory test conditions must simulate closely the field conditions with regard to those factors. Depending on the loading rate, drainage condition, and backfill/foundation materials, GRS wall construction may be simulated as either drained or undrained conditions. However, the backfill and foundation in the field usually behave between these two extremes, therefore selection of the parameters could be difficult.

Some representative parameters of compacted soils tested under drained conditions are presented in Tables 3.2 and 3.3. These parameters are useful for preliminary analyses.

Table 3.2: Representative Parameter Values of the Modified Hyperbolic Duncan-Chang Soil model (After Duncan et al, 1980)

Unified Soil Classification	RC* Stand. AASHTO	γ_m k/ft^3	ϕ_o deg	$\Delta\phi$ deg	c k/ft^2	K	n	R_f	k_b	m
GW, GP SW, SP	105	0.150	42	9	0	600	0.4	0.7	175	0.2
	100	0.145	39	7	0	450	0.4	0.7	125	0.2
	95	0.140	36	5	0	300	0.4	0.7	75	0.2
	90	0.135	33	3	0	200	0.4	0.7	50	0.2
SM	100	0.135	36	8	0	600	0.25	0.7	450	0.0
	95	0.130	34	6	0	450	0.25	0.7	350	0.0
	90	0.125	32	4	0	300	0.25	0.7	250	0.0
	85	0.120	30	2	0	150	0.25	0.7	150	0.0
SM-SC	100	0.135	33	0	0.5	400	0.6	0.7	200	0.5
	95	0.130	33	0	0.4	200	0.6	0.7	100	0.5
	90	0.125	33	0	0.3	150	0.6	0.7	75	0.5
	85	0.120	33	0	0.2	100	0.6	0.7	50	0.5
CL	100	0.135	30	0	0.4	150	0.45	0.7	140	0.2
	95	0.130	30	0	0.3	120	0.45	0.7	110	0.2
	90	0.125	30	0	0.2	90	0.45	0.7	80	0.2
	85	0.120	30	0	0.1	60	0.45	0.7	50	0.2

* RC = relative compaction, in percent

Table 3.3: Representative Duncan-Chang Drained Parameters for Compacted Soils (Lin, R-S, 1987)

Unified Classification	T-99 Density(%)	γ_t lb/cu in.	ϕ_o deg	$\Delta\phi$ deg	C psi	K	n	R_f
SW	61	0.0523	29	0	0	54	0.85	0.9
	85	0.0729	38	2	0	450	0.35	0.8
	95	0.0815	48	8	0	950	0.60	0.7
ML	49	0.0380	23	0	0	16	0.95	0.55
	85	0.0658	30	0	3	110	0.25	0.85
	95	0.0735	34	0	4	440	0.40	0.95
CL	45	0.0325	23	11	0	16	0.95	0.75
	85	0.0613	18	8	6	50	0.60	0.90
	95	0.0685	15	4	9	120	0.45	1.00

3.3.2.1.3 Extended Anisotropic Cam-clay Model

The original soil model incorporated in DACSAR is the Sekiguchi & Ohta (1977) model. This is an elasto-viscoplastic model which is capable of simulating the anisotropic behavior of clay, including complicated responses to rotation of principal stress directions. This model reduces to the original Cam-clay model (Roscoe, Schofield and Thurairajah, 1963) under the condition of isotropic initial stress state. Therefore, the Sekiguchi and Ohta model may be considered an extended anisotropic Cam-clay model, or a generalized Cam-clay model, with the original Cam-clay being a special case under isotropic conditions.

Detailed derivation of the soil model has been given by Sekiguchi & Ohta (1977), Ohta & Sekiguchi (1979) and Iizuka & Ohta (1987). A brief summary of its main features is presented herein.

Inviscid Formulation

Rather comprehensive experimental studies of volumetric-deformation characteristics of clay have been carried out at Kyoto University, Japan. On the basis of these studies, Ohta, Sekiguchi and their co-workers proposed the anisotropic Cam-clay model to account for consolidation induced anisotropy of clay. The constitutive equation proposed by Sekiguchi and Ohta was derived based on the plasticity theory presented by Drucker, Gibson and Henkel (1957) and was

characterized by furnishing both the plastic volumetric strain hardening and the associated flow rules. The yield condition is associated with plastic volumetric strain as the hardening parameter in the following form:

$$f(\sigma_{ij}) - F(v^p) = 0 \qquad (3.6)$$

where f is the yield function, F is the hardening functions, σ_{ij} is effective stress tensor and v^p is the plastic volumetric strain.

The critical state lines and yield loci for normally consolidated soils (wetter than critical) and over-consolidated soils (drier than critical) are shown in Figure 3.1.a and 3.1.b, respectively. These loci are similar to those obtained from the Cam-Clay model, except that anisotropic consolidation has been taken into account, and the stress paths start from the normal consolidation lines.

The Sekiguchi-Ohta model assumes that the volume change of a soil has two components, volumetric strain due to consolidation (v_c) and that due to dilatancy (v_d), as shown in Figure 3.2. Dilatancy is defined as the volume change under a loading system which keeps the effective mean principal stress σ_m, or p, constant (Ohta, Yoshitani & Hatta, 1975). In other words, dilatancy is induced by a change of deviatoric stress.

Adopting the associated flow rule, it follows that:

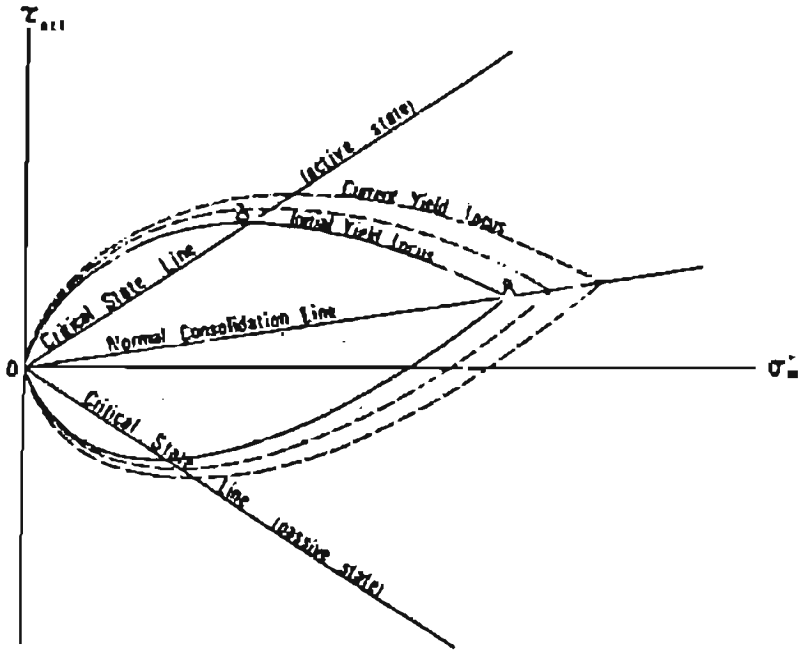

(a) Wetter Than Critical (Work-Hardening)

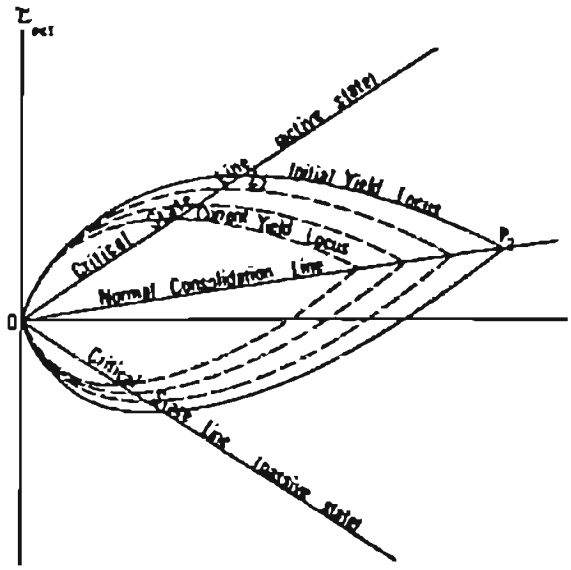

(b) Drier than Critical (Work-Softing)

Figure 3.1: Critical state line and yield loci for Sekiguchi-Ohta model (After Sekiguchi & Ohta, 1977)

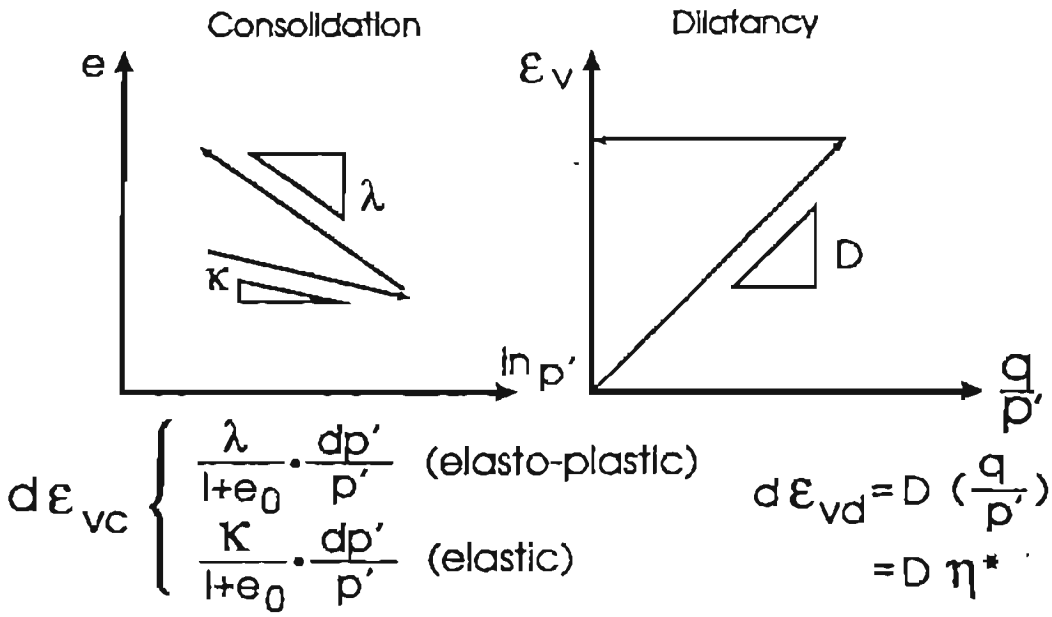

Figure 3.2: Volume Change of Soils Due to Consolidation and Dilatancy, Sekiguchi-Ohta Model (After Iizuka, 1987)

$$\delta\varepsilon^{p}_{ij} = \psi \frac{\partial f}{\partial \sigma_{ij}} \tag{3.7}$$

where $\delta\varepsilon^{p}_{ij}$ are the components of the plastic strain increment tensor, ψ is the proportional constant, and σ_{ij} are the components of effective stress tensor. The magnitude of plastic strain increment can be obtained from Equation (3.7), and its direction can be determined by Figure 3.3.

Finally, the total strain increment is the sum of the plastic and elastic components, that is:

$$\delta\varepsilon_{ij} = \delta\varepsilon^{p}_{ij} + \delta\varepsilon^{e}_{ij} \tag{3.8}$$

Viscid Formulation

In the viscid formulation, Sekiguchi and Ohta (1977) added the volume change due to creep to the inviscid volume change of consolidation and dilatancy.

Sekiguchi and Ohta regarded the potential function F as the viscoplastic potential. Derivatives of F with respect to any effective stress component defined the directions of viscoplastic deformation. It was further assumed that:

$$\dot{\varepsilon}^{P}_{ij} = \varphi \frac{\partial F}{\partial \sigma_{ij}} \tag{3.9}$$

where $\dot{\varepsilon}^{P}_{ij}$ are the components of the viscoplastic strain rate tensor and φ is the viscoplastic proportional constant.

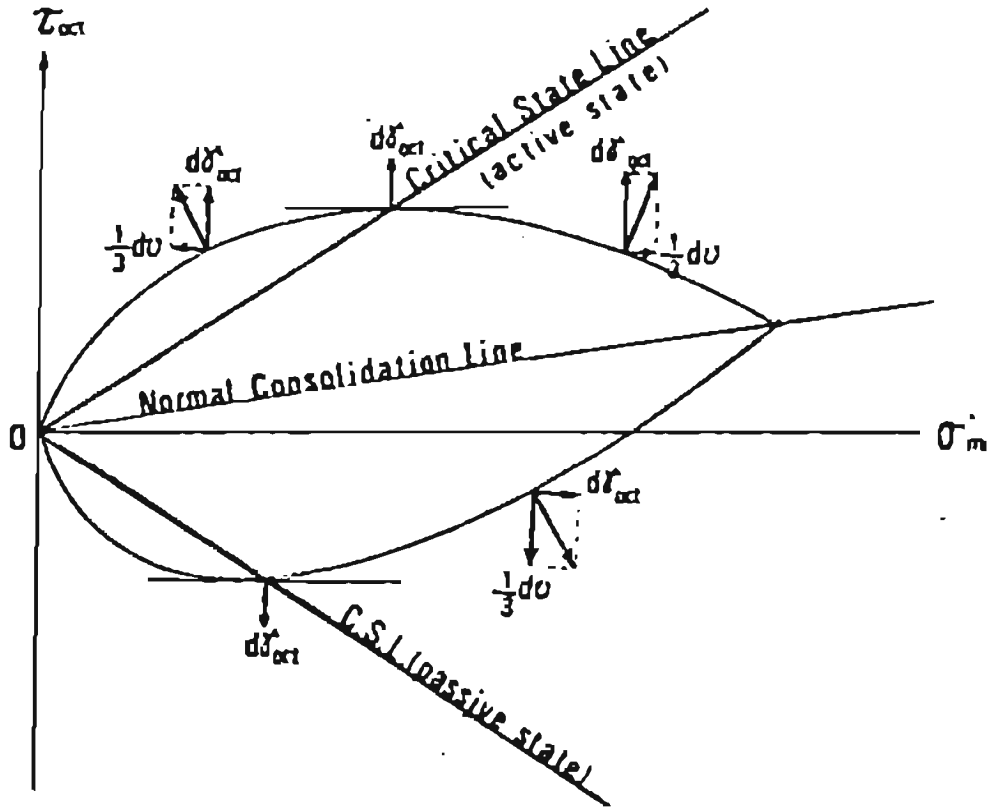

Figure 3.3: Associated Flow Rule for the Sekiguchi-Ohta Model (After Sekiguchi & Ohta, 1977)

By using this rheological model, creep (i.e., under a constant stress) and stress relaxation (i.e., under a constant deformation) can be incorporated in the FEM analyses. The stress paths for a soil subjected to creep and stress relaxation in a p (mean effective stress) verse q (deviatoric stress) diagram are shown in Figure 3.4.

By incorporating all the features mentioned above (i.e., elasto-plasticity, dilatancy and rheology), Sekiguchi and Ohta developed this rather comprehensive model for normally consolidated or lightly over-consolidated clay. However, the Sekiguchi and Ohta model has the following limitations:

(1) In volume change calculation, the Sekiguchi-Ohta model considers compression, but not dilation due to shearing. Therefore, prediction of the volumetric strain and/or excess porewater pressure of stiff clay and dense sand is probably inaccurate, especially when the confining pressure is low. Similar to other Cam-clay type soil models, this model was derived for the normally consolidated clay, and the effective stress principle was employed. The applicability of this model to simulate the behavior of compacted clay or granular soil is therefore questionable; and

(2) In the Sekiguchi-Ohta model, the creep formulation uses the simple empirical "coefficient of secondary compression" approach, instead of a more

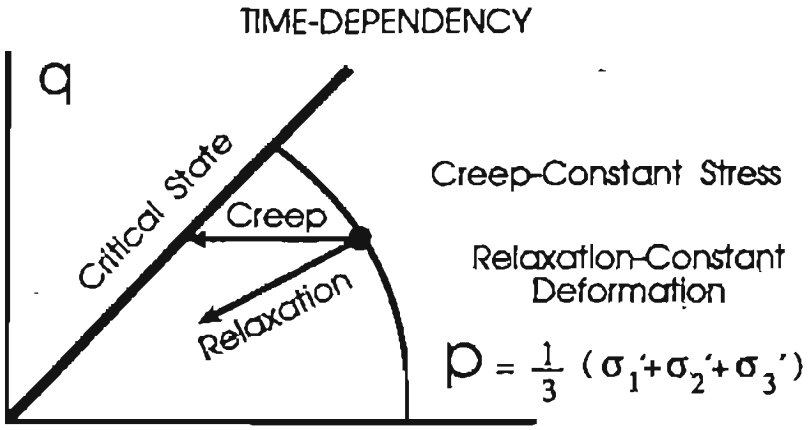

Figure 3.4: Stress Paths of a Soil in Creep and Stress Relaxation Conditions (After Iizuka, 1987)

rigorous rheological model such as Gibson and Lo (1961), etc. There are some limitations of such an empirical approach. For example, creep is defined to begin at the end of the primary consolidation, but in reality creep would start at the moment when the load is applied. Determination of the end of primary consolidation is also a difficult task. In addition, the assumption that the associated flow rule applies to the viscoplastic model is made without theoretical or experimental support.

Determination of Soil Parameters

Compared with many other constitutive models, the Cam-clay type of models use soil parameters which are clearly defined in terms of their physical significance and most closely related to the soil parameters that have been used in classical soil mechanics.

Detailed description of the determination of the Sekiguchi-Ohta model has been given by Iizuka & Ohta (1987). A brief summary is presented herein.

The soil parameters needed in the inviscid part of the Sekiguchi and Ohta model are λ, κ, e_o, and D. Parameters λ and κ are the compression index and the swelling index, respectively, e_o is void ratio at the preconsolidated state, and D is the coefficient of dilatancy defined by Shibata (1963). For simplicity, the irreversibly ratio Λ and the critical state parameter M are chosen as the soil parameters in DACSAR

rather than the parameters λ, κ, e_o. They are related by:

$$M = \frac{\lambda - \kappa}{D(1+e_o)} \qquad (3.10)$$

and

$$\Lambda = 1 - \frac{\kappa}{\lambda} \qquad (3.11)$$

The coefficient of secondary compression α and the initial volumetric strain rate $\dot{v}_0$ are needed in modelling the viscid characteristics of the material. The initial volumetric strain rate can be determined by $\dot{v}_0 = \frac{\alpha}{t_c}$, where t_c is the time required for the completion of the primary consolidation. The input parameters and laboratory tests to be determined are summarized in Table 3.4.

The parameters can be estimated by the physical properties of a soil, such as PI, Gs (Iizuka & Ohta, 1987). Wroth and Wood (1978) also indicated that the Cam-clay parameters can be estimated from the plasticity index. However, these simple empirical relationships are intended for preliminary study only. For detailed analyses, the parameters should be obtained from triaxial and consolidation tests.

3.3.2.2. Geosynthetics

The geosynthetic reinforcement can be simulated by a series of bar (truss) elements since geosynthetics, in general, exhibit only axial (tensile) and shear

Table 3.4 Summary of Soil Parameters for DACSAR (Iizuka & Ohta, 1987)

	analysis parameter	main laboratory test
material properties	λ irreversibility ratio	triaxial consolidation test
	M critical state parameter	triaxial CU test
	D coefficient of dilatancy	triaxial CD (p'=const.)test
	ν' effective poisson ratio	triaxial CU test
	α coefficient of secondary compression	triaxial consolidation test
	$\dot{v}_0$ initial volumetric strain rate	triaxial consolidation test
preconsol. stress	σ'_{V0} preconsolidation vertical pressure	oedometer test
	K_0 coefficient of earth presure at rest	triaxial K -consolidation test
initial stress	σ'_{VI} effective overburden pressure	unit weight test
	K_I coefficient of in-situ earth pressure at rest	triaxial K -swelling test
	k coefficient of permeability	permeability test

resistance and lack bending resistance. In the past, finite element analysis of reinforced soil structures typically adopted a linear elastic model for the bar elements (Seed & Duncan, 1983; Collins, 1986; Adib, 1988). This idealization does not apply to some extensible geosynthetics, such as nonwoven geotextiles, whose load-deformation behavior is nonlinear, inelastic and stress dependent.

For most geosynthetics, the load-deformation relationship of geosynthetics can be described by a hyperbola:

$$E = E_i \left(1 - \frac{T}{T_{ult}} \right)^2 \qquad (3.12)$$

where E_i = Initial tensile stiffness, and

T_{ult} = Ultimate tensile force per unit width.

Both E_i and T_{ult} can be obtained by the transformed linear relationship:

$$\frac{\varepsilon}{T} = \frac{1}{E_i} + \frac{\varepsilon}{T_{ult}} \qquad (3.13)$$

It has been recognized that some geosynthetics have different load-elongation properties when they are tested in isolation (air) and in the confinement of soil (McGown, Andrawes & Kabir, 1982; El-Fermaoui and Nowatzki, 1982; ; Siel, Wu and Chou, 1987; Wu, 1991; Ling, Wu and Tatsuoka, 1992). Both T_{ult} and E_i increase with increasing normal stress. To account for the

confining stress effect under the service load, a simple linear relationship can be assumed (Lin & Tatsouka, 1992):

$$E_i = E_{i,o} + \sigma_n \cdot S_1 \qquad (3.14)$$

and

$$T_{ult} = T_{ult,o} + \sigma_n \cdot S_2 \qquad (3.15)$$

where $E_{i,o}$ = initial stiffness in unconfined condition

$T_{ult,o}$ = ultimate load in unconfined condition

S_1 = increase rate of E_i with respect to the confining pressure, and

S_2 = increase rate of T_{ult} with respect to the confining pressure.

The author has implemented Equations 3.12, 3.14 and 3.15 in the bar element formulation in DACSAR, to account for the nonlinear load-elongation relationship and the stress dependent effect of the geosynthetics.

Determination of Geosynthetic Parameters

The ASTM recommends that a wide-width strip method (ASTM D-4595) be used to determine the in-air load-extension properties of a geosynthetic. A minimum aspect ratio (width/length) of two is required, but a larger aspect ratio is preferred, to avoid necking

which results in non-uniform stress distribution. The geosynthetic specimens should be strained at a constant rate, such as 2% per minute until failure occurs.

Several confined test methods and apparatuses have been developed and used (McGown, Andrawes & Kabir, 1982; El-Fermaoui & Nowatzki 1982; Christopher, Holtz and Bell, 1986; Leshchinsky & Field, 1987; Juran & Christopher, 1989). Wu (1991) evaluated these existing test methods and pointed out that all the methods suffer from the following problems:

(1) They are not "element" tests and the measured properties can be significantly affected by boundary effects.

(2) Most tests hold the confining soil stationary while the geosynthetic deforms, simulating an unrealistic condition in which soil-geosynthetic slippage "must" occur in order for the geosynthetic to deform. In other words, the frictional resistance between the geosynthetic and the stationary confining soil has to be overcome before tensile strain in the geosynthetic can be developed. As a result, the resistance to the applied load is a combination of the friction and stiffness of the geosynthetic, and it is very difficult to de-couple the two effects; and

(3) The measured load-extension properties are on the "unsafe side" in design computation.

To overcome these drawbacks, Wu (1991) and Ling, Wu and Tatsuoka (1992) developed a test method that can be used to measure the inherent load-elongation behavior of geosynthetics under in-membrane and in-soil conditions. For the in-membrane test, the geosynthetic specimen is confined by a rubber membrane and is subjected to a confining pressure through suction or by applying a normal stress (see Figure 3.5). When the geosynthetic specimen is being tested, both the membrane and geosynthetic deform the same amount and no relative displacement developed between them. For the in-soil test, the confining pressure was applied to the geosynthetic specimen through two thin soil "cakes". It was found that the in-membrane test yielded the same effect of stress confinement as did the in-soil test. This suggests that the in-membrane test, which is easier to perform, is a superior alternative for determining the load-extension behavior of a geosynthetic under stress-confined conditions.

3.3.2.3. Facing

The behavior of wall facing can be simulated in DACSAR by a series of beam elements with bending and axial resistances. Various facings (see Figure 3.6) have been used for GRS wall construction, and their FEM simulations are described as follows:

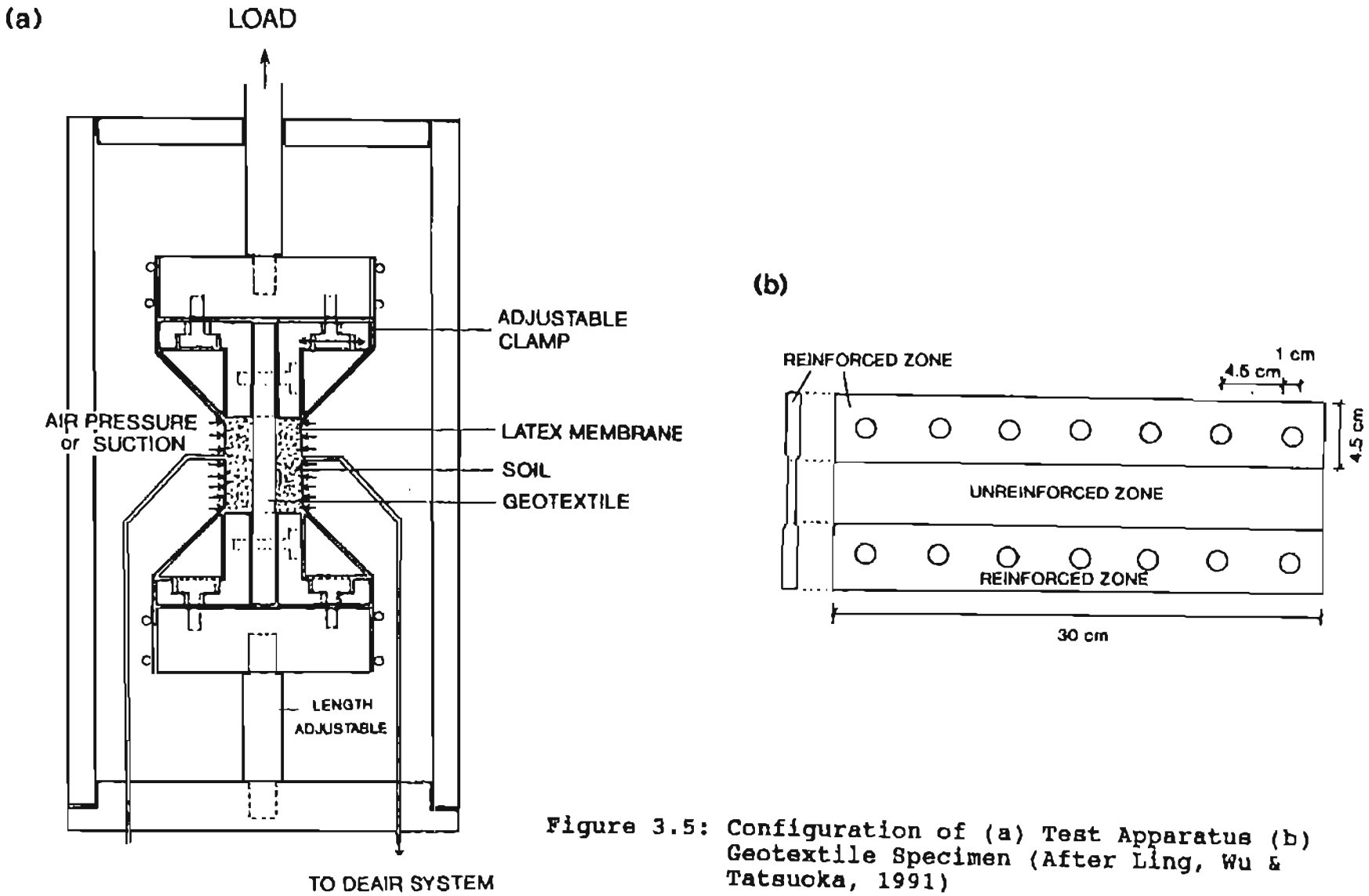

Figure 3.5: Configuration of (a) Test Apparatus (b) Geotextile Specimen (After Ling, Wu & Tatsuoka, 1991)

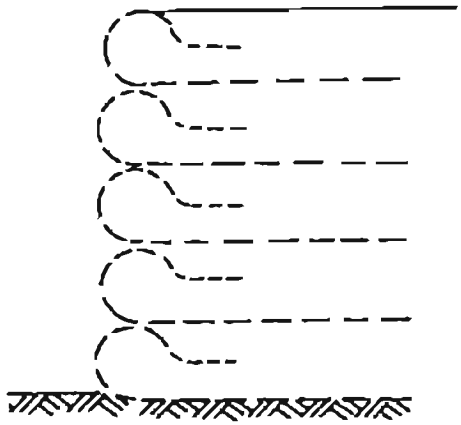

(a) Wrap Around Facing

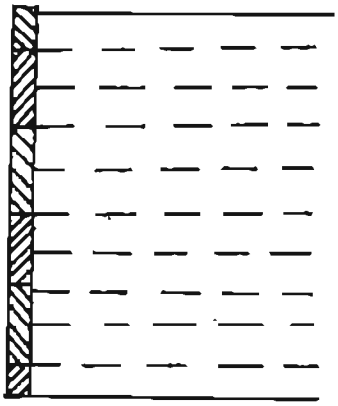

(b) Timber Facing

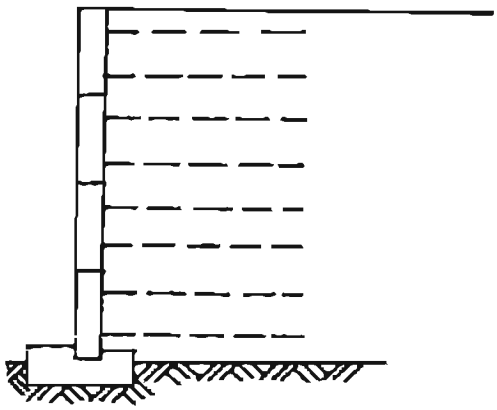

(c) Articulated Concrete Panels

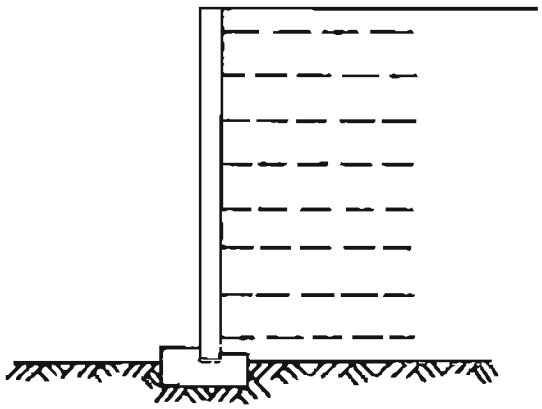

(d) Continuous Concrete Panels

Figure 3.6: Types of Wall Facings

(1) Geosynthetic wrap-around: with negligible bending resistance, and the geosynthetic can be simulated by bar elements;

(2) Timber/plywood system: with moderate local and global bending resistances;

(3) Articulated precast panels (modular blocks): with high local bending resistance but little global bending resistance; and

(4) Continuous cast-in-place or precast panels: with high local and global bending resistances.

The stiffness (rigidity) of a facing element generally can be determined by a simple flexural and tension/compression test. For articulated and timber/plywood facings, however, determination of the rigidity can be difficult. Collin (1986) employed a trial and error method to determine the distance between the hinges in FEM simulation of the articulated facing for a Reinforced Earth Wall. A series of beam lengths were assumed, and the FEM simulations were compared with field measurements before an equivalent beam length for an articulated panel was determined. Another example is the Denver Test Walls. The timber facing blocks were inter-connected by plywood boards in a manner that the facing was "semi-continuous". The determination of facing stiffness, using the continuous beam theory, is at best an approximation.

3.3.2.4. Soil-Reinforcement Interface

The interface (joint) element used in DACSAR is similar to the one proposed by Goodman, Taylor & Brekke (1968). Two linear spring constants, K_s (shear stiffness) and K_n (normal stiffness), are used to simulate the interface behavior on normal and tangent directions. The shear deformation is assumed to be linear with the shear stress until the bond strength of the interface is reached, beyond which slip is said to have occurred. The bond strength is assumed to be governed by the Mohr-Coulomb criterion.

The interface elements are not used in this research study because:

(1) The interface model has a number of serious theoretical problems (Wu, 1980). For example, the value of shear stiffness is affected by the size of sample tested. Unless the size of the sample tested is equal to or close to the size of the finite element meshes at the interface, the stiffness obtained from the laboratory could be drastically misleading; and

(2) In this research emphasis is placed on studying the performance of GRS walls under service loads. It is believed that slippage between the geosynthetic and adjacent soils is unlikely to occur under service loads (less than 15 psi surcharge).

3.3.3 Other Features

3.3.3.1 Consolidation (Coupling) Analysis

The consolidation (coupling) analysis technique originally formulated by Akai and Tamura (1976) was incorporated in DACSAR. In this method the water pressure is defined at the center of each element. Time is tracked by a backward difference scheme to ensure better numerical stability of the computations.

3.3.3.2 Nonlinear Solution Technique

In DACSAR, material nonlinearity is accommodated by an incremental procedure with a tangential stiffness approach. The size of the load increments governs the accuracy with which equilibrium between the equivalent and applied nodal force is satisfied at the end of each load increment. DACSAR allows each load increment to be divided into several steps to achieve better accuracy. The number of load increments has to be selected considering a balance of the accuracy and the cost. In this study the load increment was limited to 0.3 psi.

3.4. An Example Application of DACSAR: Analysis of a Reinforced Earth Wall Constructed Over a Soft Clay Foundation

DACSAR has been used to predict or simulate the behavior of embankments over soft clay foundations (Sekiguchi,1991; Ohta, Mochinaga & Kurihara, 1980; Iizuka, 1987). These analyses have been successful, especially for porewater pressure prediction (Iizuka, 1987).

This section demonstrates using DACSAR for simulating the behavior of a soft clay foundation under the load of a 40-ft high Reinforced Earth wall. The author and his colleagues have tested the external stability of this wall, using conventional stability analysis methods (Chou & Su, 1990). Settlement and lateral deformation of the soft clay, as well as the shear strength increase due to staged construction, have been analyzed by DACSAR (Chou, Chao, Chang & Ni, 1991).

3.4.1 Description of the Case History

3.4.1.1 Introduction

The Colorado Department of Transportation (CDOT) decided to construct a grade separation structure over the Union Pacific Railroad tracks on State Highway 385 near Julesburg, Colorado (Figure 3.7). To allow for future widening of the railroad and to provide sufficient clearance from the tracks, a Reinforced Earth (RE) wall was constructed. The wall was approximately 1000 feet long, with heights ranging from 5 feet at the two ends to 40 feet near the center, as depicted in Figure 3.8.

The Julesburg area is located in the lower South Platte River Valley. The typical subsurface at the proposed location of the wall consists of soft silty clay overlying loose to dense sand and gravel. Bedrock was encountered at depths ranging from 28 to 70 feet.

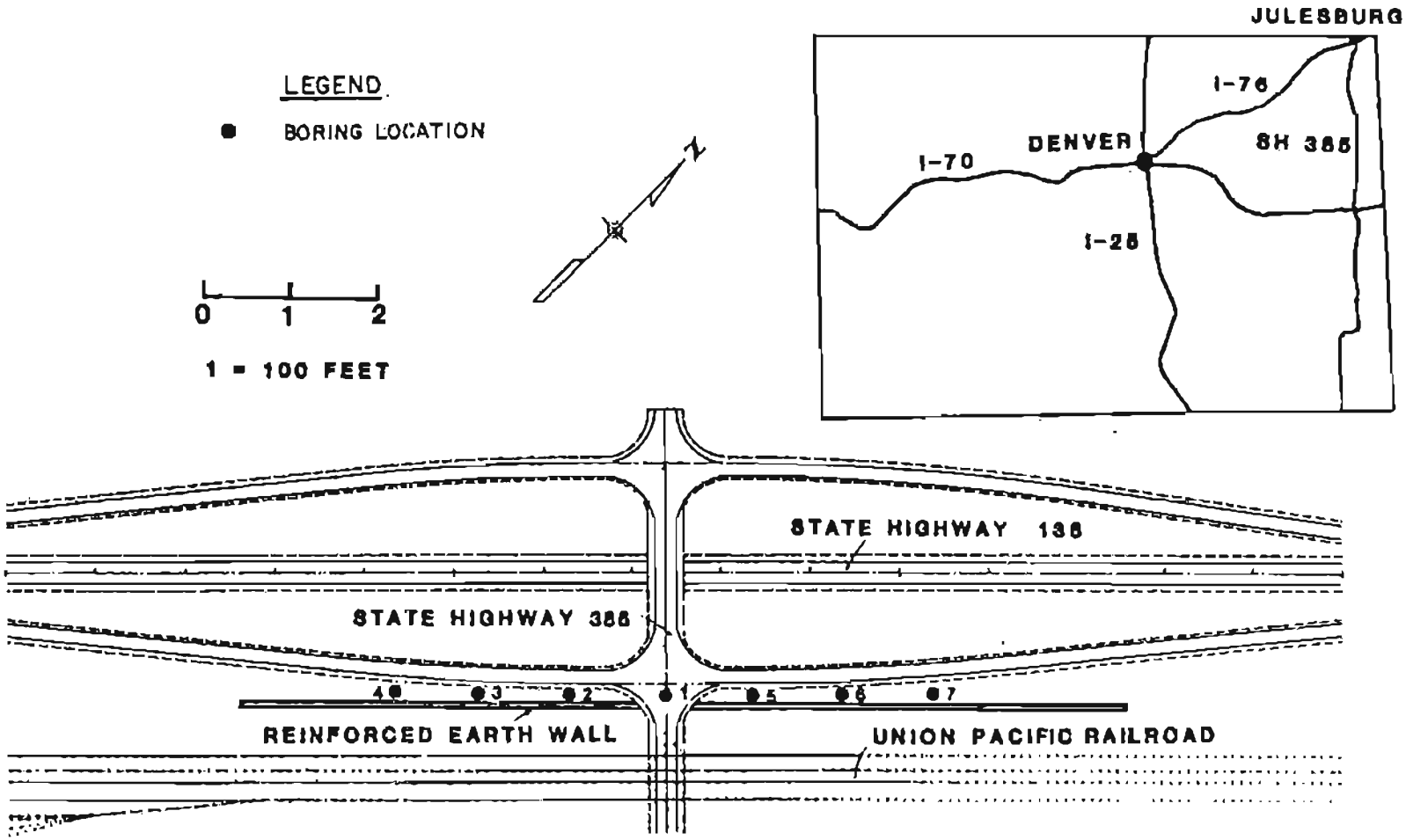

Figure 3.7: Site Location of Julesburg Reinforced Earth Wall

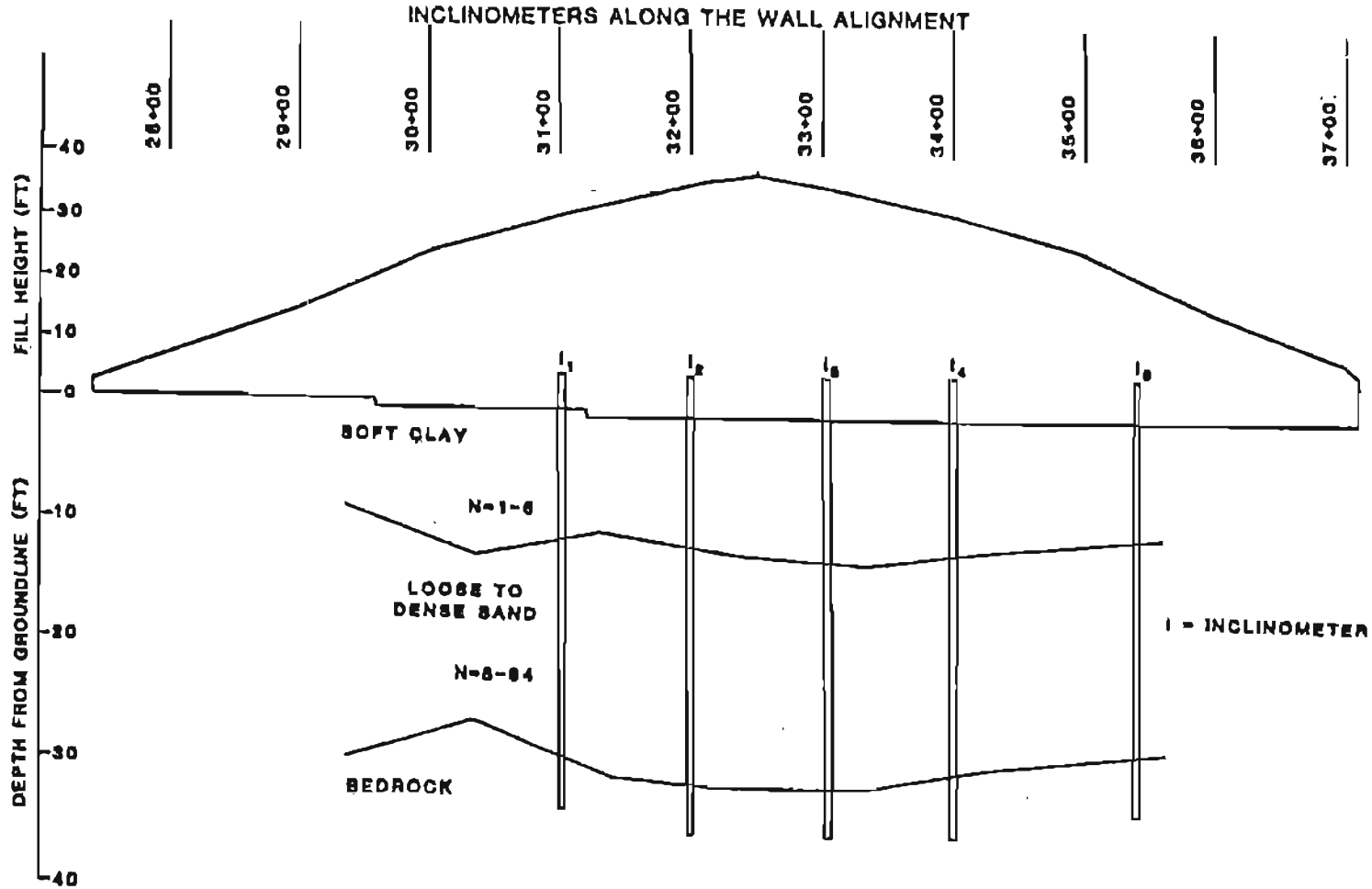

Figure 3.8: Wall Profile and Typical Subsurface Strata of the Julesburg wall

The water table was approximately 4 feet below the ground surface; pumping of the ground surface occurred when construction vehicles passed. The subsoils in the area comprised four strata, as shown in Table 3.5. Figure 3.9 illustrates the typical subsurface strata and a cross section of the wall.

Laboratory tests were conducted primarily to study the engineering characteristics of the soft clay stratum. The tests included classification, vane shear, direct shear, unconfined compression, triaxial, and 1-D consolidation. The silty clay was classified as CL by the Unified Soil Classification and as A-7-6 by the AASHTO Classification System. The typical soil properties, as obtained from the laboratory tests, are shown in Table 3.6.

The original geotechnical investigation was performed by a local consulting firm. The author reviewed the design and decided to perform an independent study on the external stability of the wall.

3.4.1.2 Stability Analyses

An MSE wall must satisfy the requirements of both external and internal stability. After reviewing the design plan, the internal stability of the wall (designed by the manufacturer) was judged satisfactory. However, the external stability was considered questionable. Several possible failure modes for

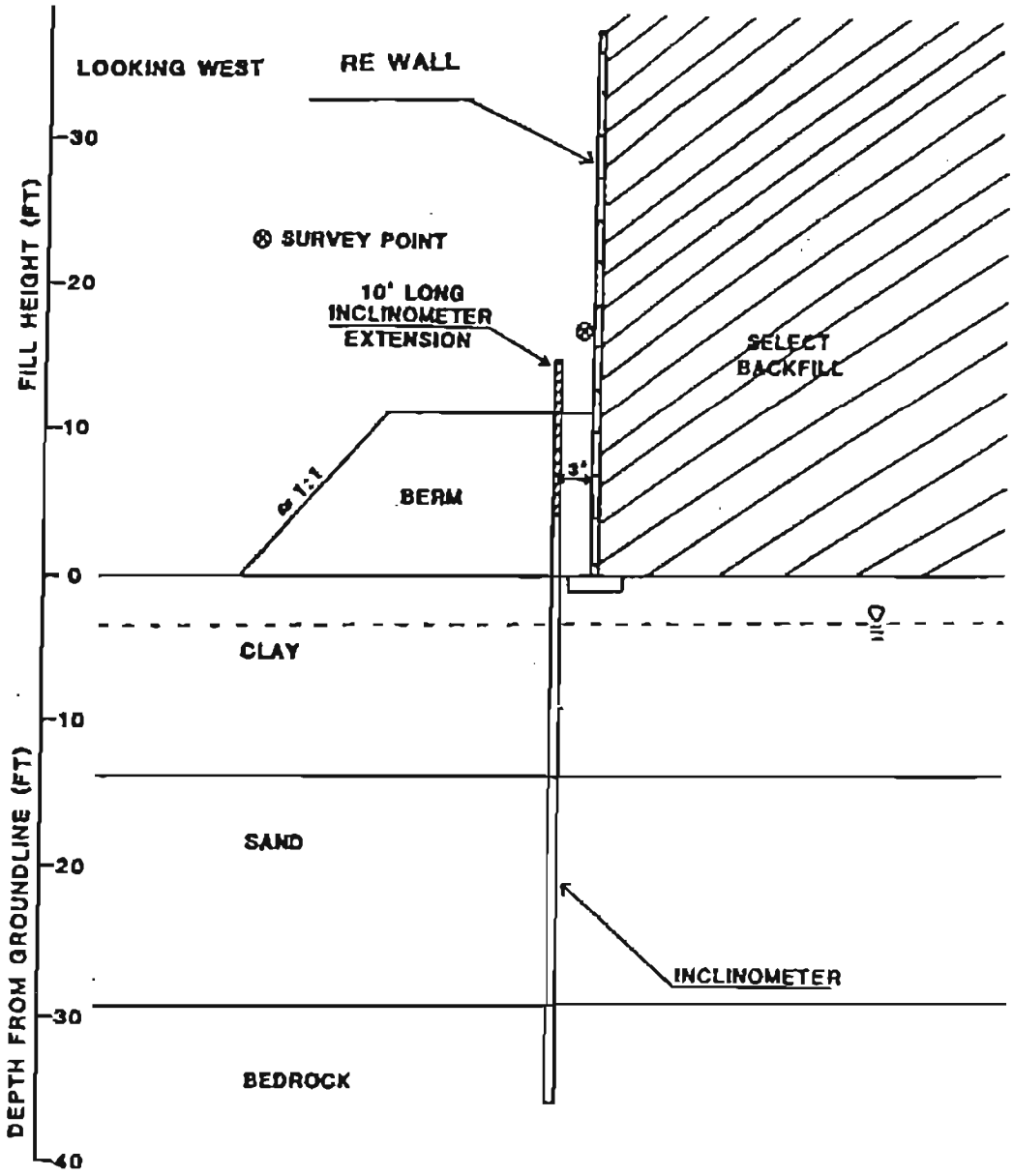

Figure 3.9: Typical Cross-Section of Julesburg Wall

Table 3.5: Subsoil Properties of the Julesburg Wall Site

Depth (ft)	Soil Description	N (blows per ft)
0 - 4	CLAY, silty, medium stiff (crust)	3-6
4 - 14	CLAY, silty, very soft	1-4
14 - 21	SAND, loose	5-9
21 - 31	SAND, medium dense to dense	20-64

Table 3.6: Properties of Subsoils, Julesburg Wall Project

Depth (ft)	Soil Description	W(%)	LL	PI	S_u[1](psf)	ϕ[2](deg.)
4	Silty Clay (Crust)	21.0	26	10	480-1000 422 (Avg.)	-
4 - 14	Soft Silty Clay	39.6	45	23	40-790 415 (Avg.)	-
14 - 21	Loose Sand	12.5	-	-	-	35
21 - 31	Dense Sand	10.5	-	-	-	40

1 - Obtained from vane shear tests
2 - Obtained from direct shear tests

external stability, evaluated by assuming the reinforced earth mass as a rigid composite, were analyzed; the calculated safety factors are shown in Table 3.7. The average shear strength parameters shown in Table 3.6 were used in these analyses.

The overall slope stability (see Figure 3.10) and bearing capacity were of major concern. Based on the average undrained shear strength of 415 psf for the soft clay, a low safety factor of 0.86 for bearing capacity was obtained. The Junbu, Ordinary, and Modified Bishop methods were used in the slope stability analyses, with calculated safety factors ranging from 0.85 to 1.08. At the time of design, the source of the embankment fill material had not been finalized. Calculations were based on the assumption that the embankment fill was to be borrowed from a nearby pit. Possible borrow materials from nearby pits ranged from silty sand to silty clay, with strength parameters shown in Table 3.8.

An embankment on a soft foundation may fail progressively because of differences in the stress-strain characteristics between the embankment and foundation. The strength of both the embankment and foundation material may be reduced to account for the progressive failure, using reduction factors obtained from the FEM analysis performed by Chirapuntu and Duncan (1975). A reduction factor (Re) of 0.67 was

Table 3.7: Calculated Safety Factors Based on Various Failure Modes

Failure Mode	Safety Factor Calculated	Required
Bearing capacity	0.86	2.0
Overturning	4.34	1.5
Sliding	1.30	1.5
Slope stability (at the end of construction and in an undrained condition)		
- Janbu Method	0.93	1.25-1.50
- Ordinary Method	0.85	1.25-1.50
- Modified Bishop Method	1.08	1.25-1.50

Table 3.8: Overall Slope Stability Analyses Using Different Embankment Fills

Borrow Soil	Embankment Soil Strength Properties				F. S.
No.	C(psf)	ϕ(deg.)	C^1(psf)	ϕ^1(deg.)	(Janbu)
1	150	39	100	28	0.934
2	300	35	200	25	0.961
3	450	28	300	20	0.988
4	750	22	500	15	1.106
5	1500	14	1000	9	1.401

1 - Values After Duncan's Strength Reduction

employed, which reduced the cohesion (c) and internal friction (tanϕ) of the soils by one third. The safety factors calculated by the Janbu method, based on various borrow site soil properties, are also listed in Table 3.8. Using the reduction factor, the safety factors against overall slope failure, except for soil No. 5, were all close to 1.0.

Based on the above analyses, borrow soil No. 5 was chosen. The material was a silty clay, with AASHTO classification A-7-6(11).

3.4.1.3 Remedial Measures

The following measures were taken to allow safe construction of the wall:

(1) Use of cohesive backfill for embankment: The cohesion would give a significant increase of the safety factor against slope failure. Since the quantity of this cohesive soil was limited, it was sandwiched between the granular backfill in the middle portion of the embankment (see Figure 3.10).

It should be noted that although cohesive backfill for embankment construction is not recommended in other areas due to possible water infiltration and long-term deformation, cohesive backfill has been successfully used in many CDOT projects for more than 20 years. This is because Colorado is located in a semi-arid area.

(2) Construction of a 10-Foot High Temporary Berm: This option was considered a cost-effective measure to increase the safety factor for both slope stability and bearing capacity. In addition, stability against sliding also would be improved.

(3) Staged Construction: The wall was constructed in four phases, each 10 feet in height, with at least a one-month waiting period between each phase. Construction time of the entire project (including several other bridges and embankments) would take about one year to complete, which made this option feasible.

(4) Instrumentation: A monitoring system was employed to measure the behavior of the wall and foundation soils during and after construction. Instruments used included inclinometers, piezometers, and survey points.

3.4.1.4 Staged Construction

During construction of the wall, the undrained shear strength (S_u) increased due to consolidation. The gain of undrained shear strength, dS_u, was calculated by the following equation (Chou, et. al. 1980):

$$dS_u = m \times I \times d\sigma_c \times U\% \qquad (3.16)$$

where m = Slope of S_u vs σ_c curve

I = Influence factor of loading

$d\sigma_c$ = Increase in mean value of consolidation pressure; and

U (%) = Percentage of consolidation.

Using the Mohr-Coulomb failure envelope obtained from the triaxial CU tests, as shown in Figure 3.11, one can establish the relationship between the undrained shear strength and the consolidation pressure. By moving the points representing the stress on the failure plane horizontally to the corresponding σ_c values (i.e. A to A' and B to B'), the slope (m) between σ_c and S_u can be obtained.

Total shear strength gain with resulting improvement in safety factors on bearing capacity are presented in Table 3.9. This table also shows the shear strength gain (dSu) at each 10 foot increment of staged construction. From Table 3.9, it can be seen that the safety factors of bearing capacity, during each stage of construction, increased significantly when the strength increase was taken into account.

Table 3.10 shows the improvement of stability safety factor for each potential failure when all of the remedial measures were employed.

3.4.1.5 Monitoring of Wall Performance

During construction, the behavior of the wall was monitored by instrumentation. The instruments used for the monitoring program are listed in Table 3.11.

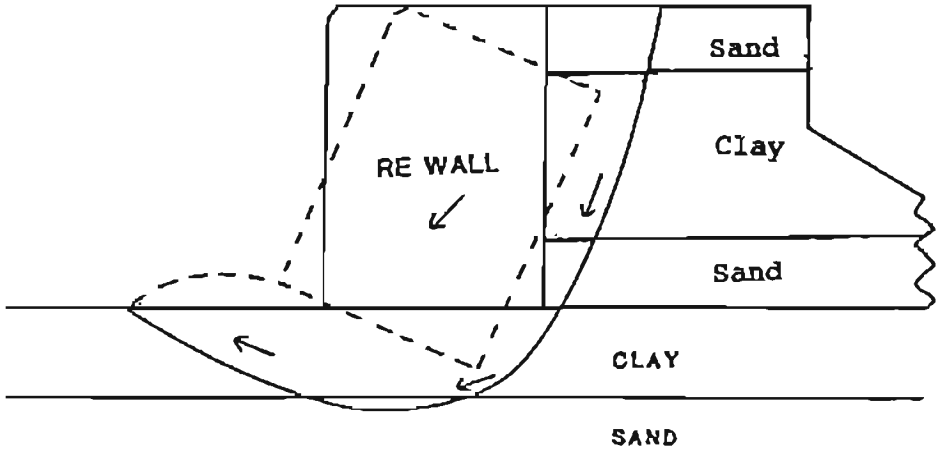

Figure 3.10: Possible Slope Stability Failure Mode

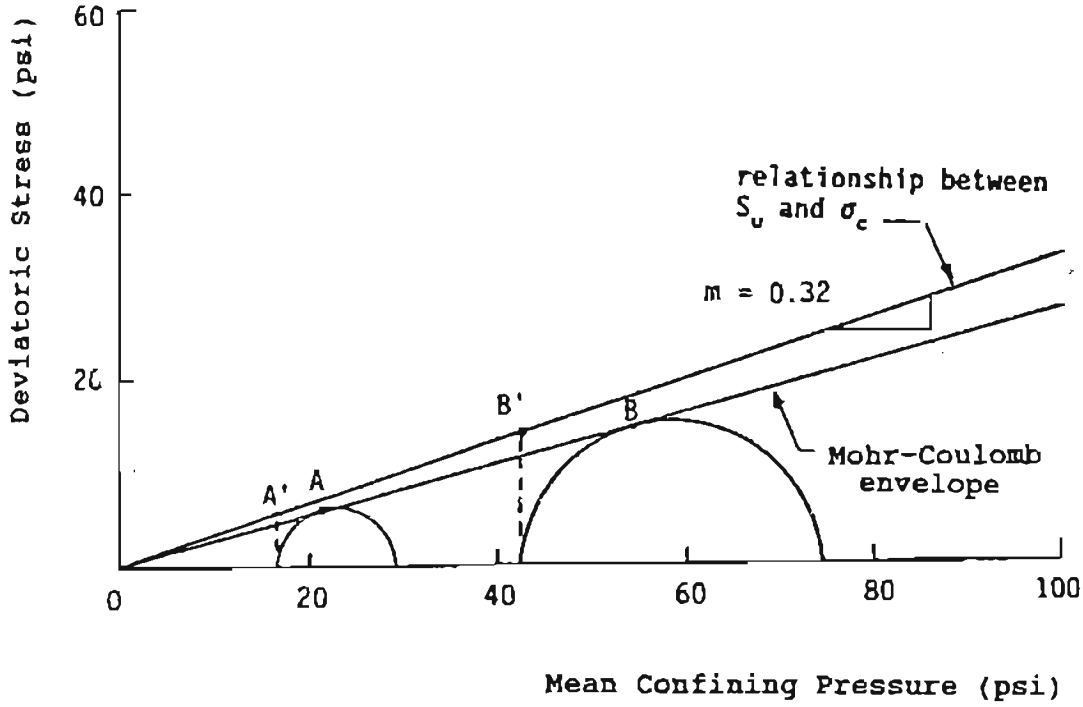

Figure 3.11: Undrained Shear Strength Increase with Consolidation from a CAU Test

Table 3.9: Comparison of RE Wall Bearing Capacity With and Without Staged Construction

Fill Ht (ft)	dS_u (psf)	S_u+dS_u (psf)	Safety Factor W/O Staged Const.	Safety Factor W/ Staged Const.
10	0	415	1.78	1.78
20	180	595	1.05	1.27
30	205	800	0.89	1.14
40	230	1030	0.86	1.10
Long term	409	1439	--	1.54

Table 3.10: Comparison of Safety Factors Before and After the Remedial Measures

Failure Mode	Safety Factor Before	Safety Factor After
Bearing capacity	0.86	1.10
Overturning	4.34	8.88
Sliding	1.30	7.09
Slope stability	0.93	1.40

Table 3.11: Instrumentation Used for the Julesburg Wall

Item	Number Installed	Function
Piezometer	9	Monitor excess porewater in soft clay during staged construction
Inclinometer	5	Monitor horizontal deformation of Foundation soils
Liquid Settlement Transducer	2	Monitor settlement at the base of RE wall
Survey Point	8	Monitor deformation of RE wall panels
Stand Pipe	2	Monitor local ground water elevation

The monitoring system was designed to detect early signs of potential wall failure. In the event of a potential failure, the protective berm was to be immediately increased in height. As it turned out, the wall was constructed on schedule to a maximum height of 40 feet and the instrumentation functioned satisfactorily.

3.4.2 FEM Analysis

3.4.2.1 Introduction

The effectiveness of using staged construction for increasing wall stability was investigated by FEM using DACSAR. The behavior of the soft clay foundation was simulated by the Sekiguchi-Ohta model. The foundation sand, crust, embankment fill and berm were simulated by the Duncan-Chang hyperbolic model.

The composite approach (see Section 2.3.3) was used for simulating the RE wall (including granular backfill, reinforcement and facing). The composite material was modeled by a linearly elastic model. Since the rigidity of the RE wall may be several orders higher than that of the foundation soil, it is believed that using the composite approach is appropriate. The RE wall mass was assumed to have a very large stiffness.

The soil parameters of the Sekiguchi-Ohta and Duncan-Chang models used in the analyses are shown in Tables 3.12.a and 3.12.b, respectively. The parameters for the soft clay

Table 3.12.a: Soil Parameters of Soft Clay Foundation Used in the FE Analysis, Sekiguchi-Ohta Model

D	Coefficient of dilatancy	0.022
Λ	Irreversibility Ratio	0.643
M	Critical state parameter	1.370
ν'	Effective Poisson ratio	0.3
k_x	Coefficient of permeability of x direction (ft/day)	0.003
k_y	Coefficient of permeability of y direction (ft/day)	0.003
σ'_{vo}	Preconsolidation pressure (psf)	1720
K_o	Coefficient of earth pressure at rest	0.428
α	Coefficient of secondary compression	0.00124
$\dot{v}_o$	Initial volumetric strain rate (day^{-1})	0.0000036
λ	Compression index in the e and $\ln(p'/p'_o)$ relationship	0.0826
e_o	void ratio corresponding with σ'_{vo}	0.765
λ_k	Gradient of e and ln(k) relationship	0.0826

Table 3.12.b: Soil Parameters of Embankment, Berm, Sandy Foundation and Crust for FE Analyses, Duncan-Chang Model

Material property description	* 1	* 2	* 3	* 4	* 5
Unit weight (pcf)	120	115	110	120	100
Young's modulus number, k	1100	410	200	326	250
Young's modulus exponent, n	0.36	0.69	0.00	0.25	0.00
Failure ratio, R_f	0.85	0.90	0.80	0.90	0.80
Bulk modulus number, K_b	900	260	100	150	130
Bulk modulus exponent, m	0.00	0.15	0.00	0.30	0.00
Cohesion, C (psf)	0	0	400	1900	500
Angle of internal friction (deg.)	40	35	14	7	14
At-rest lateral earth pressure coeff., K_o	0.50	0.50	0.50	0.80	0.50

* - 1 - Sand, medium dense to dense
  - 2 - Sand, loose
  - 3 - Clay, Silty, medium stiff (crust)
  - 4 - Embankment material (clay)
  - 5 - Berm material (random)

were determined directly from the triaxial and 1-D consolidation tests.

3.4.2.2 Comparison of FEM Analysis and Field Measurements

During construction, the behavior of the wall was monitored by the instrumentation. The fill height reached a maximum of 40 feet on December 3, 1987. The settlement and lateral deformation measurements were taken between June 2, 1987 and December 3, 1987, during the staged construction. The construction procedure was simulated in the analyses (i.e., sequential loading plus staged construction) with a waiting period of one month between each stage. Figures 3.12 and 3.13 show, respectively, the original finite element mesh and the deformed mesh at the end of construction.

The results of the lateral movements of the foundation soils versus depth at Station 32+00 (i.e. where the wall is the highest) and the corresponding FEM results are shown in Figure 3.14. The inclinometers installed 3 feet in front of the wall, indicated that there were up to 2.2 inches of lateral movement at this location. The FEM simulation agrees with the trend of field data that were collected on five different dates. The simulated maximum lateral movement (5.8 in.) was, however, significantly larger than the measured values. Using DACSAR, Iizuka (1991) also experienced similar behavior in predicting the lateral deformation of a soft clay

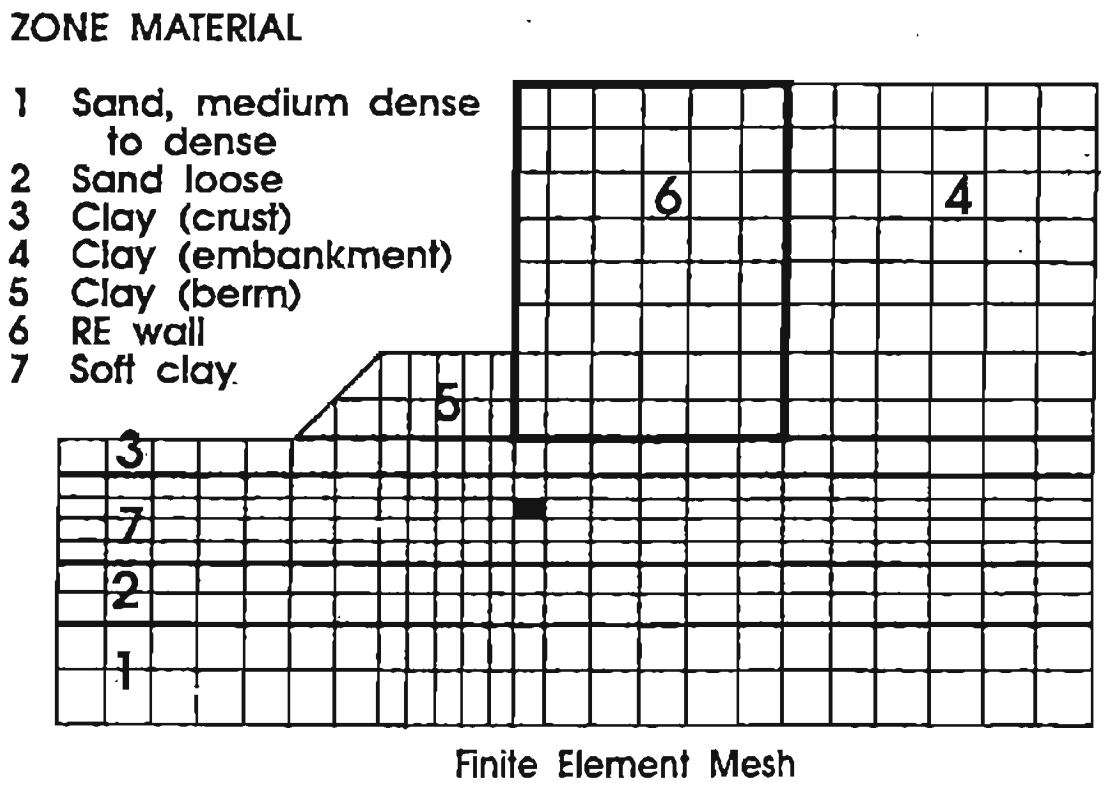

Figure 3.12: The Finite Element Mesh Used in Analysis

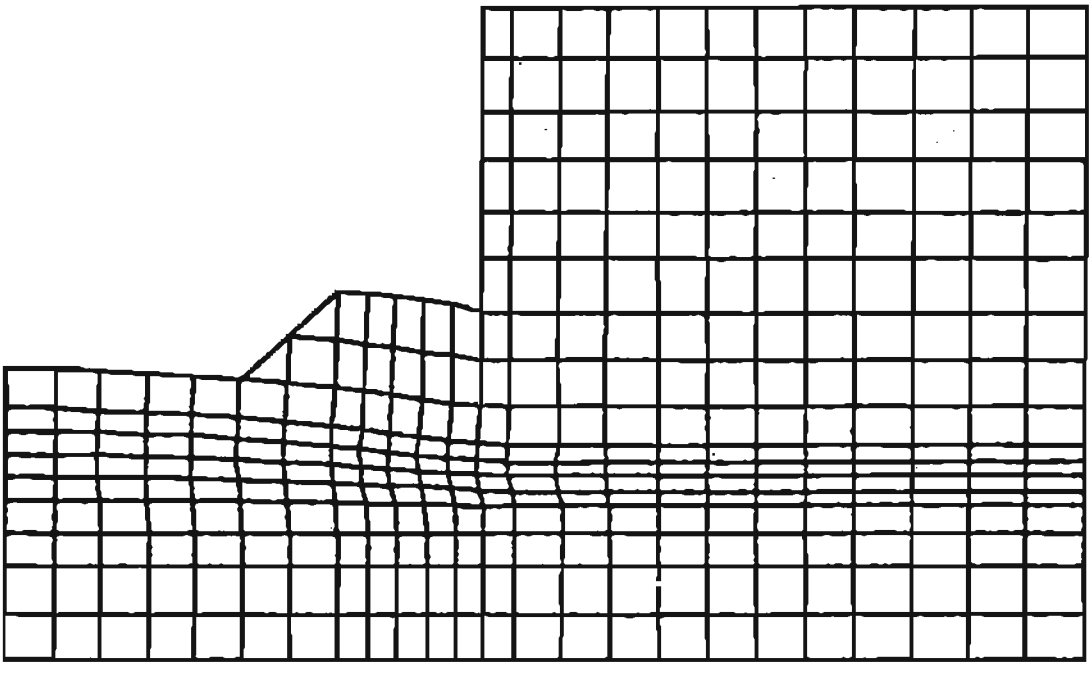

Figure 3.13: Deformation of the Mesh at the End of Construction (Displacement enlarged by 5 times for plotting)

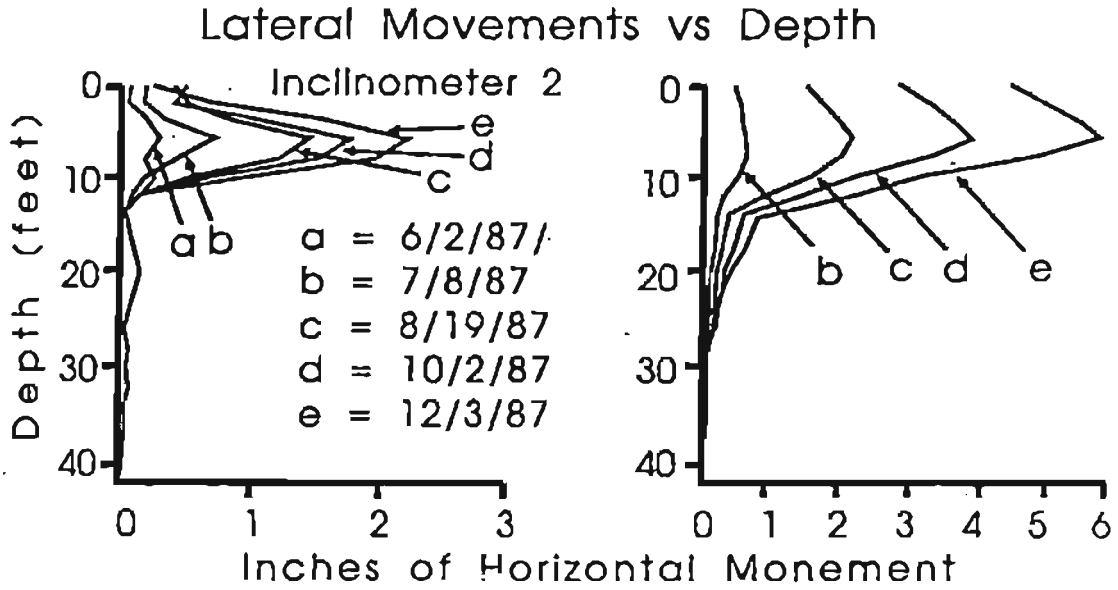

(a) Field Measurements (b) FEM Results

Figure 3.14: Measured and Simulated Lateral Movements of the Foundation Soils

loaded by an embankment. The author suspects that the overestimation is due to the use of the original Cam-clay model.

The settlements measured at Station 32+00 and the corresponding simulation are shown in Figure 3.15. The field data indicated that the settlement of the wall footings at this location was 9.5 inches at the end of construction, which agreed well with the FEM analysis of 8.9 inches. The results from the FEM analysis on the four different dates (see Figure 3.15) also show close agreement with the field data.

3.4.2.3 Strength Increase Due to Staged Construction

As stated previously, staged construction can significantly improve the stability of a wall constructed over a soft clay foundation because of the increase of undrained shear strength by consolidation. The increase of the undrained shear strength due to consolidation, as presented in Equation 3.16, may be validated by DACSAR. The soil was assumed to be a linear elastic material (same as the Terzaghi's 1-D consolidation theory), and the relationship of deviatoric stress and percent of consolidation was obtained from DACSAR (Figure 3.16). A linear relationship was obtained from the analytical result, and therefore Equation 3.16 is valid, provided that the behavior of the soil is linearly elastic.

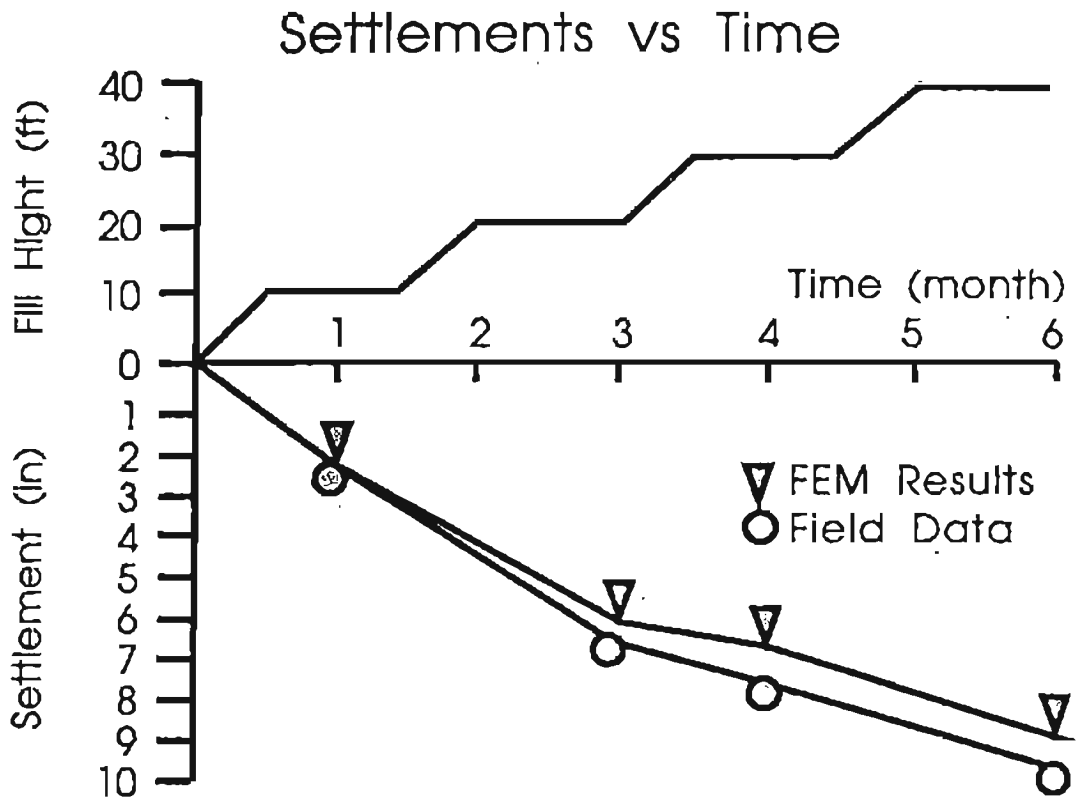

Figure 3.15: Simulated and Measured Settlements
Sta. 32+00, Julesburg wall

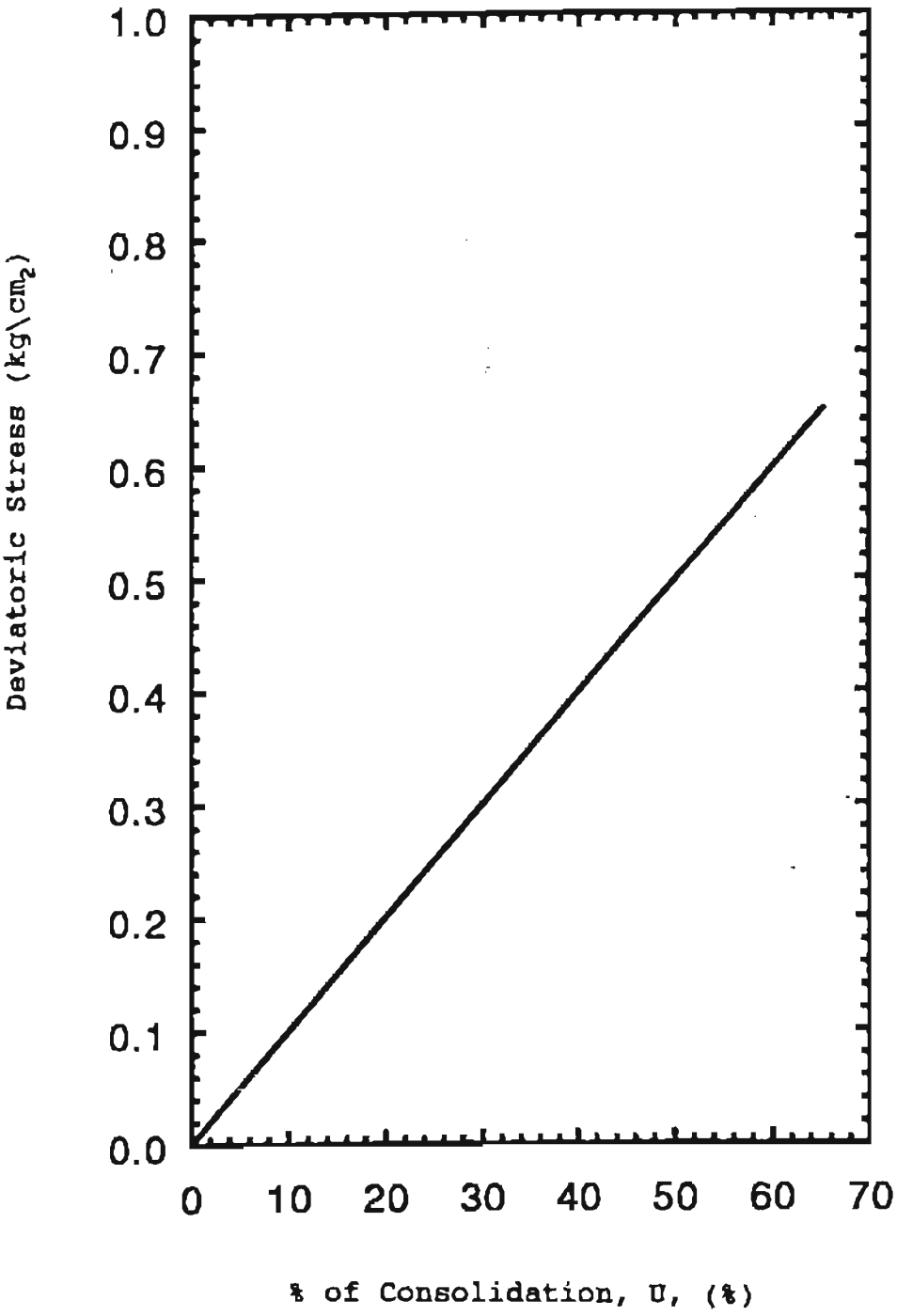

Figure 3.16: S_u vs U% Relationship

The benefits of staged construction also can be examined by the FEM analysis. Figure 3.17 shows the stress path during the wall construction for a typical soft clay element underneath the footing at station 32+00 (the location of this element is shown in Figure 3.12 as a solid element). From Figure 3.17.a, it is clear that without staged construction, the Effective Stress Path (ESP) would have reached the failure (K_f) line. Due to the effect of staged construction, with the contribution of consolidation, the excess porewater pressures dissipated partially, and the ESP for this element was below the failure line (see Fig 3.17.b). Since there was no noticeable sign of failure, it was concluded that the overall stability margin of the RE wall was adequate.

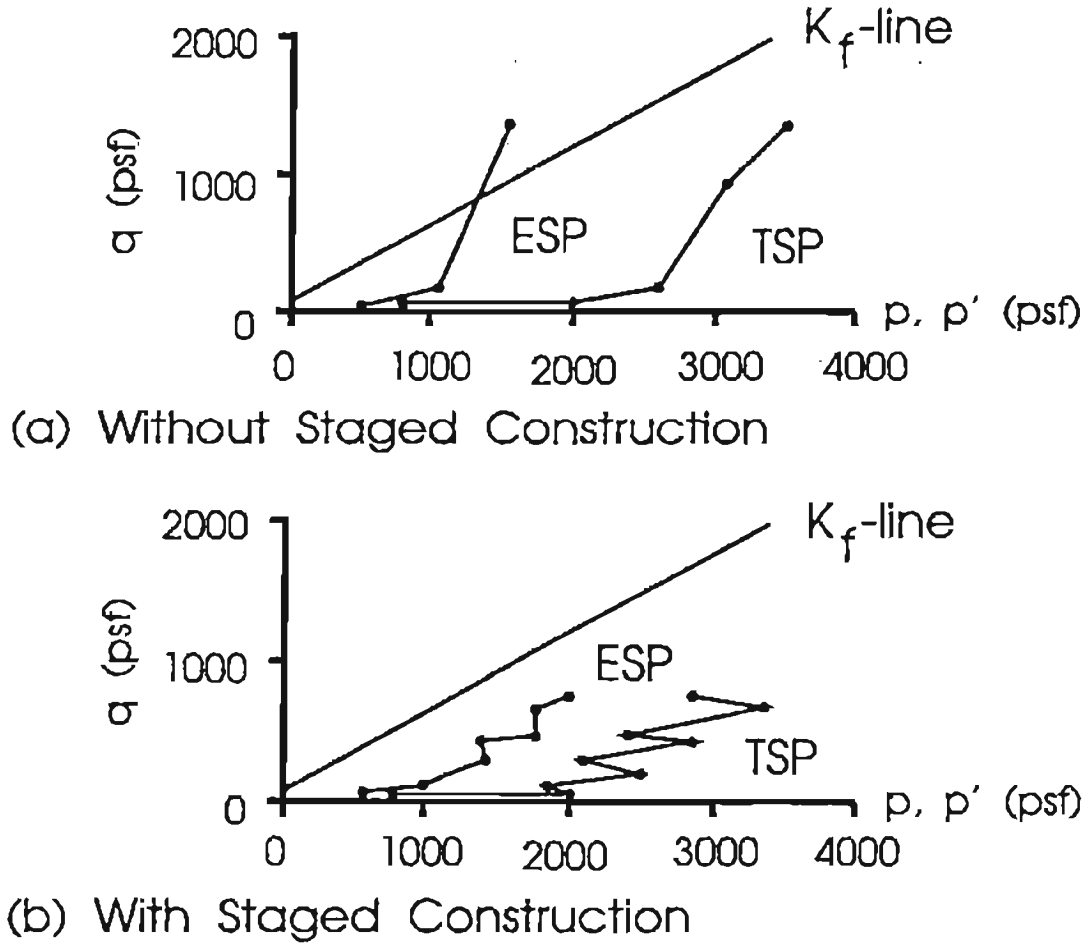

Figure 3.17: Stress Path for a Typical Soil Element Beneath the Footing

CHAPTER IV

VALIDATION OF DACSAR FOR GEOSYNTHETIC WALL SIMULATION

4.1 General

Validation of a finite element program may be conducted by one or more of the following methods:

(1) Comparison with closed-form solutions (for validation of the basic logic of the program);

(2) Comparison with results of soil element tests, such as triaxial tests (for validation of the soil models);

(3) Comparison with results of reduced-scale tests performed in the laboratory, including centrifugal tests;

(4) Comparison with results obtained by using other reliable analytical methods or by other validated FEM computer programs;

(5) Comparison with results of full-scale tests performed under control conditions.

In this study, validation of the FEM program DACSAR was conducted by:

(1) Comparing the analytical results using linear elastic model with the Terzaghi 1-D consolidation theory (closed-form solution);

(2) Comparing the analytical results using the results of Duncan-Chang and Sekiguchi-Ohta soil models

with the triaxial and 1-D consolidation/compression tests;

(3) Comparing the analytical results using the hyperbolic model (Section 3.3.2.2) for bar element with the results of a wide-width tensile test of a geosynthetic;

(4) Comparing the analytical results using beam elements with the results of a timber/plywood test;

(5) Comparing the analytical results of a 12-ft wall with the results of another FEM program, SSCOMP;

(6) Comparing the analytical results with two full-scale, well-controlled GRS walls (the Denver Test Walls) with granular and cohesive backfills.

4.2 Validation of the Linear Elastic Model and Consolidation Analysis

To validate the consolidation (coupling) analysis of DACSAR program and to check the basic logic of the program, a linear elastic soil model was used to simulate a one-dimensional consolidation test for clay. The excess porewater pressure distribution was compared with the Terzaghi closed-form solution (Iizuka, 1987).

The finite element mesh and material parameters used in the analysis are summarized in Figure 4.1.a. Water was assumed to drain through the upper boundary, and the drainage path H was equal to 3.5 cm. A uniform pressure of 4.0 Kg/cm^2 was applied at the top of the sample. The excess porewater pressure was obtained at

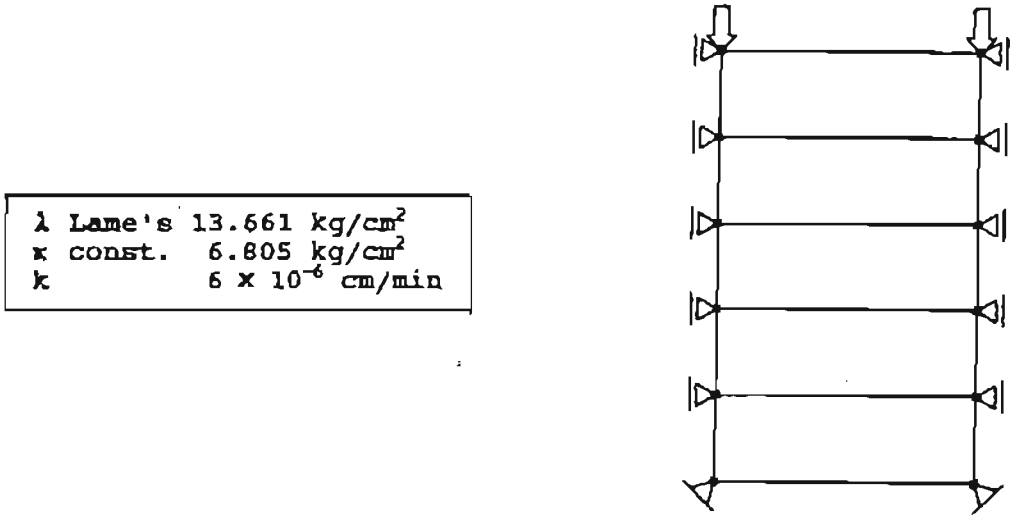

(a) FE Mesh

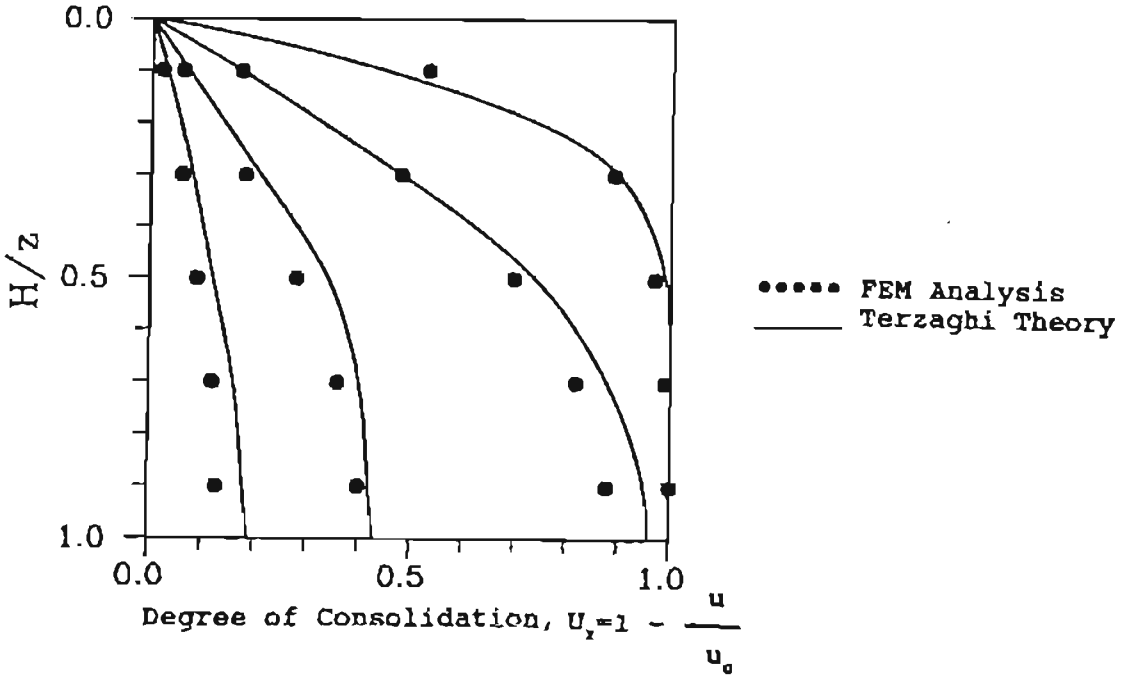

(b) Isochrones of excess porewater pressure

Figure 4.1: Comparison of Terzaghi's Theory and FEM Simulation of 1-D Consolidation Test (After Iizuka, 1987)

the center of each element, at the elapsed times of 0.1, 0.2, 0.5, 1, 2, 4, 8, 15, 30, 60, 120, 240, 80, 960, and 1440 minutes. Figure 4.1.b shows the dissipation of porewater pressure under the axi-symmetric condition. The analytical results agreed closely with Terzaghi's theory.

4.3 Validation of the Duncan-Chang Model by Soil "Element Tests"

The Duncan-Chang model in DACSAR was verified through comparisons with measured data of triaxial and 1-D compression (or 1-D consolidation) tests.

4.3.1 Triaxial CD Tests

A set of Consolidated Drained (CD) triaxial tests was performed on a sandy clay. This soil is one of the backfills used in the Denver Test Walls (see Section 4.8.1).

The samples were compacted at 95% of maximum dry density determined by the Standard Proctor test, at the moisture content about 2.5% over the OMC. The samples were consolidated at the confining pressures of 10 and 30 psi, and sheared at a constant strain rate of 0.0003 inches per minute. No attempt was made to saturate the samples before consolidation.

Using the Duncan-Chang soil model, the stress-strain relationship of soil samples are well simulated by DACSAR, as shown in Figures 4.2. No dilation was observed during shearing, probably because the moisture

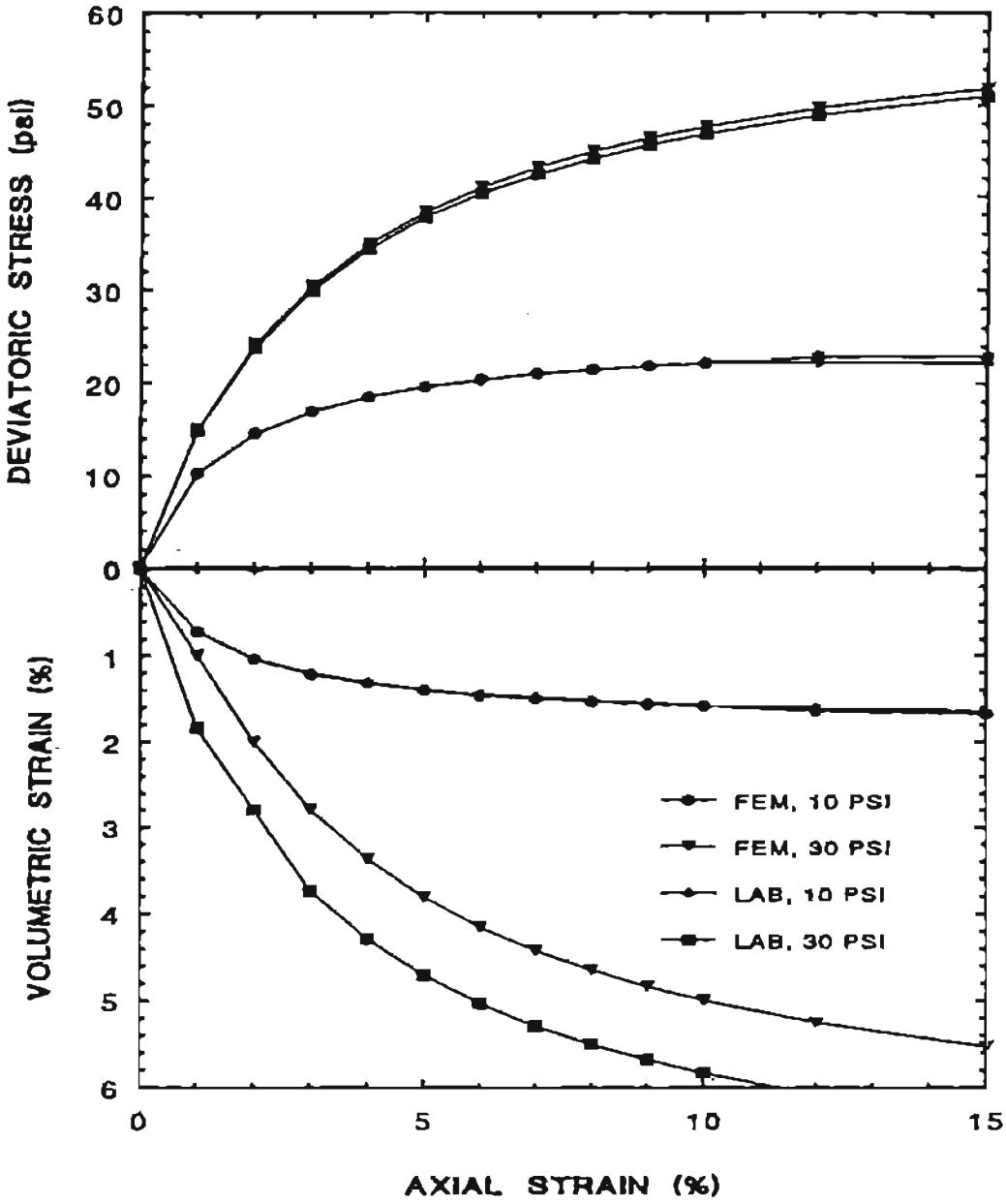

Figure 4.2: Simulated and Measured Stress-Strain-Volume Change Relationship, Moist Sandy Clay, Duncan-Chang Model

contents were on the wet side of the OMC. The volumetric strain simulation is also fairly good (See Figure 4.2). The Duncan-Chang parameters used for simulation of the triaxial CD tests are listed in Table 4.1.

4.3.2 1-D Compression/Consolidation Tests

Two one-dimensional compression/consolidation tests were conducted for the same sandy clay, one in saturated (wet) condition and the other in unsaturated (moist) condition. The deformations were measured at the end of 24 hours for each load increment. For the wet sample, water was added at 10 psi normal pressure. No water was added for the moist sample throughout the test.

To simulate the 1-D compression tests by DACSAR, the same parameters (except K_o) used for the simulation of the triaxial CD tests (See Table 4.1) were employed. The simulated and measured ϵ-log p curves for the saturated (wet) and unsaturated (moist) samples are shown in Figures 4.3 and 4.4, respectively.

The coefficient of at-rest earth pressure (K_o) is not readily available from the 1-D consolidation/ compression test. The following procedure was used to estimate the value of K_o:

(1) Based on the ϵ-log p curve of the 1-D consolidation/compression test, determine the pre-consolidation pressure;

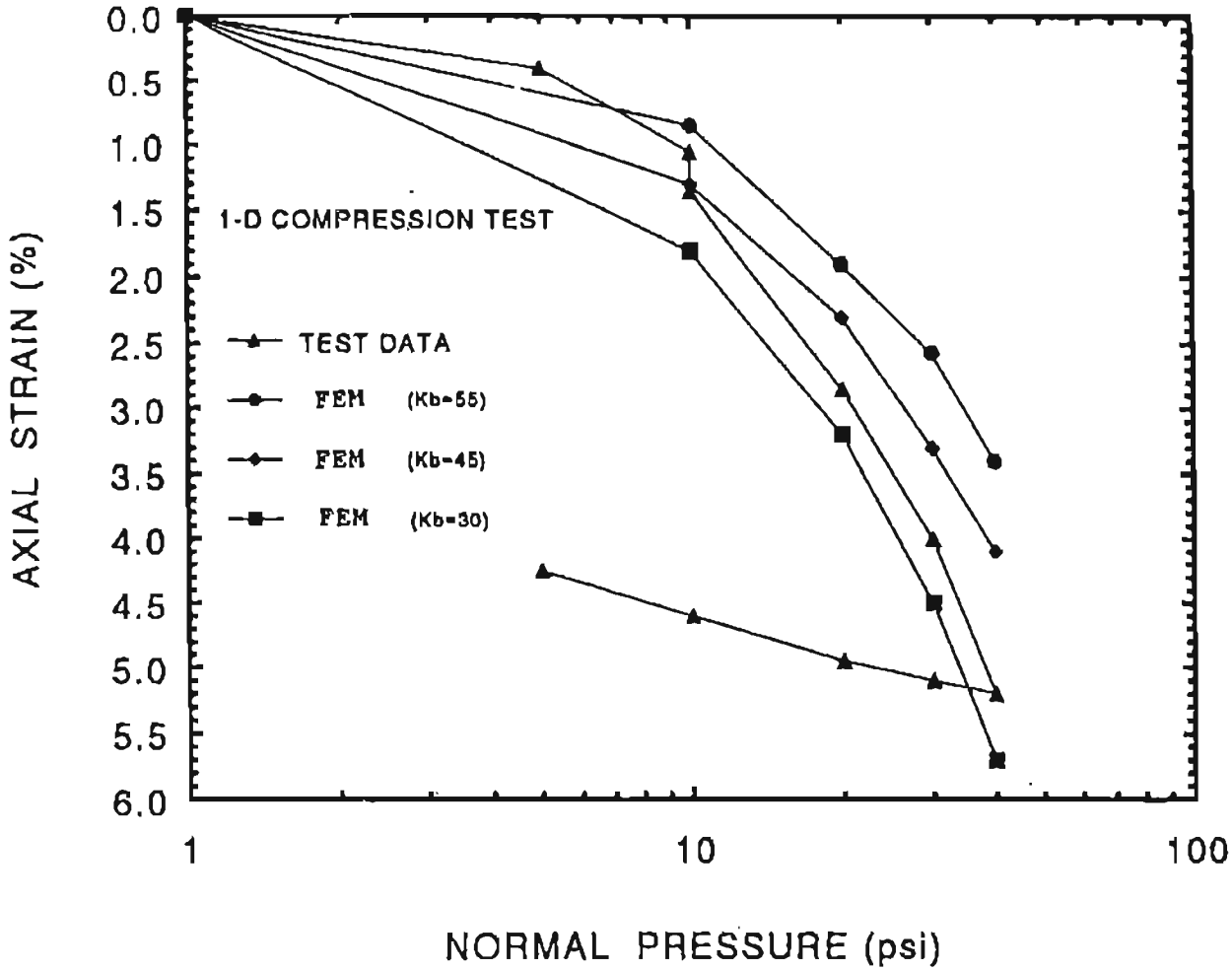

Figure 4.3: Simulated and Measured Strain-Pressure Relationship in 1-D Compression Test, Saturated Sandy Clay

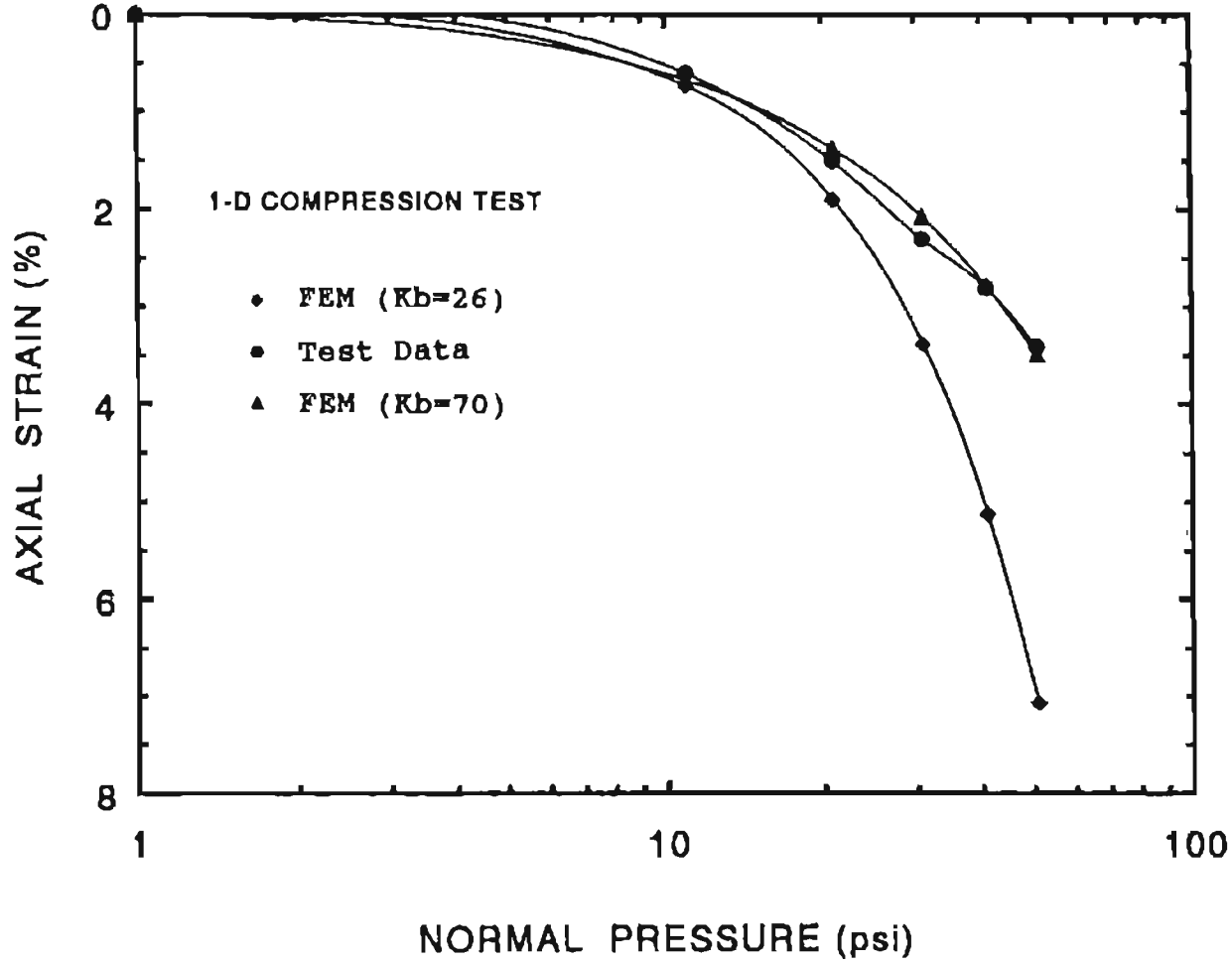

Figure 4.4: Simulated and Measured Strain-Pressure Relationship in 1-D Consolidated Test, Moist Sandy Clay

(2) Determine the Over-Consolidation Ratio (OCR).

(3) Use the following equation to calculate K_o (Parry, 1982):

$$K_o = K_{nc} (OCR)^{\phi} \tag{4.1}$$

where K_{nc} is the coefficient of at rest earth pressure under a normally consolidated condition, which was obtained by:

$$K_{nc} = 1-\sin\phi \tag{4.2}$$

A K_o of 3.0 as obtained from the above calculation was used in the simulation.

Since no porewater pressure was considered in the 1-D compression test, a single element was used in the finite element analysis. Small vertical stress increments are required to simulate the 1-D compression test, due to the confining stress dependent nature of both the incremental Young's modulus and volumetric strain.

By using the same K_b and m values obtained from the triaxial CD test simulation (Table 4.1), it was found that the strains in 1-D compression test were overpredicted for the moist sample, and underpredicted for the wet sample. These discrepancies are attributed to:

(1) The Duncan-Chang parameters are derived from the triaxial test, instead of from the 1-D

consolidation/ compression test. The stress path of these two tests are different; and

(2) The assumption that bulk modulus is independent of the shear stress (Equation 3.5) is overly simplified. To improve the simulation, various combinations of K_b and m values were used. Since the stress-strain relationship is not very sensitive to m, it was assumed that m was constant, and the value of K_b was varied until a close agreement was achieved. The sets of K_b=45 and m=0 (See Figure 4.3), and K_b=70 and m=0 (See Figure 4.4) represent a good-fit for the wet and moist clays, respectively. The soil parameters used in the 1-D compression tests are also listed in Table 4.1.

4.4 Validation of the Sekiguchi-Ohta Model by Element Tests

In this section, the Sekiguchi-Ohta model was validated by the Consolidated Undrained (CU) triaxial and 1-D consolidation tests. Consolidation and creep models were used in the analyses.

4.4.1 Triaxial CU Tests For NC Clay

Three triaxial CU tests were performed on a Normally Consolidated (NC) clay, and the results were compared with the FEM simulation. The samples were obtained from the undisturbed Shelby tubes taken from the CDOT Julesburg wall site. The soil was classified as CL, with an average undrained shear strength of 415

psf. Other soil properties obtained from lab tests were: w=29.7%, e_0=0.95, γd=94.1 pcf, LL=32, PI=10, Gs=2.68.

The samples were saturated and consolidated under confining pressures of 10, 30 and 60 psi. A back pressure was applied to accelerate saturation of the samples until the Skempton's porewater pressure parameter B was equal to or greater than 0.95. The simulated and measured stress-strain relationships are shown in Figure 4.5. The simulated and measured porewater pressures are shown in Figure 4.6. Figures 4.5 and 4.6 are compromise of the best-fitted stress-strain and the porewater pressure-strain relationships. A comparison of the measured and simulated P (mean stress) versus Q (deviatoric stress) diagrams for the clay is shown in Figure 4.7. The comparison indicates that the Sekiguchi-Ohta model reasonably simulate the stress-strain-strength and porewater pressure response of a NC clay.

The material parameter values for the CU test are listed in Table 4.2.

4.4.2 One-Dimensional Consolidation and Creep Tests For NC Clay

One-dimensional consolidation and creep tests were performed on a NC clay to validate the elasto-visco-plastic formulation of the Sekiguchi-Ohta model. The

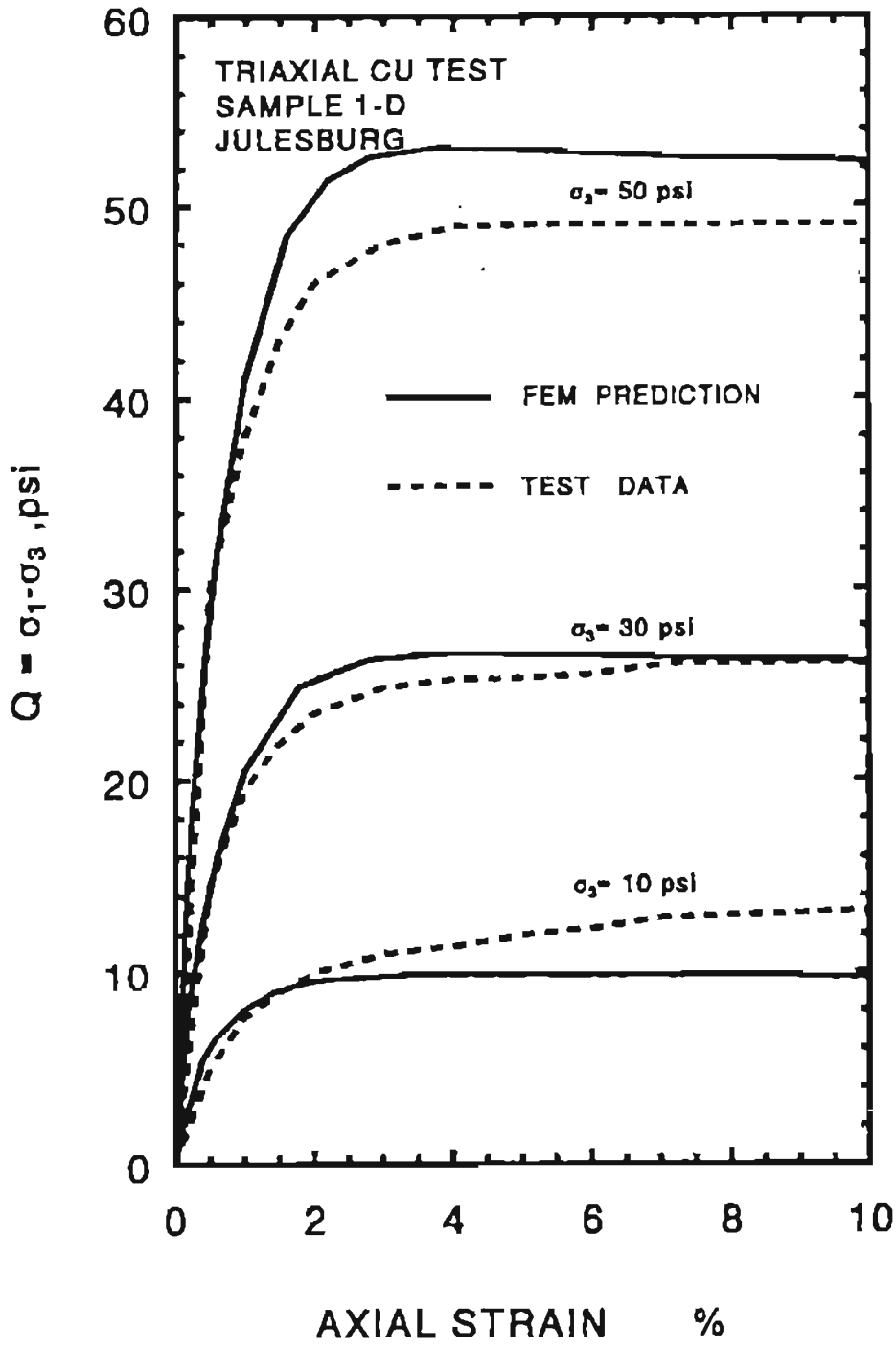

Figure 4.5: Simulated and Measured Stress-Strain Relationship in Triaxial CU Tests, Julesburg Clay, Sekiguchi-Ohta Model

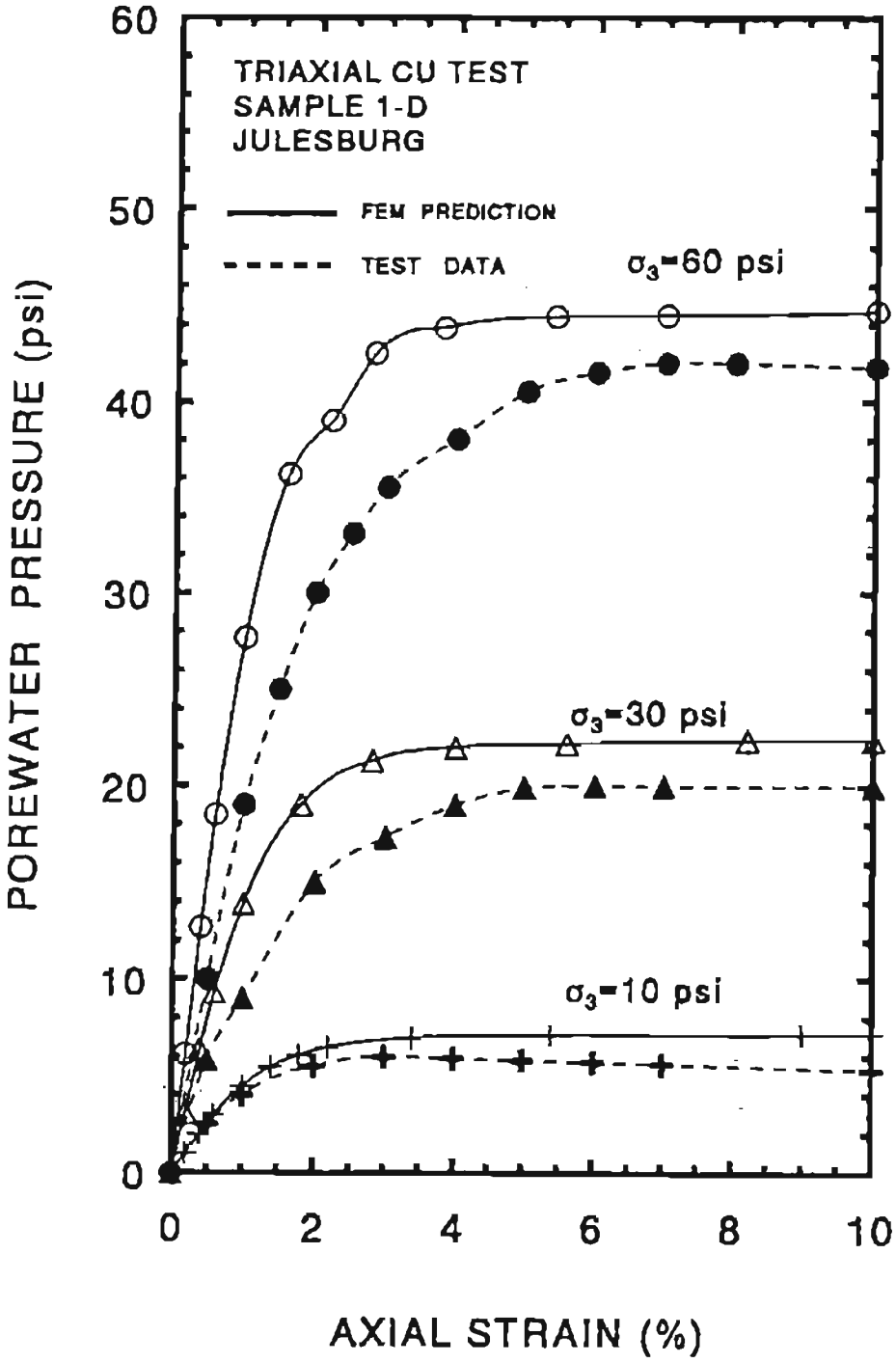

Figure 4.6: Predicted and Measured Porewater Pressure in Triaxial CU tests, Julesburg Clay, Sekiguchi-Ohta Model

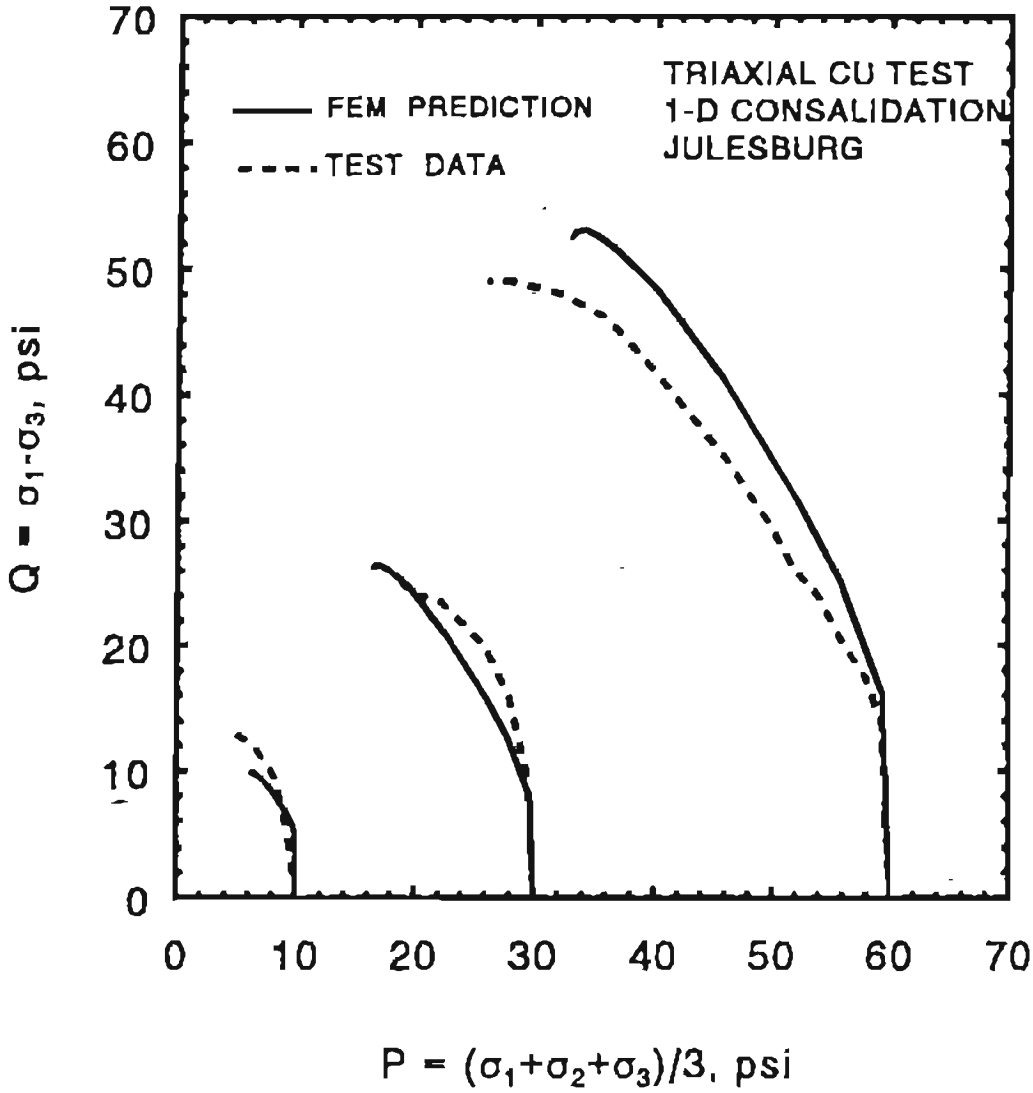

Figure 4.7: P-Q Diagram for Julesburg Clay in CU Test, Sekiguchi-Ohta Model

Table 4.1: Parameter Values Used in the Simulation of Duncan-Chang Model

Element Test	C (psi)	ϕ (deg)	$\Delta\phi$ (deg)	K_b	m	K_{ur}	K_o	K	n	R_f
CD (Unsat.)	1.71	26.5	0	26	-.52	52	1.0	121	.13	.87
1-D Comp. (Sat.)	0.1	30.5	0	45	0	70	3.0	278	.06	.91
1-D Comp. (Unsat.)	1.71	26.5	0	70	0	70	3.0	121	.13	.87

Table 4.2: Parameters Values Used in the Simulation of Sekiguchi-Ohta Model

Element Test	D	Λ	M	ν	k/γ_w (ft^4/lb-lb)	K_0	K_i	α	v_0	e_0	λ	k
CU (Soft Clay)	.021	.642	1.60	.15	.00007	1.0	1.0	.00124	.0000124	.815	.0826	.0296

soil sample was also obtained from the Julesburg site, and had properties similar to those shown in Section 4.4.1.

The sample was saturated under a small initial load and then incremental loads were applied and the time-settlement data recorded. The 1-D consolidation simulation procedure was similar to that described in Section 4.2, except that the elasto-visco-plastic model, instead of the linear elastic model, was used.

Figure 4.8 depicts the simulated and measured ϵ-log p relationship. A good agreement was obtained. Figure 4.9 shows the simulated and measured ϵ-log t curves under a normal pressure of 2 tsf. The consolidation and creep models in DACSAR successfully predict the general trend of the strain-time relationship, although the models tend to overestimate deformation of the clay.

The parameter values used in the above analysis are also listed in Table 4.2. Ohta and Iizuka (1987) recommended obtaining the creep parameters, α (coefficient of secondary compression) and $\dot{v}_0$ (initial volumetric strain rate) from the triaxial consolidation tests. Since there is no triaxial consolidation data available for this soil, it was assumed that α value from the triaxial test is equal to that from the 1-D consolidation test. The initial

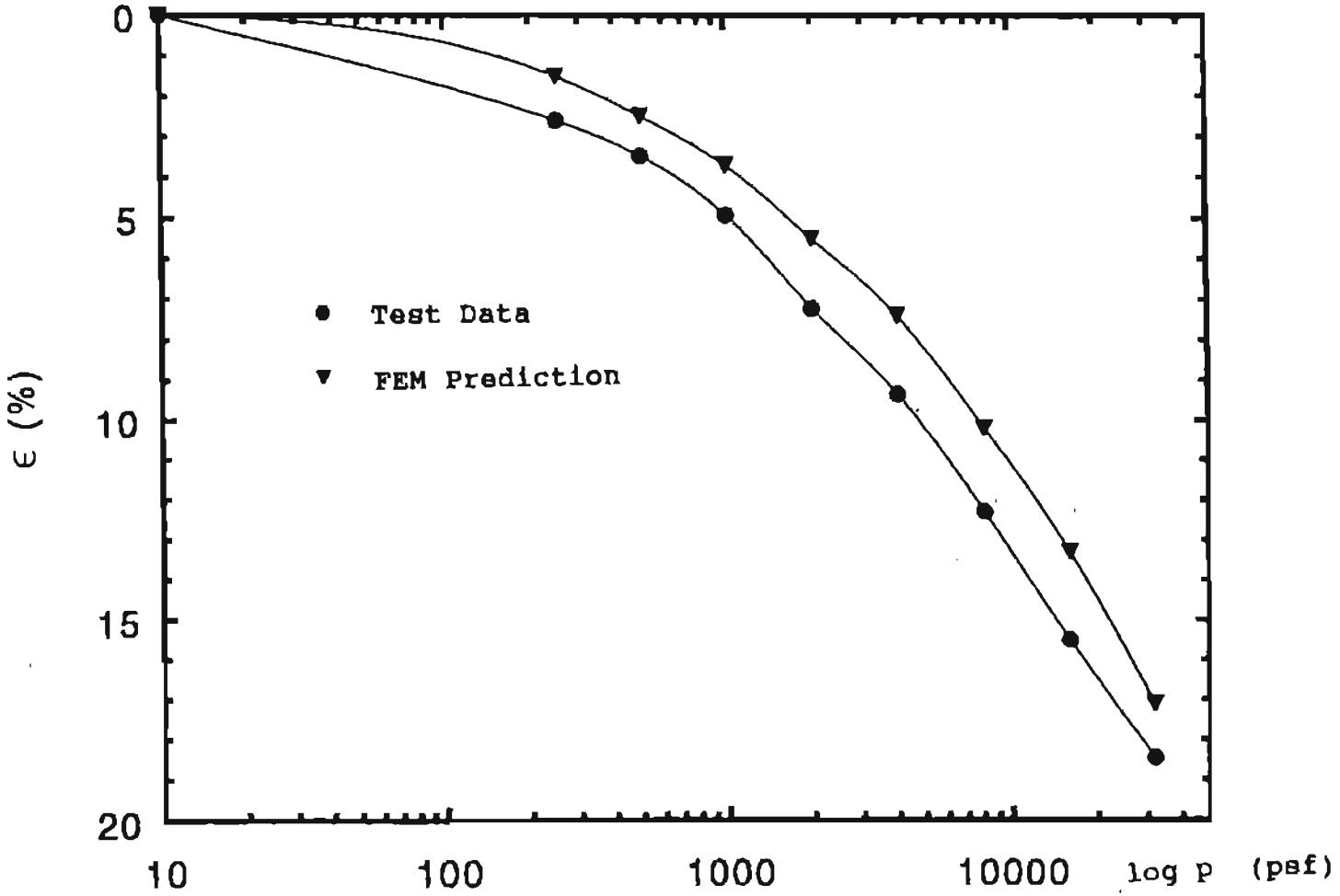

Figure 4.8: Simulated and Measured 1-D Consolidation Test of Soft Clay, Strain-Pressure Relationship, Simulated by the Sekiguchi-Ohta Model

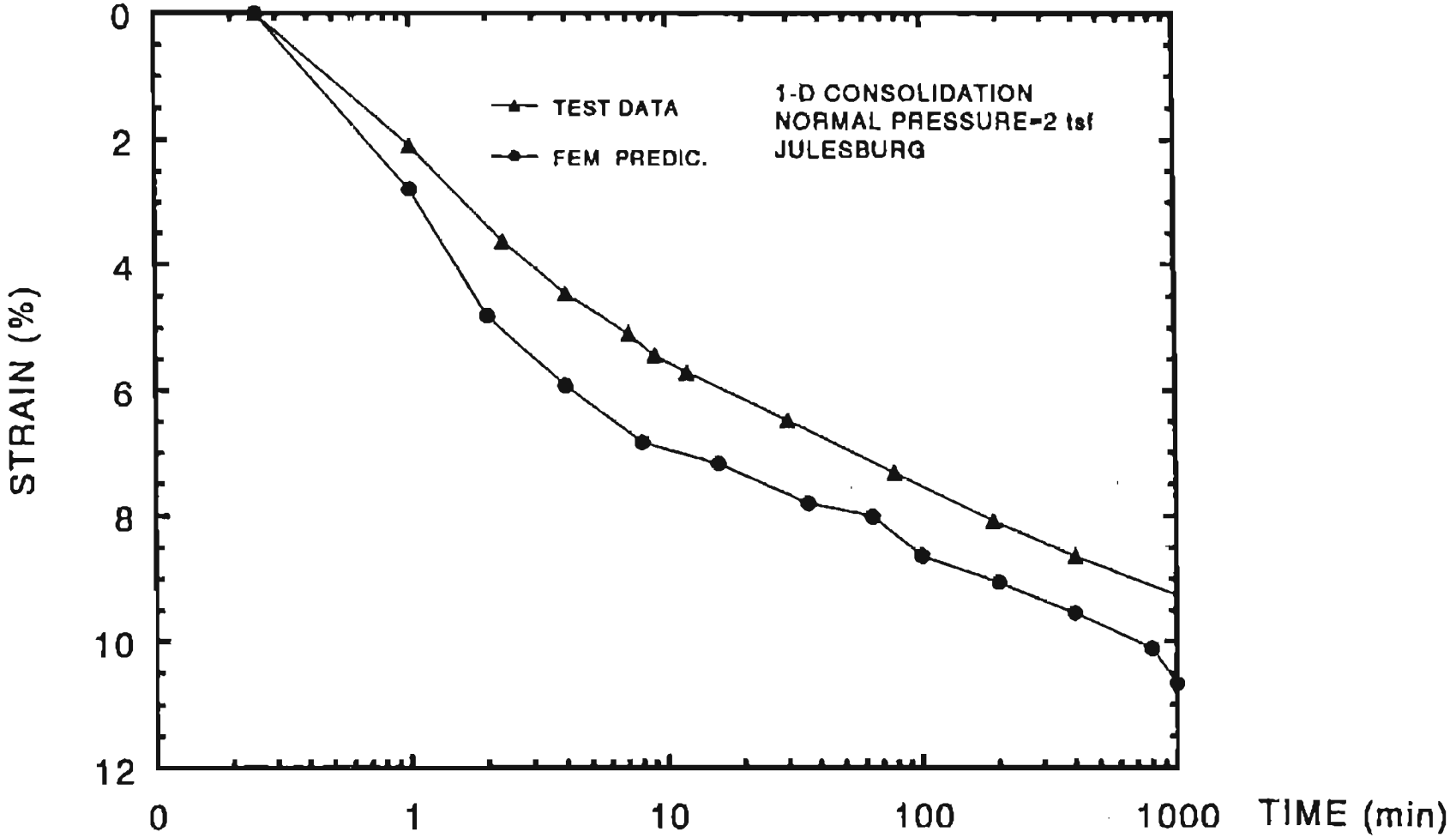

Figure 4.9: Simulated and Measured 1-D Consolidation Test of Soft Clay, Strain-Time Relationship Under a Surcharge of 2 tsf, Simulated by the Sekiguchi-Ohta Model

volumetric strain rate, $\dot{v}_0$, can be obtained from the following equation:

$$\dot{v}_0 = \frac{\alpha}{t_c} \tag{4.3}$$

where t_c is the time required for completion of primary consolidation.

Since t_c obtained from the triaxial consolidation test could be different from that of the 1-D compression test, some adjustment was necessary. As shown in Figure 4.8 and 4.9, creep parameter values of α=0.00124 and $\dot{v}_0$=0.000012 min^{-1} , successfully simulated the lab test data for both strain-log (pressure) and strain-log (time) curves.

The success in the above simulation indicates that the Sekiguchi-Ohta model is capable of simulating the elasto-visco-plastic behavior of the normally consolidated clay. This capability is important for simulating a GRS wall constructed over a soft foundation.

4.5 Validation of Geosynthetic Material Model

As described in Chapter 3, a hyperbolic model was implemented in DACSAR to simulate nonlinear, stress-dependent load-deformation relation of the reinforcement. Two parameters, the initial tangential modulus (E_i) and the ultimate tensile strength (T_{ult}), are required in this model. To validate the hyperbolic

model, a load-deformation curve obtained from a wide-width tensile test (Ling, Wu and Tatsuoka, 1991) for a nonwoven heat-bound polypropylene geotextile, TYPAR 3301, as shown in Figure 4.10, was used. The specimens were 30 cm in width and 3.75 cm in gage length (see Figure 4.10) and were tested at a constant strain rate of 2% per minute. The simulated tensile force vs. strain curve is also plotted in Figure 4.10. It is seen that the model gives a good representation of the test results.

Simulation of the creep behavior of the geosynthetic was not considered because creep of geosynthetics is usually not a major concern under service leads. For example, the Denver Test Walls with both sand and clay backfills did not demonstrate any noticeable creep under a surcharge pressure of 15 psi for a period of 100 hours (see Section 4.8.4). Other field case histories (i.e. the Seattle Wall and the Glenwood Canyon Test Wall) also indicated that creep is not a major concern under service loads.

4.6 Validation of Beam Element Formulation

A flexural test (Figure 4.11) was performed to obtain the bending stiffness of the timber/plywood facing in the Denver Test Walls. The test unit consists of five timber blocks (4" x 6" x 6" each) connected to two plywood forming elements (12" x 6" x

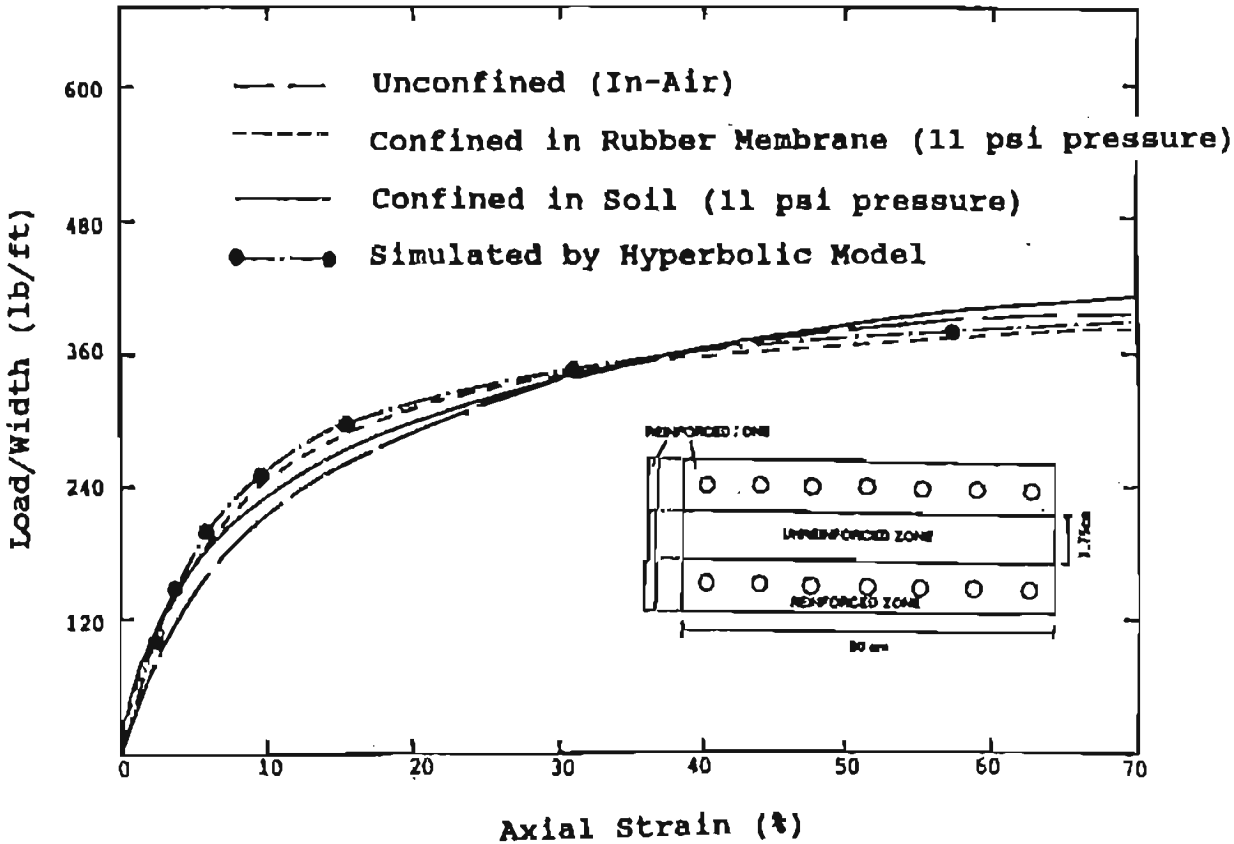

Figure 4.10: Simulated and Measured Load-Deformation Curves by the Hyperbolic Model (After Ling, Wu and Tatsuoka, 1991; Chou, 1992)

Timber/Plywood Facing Test

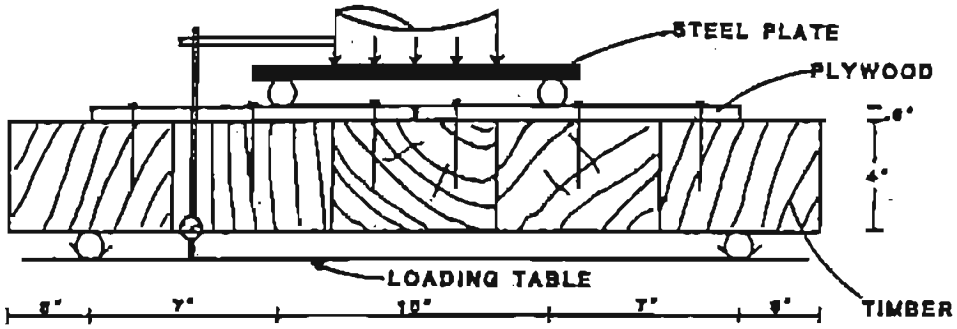

Side View

(a) Test Set-Up

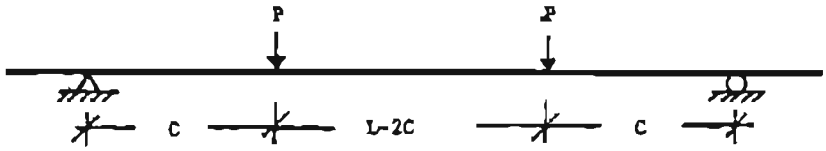

(b) Simulated Model

Figure 4.11: Timber/Plywood Facing Flexural Test and the Structural Model

3/8" each) by 3" long deck screws (one screw per element).

Two concentrated line loads of equal magnitude were applied to the plywood side of the connected blocks. The timber/plywood test was modelled by a continuous long beam, as shown in Figure 4.11.b. The results of the total applied loads vs. vertical movement of the loading piston (which is the same as deflection at the loading locations) is shown in Figure 4.12.

To evaluate the bending stiffness of the test unit, the following assumptions were made:

(1) The test unit was assumed to be a continuous long beam, although these 4" x 6" x 6" timbers are individual blocks connected to the plywood by six 3 inch screws. This assumption is probably acceptable under service loads;

(2) The two simple supports were assumed to be a hinge on one side and a roller on the other side (Figure 4.11.b)

(3) There is no friction generated between the timber blocks when they are subjected to loads.

Based on the linear portion of the load-deflection curve, a total applied load of 100 pounds would induce a deflection of 0.14 inch. An EI value of 21,000 lb-in sq was calculated from the following equation:

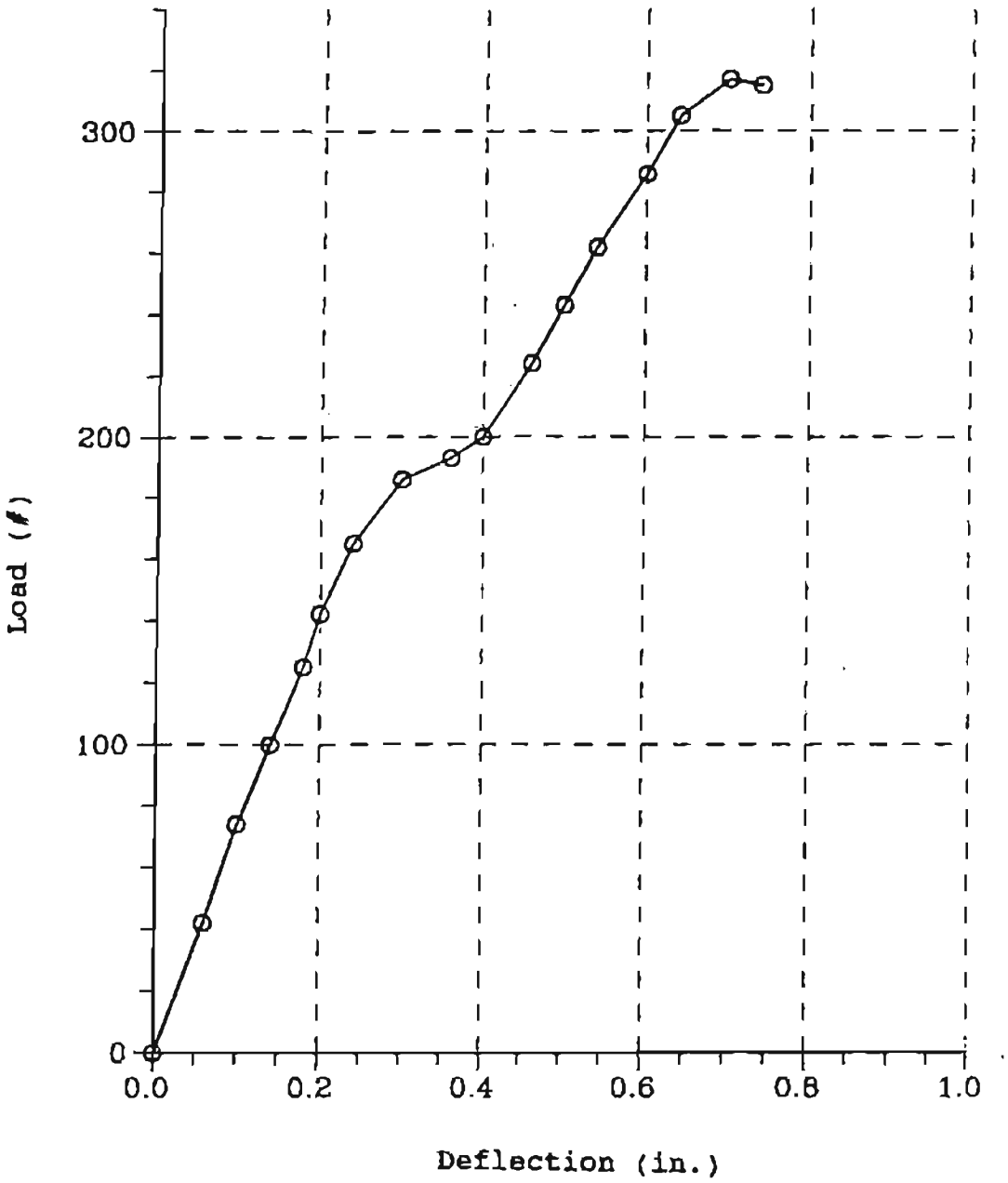

Applied Load vs. Movement Curve of the Timber Facing Unit.

(Note: Deflections are measured from dial guage on loading table)

Figure 4.12: Load-Deflection Curve for the Timber/Plywood Facing Test

$$y = \frac{Pc^2}{EI_z}\left(\frac{L}{2} - \frac{2c}{3}\right) \qquad (4.4)$$

where:

y = deflection at the location of the applied load

c = distance from roller/hinge to where the load is applied

l = length between supports

E = Young's modulus

I = Moment of inertia of the beam

To validate the beam element formulation in DACSAR, a three element continuous beam was used for the simulation. A force of 8.33 pounds per inch (equivalent to 100 pounds of total load applied to the test beam) and an EI value of 21,000 lb-in sq were selected for the analyses. The FEM analysis gave a deflection of 0.14 inch at the loading locations, which was identical to the lab test result.

4.7 Validation By Comparison With SSCOMP

As described in Section 4.1, one approach to validate a FEM program is to compare the results with those obtained from other FEM programs. SSCOMP was chosen for the comparison because it has been used for MSE walls analyses (Collin, 1986; Adib, 1988; Wu & Lin, 1991).

A 12-ft high GRS wall was used for the comparison. The wall was assumed to be constructed over a rigid foundation, with the following conditions:

(1) Geometry:

Wall height H = 12 ft

Reinforcement spacing S = 2 ft

Reinforcement length L = 9 ft

Contious concrete facing, with the following properties:

E = 3,055,000 psi

I = 31.1 in^4/in

A = 7.2 in^2/in

(2) Backfill:

A uniform, medium-dense, GP soil compacted to 95% Standard Proctor, with the following Duncan-Chang model parameters: γ= 125 pcf, K= 600, n= 0.6, R_f= 0.7, K_b= 175, m= 0.2, C=0 psi, ϕ = 39 deg., $\Delta\phi$= 7 deg, K_o= 0.37, K_{ur}= 600.

(3) Uniform surcharge is assumed to be 0.2 x γh.

Wu & Lin (1991) have previously analyzed this wall using SSCOMP. No compaction induced horizontal stress was considered in their analyses. Using the same parameters in their analyses, an analysis was performed by DACSAR.

As shown in Figure 4.13, the lateral deformations of the wall face calculated by using the two programs

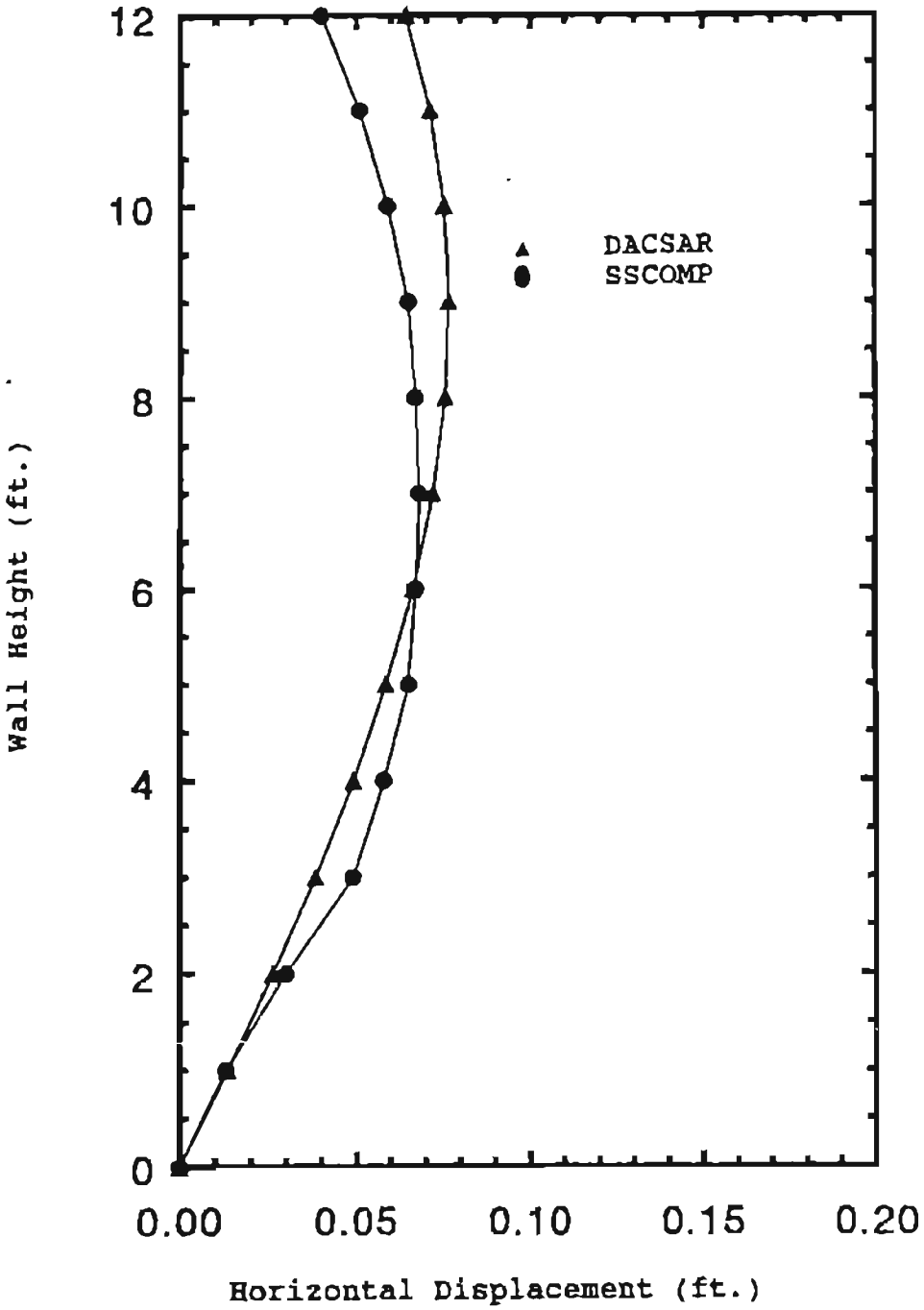

Figure 4.13: Comparison of prediction by DACSAR and SSCOMP Analyses
- Horizontal Displacement

are fairly close, the maximum lateral wall deflection was 0.077 ft (0.92") for DACSAR and 0.069 ft (0.82") for SSCOMP. The location of maximum deflection obtained from DACSAR is 9 ft (measured from wall base), compared with 7 ft from SSCOMP.

A comparison of the horizontal stress distributions (earth pressures) against the wall face are shown in Figure 4.14. Both programs gave very high stresses near the rigid base, although the stresses calculated by DACSAR are small than those calculated by SSCOMP. Figure 4.15 shows a comparison of the tensile forces in the reinforcement at 3, 7 & 11 feet above the wall base. The tensile forces were similar for the lower and middle layers of the reinforcement. DACSAR calculated slightly lower tension at the 3 foot level reinforcement, but higher tension at 7 and 11 foot reinforcement levels.

Although there are some discrepancies in the results of DACSAR and SSCOMP, the agreement is considered satisfactory.

4.8 Validation of DACSAR By the Denver Test Walls

4.8.1 The Denver Test Walls

Two 10-ft high, instrumented and well-controlled GRS walls were constructed at the geotechnical lab of the University of Colorado at Denver. The test walls, referred to as the Denver Test Walls, was a joint research of the CDOT and CU-Denver. The author was

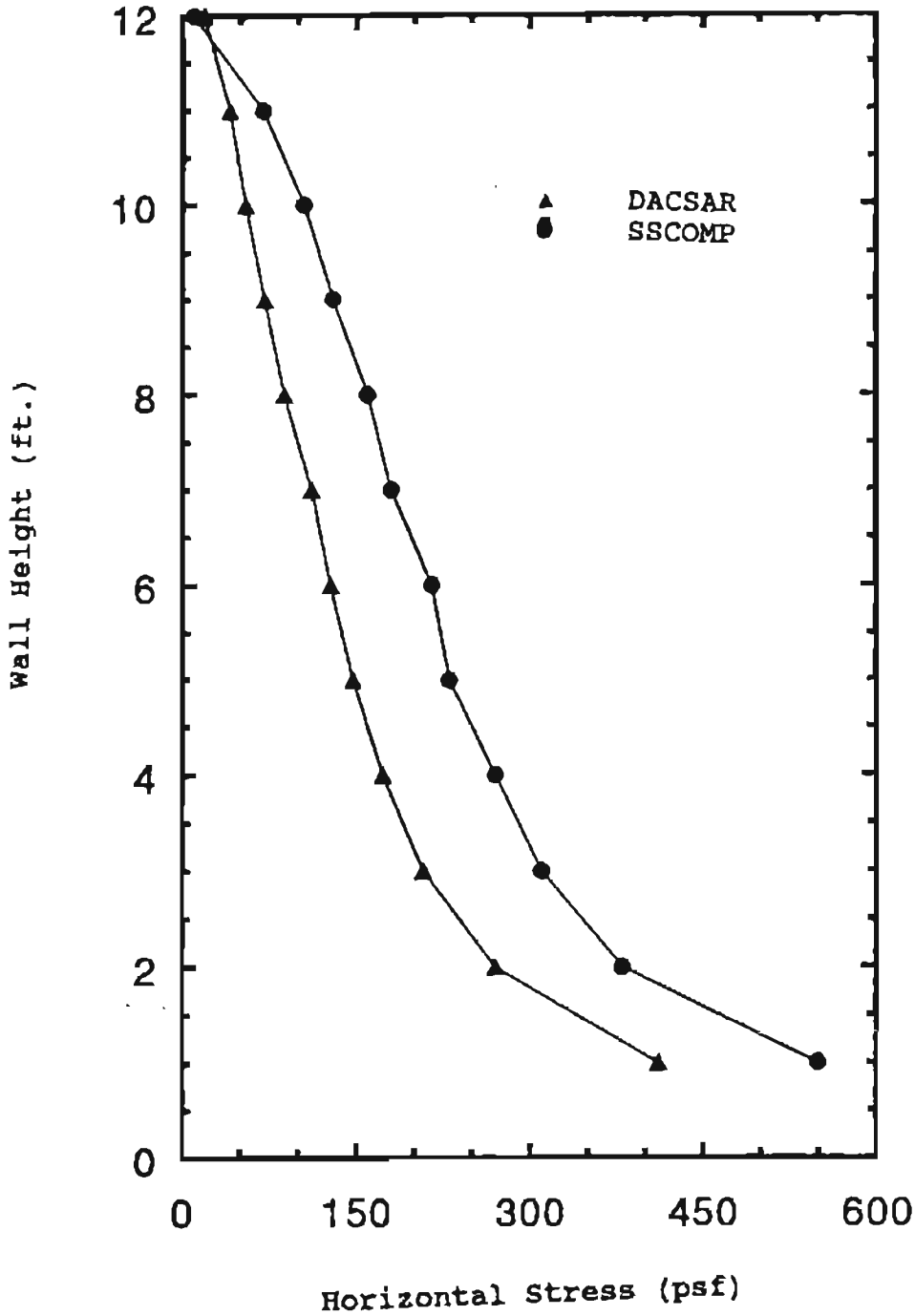

Figure 4.14: Comparison of prediction by DACSAR and SSCOMP Analyses
- Horizontal Stresses Against Facing

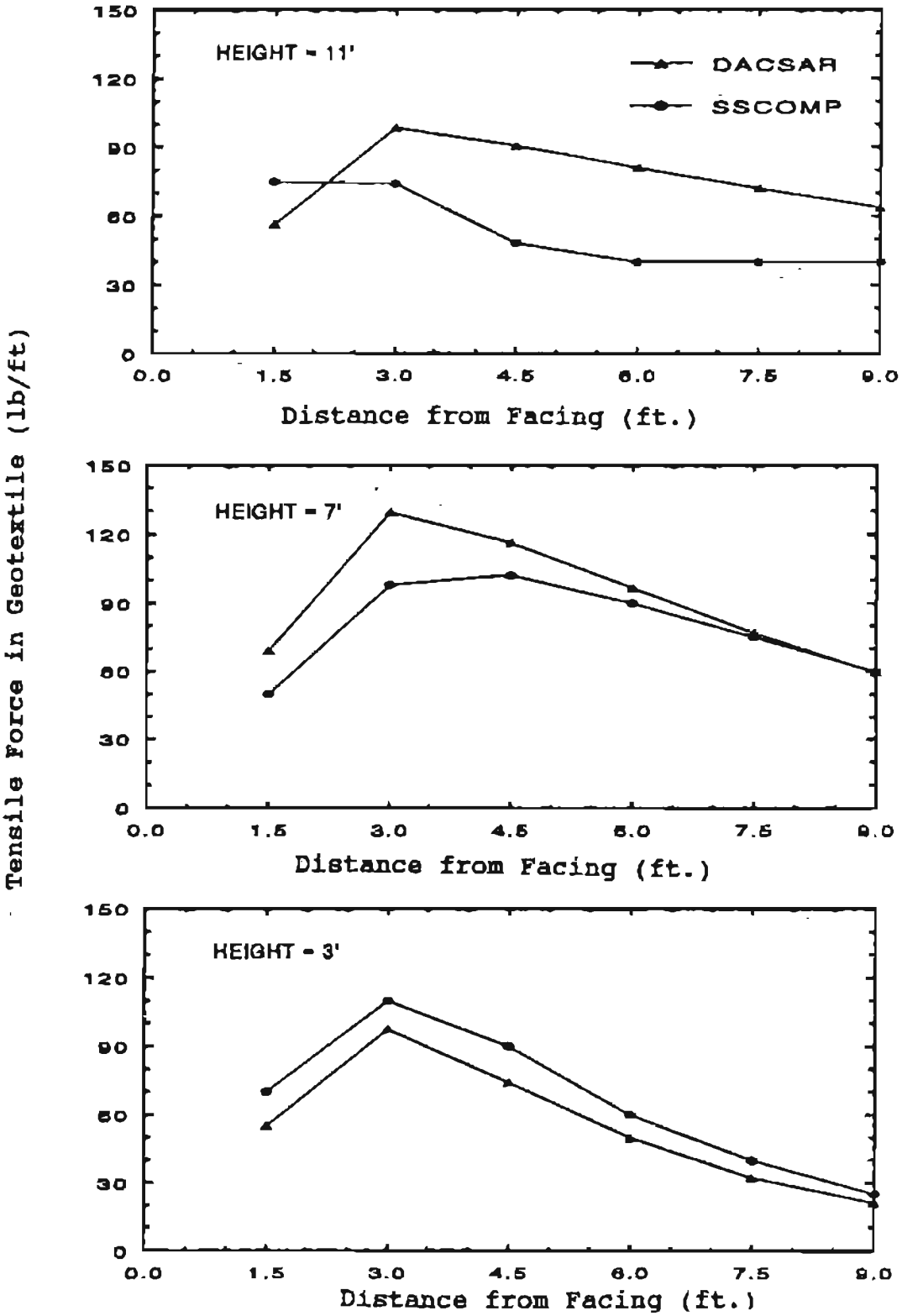

Figure 4.15: Comparison of prediction by DACSAR and SSCOMP Analyses
- Tensile Forces in Geotextile

heavily involved in planning, design and coordination of the test program, laboratory tests and construction of the walls.

Detailed information of the Denver Test walls has been presented by Wu (1992a). Only a brief summary is predicted herein. One of the two test walls was backfilled with a granular soil, and the other with a cohesive soil. The granular backfill was emplaced by an air-pluviation method, using a specially designed hopper. The cohesive backfill was emplaced by compacting the soil at 2% wet of optimum and 95% relative compaction (Standard Proctor) using a vibratory plate.

Each wall was constructed with an incremental timber/plywood facing and reinforced by 12 layers of a nonwoven polypropylene heat-bonded geotextile. The walls were constructed within a rigid loading facility in the laboratory to achieve better control of the test conditions. The side walls of the loading facility were lubricated to a near frictionless state to achieve a plane strain condition. The configuration of the test walls and the loading facility is depicted in Figure 4.16. The construction procedure for the cohesive backfill wall is illustrated in Figure 4.17.

A uniform surcharge was applied in 3 psi increments, using an air bag, on the top surface of the backfill. Upon arriving at a surcharge pressure of 15

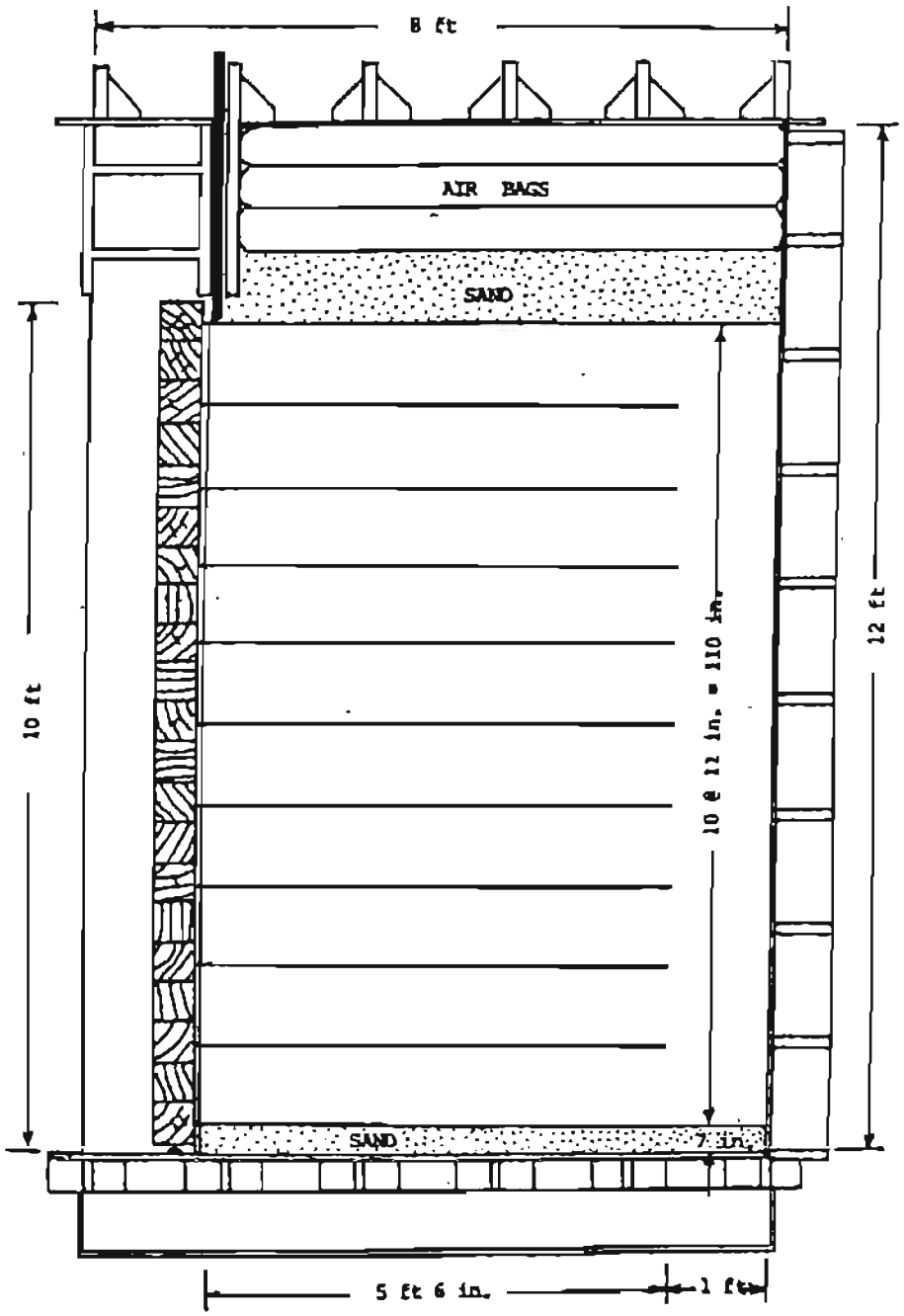

Figure 4.16: Loading Facility and Configuration of the Denver Test Walls (After Wu, 1992)

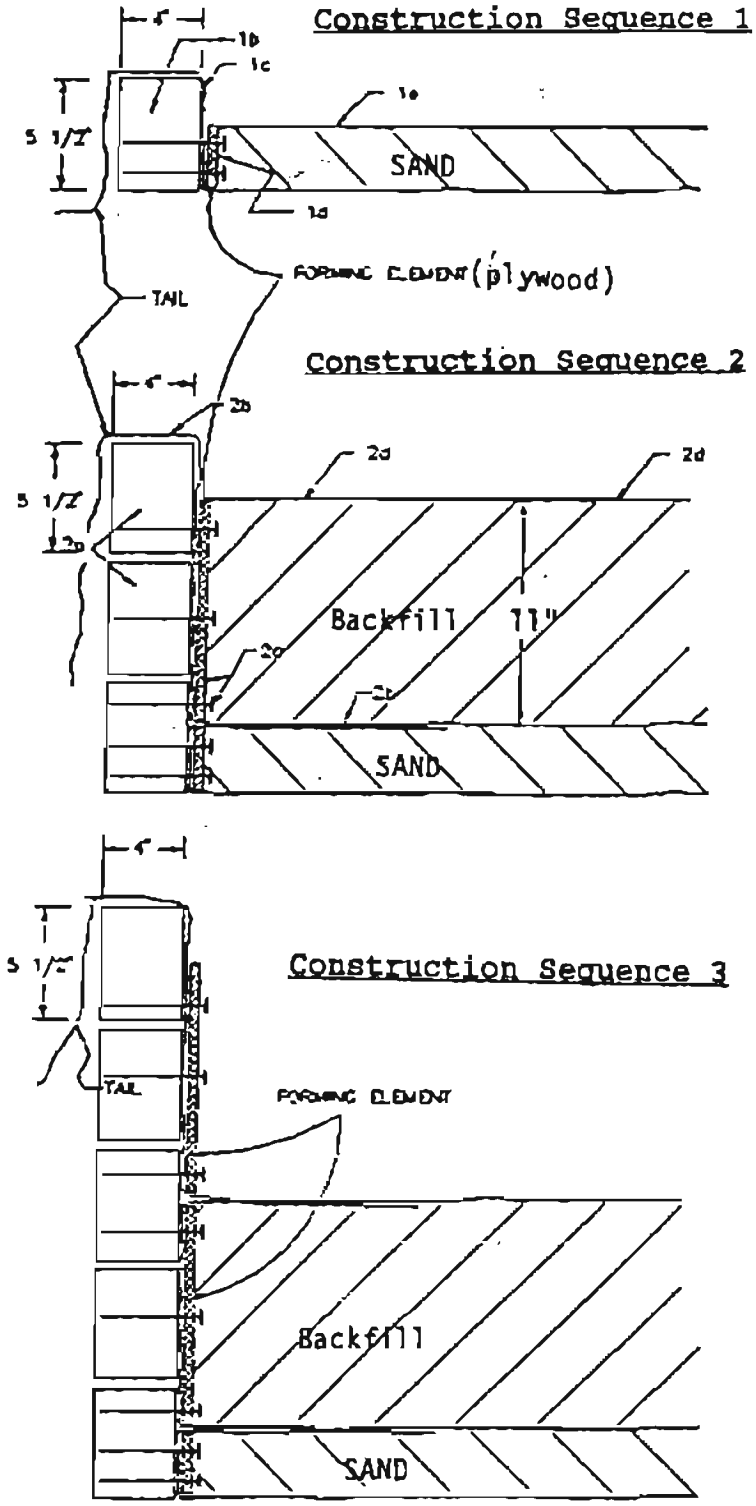

Figure 4.17: Construction Sequence of the Cohesive Backfill Test Wall

Figure 4.17: (Continued)

GEOFABRIC WALL CONSTRUCTION DETAIL

Construction Sequence 1

Step 1a: Level wall site.
Step 1b: Place initial row of 4" (width) x 5-1/2" (height) timber.
Step 1c: Place initial fabric layer.
Step 1d: Attach initial fabric layer to initial timber by connecting forming element (3" height) to timber, using 3" long deck screws.
Step 1e: Backfill to top of forming element.
Step 1f: Compact lift to 95% of max dry density from standard proctor test @ 2% wet of optimum moisture.
Step 1g: Fold the fabric tail over onto the compacted backfill.

Construction Sequence 2

Step 2a: Place two timbers.
Step 2b: Place fabric layer.
Step 2c: Attach fabric layer to timbers, using 3" long deck screws through the forming element, as shown (11" height).
Step 2d: Place backfill and compact to the density and moisture as in 1f.
Step 2e: Fold the fabric tail over onto the compacted backfill.
Note: Center forming element between timber, as shown.

Construction Sequence 3

Step 3a: Same as 2a.
Step 3b: Same as 2b.
Step 3c: Same as 2c.
Step 3d: Backfill with fill material to top of forming element and compact.
Step 3e: Repeat sequences 2 and 3 until full height is achieved. (The tail length on the final layer is 6-1/2 ft, and on other layers is 3 ft.)

psi, the walls were allowed to creep for a duration of 100 hours. Thereafter, the surcharge pressure was increased until a failure condition developed or until the capacity of the loading mechanism was reached.

The performance of the test walls was monitored during construction and during application of the surcharge pressures. The instrumentation of the test walls included:

(1) Strain gages along the length of the reinforcement to monitor the strain distribution in the reinforcement;

(2) Tracing magnets (0.06 inch thick and 1/16 inch in diameter each) on the reinforcement at selected points, to monitor displacements of the reinforcement by using a hall generator probe with a magnetic sensor;

(3) Pressure transducers on the back of the timber facing to monitor the earth pressure against the facing;

(4) Paper targets on the front facing to monitor the facing movements; and

(5) A side-wall grid system on the side wall transparent plexiglass to monitor the internal movement of the backfill, including the displacements of the top fill surface.

To assess the state-of-the-art analytical capabilities and to gain a better understanding of the performance of GRS walls, an international symposium on

GRS walls was held in Denver, Colorado on August 8 and 9, 1991. The Denver walls were featured in the Symposium. Fourteen teams, including the author, submitted their predictions prior to construction of the walls.

Each predictor was provided detailed information concerning the geometry, the material properties, the construction procedure, and the loading schedule of the test walls. The material properties provided to the predictions include:

- Geotextile: wide-width tensile test (confined and unconfined);

- Backfills: direct shear test, isotropic compression test, triaxial CD test for the granular backfill; compaction (Proctor) test, 1-D compression test, triaxial UU, CU and CD tests for the cohesive backfill;

- Soil-reinforcement interface: pullout test and direct shear test;

- Timber/plywood facing: flexural test.

Details of the prediction information, the construction and instrumentation of the walls, and the measured behavior of the walls have been presented by Wu (1992a, 1992b, 1992c).

4.8.2 FEM Prediction By DACSAR

4.8.2.1 General

Class-A prediction of the following wall performance characteristics were requested:

(1) Facing displacement profile;

(2) Settlements at the top of backfill;

(3) Strains in the geotextile reinforcements;

(4) Earth pressure against the timber facing; and

(5) The failure load and failure mode.

The performance characteristics 1 to 4 were for the following three loading conditions.

- at the end of construction (EOC)
- under the 15 psi surcharge
- at the end of the 100-hour creep with 15 psi surcharge.

The following FEM analyses, performed using DACSAR, are based on the author's predictions submitted for the Symposium. After the Symposium, additional analyses were performed, which are presented in Section 4.8.6.

The finite element mesh used for the prediction is shown in Figure 4.18. A total of 403 soil elements, 31 beam elements (for facing) and 125 bar elements (for reinforcement) were used in the analysis. Interface elements were not used. Each analysis typically took about three hours of CPU time in a VAX 8800 mini-computer environment.

The analyses of the wall were conducted by an incremental technique, following the construction

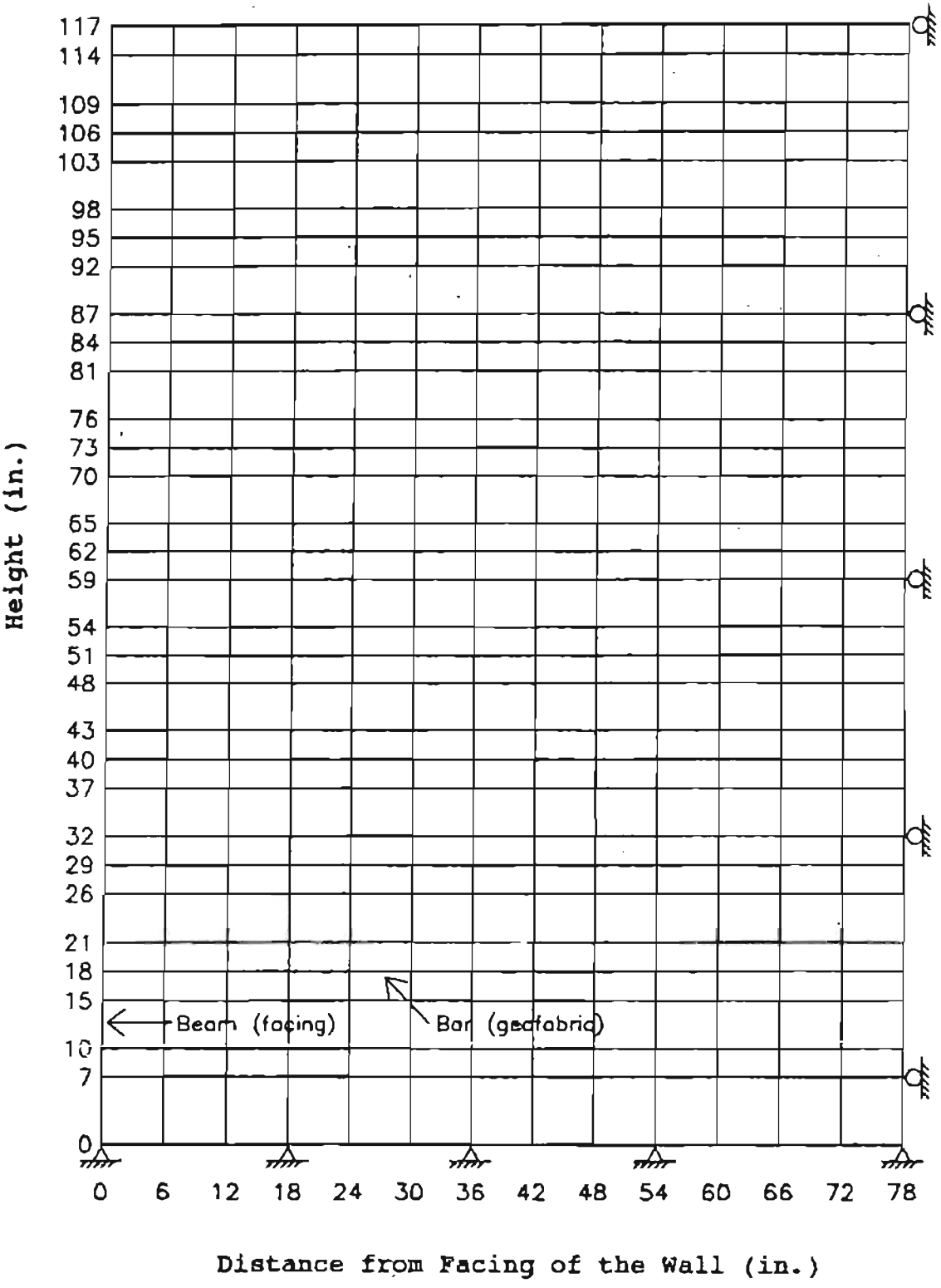

Figure 4.18: FEM Mesh for the Analysis of the Denver Test Walls

sequence. Each increment represents an 11-inch construction lift of fill and placement of a layer of reinforcement. After reaching the full-height of the wall, the top of the backfill was subjected to three psi uniform pressure increments. The lateral deformations, settlements, axial forces and strains along the geotextile layers, as well as the earth pressures against the facing, were determined at each increment of the analyses.

4.8.2.2 Selection of Material Models Soils

The Duncan-Chang hyperbolic model was employed for simulating both the cohesive and granular backfills, for the following reasons:

(1) The backfills were placed and loaded under an unsaturated condition. Compared with the Sekiguchi-Ohta model, the Duncan-Chang model is more suitable for dry sand and compacted clay (as discussed in Section 3.3.2.1.3). Using the total stress approach, the Duncan-Chang model avoids the inherent difficulties in determining the effective stress parameters from unsaturated triaxial and consolidation tests; and

(2) The behavior of test walls with different backfill (sand and sandy clay) can be analyzed and compared by using the same soil model.

Reinforcement

Bar element was used to represent the reinforcement. The load-deformation behavior of the

reinforcement was simulated by the hyperbolic model described in Section 4.5. Because the confining pressure did not influence the stiffness/strength of the heat-bonded geotextile, the confining pressure was not accounted for in the analyses. The creep of the soil and geotextile was not included in the analyses.

Facing

Two-node beam elements with axial shear and bending stiffness were used to simulate the timber/plywood facing.

4.8.2.3 Boundary Conditions

Because the walls were rested on a rough gravelly surface, a high friction angle between the bottom backfill and the base was expected. The bottom of the test walls were therefore assumed to be fixed. The soil along the backface of the wall (the contact surface between the unreinforced fill and the backpanel loading facility) was assumed to be able to move freely downward.

4.8.3 Determination of Material Parameter Values

4.8.3.1 Soil Parameters

For the dry granular backfill, the Duncan-Chang parameters were obtained from the triaxial CD test, since the behavior of the granular backfill is considered to be in a "drained" condition during loading.

Parameter determination for the cohesive backfill is more difficult. The surcharge loads were expected to be applied rather quickly, compared to the pore pressure dissipation rate. In addition, each incremental load was anticipated to be held for only 30 minutes before adding the next load increment, it was decided that "undrained" parameters would give a better representative of the test condition. Since the bulk modulus cannot be determined by the undrained triaxial test, it was decided that K_b & m be estimated from back-calculation using the 1-D compression test result.

The Duncan-Chang soil parameters used in the test wall predictions are summarized in Table 4.3.

4.8.3.2 Reinforcement Parameters

Using the hyperbolic model for load-deformation relationship of geosynthetics (see Section 4.5), the initial tangent modulus (E_i) and the ultimate tensile strength (T_{ult}) of the reinforcement were determined as 555 lb/in and 35 lb/in, respectively. As shown in Figure 4.17, the front three feet of the geotextile was folded back toward the back of wall. This segment of the geotextile was modeled by doubling the cross sectional area of the reinforcement.

4.8.3.3 Facing parameters

Assuming a continuous beam for facing elements, the EI value of the facing/plywood unit can be determined, as discussed in Section 4.6. For a unit

width of one inch, an EI value of 21,000 lb-sq. in. was obtained from the facing/plywood test.

4.8.4 Measured Behavior of the Denver Walls

The following test wall behavior was reported by Wu (1992b, 1992c): (1) Axial strains in the geotextile reinforcement (measured by strain gages); (2) Displacements of the timber facing (measured by paper targets and rectilinear potentiometers); and (3) Internal movement of the backfill and displacements of the top fill surface (measured by side wall latex membrane grids).

The measured settlements and lateral displacements for the granular backfill test wall (at the EOC, 9, 15, 27, 29 psi) are shown in Figures 4.19 and 4.20, respectively. Figures 4.21 and 4.22 depict, respectively, the measured settlement and lateral facing movement profiles for the cohesive backfill wall at EOC, 9, 15, 33 psi and when reloaded to 34 psi surcharge pressures.

There was some movement in the timber facing during construction; as a result, the facing was not vertical at the end of construction. The facing movement profiles shown in Figures 4.20 and 4.22 were plotted using the EOC condition as the reference (i.e. the displacements shown in those figures are the displacements that occurred after the end of construction).

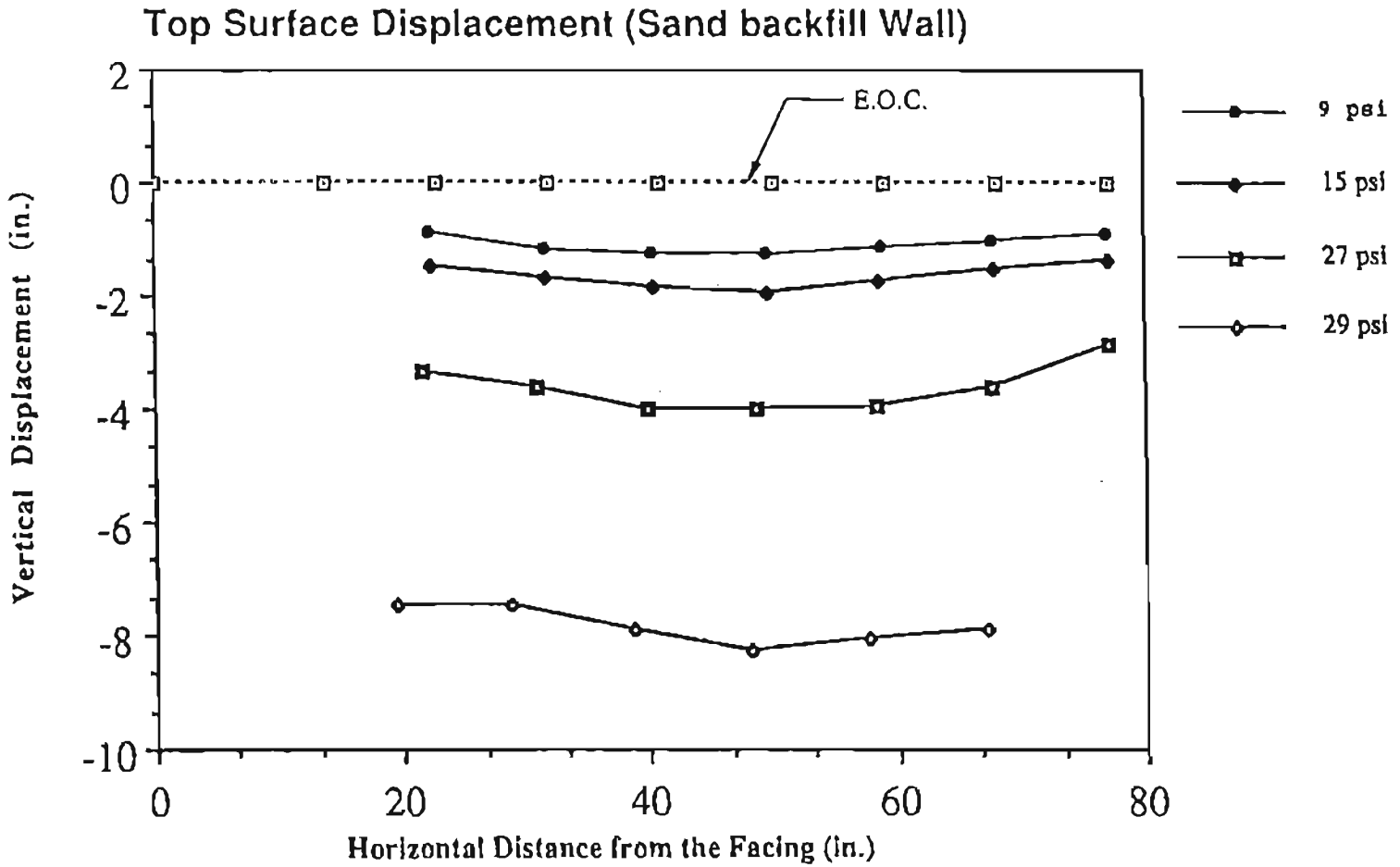

Figure 4.19: Measured Top Surface Displacement (Settlement) of the Granular Backfill Wall (After Wu, 1992)

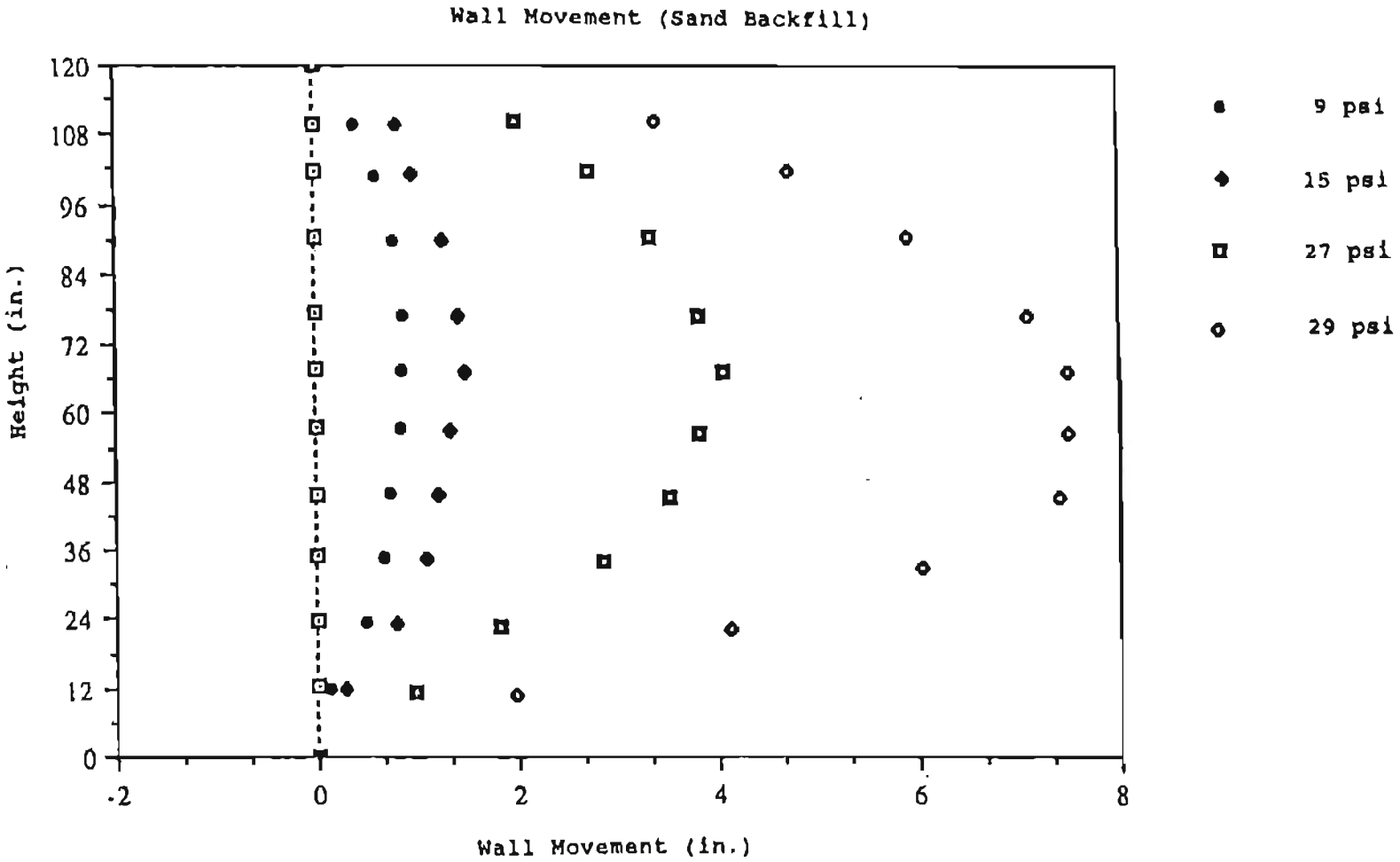

Figure 4.20: Measured Lateral Wall Displacement of the Granular Backfill Wall (after Wu, 1992)

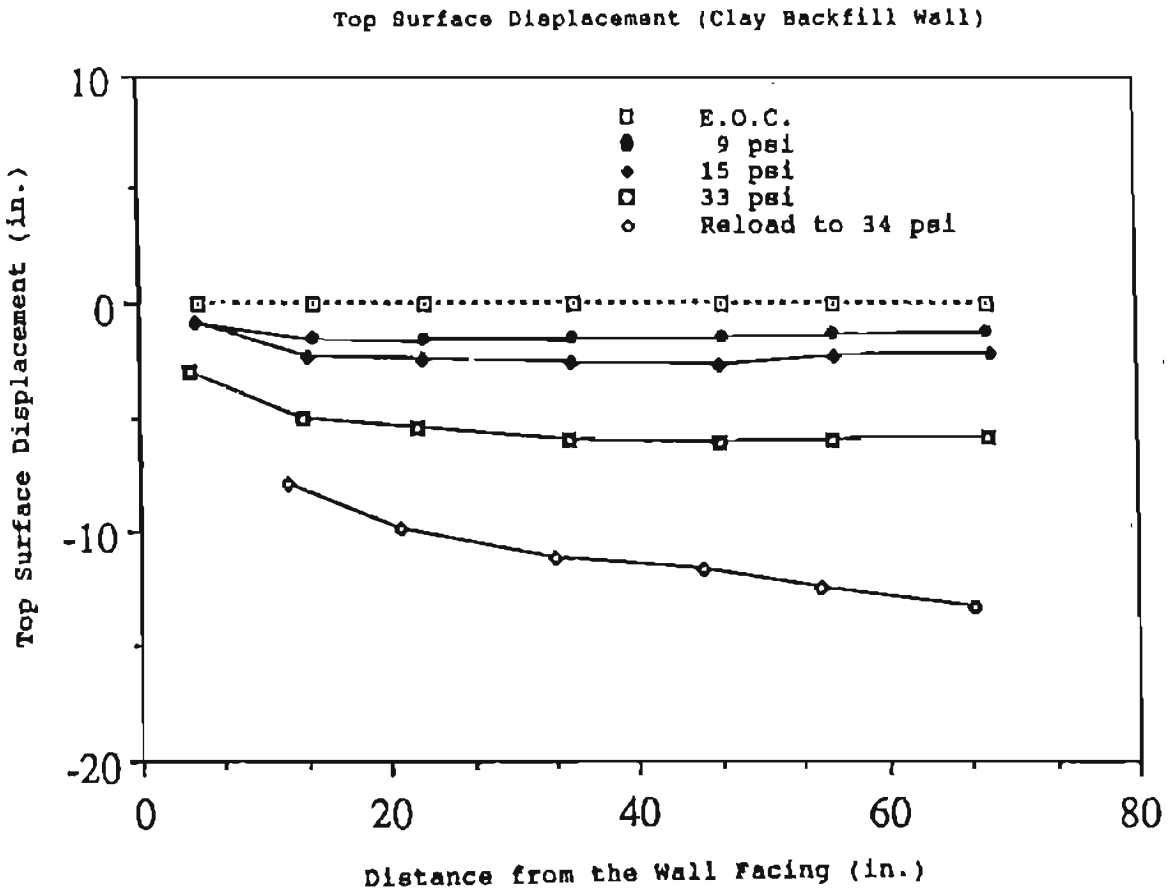

Figure 4.21: Measured Top Surface Displacement (Settlement) of the Cohesive Backfill Wall (After Wu, 1992)

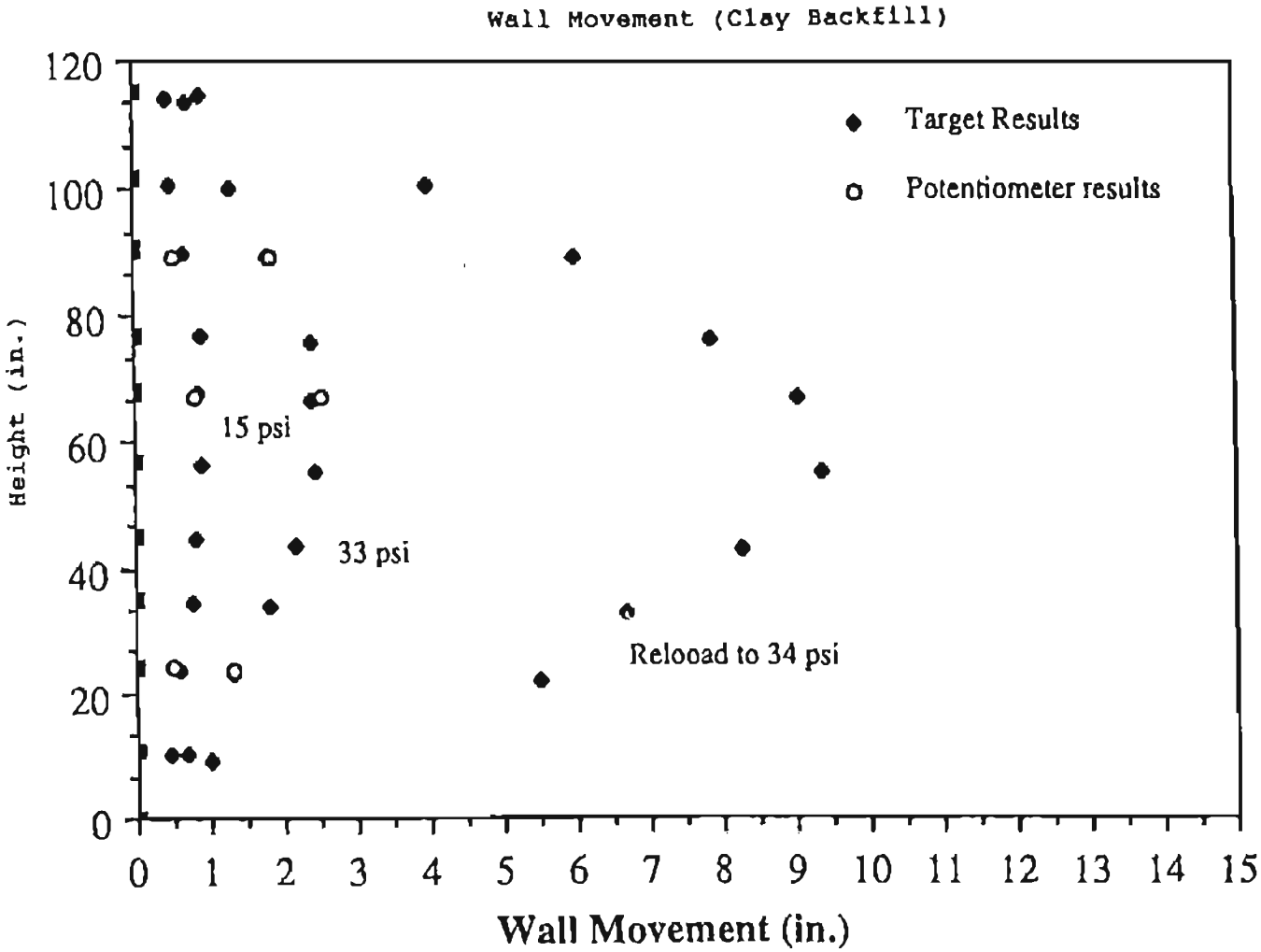

Figure 4.22: Measured Lateral Wall Displacement of the Cohesive Backfill Test Wall (After Wu, 1992)

The measured strains induced in the reinforcement for the granular and cohesive backfill walls are illustrated in Figures 4.23 and 4.24, respectively. It is to be noted that the loci of the maximum tensile strain deviate significantly from the Rankine Failure plane.

The granular backfill wall experienced much larger deformation than the previous pressure increments as the surcharge pressure was increased from 27 to 30 psi. At the 29 psi pressure, the air bags burst. The wall deformed very significantly again in the range of 27 to 29 psi when it was reloaded using new air bags. Failure was said to occur at 29 psi surcharge pressure. The final appearance of the wall facing is shown in Figure 4.25.

For the cohesive backfill wall, the largest deformations of the wall occurred as the surcharge pressure was increased from 30 to 33 psi. The air bags burst when the pressure reached 33 psi. The wall was later reloaded using new air bags that burst at a 34 psi surcharge pressure and the test was then terminated. Figure 4.26 shows the final appearance of the cohesive backfill wall. Although overall shear failures had not been reached at these surcharge pressures, it was evident that the wall was approaching failure. At the end of each test, fairly well-defined

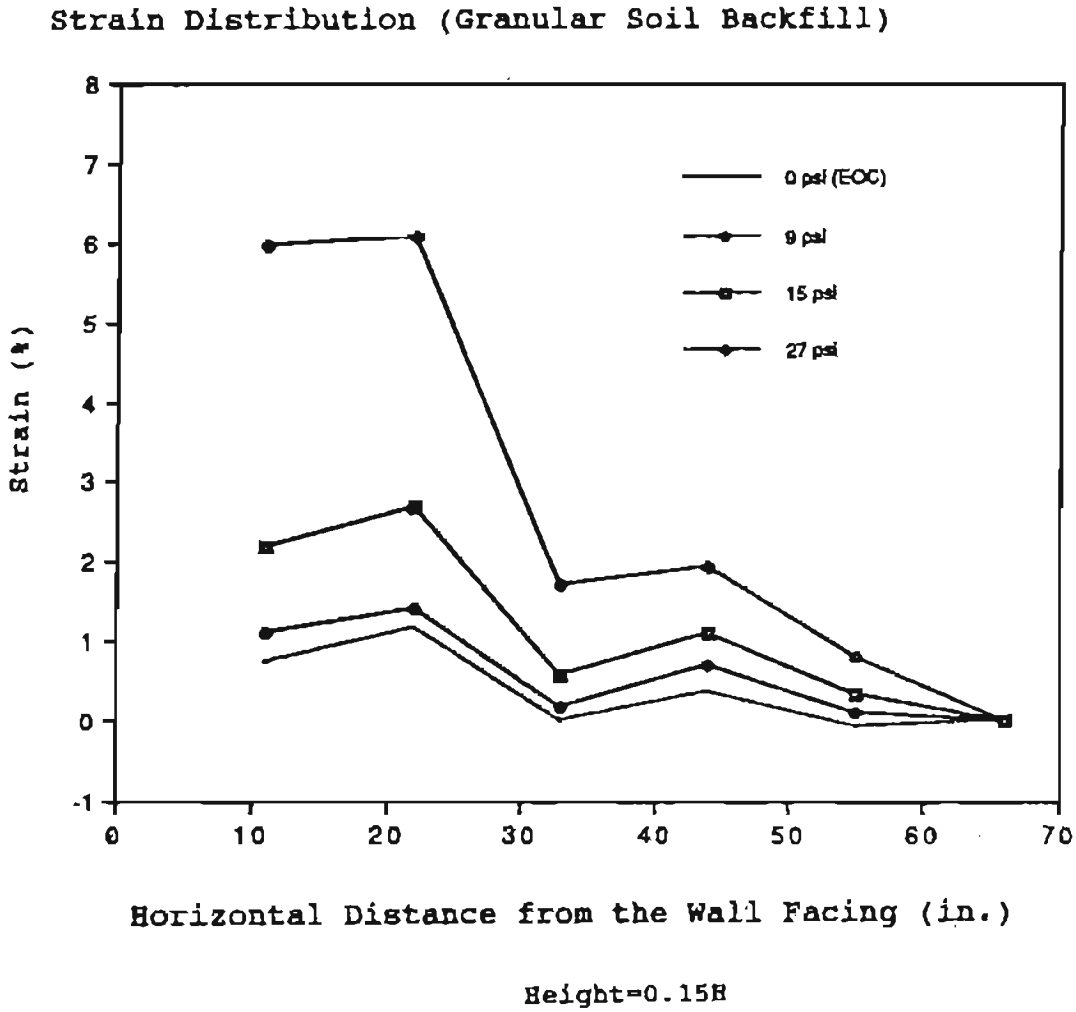

Figure 4.23a: Measured Strain Distribution in Reinforcement at Lower Level, Granular Backfill Wall (Wu, 1992)

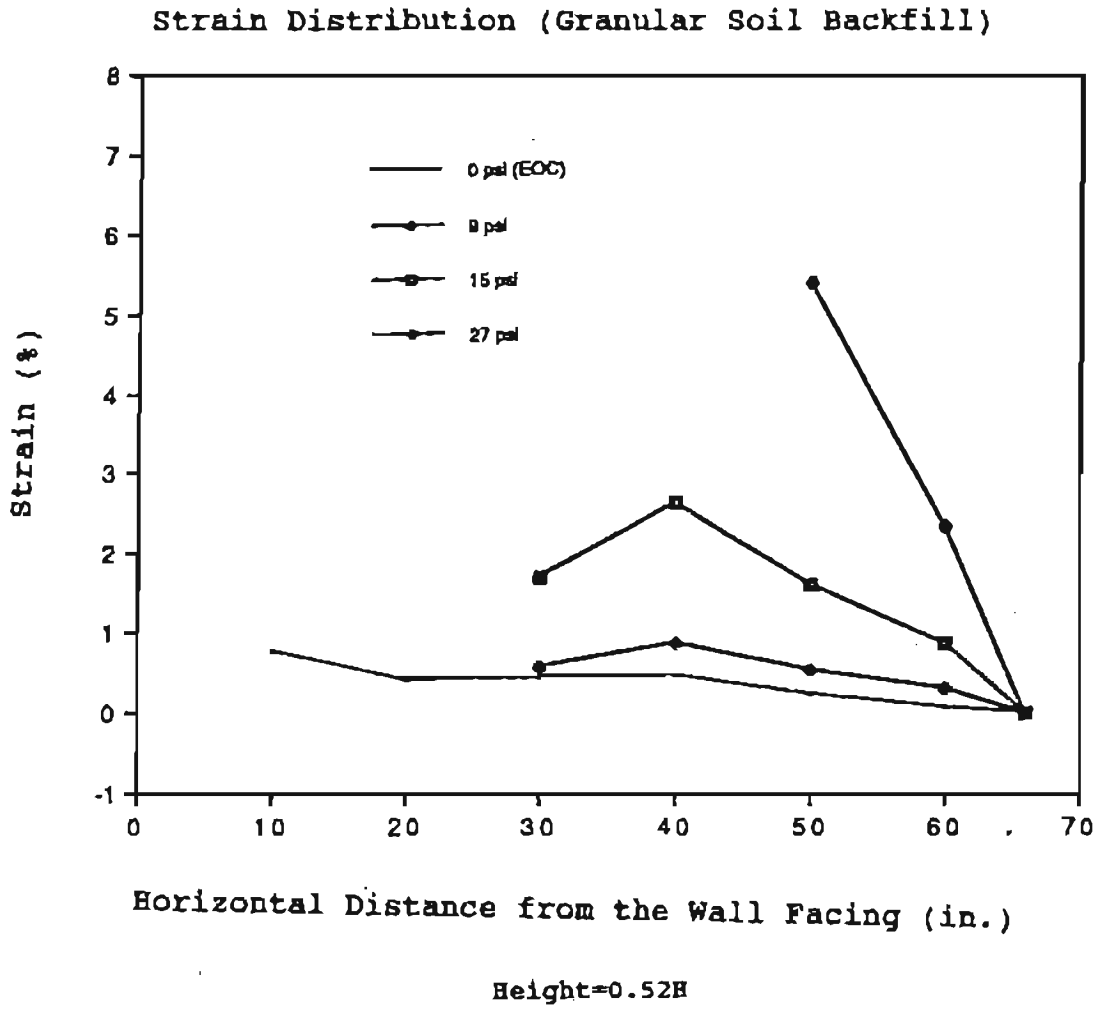

Figure 4.23b: Measured Strain Distribution in Reinforcement at Middle Level, Granular Backfill Wall (Wu, 1992)

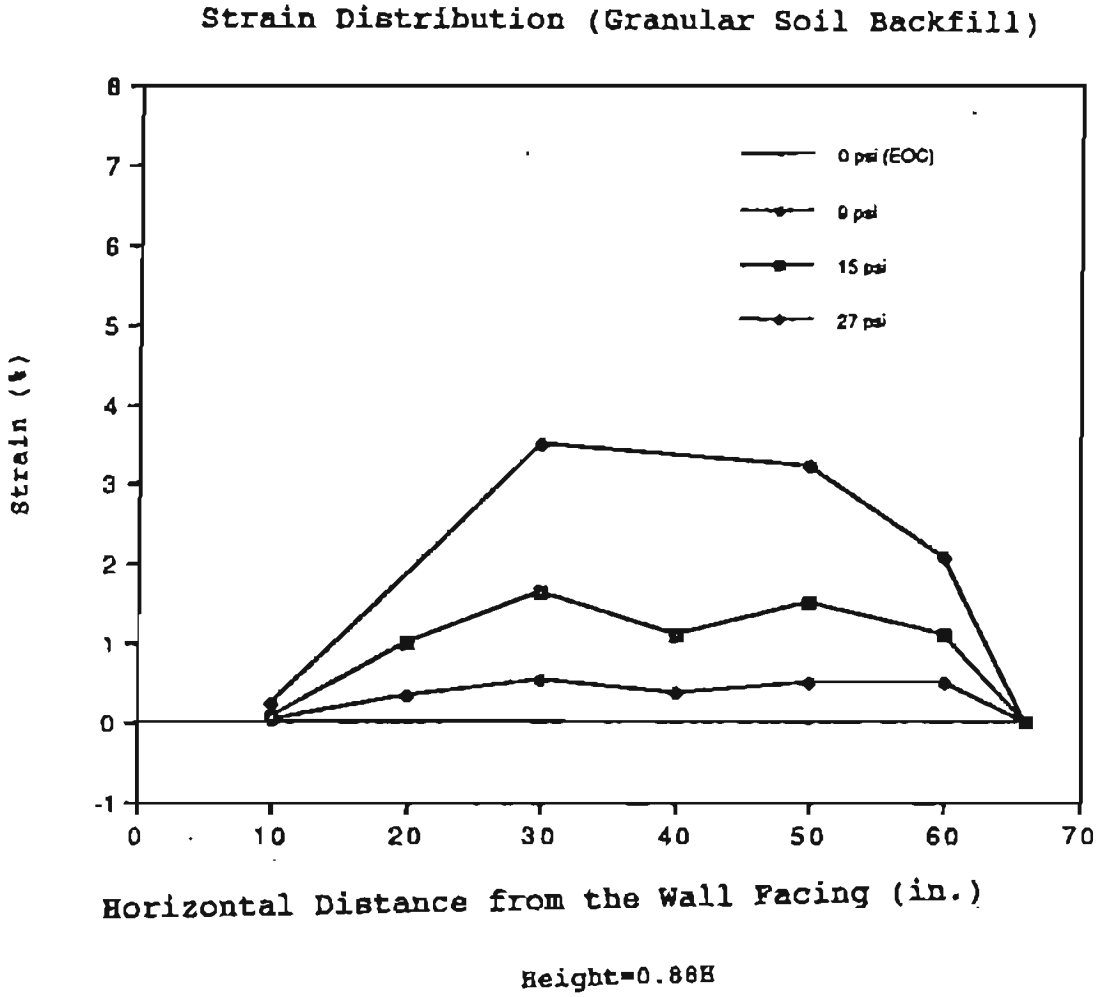

Figure 4.23c: Measured Strain Distribution in Reinforcement at Upper Level, Granular Backfill Wall (Wu, 1992)

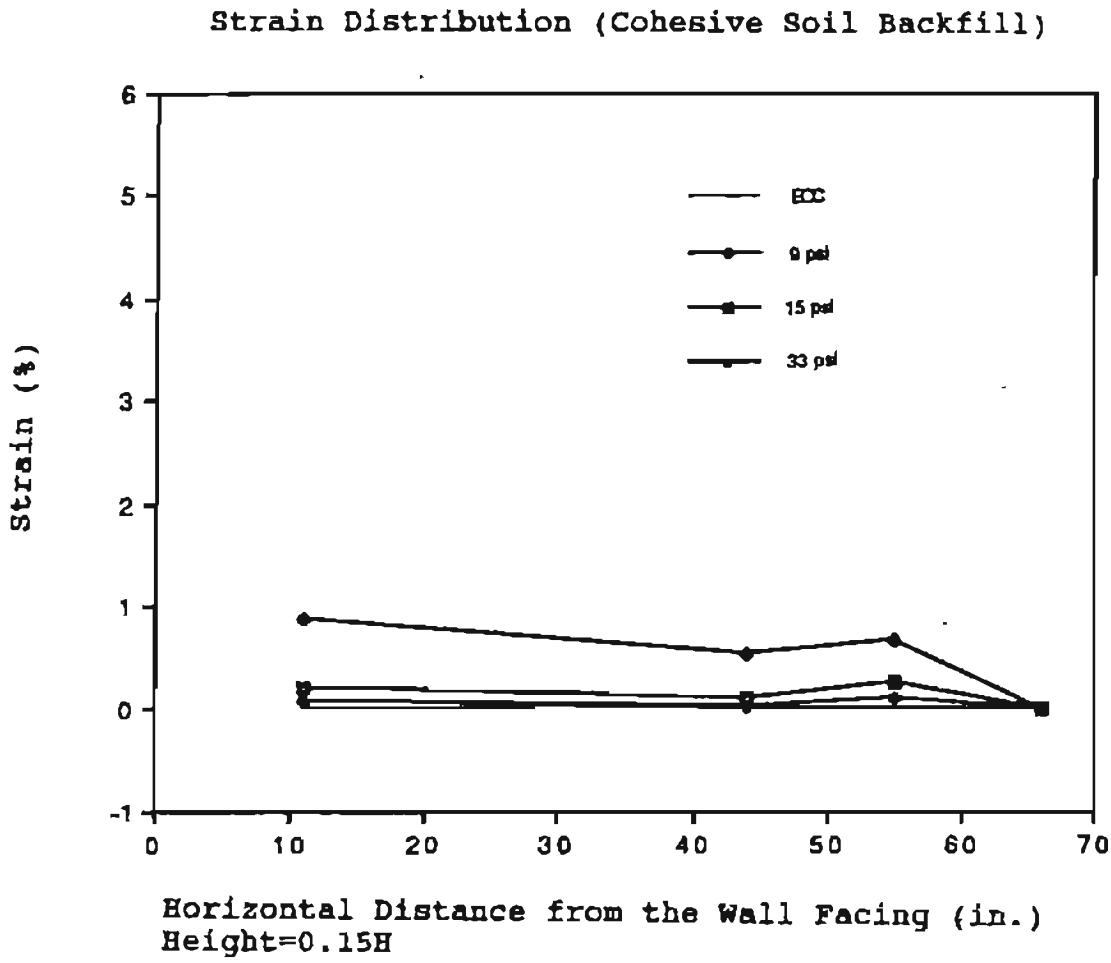

Figure 4.24a: Measured Strain Distribution in Reinforcement at Upper Level, Cohesive Backfill Wall (Wu, 1992)

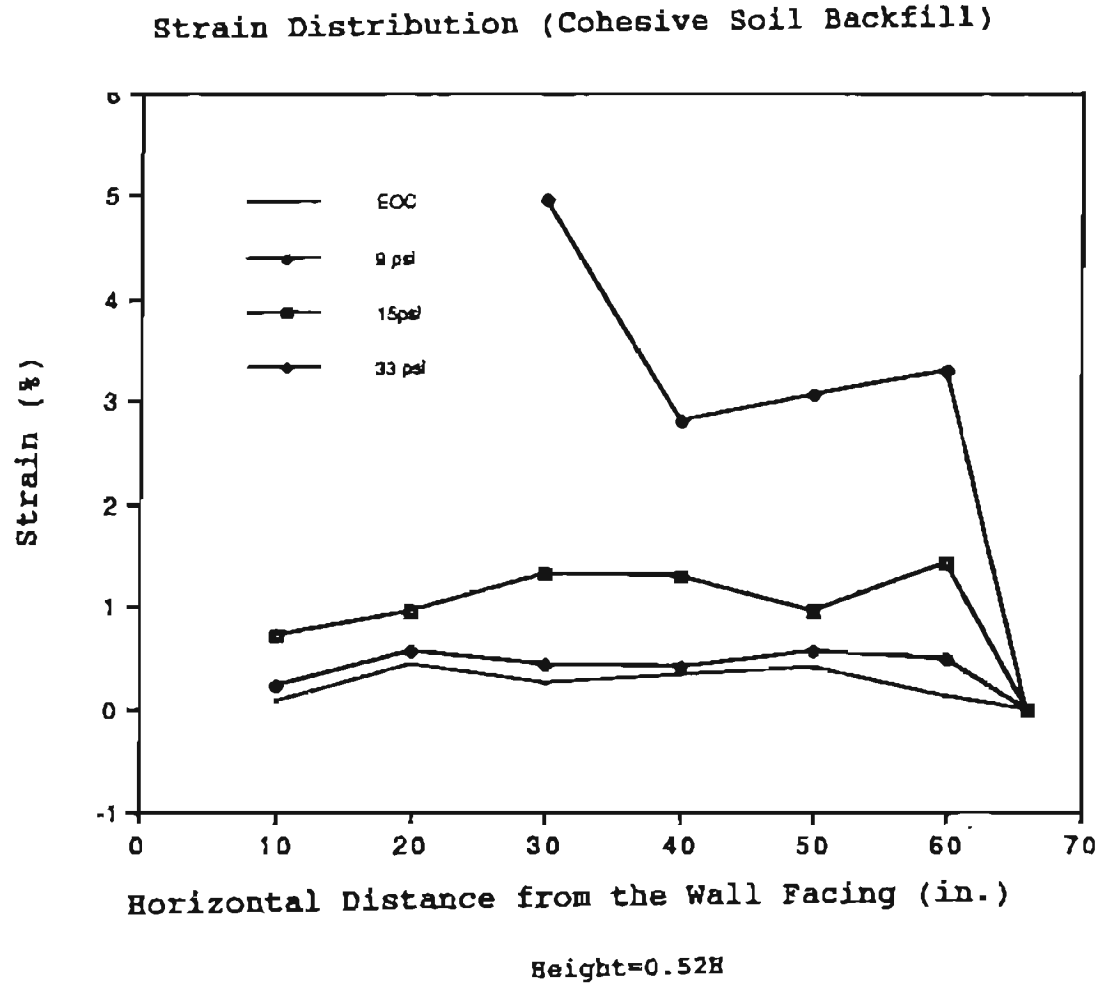

Figure 4.24b: Measured Strain Distribution in Reinforcement at Middle Level, Cohesive Backfill Wall (Wu, 1992)

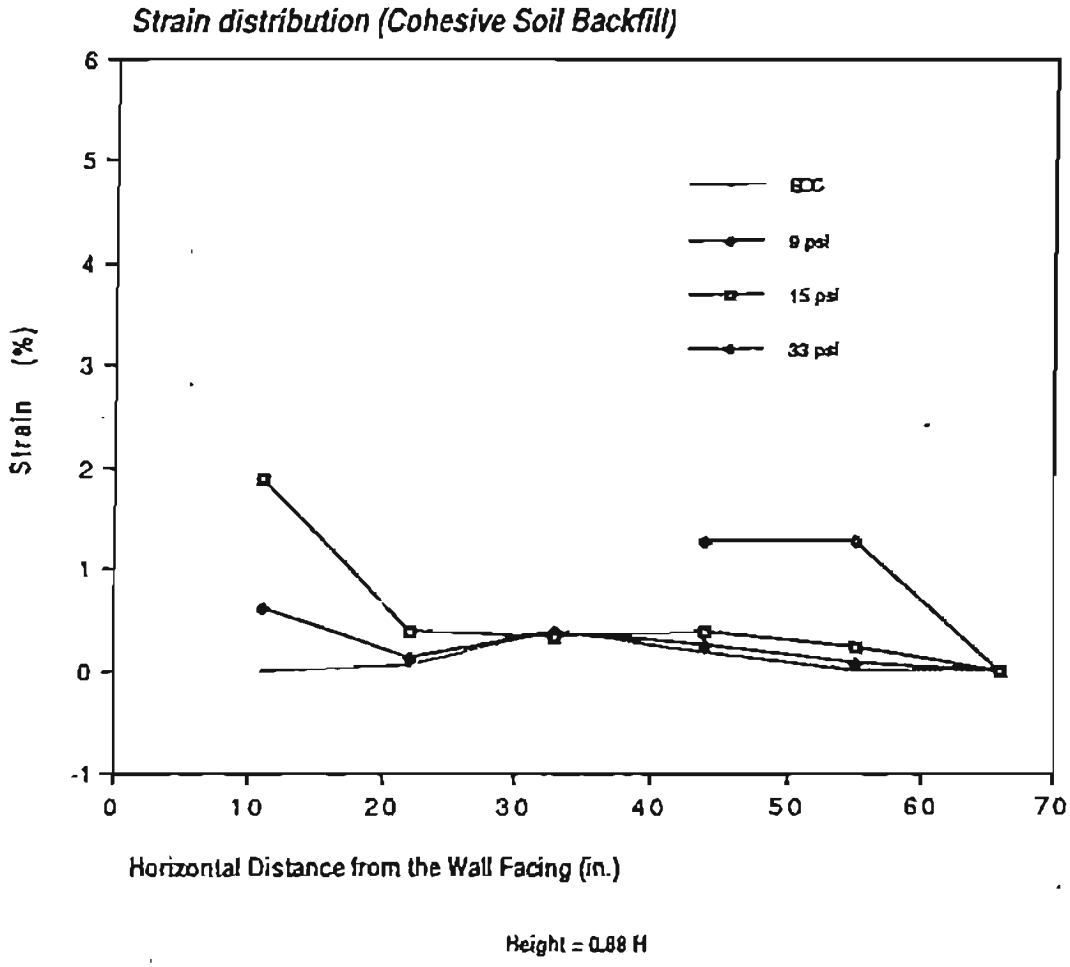

Figure 4.24c: Measured Strain Distribution in Reinforcement at Upper Level, Cohesive Backfill Wall (Wu, 1992)

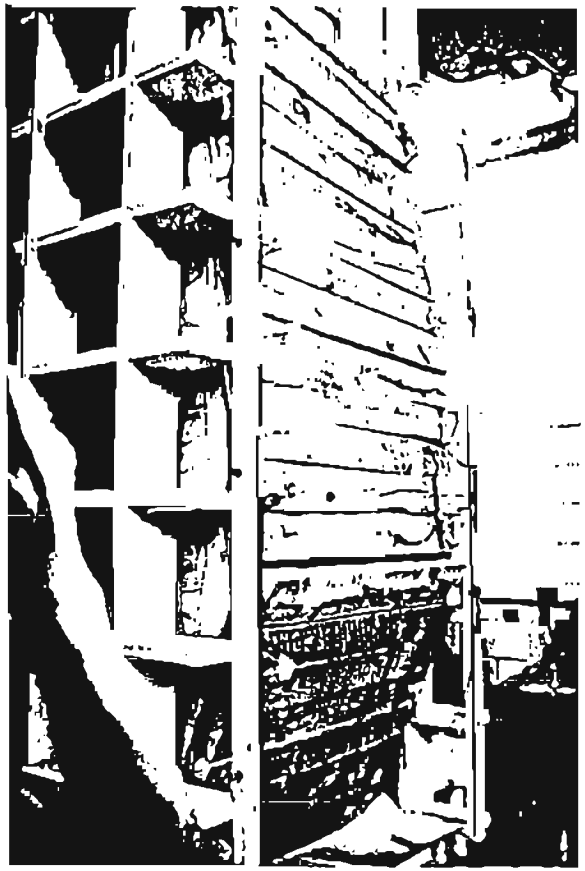

Figure 4.25: Final appearance of Granular Backfill Wall (after Wu, 1992)

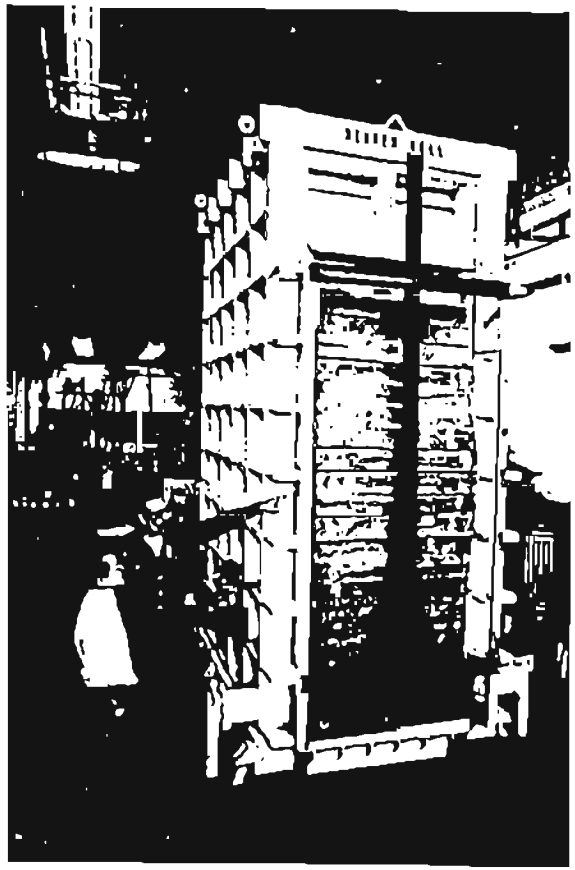

Figure 4.26: Final appearance of Cohesive Backfill Wall (after Wu, 1992)

shear bands were identified by visual inspections of the deformed latex membrane (see Figure 4.27).

The creep at 15 psi surcharge pressure was very small in both walls. The results before and after the 100-hour creep interval were therefore essentially identical at this surcharge load. However, the strains in the reinforcements recorded by an automated data acquisition system did show slight changes during the 100 hr interval.

4.8.5. Comparisons Between Predicted and Measured Results

This section compares the measured and predicted behavior of both the granular and cohesive backfill test walls. The predictions are based on the author's paper submitted for the Symposium (Chou, 1992).

An after-test analysis, including the behavior of the test walls under EOC, 9, 15, 27 (granular), and 33 (cohesive) psi surcharge pressures, will be discussed in the after-test analyses (Section 4.8.6).

4.8.5.1 Settlement and Lateral Facing Displacements

The predicted behavior at the end of construction for the granular and cohesive backfill walls is shown in Figures 4.28 and 4.29, respectively. The predicted top surface displacements (settlements) are negligible at the EOC for both test walls. Measurements of the movement of the latex grid points (through the transparent side wall plexiglass) indicated that the

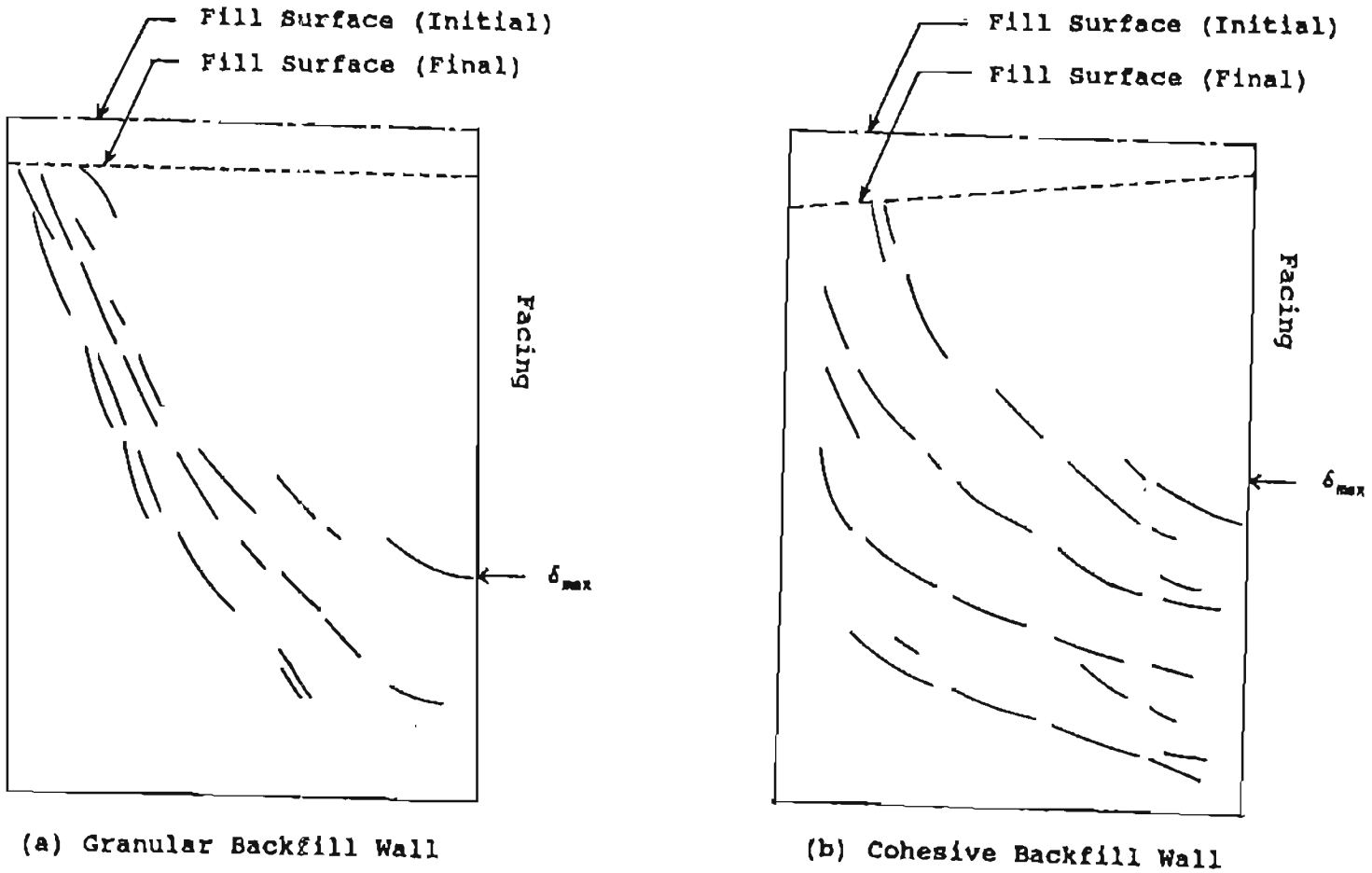

Figure 4.27: Shear Bands at the End of Test (after Wu, 1992)

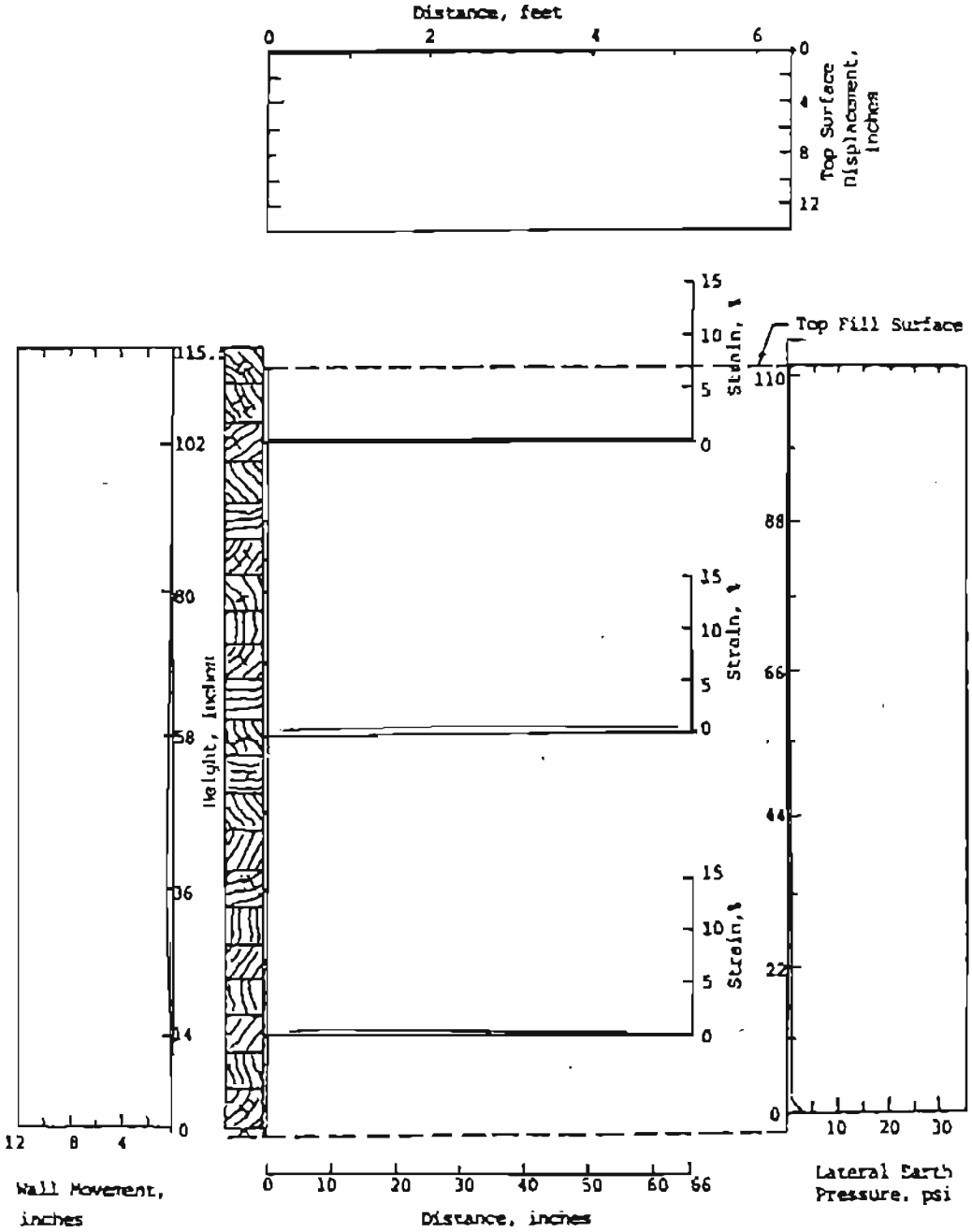

Figure 4.28: Predicted Wall Performance, with Granular Backfill, at End of Construction

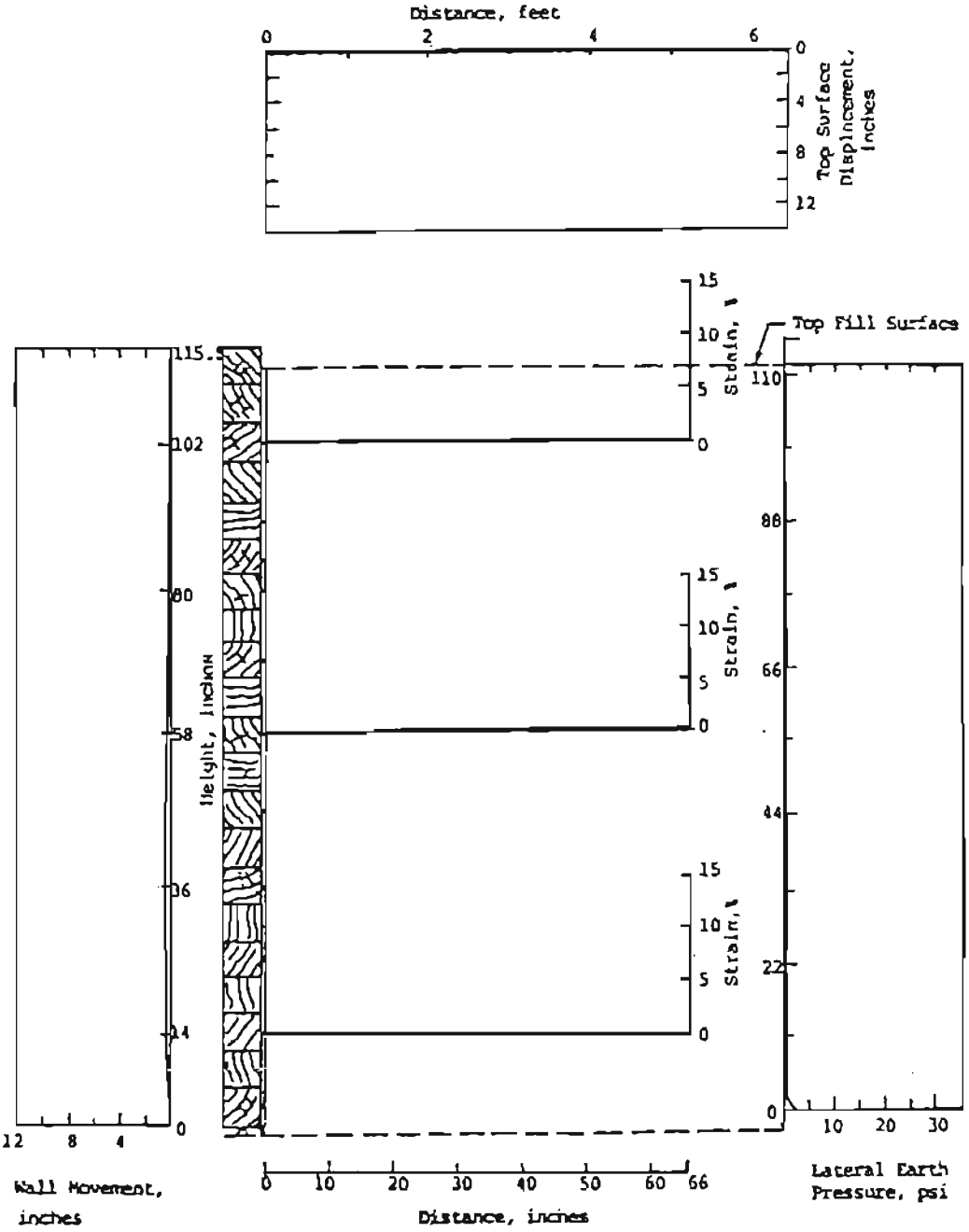

Figure 4.29: Predicted Wall Performance, with Cohesive Backfill, at End of Construction

vertical and horizontal displacements at the EOC were less than 1/4 inch. It should be noted that the top fill surface at the EOC was brought to the prescribed level (117 in. high) and was used as the reference line for measuring all the subsequent displacements. The predicted lateral facing displacements at the EOC also were negligible, which agreed well with the measurement.

The author predicted that the granular backfill test wall would fail at a surcharge of 12 psi. Therefore, no deformation data was available for comparison under 15 psi surcharge pressure.

The predicted performance of the cohesive backfill wall at the surcharge of 15 psi is shown in Figure 4.30. The predicted maximum facing displacement was 0.7 inches (compared with the measured 0.9 inches), and the predicted location of maximum facing deformation was at 0.40 H (H = wall height) from the base (compared with the measured 0.55 H). The predicted maximum settlement was 2.0 inches (compared with the measured 2.6 inches), and the predicted location of maximum settlement was at the far end of backfill, i.e., 1.0 L (L = length) from facing (compared with the measured 0.6 L). The author's prediction was quite good compared with the other predictions submitted to the Symposium.

4.8.5.2 Axial Strains in the Reinforcement

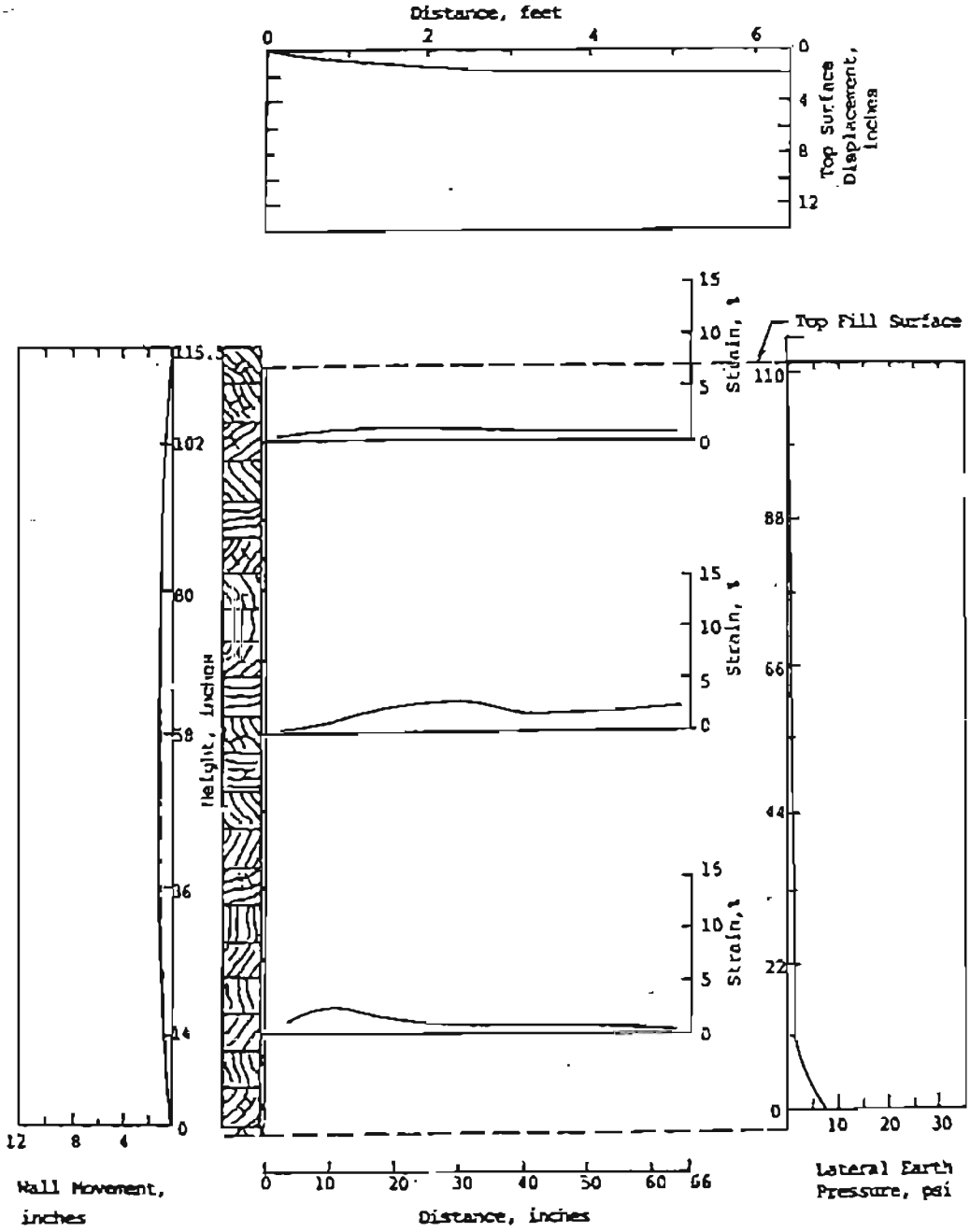

Figure 4.30: Predicted Wall Performance, with Cohesive Backfill, at 15 psi Surcharge Pressure.

The predicted tensile strain distribution in the reinforcement at three different heights: 0.15 H, 0.52 H, and 0.88 H are presented in Figure 4.28 for the granular backfill wall, and in Figures 4.29 and 4.30 for the cohesive backfill wall. The predicted reinforcement strains were negligible at the EOC conditions, which agreed with the measured behavior for both walls. For the cohesive backfill wall, at the surcharge pressure of 15 psi, the author's predictions vs. measurements were as follows:

Max. Strain in Reinforcement

Location	Predicted (%)	Measured (%)
Lower level	2.5	0.3
Middle level	2.6	1.3
Upper level	1.5	1.9

Among the predictions submitted, the author's prediction was among the most accurate on the maximum strain, location and area of the strain distribution (Wu, et. al., 1992d).

4.8.5.3 Failure Conditions

The author predicted that a 12 psi surcharge pressure would cause failure (compared with the measured 29 psi) in the granular backfill test wall. The author further predicted that when the surcharge reached 12 psi, a failure plane would be fully

developed and an external instability of the wall would be visible (see Figure 4.31).

For the cohesive backfill wall, the author predicted the surcharge pressure at failure would be 27 psi (compared with the measured > 34 psi). The author also predicted that reinforcement rupture would occur in several layers of geotextile (see Figure 4.32).

4.8.6 After-Symposium Analyses

After the Symposium, the author performed some additional analyses involving the following modifications:

(1) The front drop gate of the loading facility, used to prevent the backfill and surcharge from leaking, was included in the analysis. The boundary condition of the gate was simulated by rollers. The rollers significantly reduced the calculated lateral deformations near the top of the test walls. The predicted overall performance of the walls were moderately improved, especially for the granular backfill wall.

(2) The surcharge sand placed on the top of the test walls was included in the analysis as soil elements, instead of treating it as an equivalent 3 psi surcharge pressure (in the original prediction). The restraint due to surcharge sand reduced the lateral deformation of the walls.

Failure Condition:

(a) Surcharge Pressure at Failure = 12 lb/in^2.
or
Fill Height at Failure = _____ ft.

(b) Failure Mode: (description)
Shear failure will start to develop between the reinforced and unreinforced zones when the surcharge reaches 6 psi. However, the wall remains stable and the deformations are small. When the surcharge increases to 12 psi, the failure plane will be fully developed and the wall collapsed.

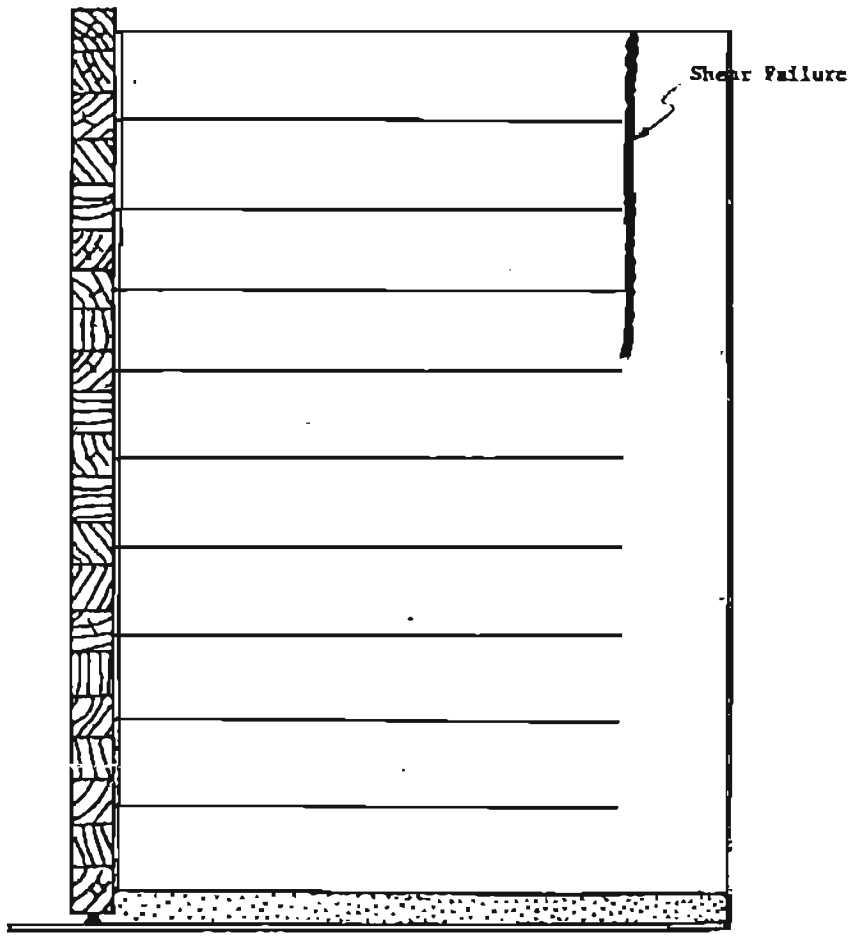

Figure 4.31: Predicted Failure Condition, Granular Backfill Test Wall

Failure Condition:

(a) Surcharge Pressure at Failure = 27 lb/in^2.
or
Fill Height at Failure = _____ ft.

(b) Failure Mode: (description)
Large deformations are expected when surcharge reaches 24 psi. Tension breaks are anticipated in geotextile when surcharge pressure reaches 27 psi, as marked.

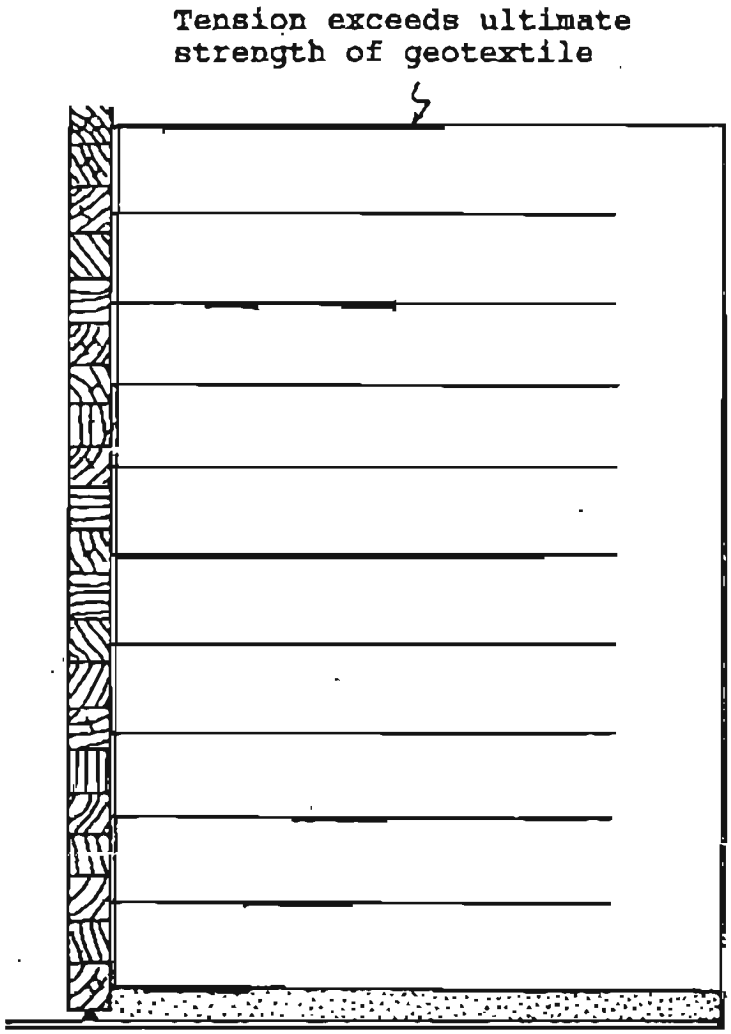

Figure 4.32: Predicted Failure Condition, Cohesive Backfill Test Wall

(3) For the cohesive backfill test wall, the actual time involved in construction and loading may allow partial dissipation of the porewater pressure. The drainage conditions of the soil should be somewhere between fully drained and fully undrained conditions. The author's original prediction was based on the triaxial CU test parameters and was therefore modified. In this after-test analyses, the average values obtained from the CU and CD tests were used. The revised Duncan-Chang soil parameters for the cohesive backfill wall analyses were: C=6.05 psi, ϕ=19 deg., Kb=70, m=0, Kur=100, K=121, n=0.13, and Rf=0.87. The revised parameters, with a higher ϕ angle and a lower cohesion, result in a better simulation.

4.8.6.1 Settlement and Lateral Facing Displacements

The settlements at the top surface of backfill and the lateral facing displacements, calculated by the after-test FEM analyses, are shown in Figures 4.33 through 4.36. To focus on the service load condition, the measured and predicted values under a surcharge pressure of 9 psi were added to the comparisons. Since in this analysis, the predicted failure surcharge pressure was greater than 15 psi for the granular backfill wall, it allowed the predicted wall displacements to be compared with the measured results.

The calculated and measured maximum settlements and lateral wall displacements for both the granular

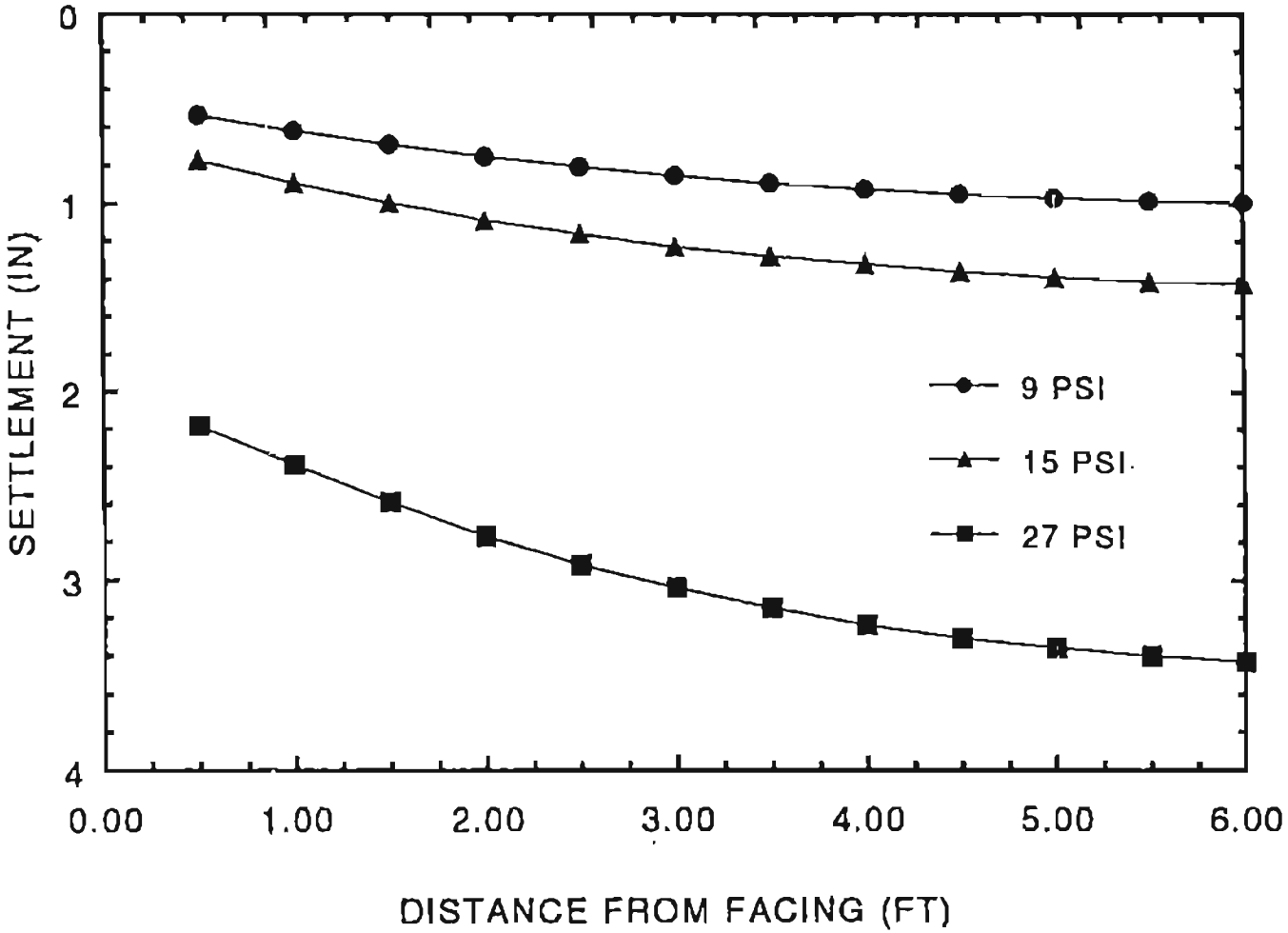

Figure 4.33: After-Test Simulation of Top Surface Settlement, Granular Backfill Test Wall

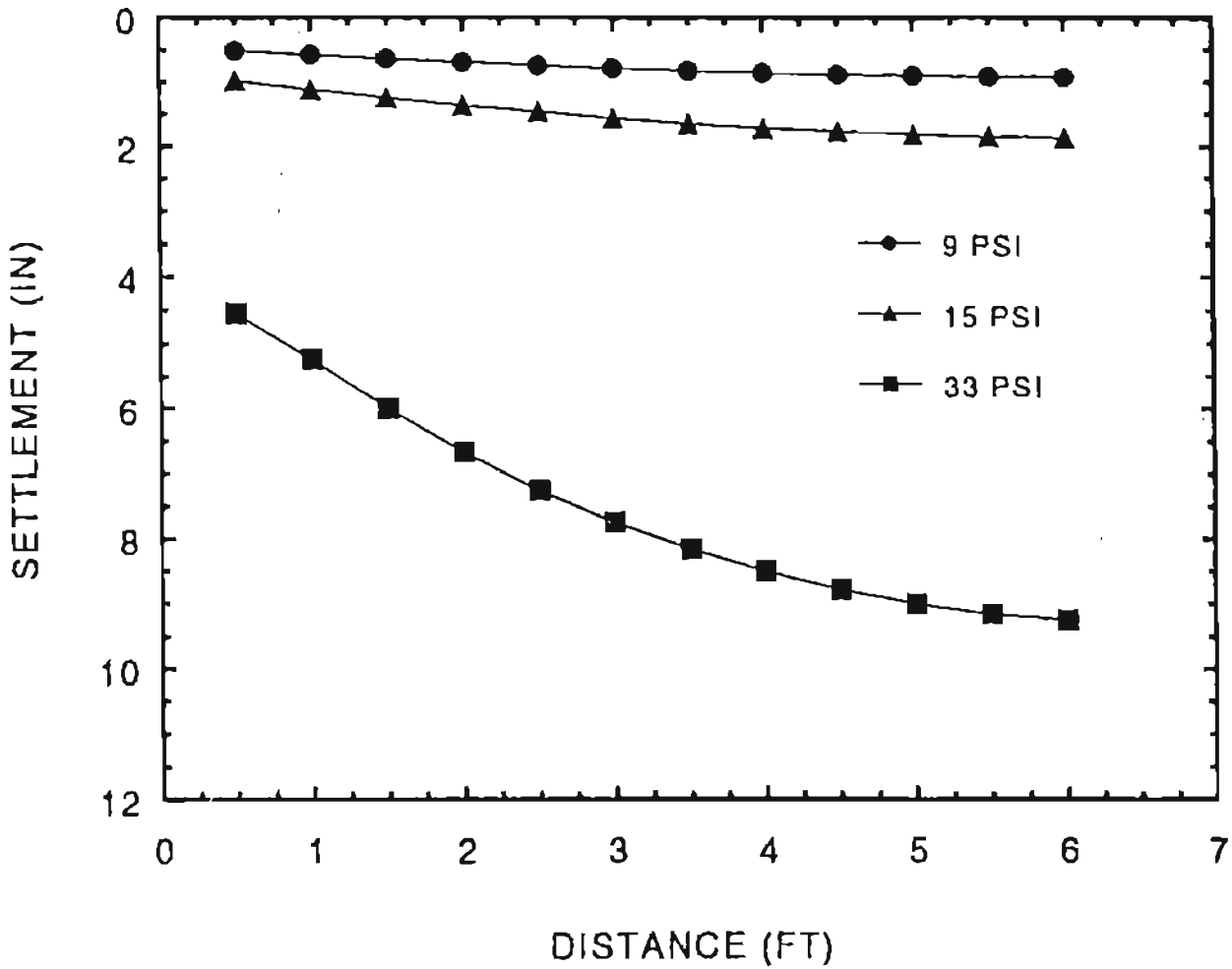

Figure 4.34: After-Test Simulation of Top Surface Settlement, Cohesive Backfill Test Wall

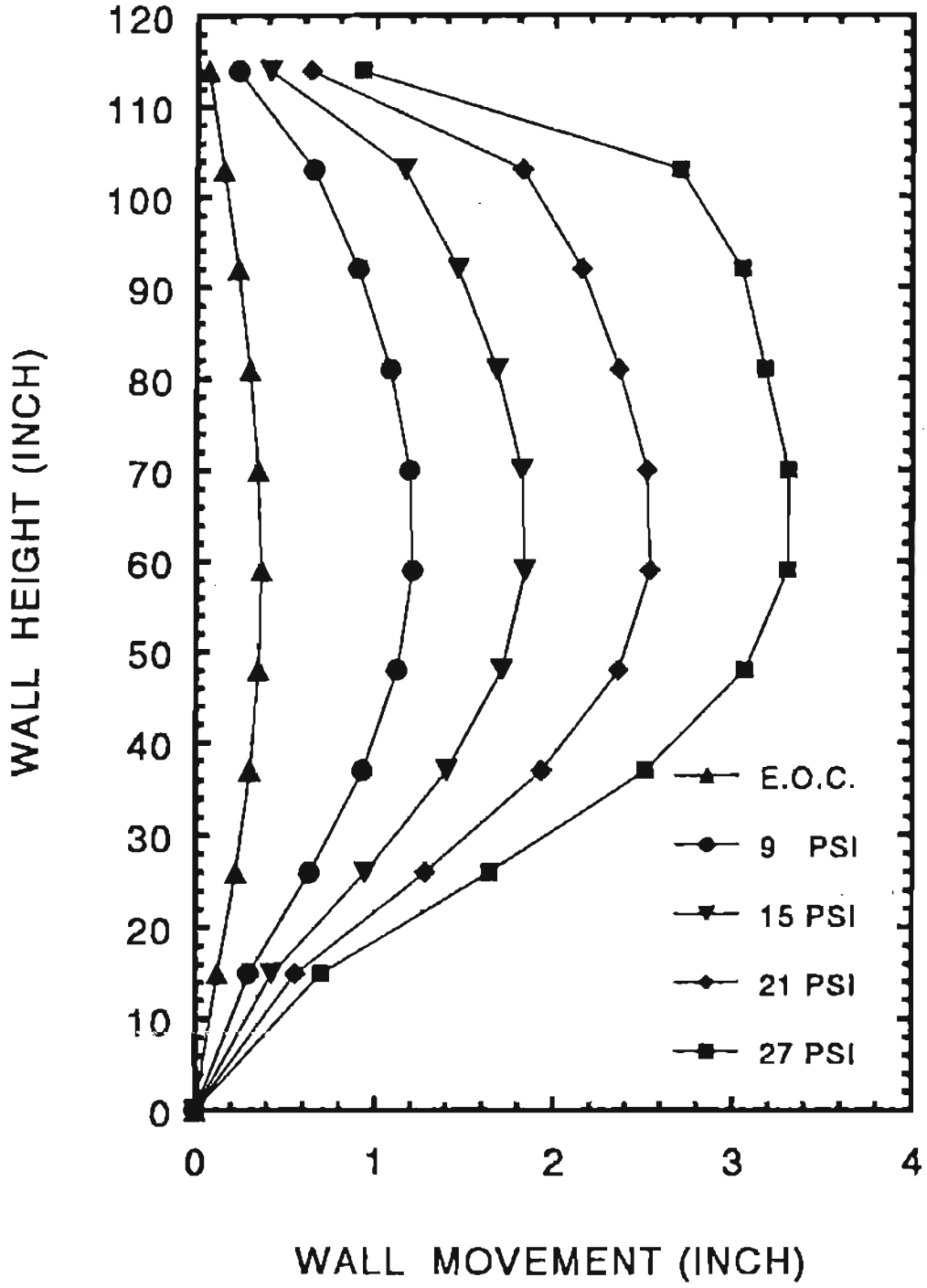

Figure 4.35: After-Test Simulation of Lateral Wall Displacements, Granular Backfill Test Wall

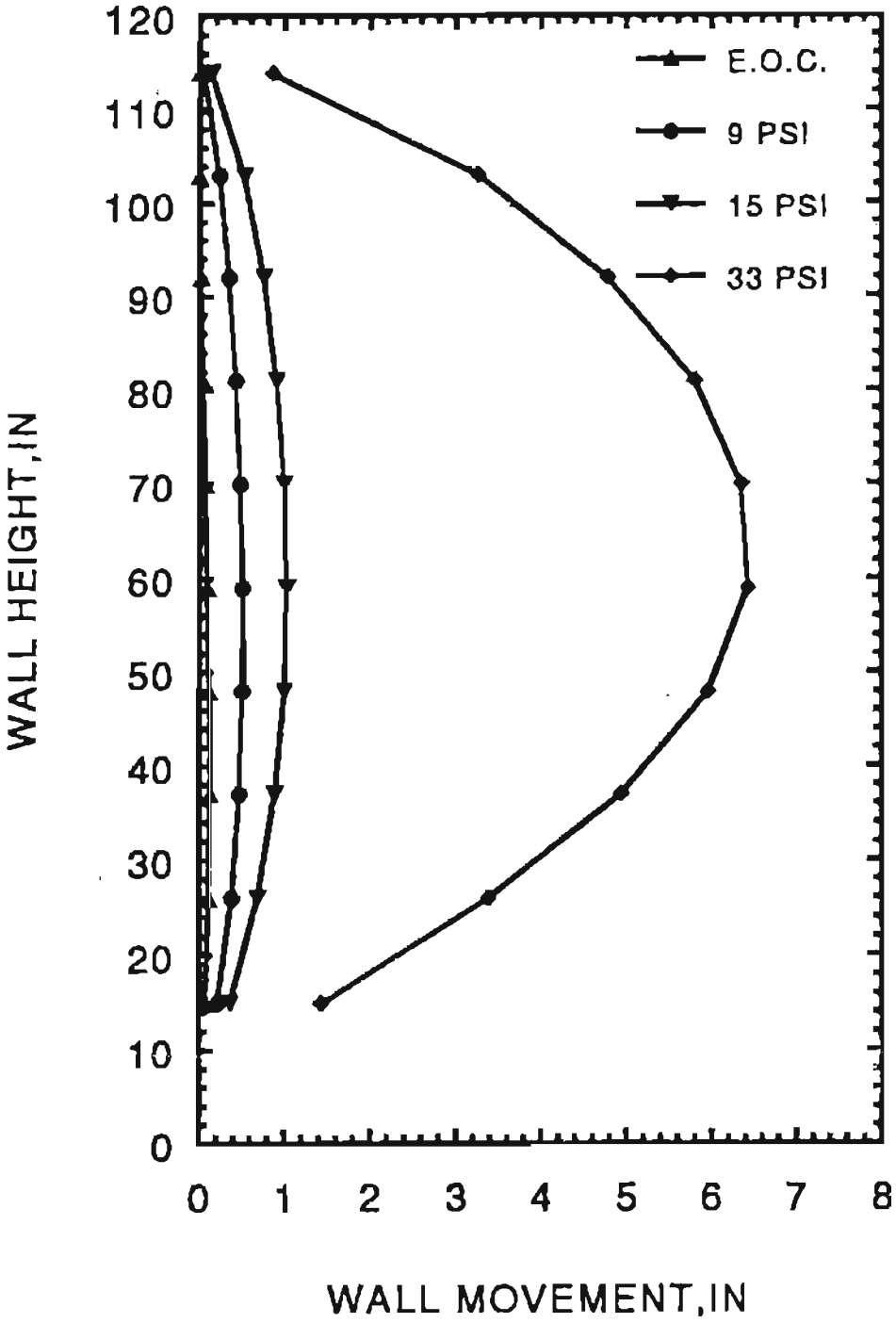

Figure 4.36: After-Test Simulation of Lateral Wall Displacement, Cohesive Backfill Test Wall

Table 4.3: Duncan-Chang Soil Parameters Used in Prediction of the Denver Test Walls

Backfill	c psi	ϕ degrees	K	n	R_f	K_b	m	K_{ur}	K_o	$\Delta\phi$
Sand	0.5	38.4	1116	0.66	0.87	907	0	1500	0.38	2
Sandy Clay	7.47	15.0	370	0.28	0.98	210	0	500	0.5	0

Table 4.4: Comparison of Simulated and Measured Wall Settlements and Lateral Displacements

Surcharge	Max. Settlement		Max. Lateral Movement	
	Simulated (in)	Measured (in)	Simulated (in)	Measured (in)
(Granular Wall)				
9 psi	1.0	1.6	0.8	0.9
15 psi	1.4	2.0	1.4	1.5
27 psi	3.4	4.1	2.9	4.1
(Cohesive Wall)				
9 psi	1.0	1.6	0.6	0.5
15 psi	1.9	2.5	1.0	1.0
33 psi	9.2	6.3	6.4	2.6

and cohesive backfill walls are compared in Table 4.4. Both the calculated settlements and lateral displacements were slightly less than the measured values for the granular backfill test wall. For the cohesive backfill wall, the calculated and measured settlements and lateral displacements were very close under the surcharge pressures of 9 and 15 psi. The calculated settlement and lateral displacement are larger than the measured values under the surcharge pressure of 33 psi. The simulation is considered satisfactory.

4.8.6.2 Backfill Displacement

The calculated and measured granular backfill displacements (at surcharge pressures of 9, 15, 29 psi) are shown in Figures 4.37 and 4.38, respectively. The simulated deformations are about half of the measured values.

The simulated and measured cohesive backfill displacements (at surcharge pressures of 9, 15, 33 psi) are shown in Figures 4.39 & 4.40, respectively. The simulated displacements were also less than the measured values, but the differences are less. However, the simulated pattern of the displacements agreed well with the measurement for both walls.

4.8.6.3 Axial Strains in the Reinforcement

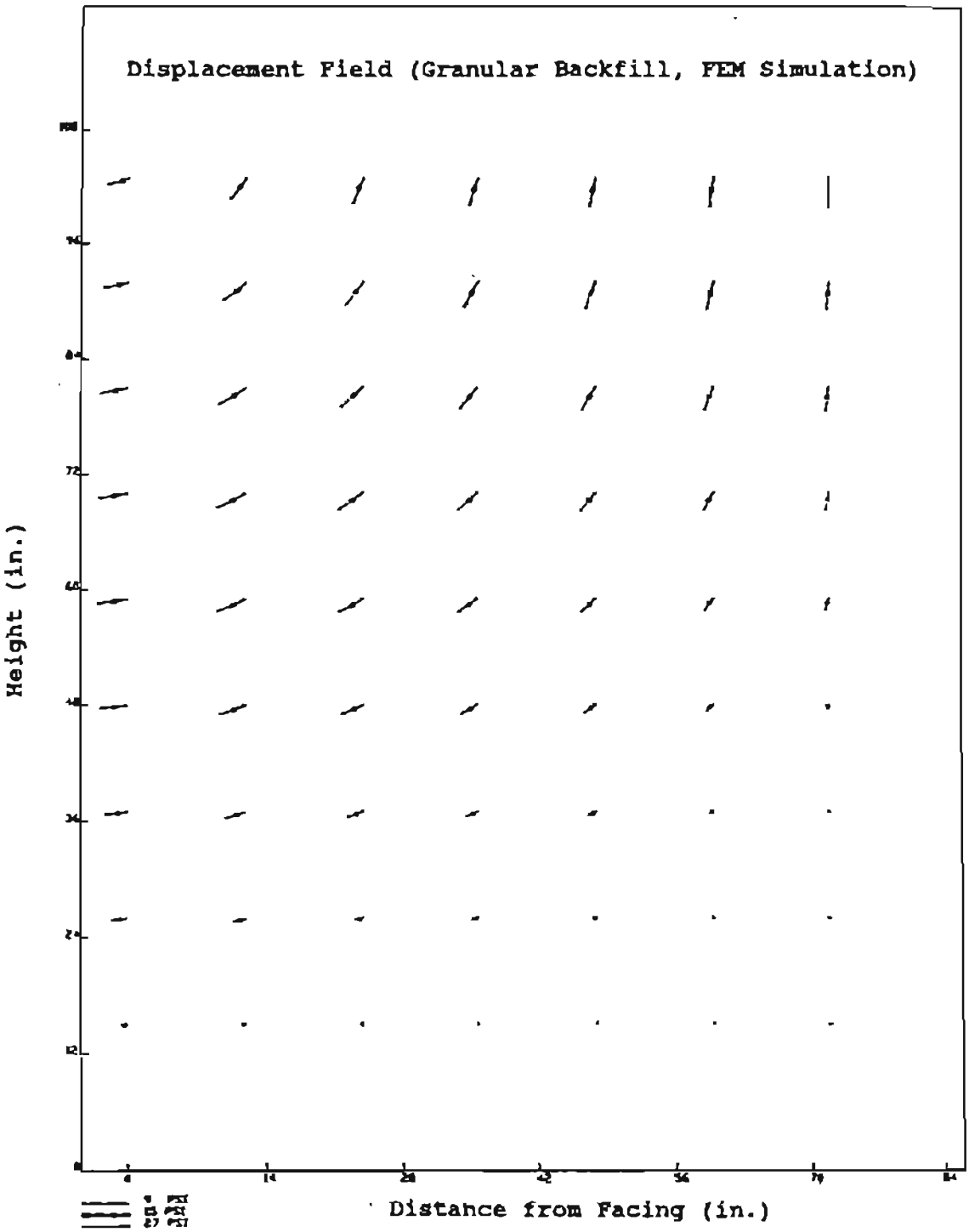

Figure 4.37: After-Test Simulation of Backfill Displacements for Granular Backfill Wall

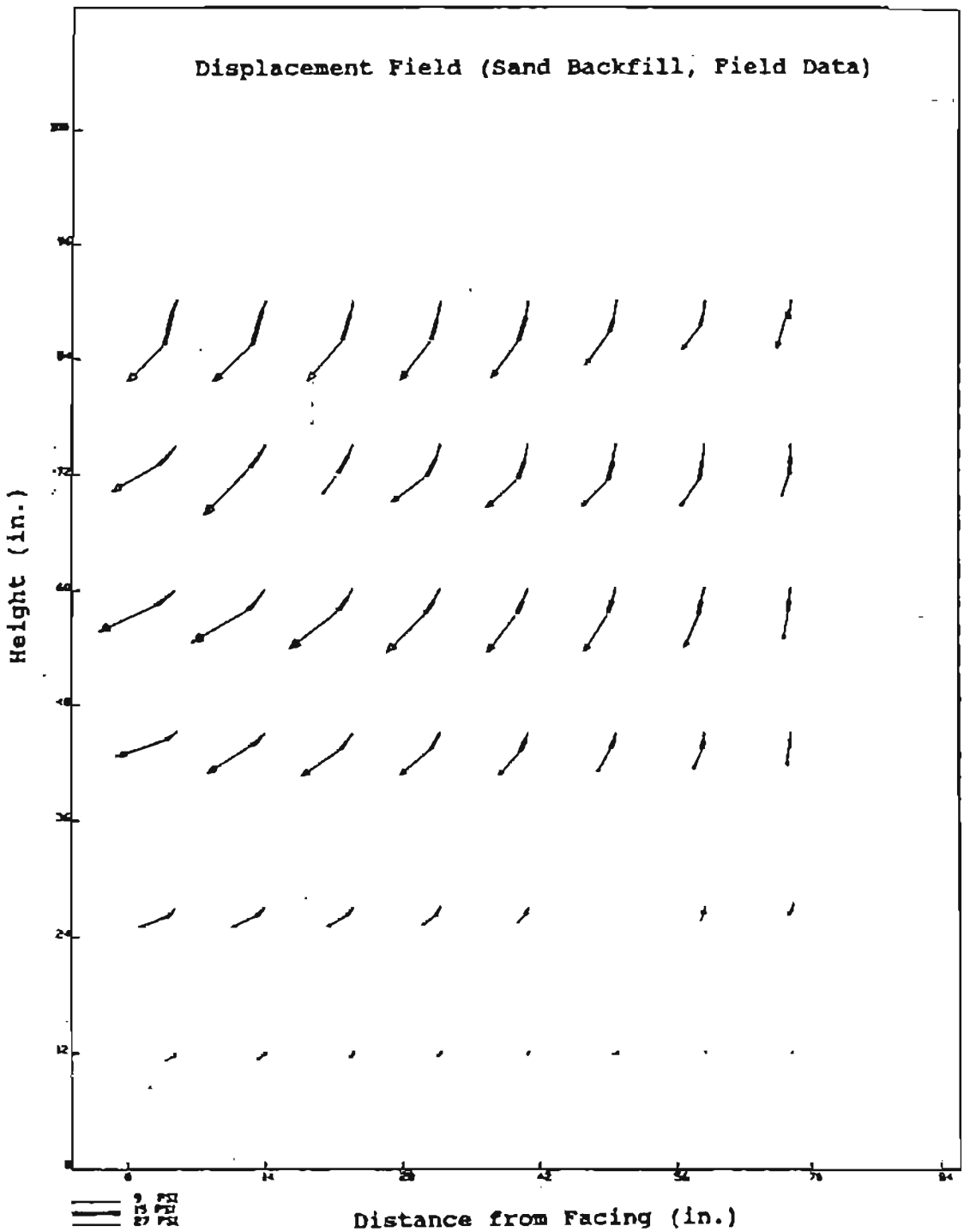

Figure 4.38: Measured Backfill Displacements for Granular Backfill Wall

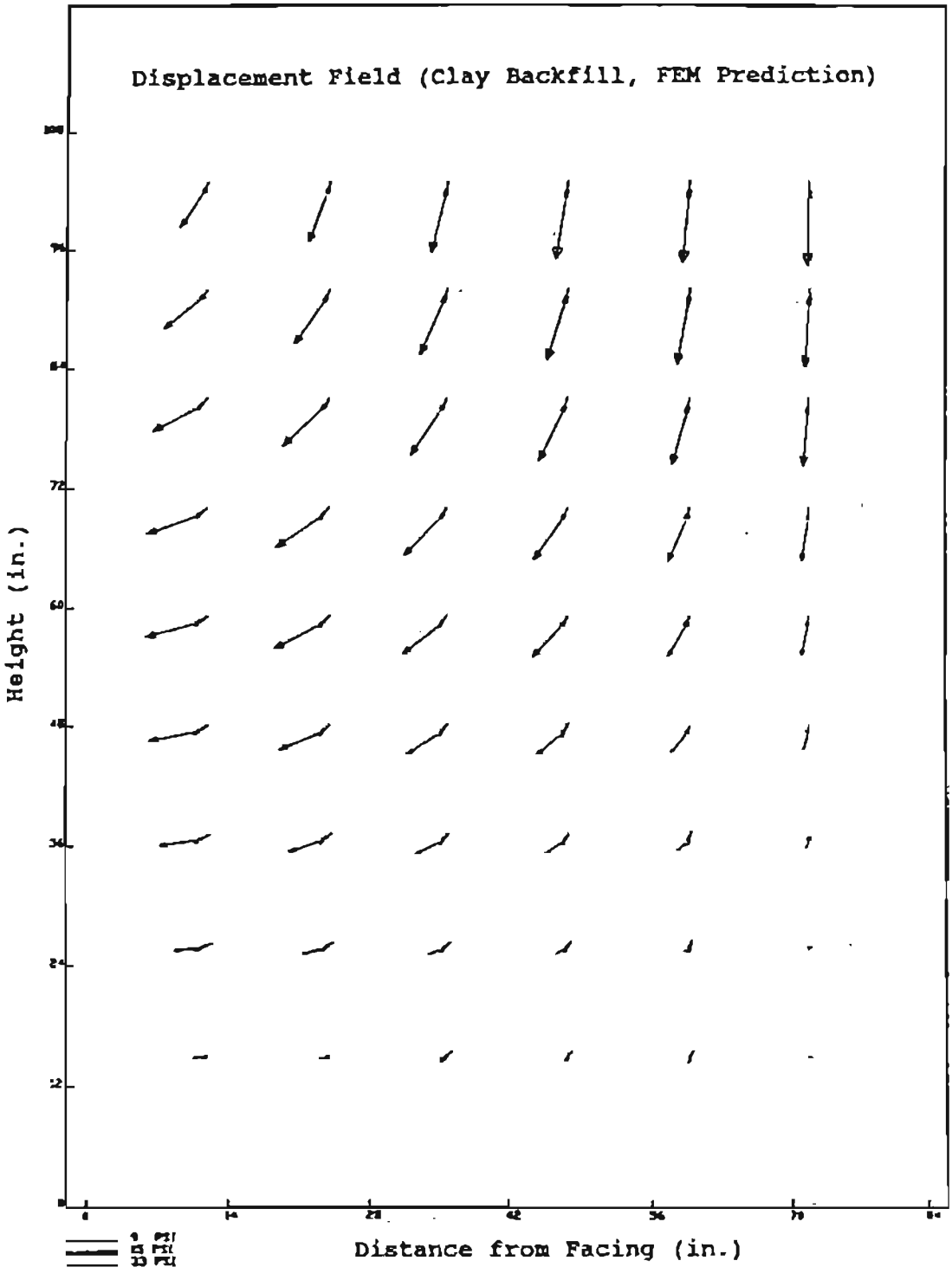

Figure 4.39: After-Test Simulation of Backfill Displacements for Cohesive Backfill Wall

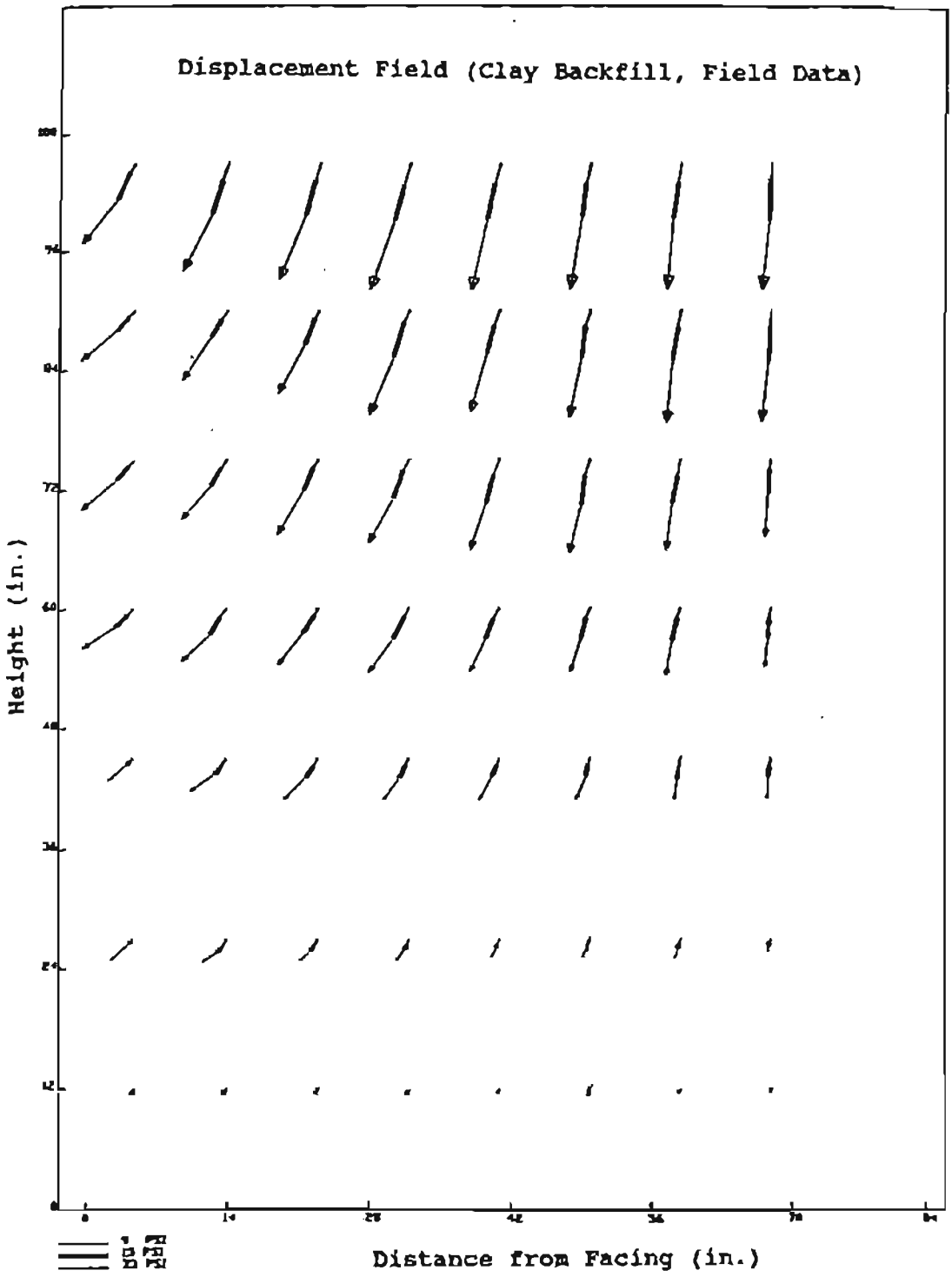

Figure 4.40: Measured Backfill Displacements for Cohesive Backfill Wall

The predicted tensile strains in the reinforcement for the granular and cohesive backfills are shown in Figures 4.41 and 4.42, respectively. The after-test simulation gave small tensile strains at the end of construction for both walls. This is probably due to the fact that construction-related strains are difficult to simulate. For example, the granular backfill wall exhibited high tensile strains (up to 1.2% and 0.75%, respectively) in the lower and middle level reinforcements, but negligible strains in the upper reinforcement. On the other hand, the cohesive backfill wall exhibited negligible strains in the lower level reinforcement, but up to 0.4% strain in the middle and upper reinforcement. The simulation of reinforcement strains under the service loads, i.e., 9 and 15 psi surcharge pressures, is considered satisfactory.

The simulated locations of the maximum tensile strains were near the facing at the bottom of the wall, at or close to the backface of the wall at the middle level, and either close to or far from the facing at the upper level.

In conclusion, when the front drop gate and the surcharge sand were included in the analysis, the simulation of the granular backfill test wall behavior

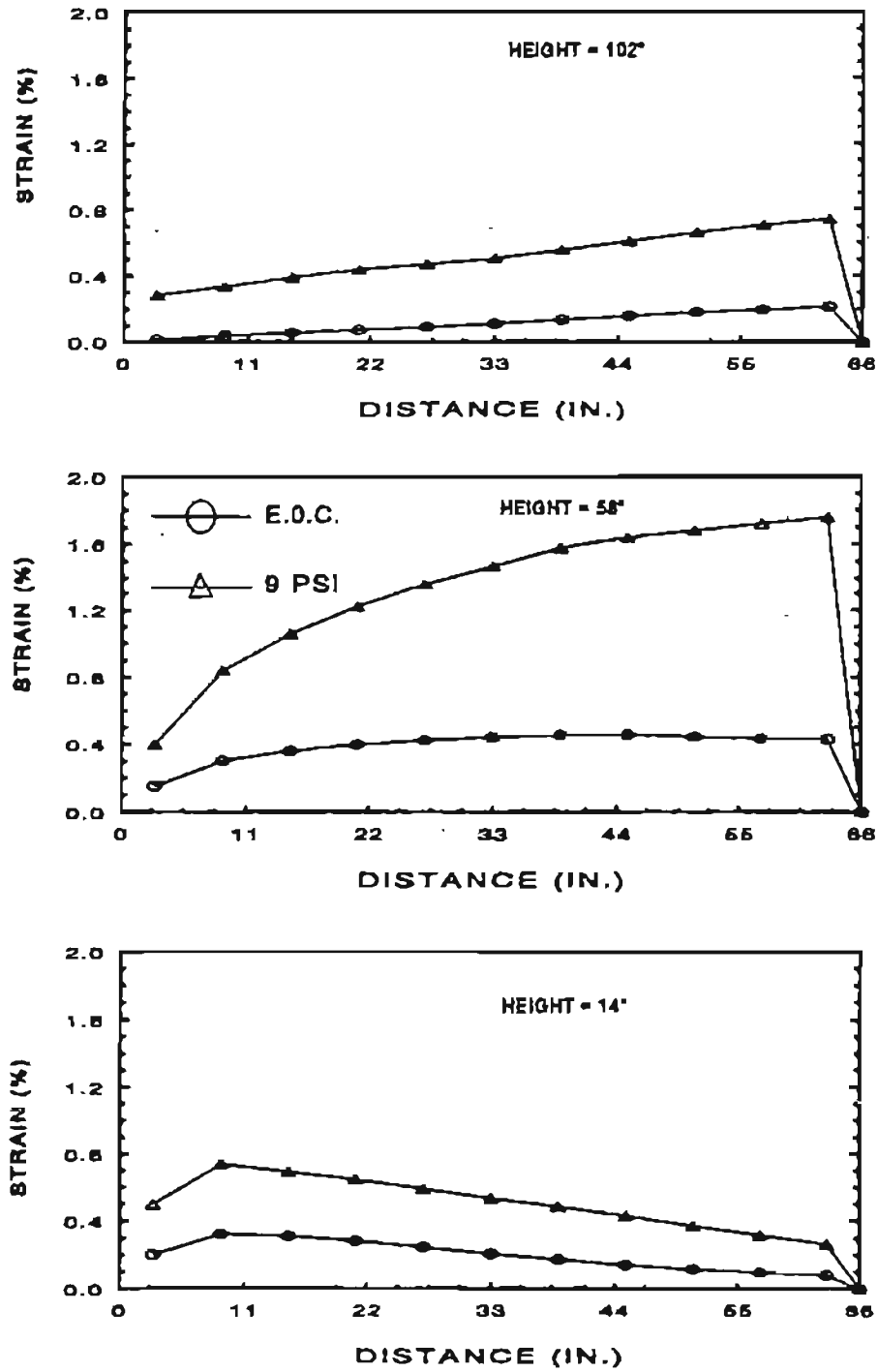

Figure 4.41a: After-Test Simulation of Strains in Reinforcement, with Granular Backfill, EOC & 9 psi Surcharge pressure

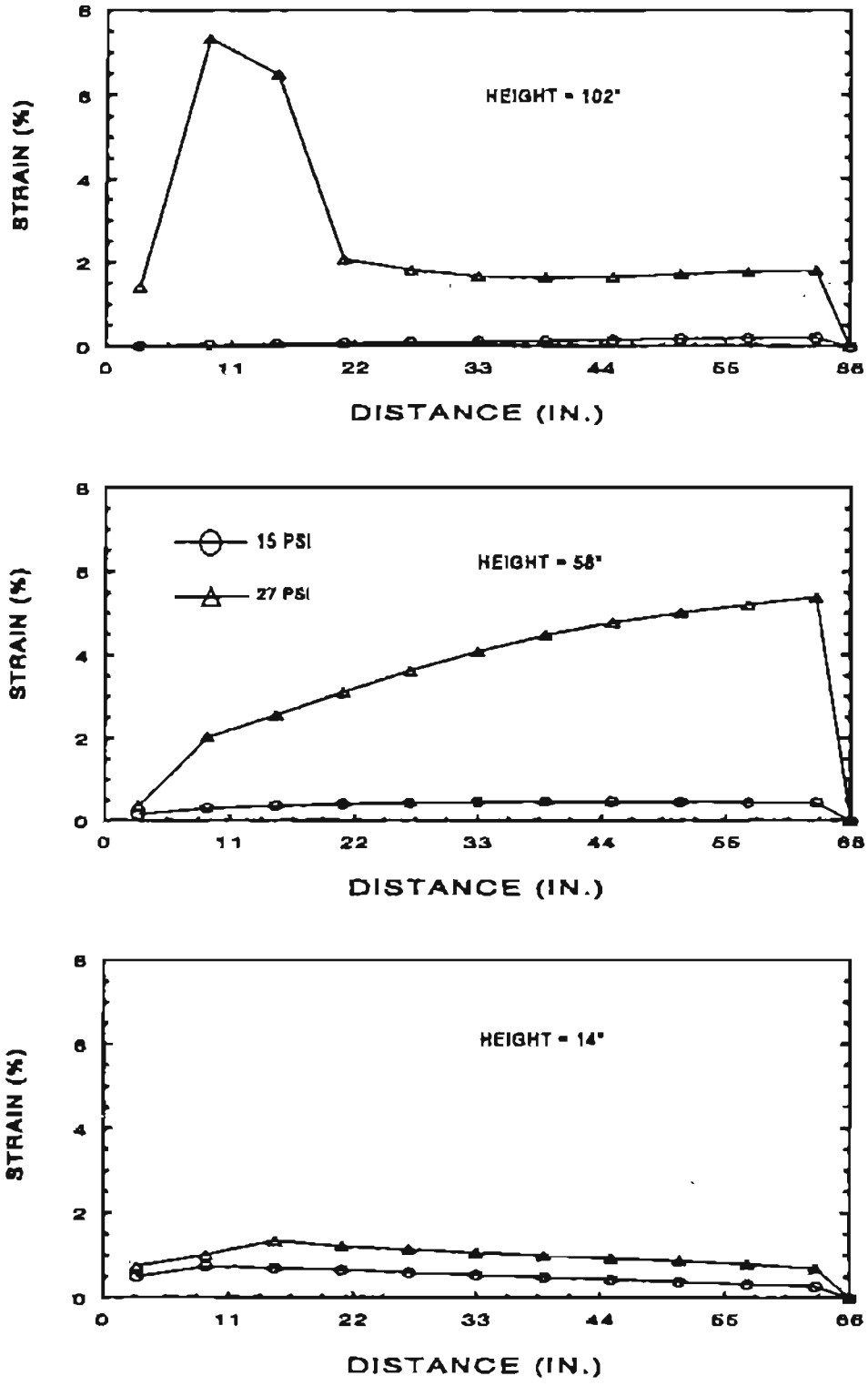

Figure 4.41b: After-Test Simulation of Strains in Reinforcement, with Granular Backfill, 15 & 27 psi Surcharge Pressures

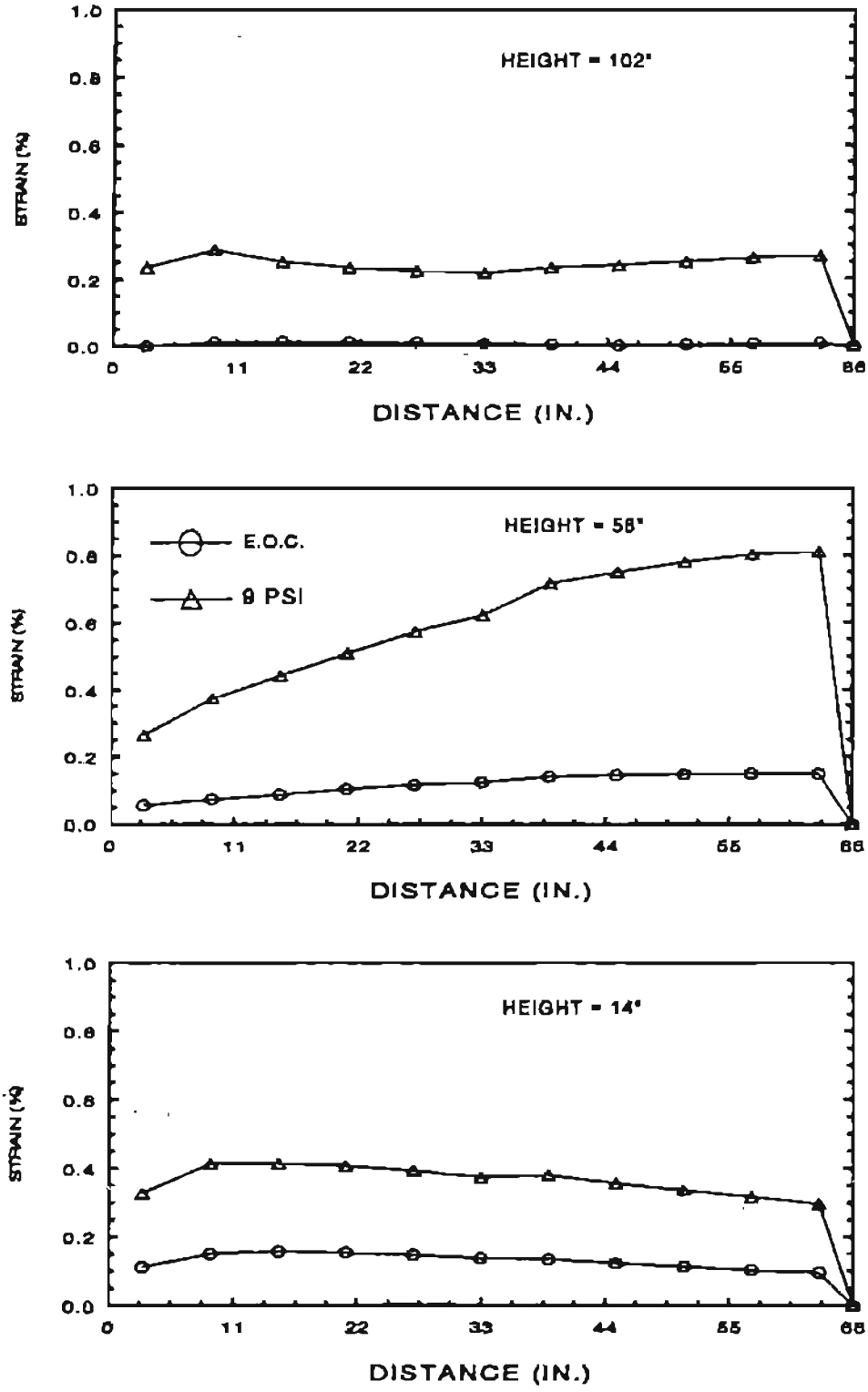

Figure 4.42a: After-Test Simulation of Strains in Reinforcement, with Cohesive Backfill, EOC & 9 psi Surcharge Pressures

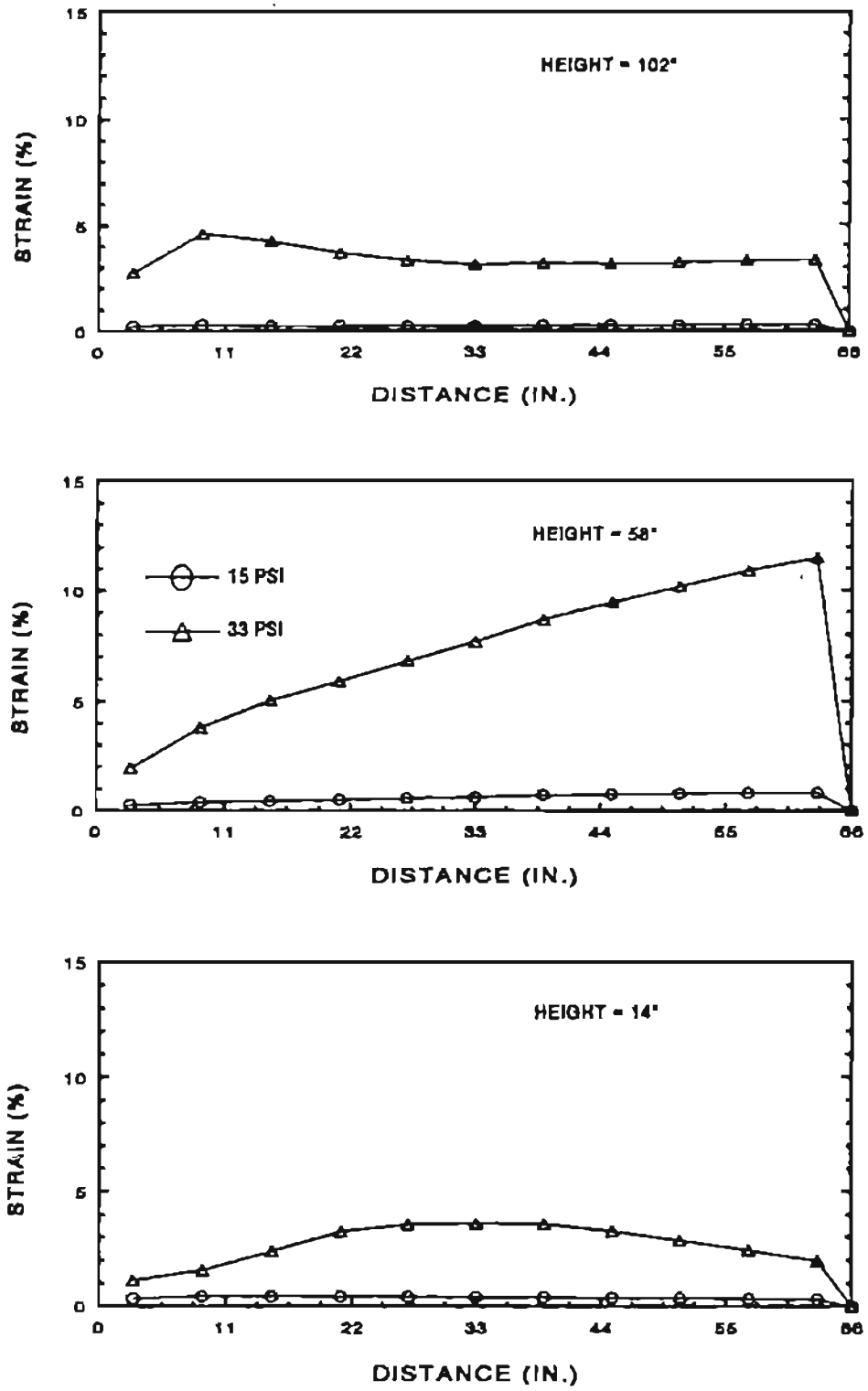

Figure 4.42b: After-Test Simulation of Strains in Reinforcement, Cohesive Backfill Wall, 15 & 33 psi Surcharge Pressures

was significantly improved. Since the original prediction on the cohesive backfill wall was satisfactory, no notable improvements were observed after the modification of the soil parameters. This study indicates that DACSAR is capable of simulating the performance of the GRS walls under service loads, provides that proper simulation procedure and simulation parameters are used.

CHAPTER V

PERFORMANCE OF GEOSYNTHETIC WALLS - A PARAMETRIC STUDY

An obvious approach for studying the performance of GRS walls is to construct and monitor a large number of full-scale control test walls. However, the cost of doing so is prohibitive. A viable approach that can reduce the number of full-scale tests is to perform a parametric study by using a validated analytical model. In the parametric study presented in this chapter, the following factors have been investigated: wall height, reinforcement geometry (wall shape), backfill properties, facing rigidity, foundation soil compressibility, reinforcement stiffness and strength, K_o (due to compaction), and combinations of these factors.

The wall response characteristics examined in this study include: lateral wall movement, axial tension in reinforcement layers, lateral earth pressure against facing, soil reaction at wall base, and settlement at backfill surface. The first two characteristics are emphasized in this study.

This parametric study was conducted by FEM analysis using DACSAR. This study includes a total of 32 cases. The Duncan-Chang model has been used for simulating compacted backfills and granular

foundations; the Sekiguchi-Ohta model was employed for simulating clayey foundations. These simulation procedures are the same as those used in the Denver Test Walls described in Chapter 4.

5.1 The Control Wall (Baseline Case)

For the purpose of comparison, a control wall (baseline case) was selected for this study. This control wall (Figure 5.1) had the following features:

Geometry

- Wall height = 12 feet
- Reinforcement spacing = 1 foot
- Reinforcement length (uniform) = 9 feet
- Vertical, timber/plywood facing (same as the one used in the Denver Test Walls)
- Horizontal crest
- Flexible foundation with a thickness of 14 ft.
- Rectangular wall shape

Materials

- Reinforced backfill: a silty sand and gravel (GP) compacted to 95% of Standard Proctor (T99 of AASHTO), with the modified Duncan-Chang model parameters shown in Table 5.1
- Unreinforced backfill: same as the reinforced backfill
- Reinforcement: a geosynthetic with hyperbolic model parameters: E_i=500 lb/in. and T_{ult}=35 lb/in.

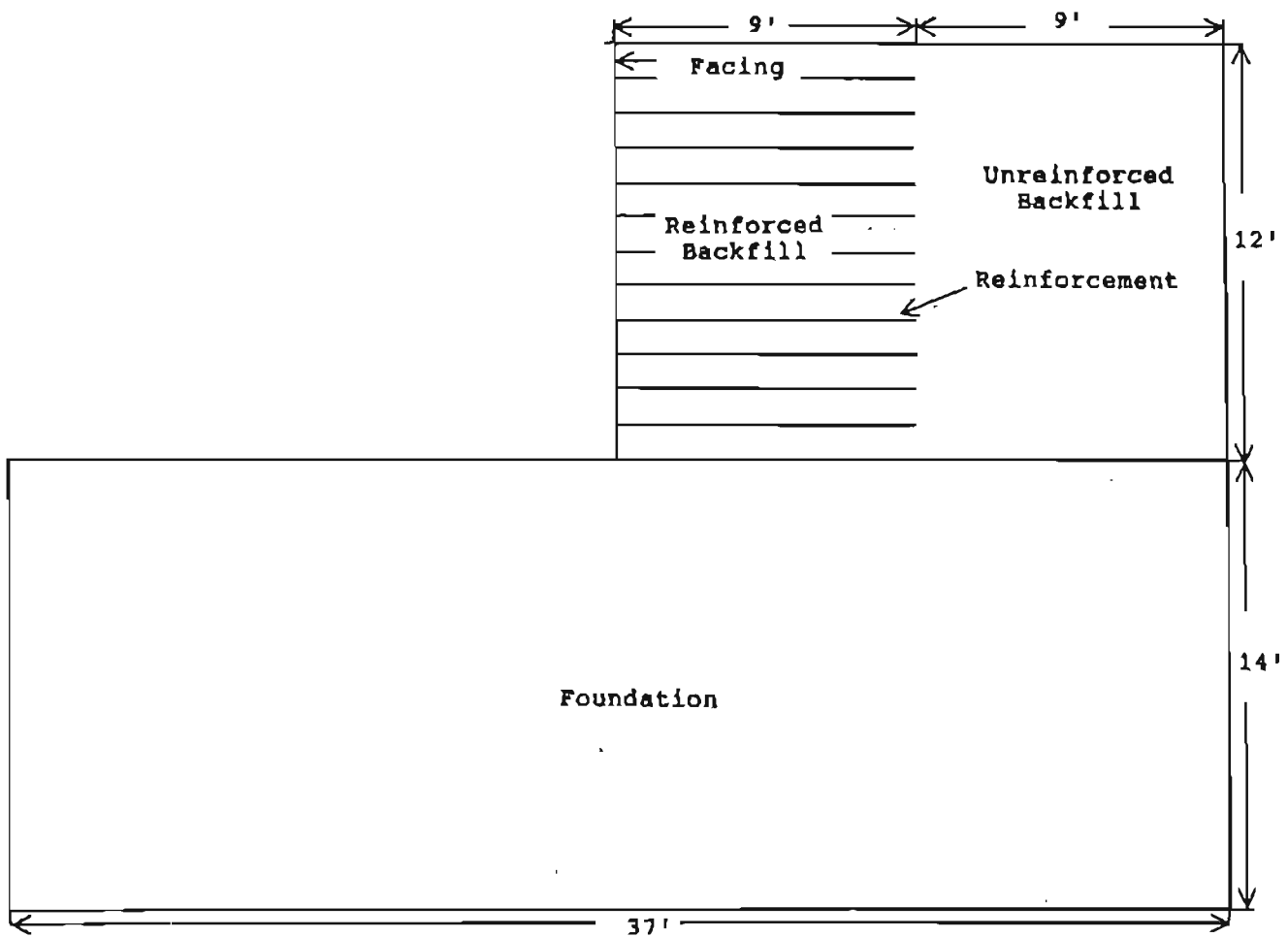

Figure 5.1: Configuration of the Control Wall

- Soil-reinforcement interface: assume no slippage at the soil-geosynthetic interface
- Facing: continuous timber/plywood facing with EI = 21,000 lb/in² and A = 4.6 in²
- Foundation soil: a medium stiff sandy clay (SC) fairly pervious and with a low plasticity and a relatively high permeability. The water table three feet below the existing ground level. This type of soil represents the most commonly encountered overburden soil in Colorado. The Sekiguchi-Ohta model parameters for the foundation soil are listed in Table 5.2. In the analyses, consolidation is considered, but not creep. The foundation soil is assumed to be uniform and underlain by a rigid stratum.

Loading

- A uniform surcharge of 5 psi was applied to the top surface of the wall, except that no surcharge was applied within 1.5 ft of facing. The surcharge represents a combination of dead and live loads of a highway embankment.

The FEM mesh used for the analysis of the control wall is shown in Figure 5.2. A total of 228 nodes, which define 200 soil elements, 66 bar elements (for the reinforcement) and 12 beam elements (for the wall facing), were employed in the mesh. The foundation soil was treated as an assembly of "pre-existing" soil

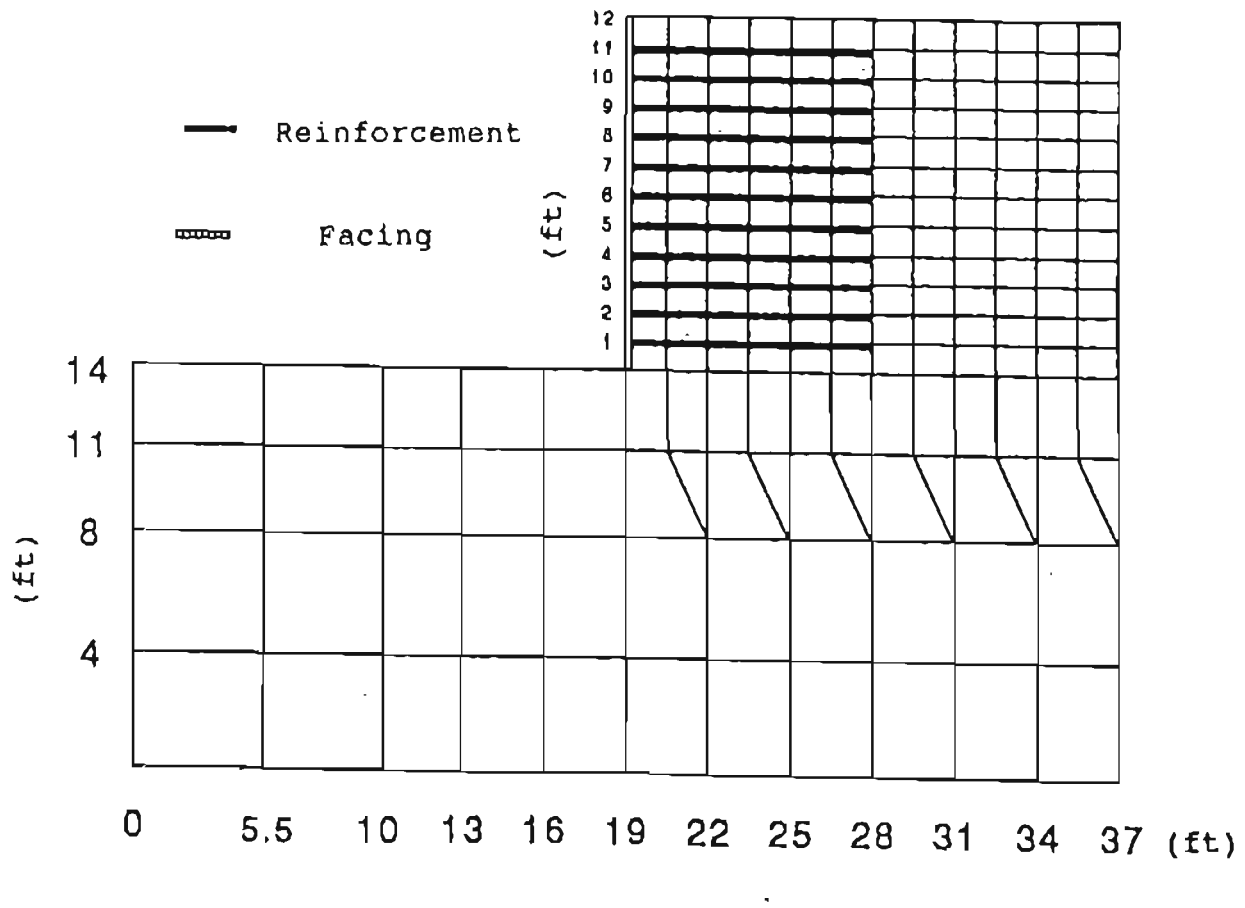

Figure 5.2: Finite Element Mesh for the Control Wall

elements. The erection of the wall was simulated in twelve construction lifts of soil placement, each one foot thick. Compaction effect was simulated by assigning a high K^o value in the compacted backfill.

It was assumed for this study that the construction took 12 days (one foot high per day) and that another 18 days elapsed before the surcharge was applied. Since the foundation soil for the control wall was assumed to be relatively pervious, the influences due to consolidation are insignificant. No creep was considered in the analysis of the control wall.

This control wall was selected as a baseline case for two reasons:

(1) It is very similar to the Denver Test Wall with granular backfill, which is modeled in Chapter 4. The major differences between the control wall and the test wall are: (a) The foundation is assumed to be flexible for the control wall, while it was rigid for the Denver Test Wall; (b) No lateral constraint is imposed at the top of the control wall; and (c) The unreinforced backfill extends 0.75 H (H = wall height) from the end of reinforcement for the control wall, while it was 0.1 H for the Denver Test Walls.

(2) The wall height, wall shape, backfill, reinforcement, foundation and facing are typical in the prevailing CDOT practice. The facing construction

technique has been successfully used by CDOT in several geotextile wall projects.

5.1.1 Wall Movement

The calculated wall movement for the control wall is shown in Figure 5.3. The shape of this deformed curve agrees qualitatively with that of the Denver Test Wall, except that about 50% of the maximum lateral movement in the control wall is due to lateral movement of the foundation soil. The magnitude of maximum deformation is 1.0 inch, or 0.68% of the wall height. The maximum deformation occurs at the middle of the wall height (i.e., 0.5H).

To compare the FEM analysis with other methods for wall deformation calculations, the same control wall situated on a rigid foundation was analyzed. The maximum lateral deformation for this case is 0.5% of the wall height, and the maximum tensile strain is 0.6%. The following three methods (see Section 2.2.2) were used for comparison:

(1) Christopher, et. al. method (Christopher, et. al., 1989)

(2) GeoService method (GeoService Inc, 1989)

(3) Jewell method (Jewell & Milligan, 1989)

A comparison of the maximum wall displacements is shown in Table 5.3. It is seen that the calculated displacements are very different from the value obtained from DACSAR.

Table 5.1: The Duncan-Chang Soil Parameters for Backfill of the Control Wall

C(psi)	ϕ(deg)	$\Delta\phi$	K_b	m	K_{ur}	K_o	k	n	R_f
0.5	35	7	175	0.2	600	2.5	600	.6	.7

Table 5.2: The Sekiguchi-Ohta Model Parameters for Foundation of the Control Wall

D	Λ	M	δ	k/γ_w	σ'_v(psi)	K_o	K_f	α	$\dot{v}_o$	$\dot{\epsilon}_o$
.023	.86	1.4	.3	$\frac{1.0\ in^4}{day\text{-}\ell}$	14	0.9	1.0	0	N/A	0.7

Table 5.3: Comparison of Maximum Wall Displacement

	FEM	FHWA	GeoService	Jewell
Deflection (% of wall height)	0.5	1.7	0.2	2.0

5.1.2 Lateral Earth Pressure Distribution

The way the "lateral earth pressure" is evaluated in a reinforced soil mass deserves some clarification. Unlike a conventional (unreinforced) retaining wall, the magnitude of the lateral earth pressure in a reinforced soil mass may vary significantly from the facing to the back of the wall. From the designer's viewpoint, the earth pressures at the following three locations may be of interest:

(1) Earth pressure against facing. The earth pressure against the facing is usually smaller than any other vertical cross sections in the fill, because part of the lateral earth thrust is resisted by the friction induced between the reinforcement and the backfill. This pressure distribution is particularly useful for the structural design of the facing and the connection between the facing and reinforcement. In the FEM analysis, the pressure distribution against the facing can be obtained by the horizontal stress in the soil elements immediately behind the facing.

(2) Earth pressure against the reinforced soil mass. This pressure distribution is useful in calculating safety factors for both external and internal stabilities (for limiting equilibrium analysis). In the FEM analysis, this pressure distribution can be obtained by the horizontal stress in the soil elements immediately behind the reinforced

zone (i.e., 9.75 feet from the facing for the control wall).

(3) Earth pressure along the plane of maximum tensile force in the reinforcement (Collin, 1986). This earth pressure distribution is useful in the tieback wedge analysis of limiting equilibrium methods. The pressure distribution can be used to evaluate the anchorage length behind the potential failure plane (Adib, 1988). In the FEM analysis, this earth pressure distribution can be obtained by the horizontal stress in the soil elements along the plane of maximum tensile force.

Figure 5.4 shows the earth pressure distributions evaluated by the above three approaches. The earth pressure against facing is smallest, the earth pressure against the reinforced soil mass is largest, while the earth pressure obtained along the maximum tensile force in the reinforcement is somewhat in-between. In the close vicinity of the foundation, the lateral earth pressure is extremely high for the earth pressure against facing, probably due to the horizontal restraint invoked by the friction between the wall base and foundation soil. For comparison purposes, the K_a and K_o earth pressure distributions are also shown in Figure 5.4. It is seen that the earth pressure distribution against the reinforced soil mass is slightly larger than Ka line.

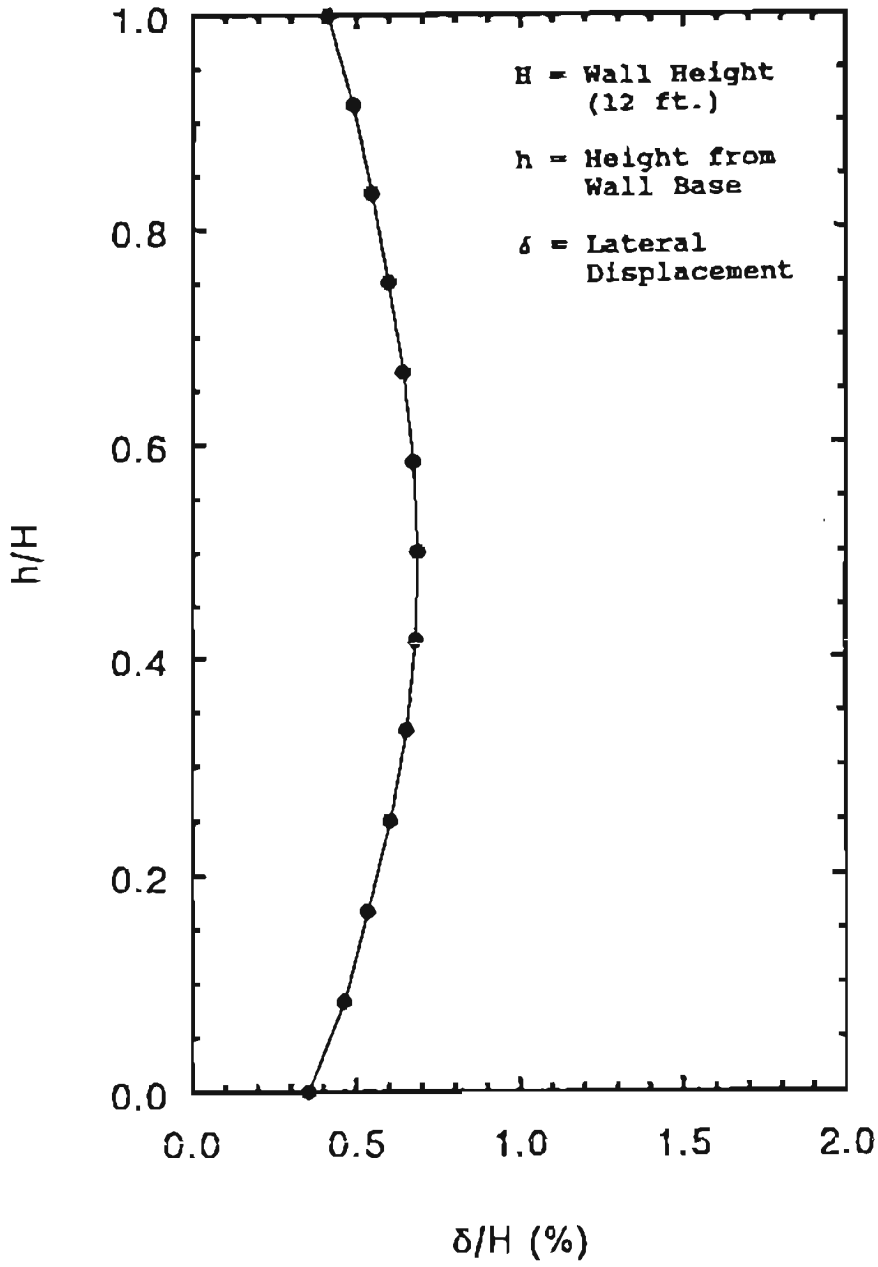

Figure 5.3: Lateral Wall Displacement for the Control Wall

5.1.3 Tension in Reinforcements

The tensile strain distribution along the reinforcement at three different heights of the control wall is shown in Figure 5.5. The location where maximum tension occurs is useful in the conventional internal stability analysis, especially for calculating the reinforcement anchorage length to resist pullout failure. The locus of the maximum tension for the control wall is shown in Figure 5.6. This locus is very different from the active Rankine failure plane, which has been used in most of the limiting equilibrium methods. It should be noted that the locus obtained from the control wall is under a surcharge of 5 psi, which is far from the failure condition.

The maximum reinforcement tension usually develops at or near the middle of the wall height. The maximum tensile strains induced at the top, middle and bottom layers of reinforcement for the control wall are 0.4%, 0.8% and 0.4 % for the upper, middle and bottom layers of reinforcement. This lead to a safety factor for reinforcement rupture failure of 5.6 (at 5 psi surcharge). The safety factor is herein defined as the ratio of the tensile strength (T_{ult}), divided by the maximum tensile force induced in the reinforcement.

5.1.4 Soil Reaction at Wall Base

The soil reaction against the foundation is important for both the external and internal stability

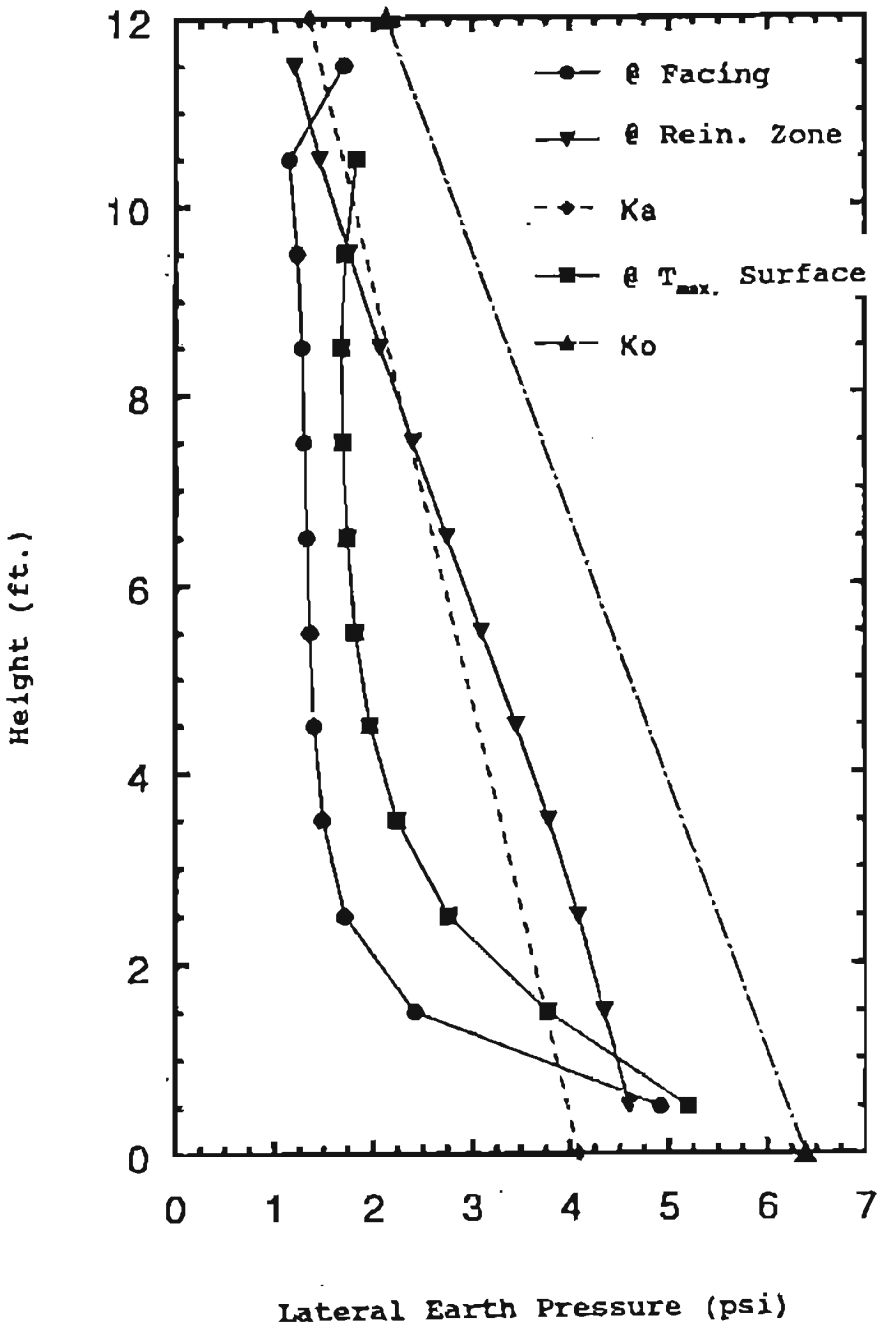

Figure 5.4: Lateral Earth Pressure Distribution for the Control Wall

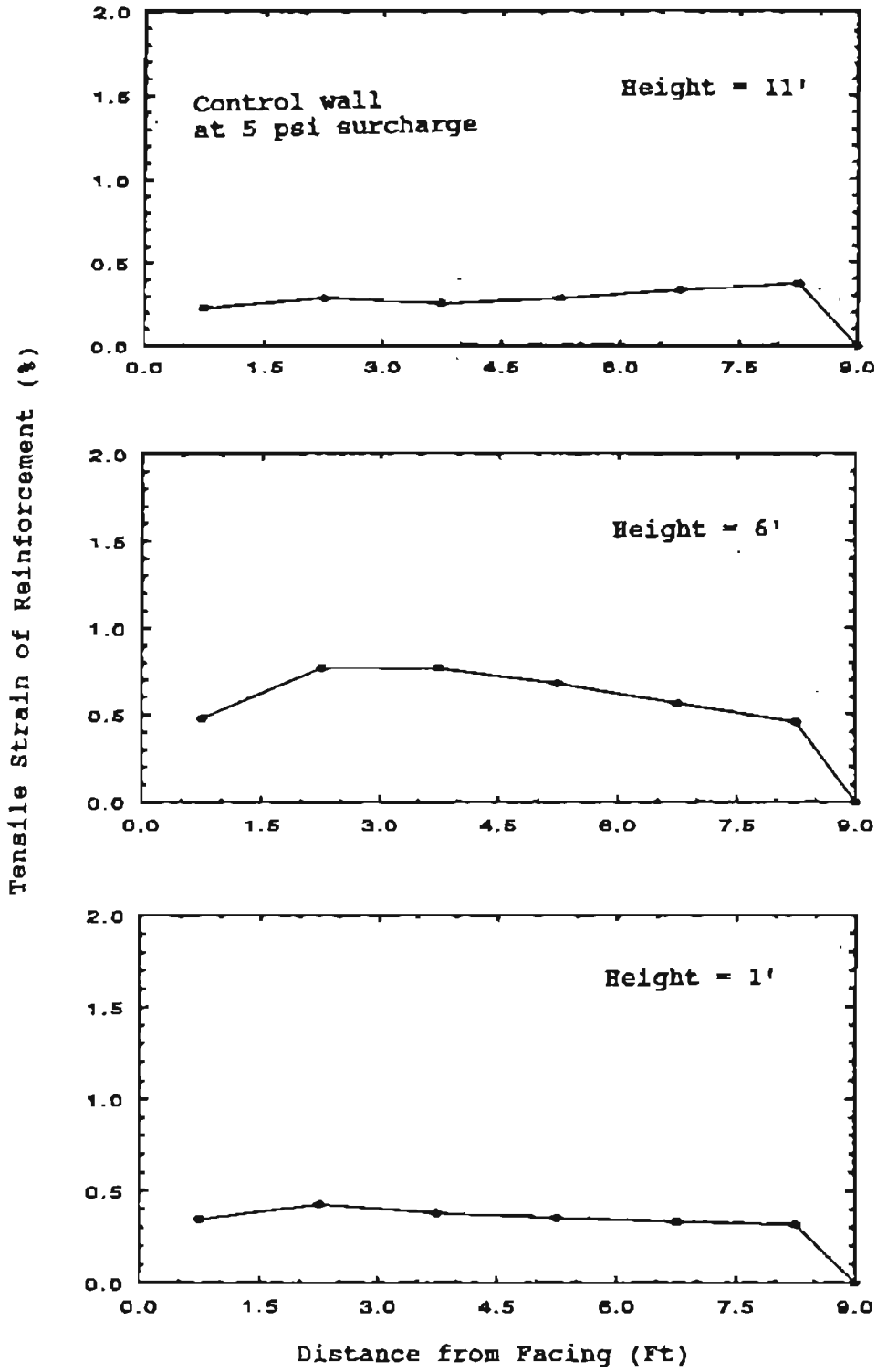

Figure 5.5: Tensile Strain Distribution in Reinforcements for the Control Wall

analyses and can be obtained from the FEM analysis. In the conventional design methods, the soil reaction is usually assumed to be a trapezoidal (Peck, Hanson & Thornburn, 1974) or Meyerhof type profile (Bonaparte et. al., 1985) for a GRS wall. The vertical reactions obtained from the FEM analysis are depicted in Figure 5.7. The soil reaction is drastically different from the trapezoidal profile, and quite different from the Meyerhof's profile within 0.5 H from the facing. The discrepancy is probably due to the stiffness of foundations assumed: the trapezoidal distribution is based on the assumption that the wall base is rigid, while the control wall is assumed to be over a semi-rigid foundation. It also should be noted that the Meyerhof's profile was developed in a limiting condition.

5.1.5 Settlement at the Top of Backfill

The settlement profile at the top of the backfill is shown in Figure 5.8. The settlements range from 0.5 to 1.3 inches under the 5 psi surcharge pressure. It is to be noted that the abrupt change in the settlement profile (near the facing) is due to the discontinuity of the surcharge load at the 1.5 ft behind the facing.

The following sections discuss the effects of a number of factors on the performance of the control wall. The factors investigated were reinforcement configuration (wall shape), backfill, facing rigidity,

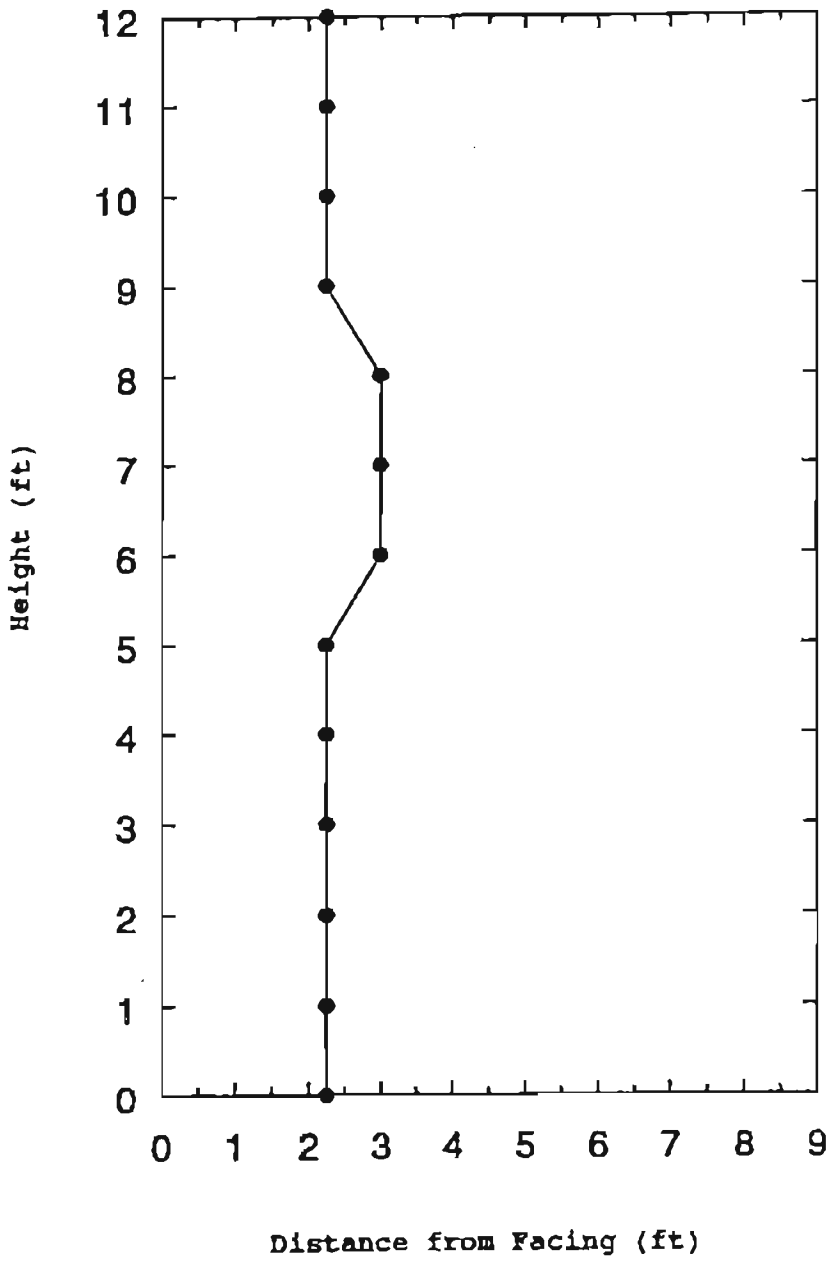

Figure 5.6: Locus of Maximum Reinforcement Tension for the Control Wall

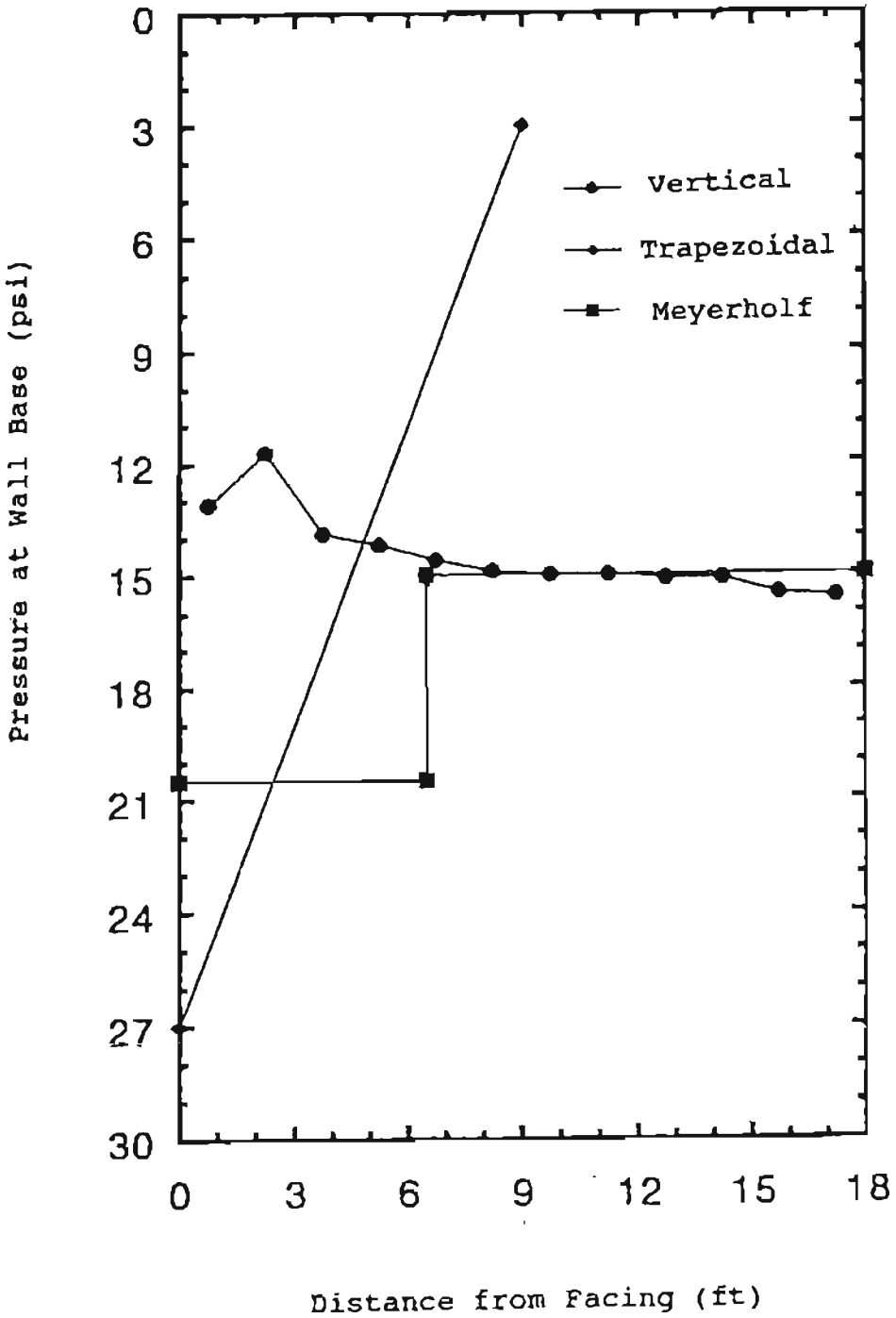

Figure 5.7: Soil Reactions for the Control Wall

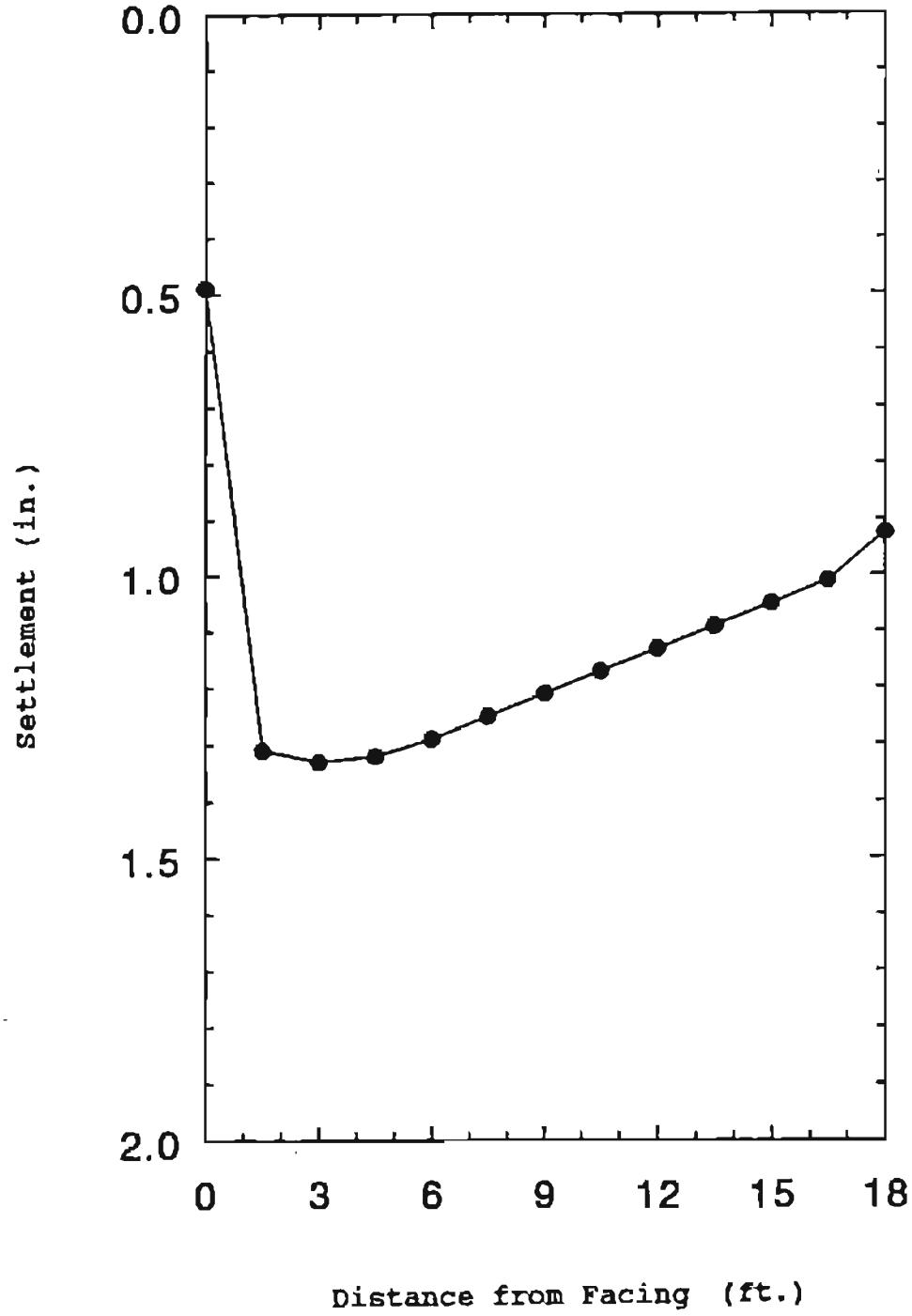

Figure 5.8: Settlement at the Top of Backfill for the Control Wall

foundation, reinforcement stiffness and strength, and K_o (due to compaction). While a factor was being investigated, all the other conditions were kept the same as the control wall. Sections 5.2 through 5.8 present the result of varying a single factor. The variations of each factor are shown in Table 5.4. The effect due to a combination of some of the factors is presented in Section 5.9.

5.2 Effect of Reinforcement Configuration (Wall Shape)

The rectangular reinforcement configuration in the control wall was replaced with a trapezoidal shaped reinforcement configuration, i.e., truncated at the base and extended at the top, to investigate the effects of wall shape. The FEM mesh for the trapezoidal wall is shown in Figure 5.9.

The total length of all the reinforcement in the trapezoidal wall was 94.5 feet, which is comparable to that of the control wall (99 ft). As expected, the lateral deformations of the trapezoidal wall were slightly larger than the control wall at the bottom half, but were smaller at the upper half of the wall (Figure 5.10). The maximum lateral deflection, occurred at a depth of 0.41 H above the base, was about 0.73% of the wall height, or about 1.1 inch.

The tensile strain distributions of the reinforcement at three different heights are shown in

TABLE 5.4: FACTORS CONSIDERED IN PARAMETRIC STUDY

A. WALL HEIGHT:

1): 12' (BASELINE)
2): 16'
3): 8'

B. WALL SHAPE:

1): RECTANGULAR (BASELINE)
2): TRAPEZOIDAL

C. BACKFILL:

1): SAND & GRAVEL (BASELINE)
2): SANDY CLAY, MOIST
3): SANDY CLAY, WET

D. FACING:

1): TIMBER FACING: (BASELINE)
2): WRAP-AROUND GEOTEXTILE FACING
3): FULL HEIGHT CONCRETE FACING
4): ARTICULATED PANELS

E. FOUNDATION SOIL:

1): MEDIUM STIFF SANDY CLAY (BASELINE)
2): SOFT CLAY
3): MEDIUM DENSE SAND AND GRAVEL.
4): RIGID FOUNDATION

F. Ko (DUE TO COMPACTION):

1): 2.5 (BASELINE)
2): 1.0
3): 0.5

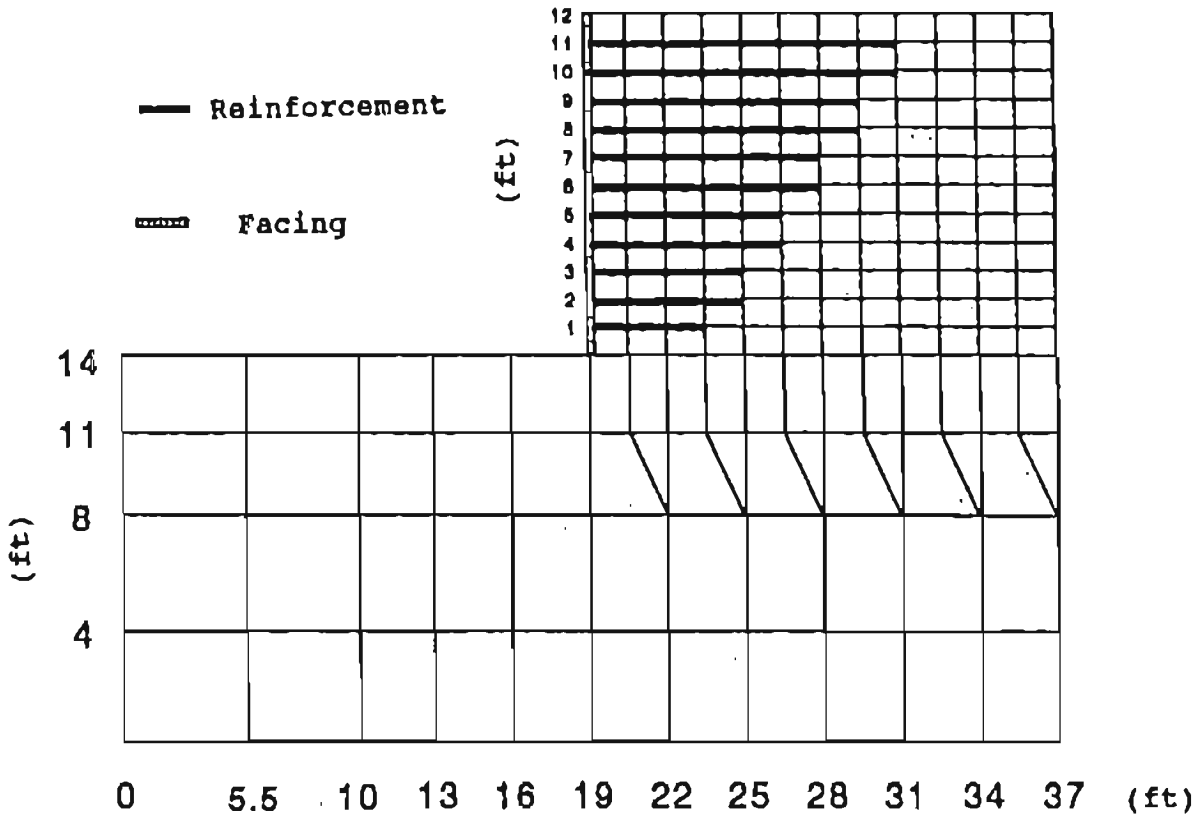

Figure 5.9: FEM Mesh for Trapezoidal Shape Wall

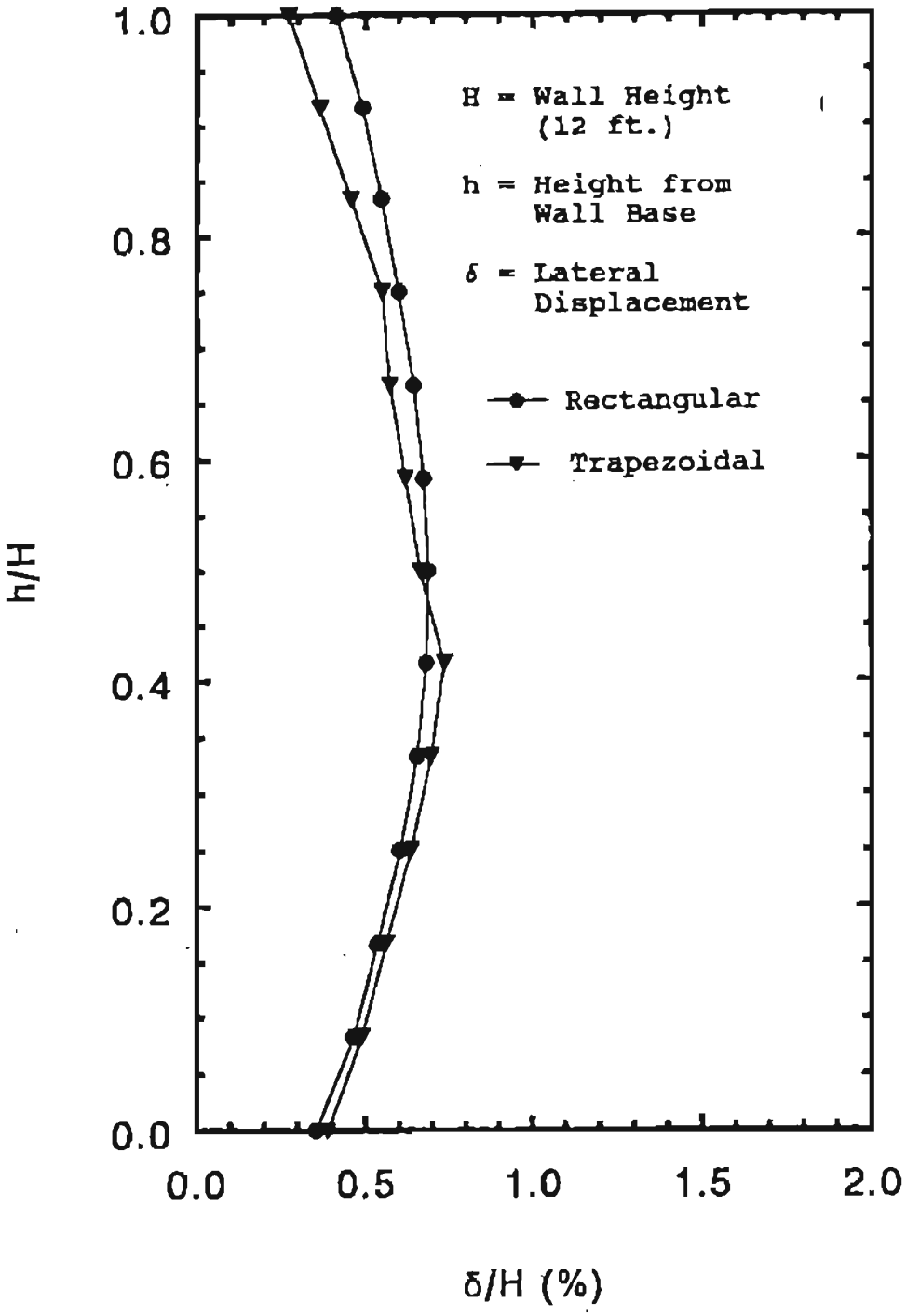

Figure 5.10: Effect of Wall Shape on Lateral Wall Displacement

Figure 5.11. The strains are generally smaller than those of the control wall.

The analysis indicates that the performance of the trapezoidal wall is as good as the rectangular one. Since the trapezoidal shaped wall could reduce excavation (if needed), it may provide a feasible alternative to the rectangular shaped wall.

5.3 Effect of Backfill

The effect of using backfills of different stress-strain-strength behaviors was examined. The following three types of backfill were studied:

(1) A sand and gravel (SP) compacted to 95% of Standard Proctor (termed the "granular" backfill); this was the backfill used in the control wall;

(2) A sandy clay (SC) compacted to 95% of Standard Proctor at 2% wet of optimum moisture (termed the "cohesive-moist" backfill); and

(3) Same as No. 2, except that the material is fully wetted after compaction (termed the "cohesive-wet" backfill). This is to simulate a "worst" condition of cohesive backfill when it becomes almost fully saturated by infiltration of water when adequate drainage is not provided.

The cohesive backfill used in the Denver Test Wall was employed in (2) and (3). The Duncan-Chang model parameters for the cohesive-moist and cohesive-wet soils are listed in Table 5.5. The parameters of the

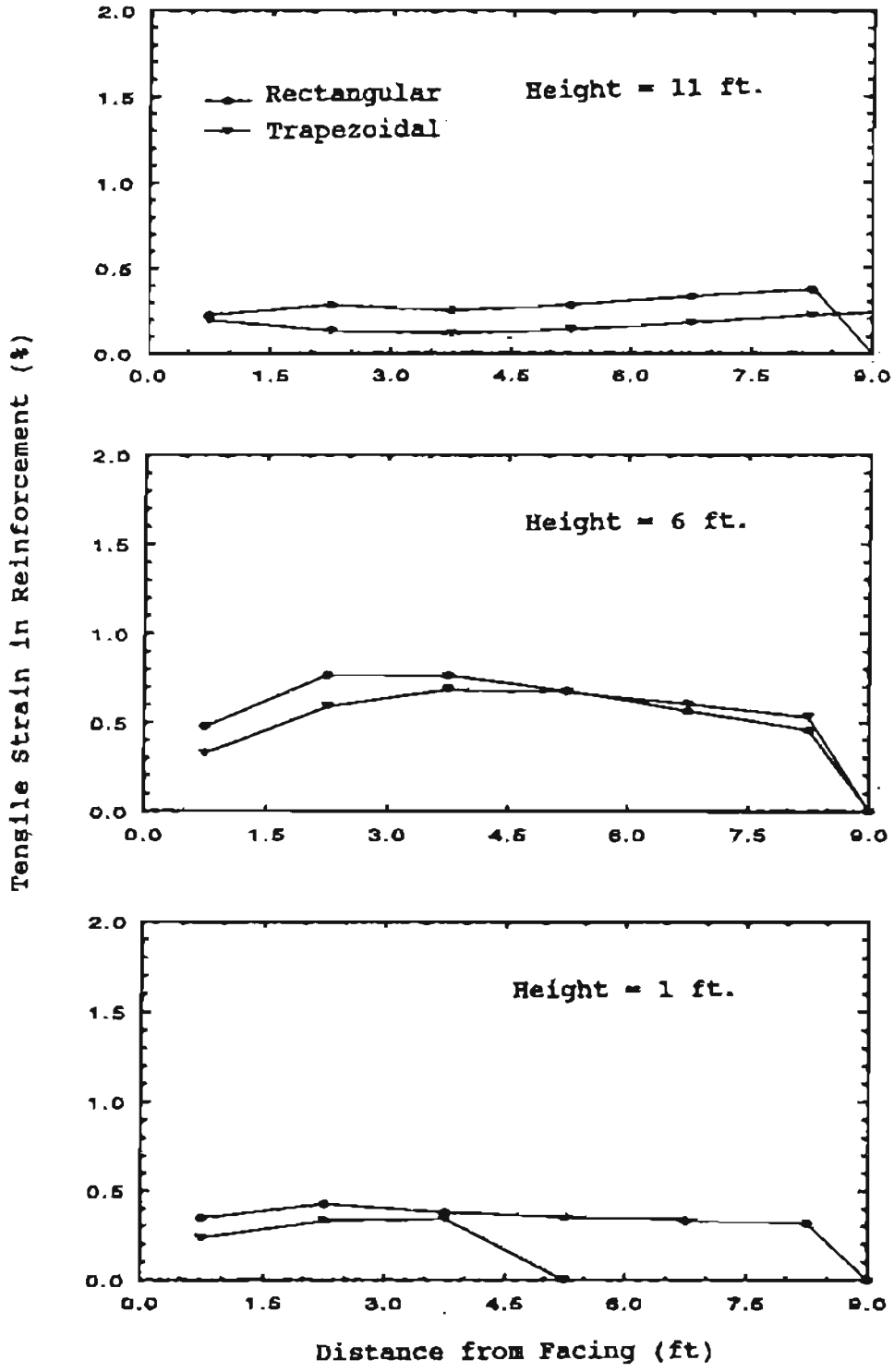

Figure 5.11: Effect of Wall Shape on Reinforcement Tensile Strains

cohesive-moist soil were obtained from the average of the triaxial CU and CD tests, while the parameters of the cohesive-wet soil were obtained from the triaxial CD tests. After consolidation was completed, the cohesive-wet samples were saturated by applying a 5 psi back pressure to both ends of samples.

Figures 5.12 and 5.13 depict, respectively, the horizontal wall displacements and the tensile strain distribution in the geosynthetic layers near the top, middle and bottom of the wall. These figures indicate that wetting the clayey backfill has a drastic effect on the wall movement and the tension induced in the reinforcement. With the cohesive-wet backfill, the bottom portion of the wall deforms more than 7% of the wall height, and the tensile strains at the middle and bottom layers of reinforcement experience much more higher strains (as high as 11%), which reveals symptoms of wall instability. Figures 5.12 and 5.13 also indicate that, when kept near the placement moisture (at 2% wet of optimum), the cohesive backfill wall can perform at least as well as the granular backfill wall.

For a conventional unreinforced wall with a cohesive backfill, the horizontal effective stress is in tension throughout the upper part of the backfill (Lambe & Whitman, 1969). Consequently, there is a tendency for tension cracks to develop at the surface of the cohesive backfill behind a retaining wall. For

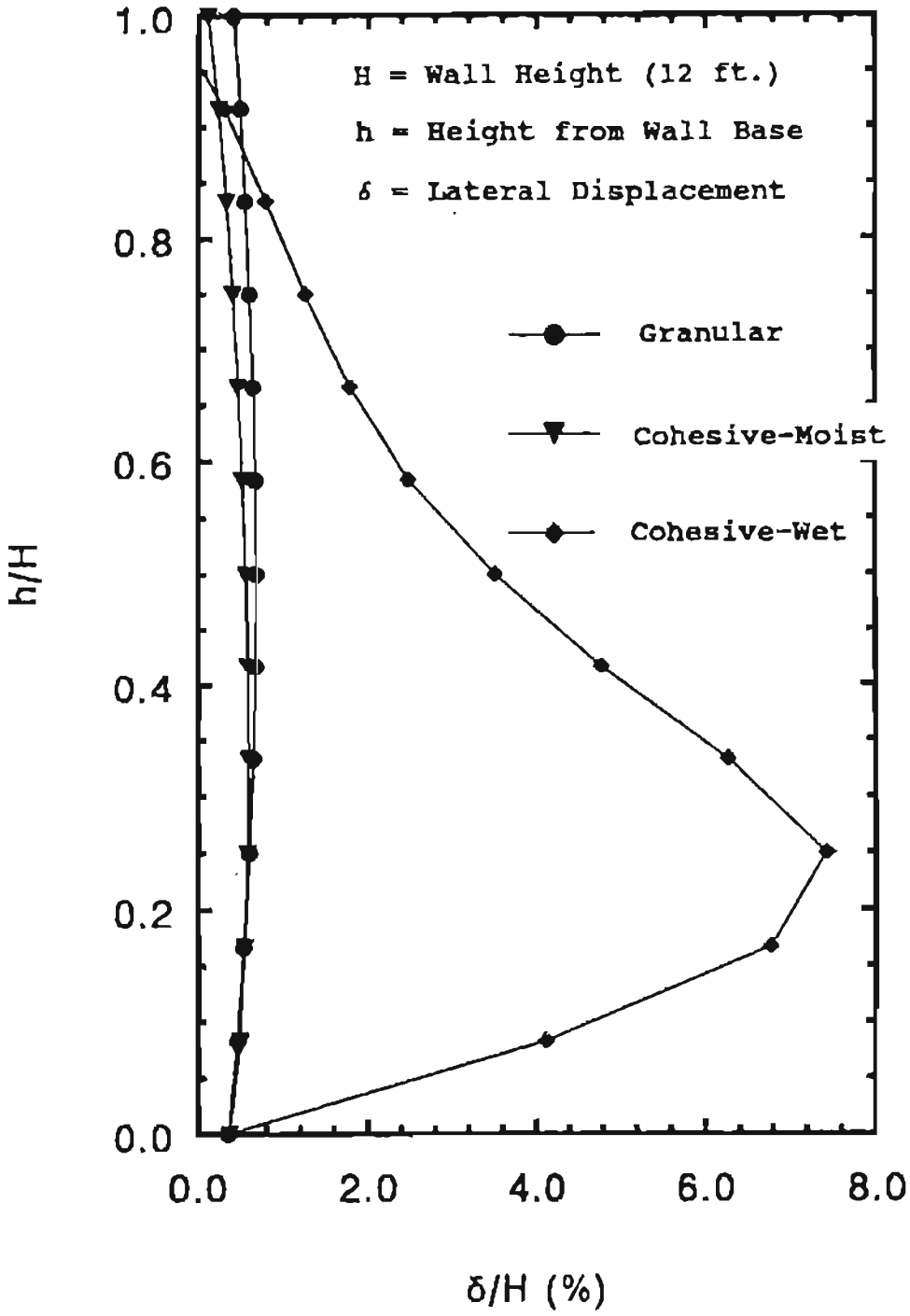

Figure 5.12: Effect of Backfill on Lateral Wall Displacement

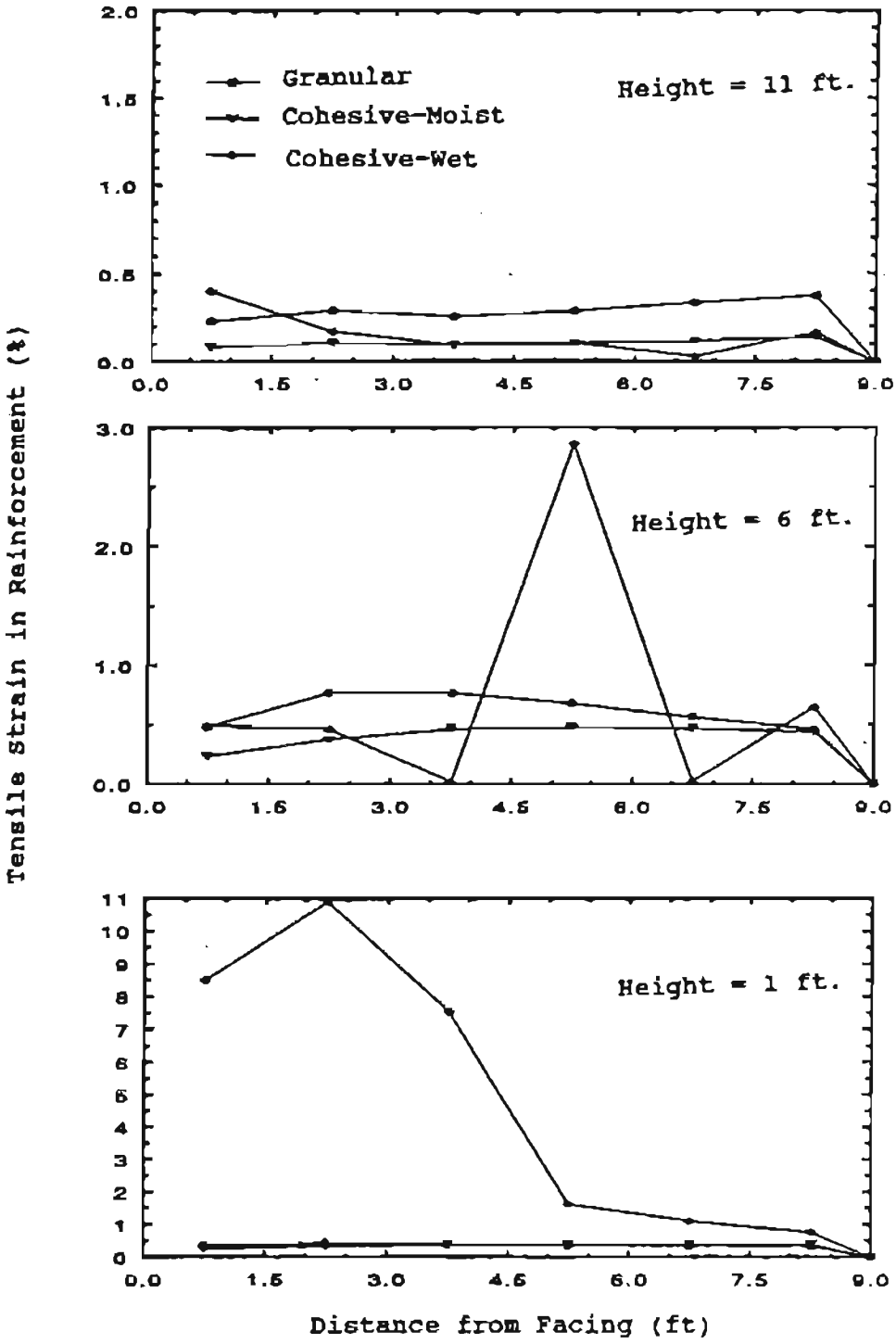

Figure 5.13: Effect of Backfill on Reinforcement Tensile Strain

a geosynthetic wall, however, tension in the upper soil may be taken effectively by the reinforcement; therefore, tension cracks in the backfill may be less likely to occur. This feature makes cohesive backfill a viable alternative for the construction of geosynthetic walls.

However, seeping of water into the compacted clay may reduce the soil suction, or destroy the bonding agent, and lead to shear failure. In the triaxial tests performed on the sandy clay, the soil was saturated by applying a back pressure to simulate wetting due to rain or snowmelt. The results of the triaxial CD tests indicate that the cohesion is lost completely, and the soil behaves as a loose granular material with a friction angle of about 30 degrees. The one-dimensional consolidation test also shows that the saturated sandy clay is much more compressible than the moist clay. Methods to alleviate the adverse effects due to wetting are discussed in Chapter 6.

5.4 Effect of Facing Rigidity

To examine the effect of facing rigidity on the wall performance, the following four types of facings were analyzed:

(1) Timber/plywood facing; assumed to be continuous, with a moderate global stiffness of $EI=21{,}000$ lb-in^2. This is the facing used in the Denver Test Wall and in the control wall.

(2) Wrap-around geosynthetic facing with little or no bending rigidity (EI=0).

(3) Continuous concrete panel with high global bending rigidity (EI=200,000 lb-in^2).

(4) Articulated (modular) concrete blocks with high local bending rigidity, but little global bending rigidity. Blocks of one foot high, similar to the Keystone or Versa-lok type blocks, were used in the analyses. It was assumed that the connections between articulated blocks could not withstand any bending moments. In the analyses, very short beam elements with negligible EI were used to simulate the connections.

Figures 5.14 and 5.15, respectively, show the horizontal wall displacement and the tensile strains induced in the geosynthetics at different heights. These figures indicate that the global bending resistance of the facing has a significant effect on the wall performance. The wall with continuous concrete facing exhibits the smallest wall movements and lowest tensile strains in reinforcement than the other facings. The timber/plywood and the modular concrete blocks are rated about equal, while the wrap-around facing shows the largest wall movement and strains. For the walls investigated, the maximum lateral wall displacements are: 0.50%, 0.67%, 0.70% and 0.80% of the wall height for continuous concrete panel,

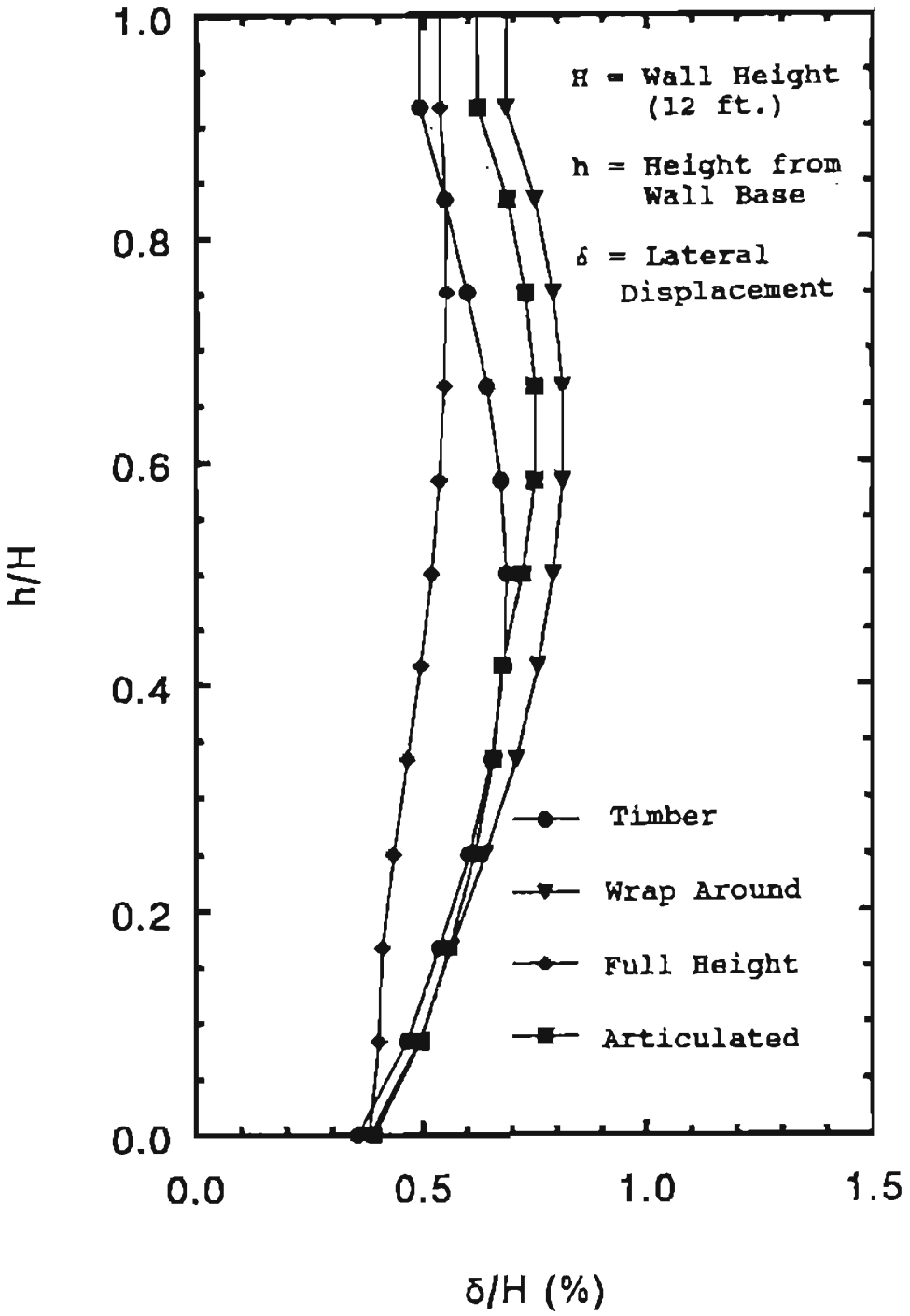

Figure 5.14: Effect of Facing Rigidity on Lateral Wall Displacement

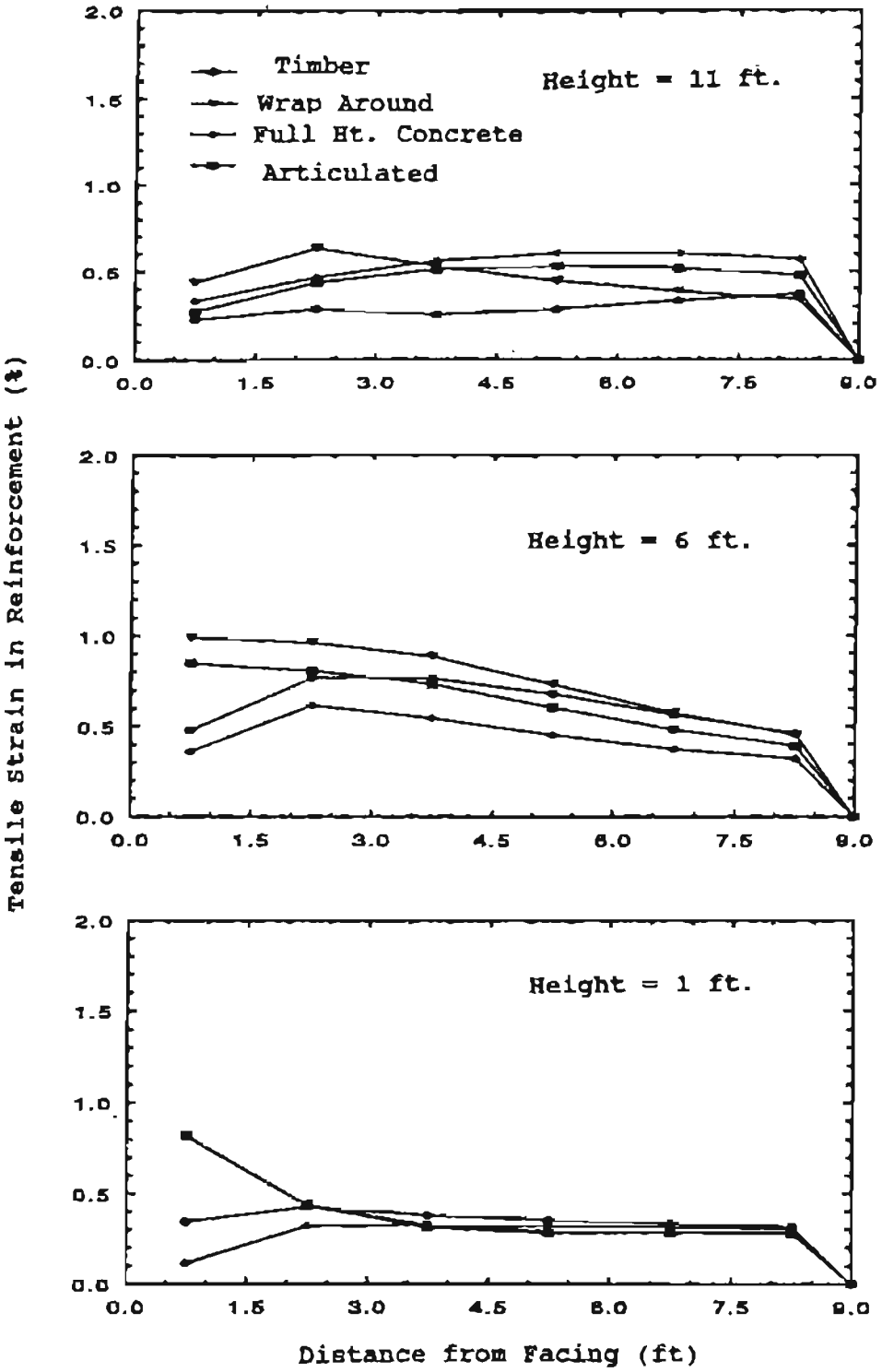

Figure 5.15: Effect of Facing Rigidity on Reinforcement Tensile Strains

timber, articulated (modular blocks), and wrap-around facings, respectively. It is to be noted that the continuous concrete facing was placed incrementally in the analysis. This is equivalent to articulated facing with very rigid connections between articulated elements.

5.5 Effect of Foundation

To study the effect of foundation on wall performance, the following subsurface conditions were analyzed:

(1) A medium-stiff sandy clay with a relatively high permeability (say, $k = 1x10^{-6}$ cm/sec) and a low PI (say, 10), referred to as "medium stiff clay" foundation. This is the foundation soil used for the control wall. The Sekiguchi-Ohta model was adopted for simulation of this foundation soil; creep was not considered in the analyses.

(2) A soft-to-medium stiff clay with a relatively low permeability (say, $k = 1x10^{-8}$ cm/sec) and a high PI (say, 30) , referred to as "soft clay" foundation. The Sekiguchi-Ohta model parameters for this material are shown in Table 5.6. Creep is considered in these analyses.

(3) A loose-to-medium dense sand, referred to as "loose sand" foundation. Neither consolidation nor creep was taken into account. The Duncan-Chang model was employed, and the parameters used are listed in

Table 5.5: The Duncan-Chang Soil Parameters for the Cohesive-Moist and Cohesive-Wet Backfills

Backfill	(psi) C	(deg) ϕ	(deg) $\Delta\phi$	K_b	m	K_{ur}	K_o	k	n	R_f
Cohesive -Moist	6.0	19	0	70	0	140	1.	121	.13	.87
Cohesive -Wet	0	30	0	33	-.06	66	1.	278	.06	.91

Table 5.6: The Sekiguchi-Ohta Model Parameters for Foundation of Soft Foundation.

D	Λ	M	$\acute{o}$	k/rw	$\sigma\grave{o}$	K_o	K_1	α	$\dot{\nu}_o$	e_o
.023	.86	1.	.3	0.01 $\frac{in}{day-\not}$ 4	14 psi	0.9	1.0	.00124	.0000124	0.7

Table 5.7: The Duncan-Chang Soil Parameters for the Loose to Medium Dense Sand Foundation.

C(psi)	ϕ(deg)	$\Delta\phi$(deg)	K_b	M	K_{ur}	K_o	K	n	R_f
2.0	30	0	110	.2	220	.5	120	.45	.7

Table 5.7.

(4) A rigid foundation; very hard, such as bedrock or very dense granular material; the settlement is negligible.

Except for the rigid foundation, the foundation depth was assumed to be 14 feet. Wu & Lin (1991) indicated that the wall movement is not sensitive to the foundation depth varying from 6 to 14 feet.

Figure 5.16 shows the lateral wall displacements for the above four foundations. As expected, the rigid foundation exhibits the least wall movement, and the wall rotates about the toe of the wall. Lateral wall movement for the medium-stiff clay and loose-sand foundations are somewhat alike, although different soil models were used. The wall with the soft clay foundation rotates about the top of the wall, due to the significant movement of the foundation. The maximum wall displacements for the rigid foundation and the soft clay foundation were 0.7% H and 3.0% H, respectively. This large difference clearly indicates the importance of including foundation soil in the analysis, especially when soft foundations are present.

The strain distribution shown in Figure 5.17 indicates that, with the soft clay foundation, the tensile strains induced in the reinforcement are much larger near the bottom of the wall, as reflected by the large wall movement. The wall with a rigid foundation

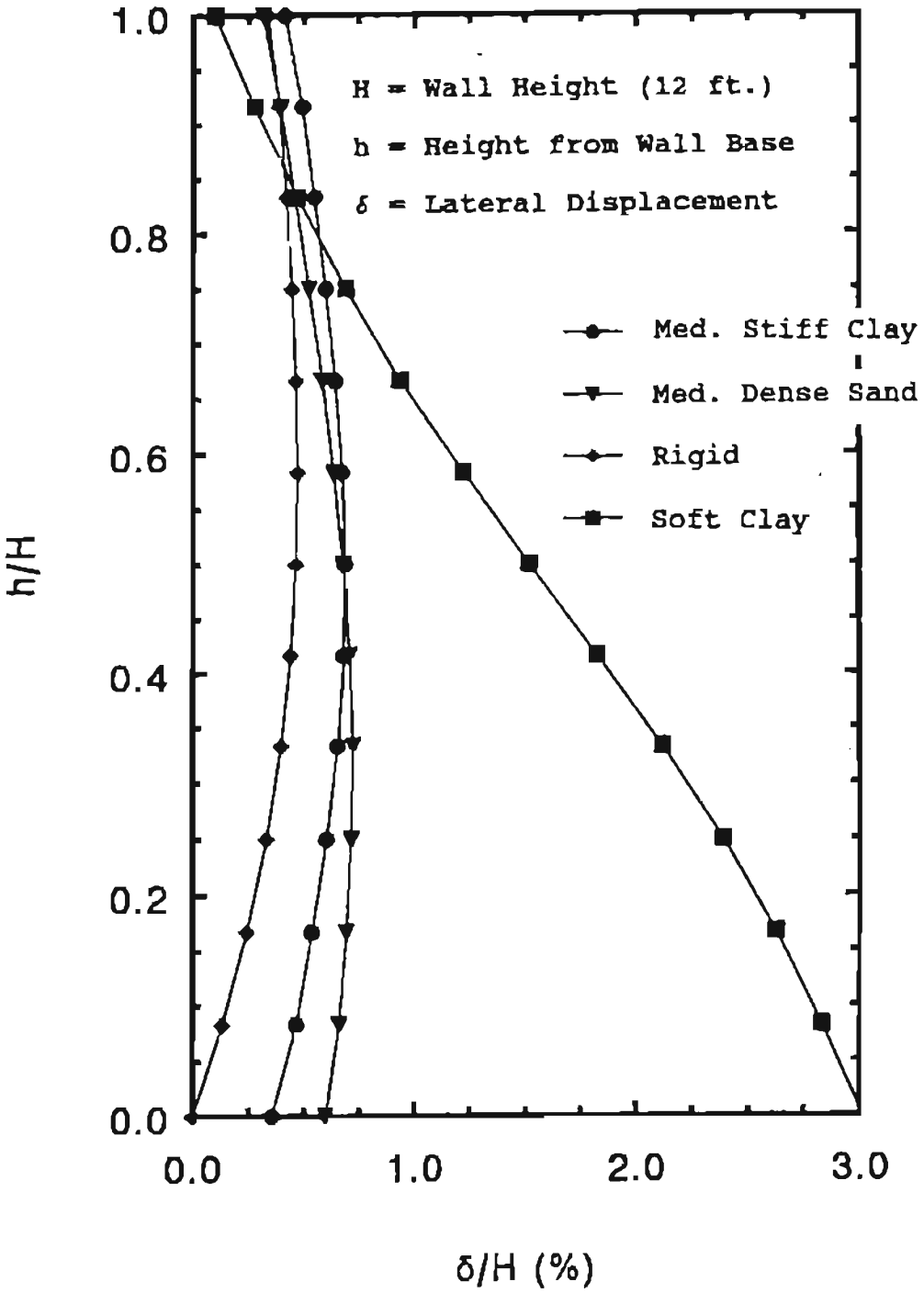

Figure 5.16: Effect of Foundation on Lateral Wall Displacement

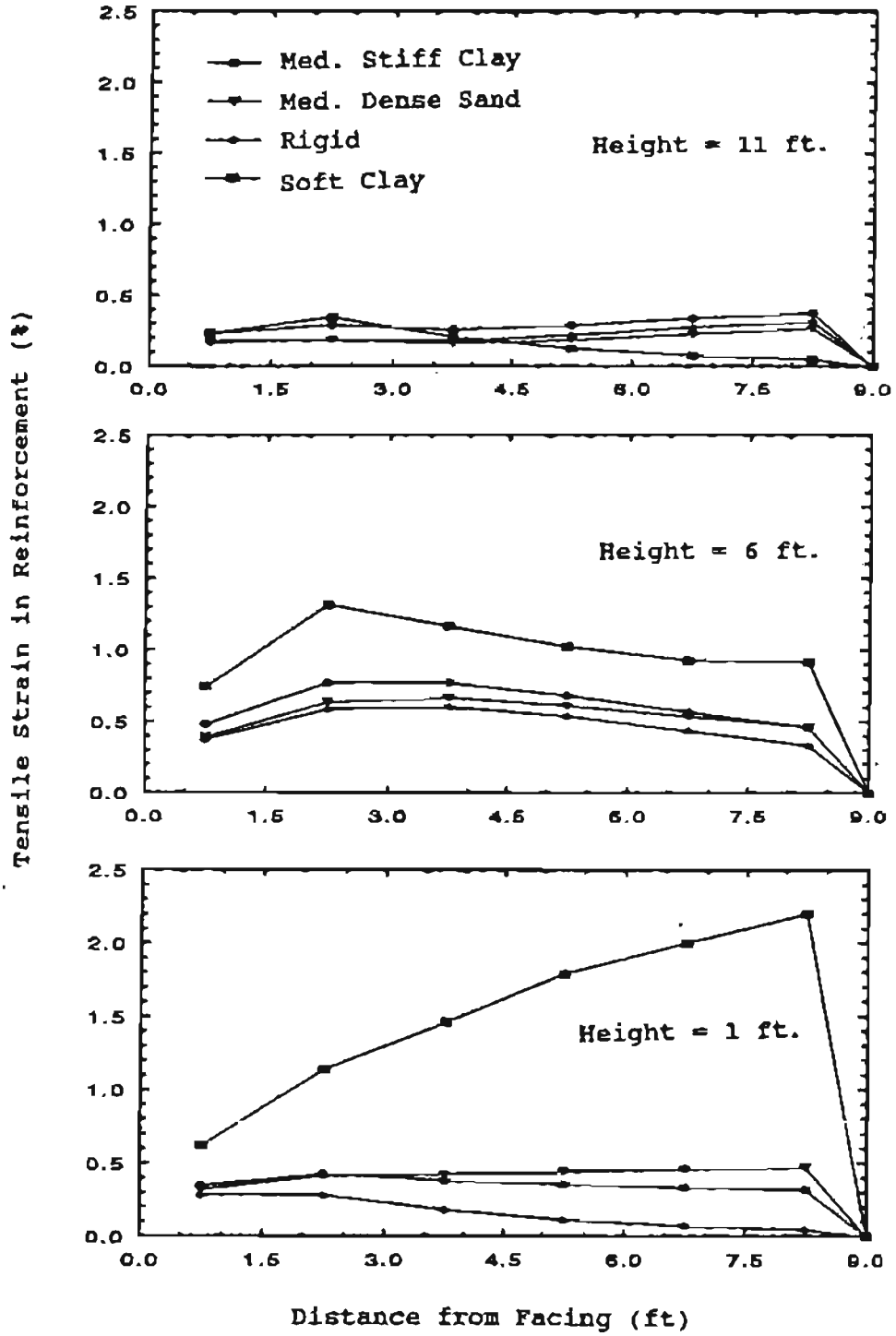

Figure 5.17: Effect of Foundation Stiffness on Reinforcement Tensile Strains

exhibits the lowest tensile strain, and the walls with loose sand and stiff clay exhibit about equal tensile strains. The patterns of the strain distribution are very similar for all four foundations.

It should be mentioned that, as discussed in Section 3.4.1.4., staged construction could be very effective for increasing the external stability of a wall constructed over a soft foundation. Wall deformation and tensile strain in the reinforcement also can be reduced effectively by staged construction. For a large wall construction project, a "slow construction" technique (i.e., limit the construction speed to an allowable rate) also may be used.

5.6 Effect of Reinforcement Stiffness and Strength

The effects of both reinforcement initial stiffness (E_i) and strength (T_{ult}) on the wall performance were examined. The values of E_i and T_{ult} investigated were:

Group 1: E_i= 500, 1000 & 2000 lb/in, and T_{ult}= 35 lb/in for the control wall (with the granular backfill).

Group 2: E_i= 500, 1000 & 2000 lb/in, and T_{ult}= 35 lb/in with the "cohesive-moist" backfill.

Group 3: E_i= 500 lb/in, T_{ult}= 35 lb/in; E_i= 5,000 lb/in, T_{ult}= 350 lb/in and E_i= 10,000 lb/in, T_{ult}= 700 lb/in with the "cohesive-wet" backfill.

Group 4: T_{ult}= 35 and 350 lb/in, and E_i= 500 lb/in for the control wall (with the granular backfill).

As shown in Figures 5.18 and 5.19, for geosynthetic walls with Group 1 properties, an increase in reinforcement stiffness reduces wall deformation and decreases tensile strain in the reinforcement. However, for walls with Group 2 properties, an increase in reinforcement stiffness does not affect the wall deformation (see Figure 5.20). For walls with Group 3 properties, the soil behaves like a loose cohesionless material; therefore, E_i becomes an important factor. As shown in Figure 5.21, the wall with a reinforcement of E_i=500 lb/in and T_{ult}=35 lb/in deformed about 7.5% of the wall height. When E_i was increased to 10,000 lb/in and T_{ult} increased to 700 lb/in, the maximum deformation reduced to 1.2% of wall height.

Unless a wall is approaching failure, an increase in tensile strength (T_{ult}) in reinforcement does not significantly improve the performance of the walls. Figure 5.22 shows that even when the reinforcement strength in the control wall is increased 10 fold, little decrease in wall deformation is noted. Naturally, the safety factor against rupture of the reinforcement is increased 10 times. For those limiting equilibrium methods which use only the strength to characterize the property of a

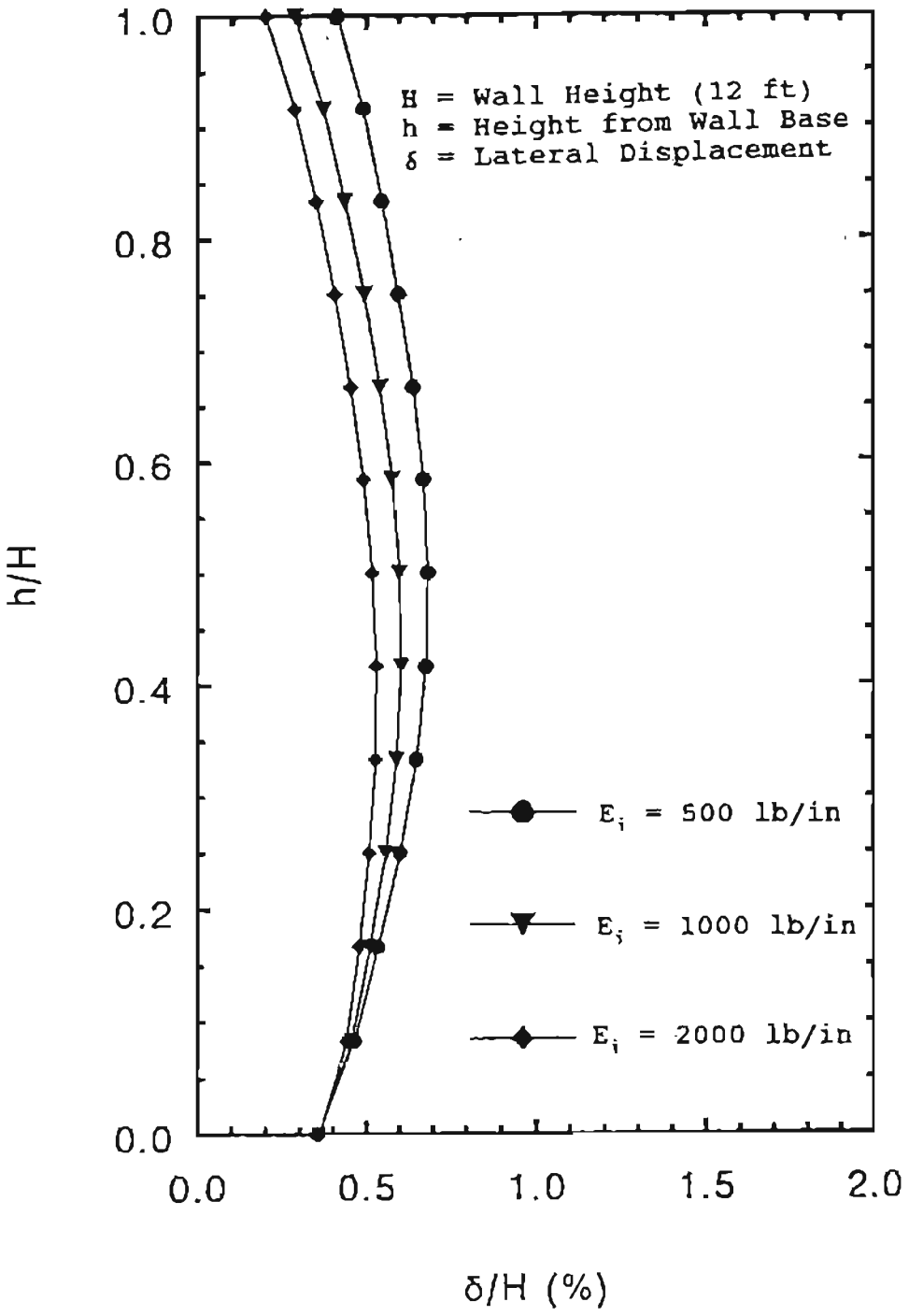

Figure 5.18: Effect of Reinforcement Stiffness on Lateral Wall Displacement, Group 1 Properties

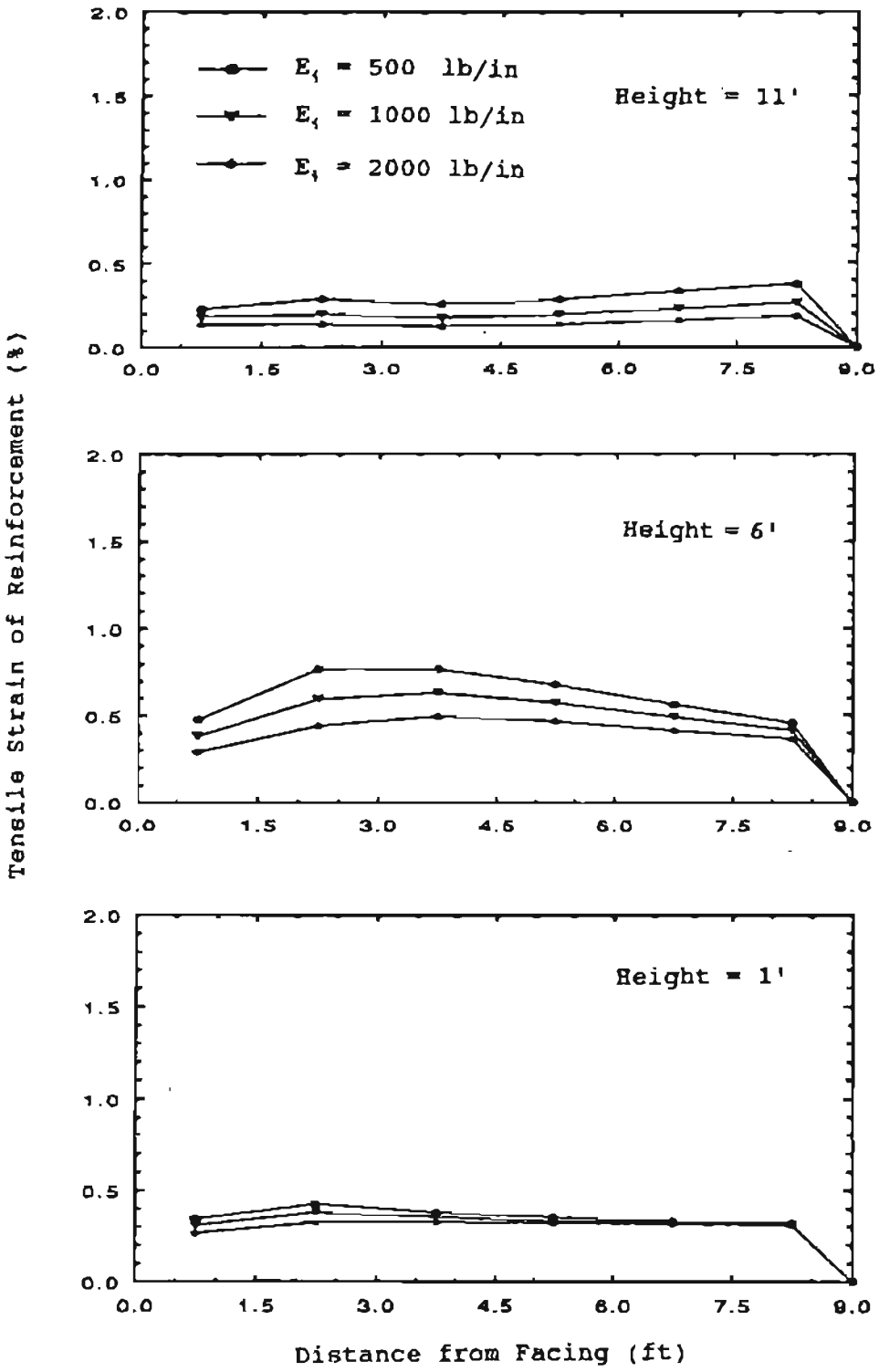

Figure 5.19: Effect of Reinforcement Stiffness on Tensile Strain, Group 1 Properties

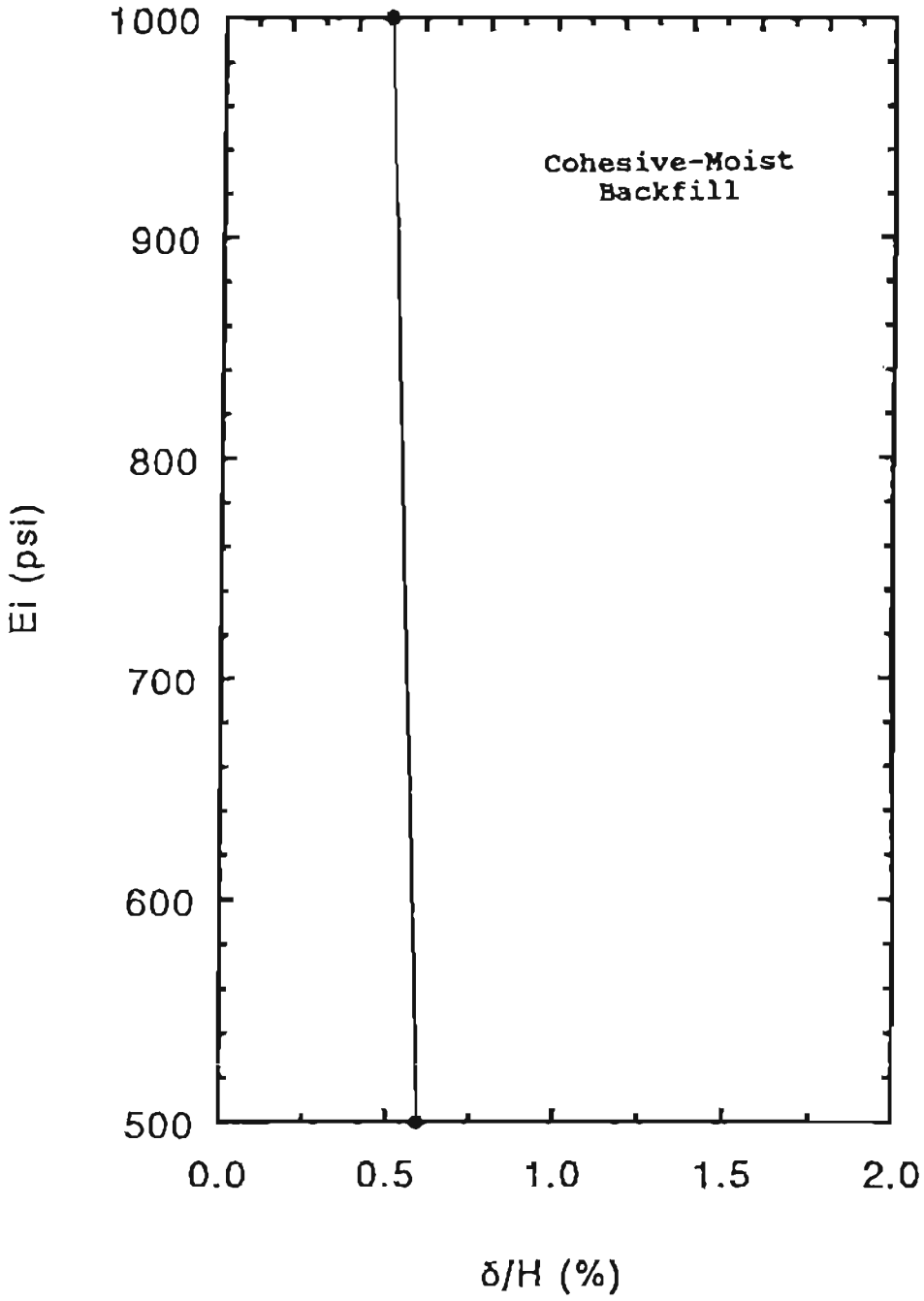

Figure 5.20: Effect of Reinforcement Stiffness on Maximum Lateral Wall Displacement, Group 2 Properties

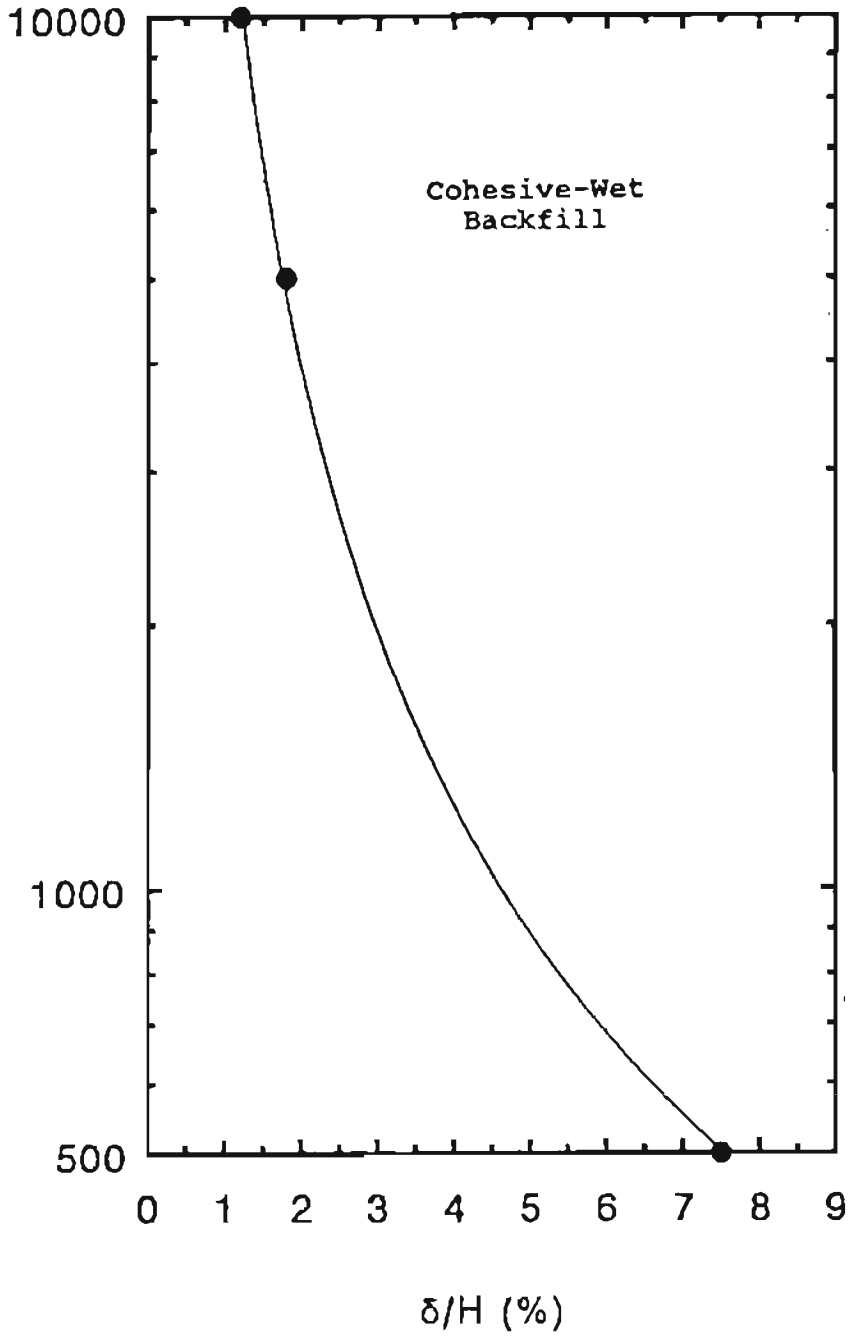

Figure 5.21: Effect of Reinforcement Stiffness on Maximum Lateral Deformation, Group 3 Properties

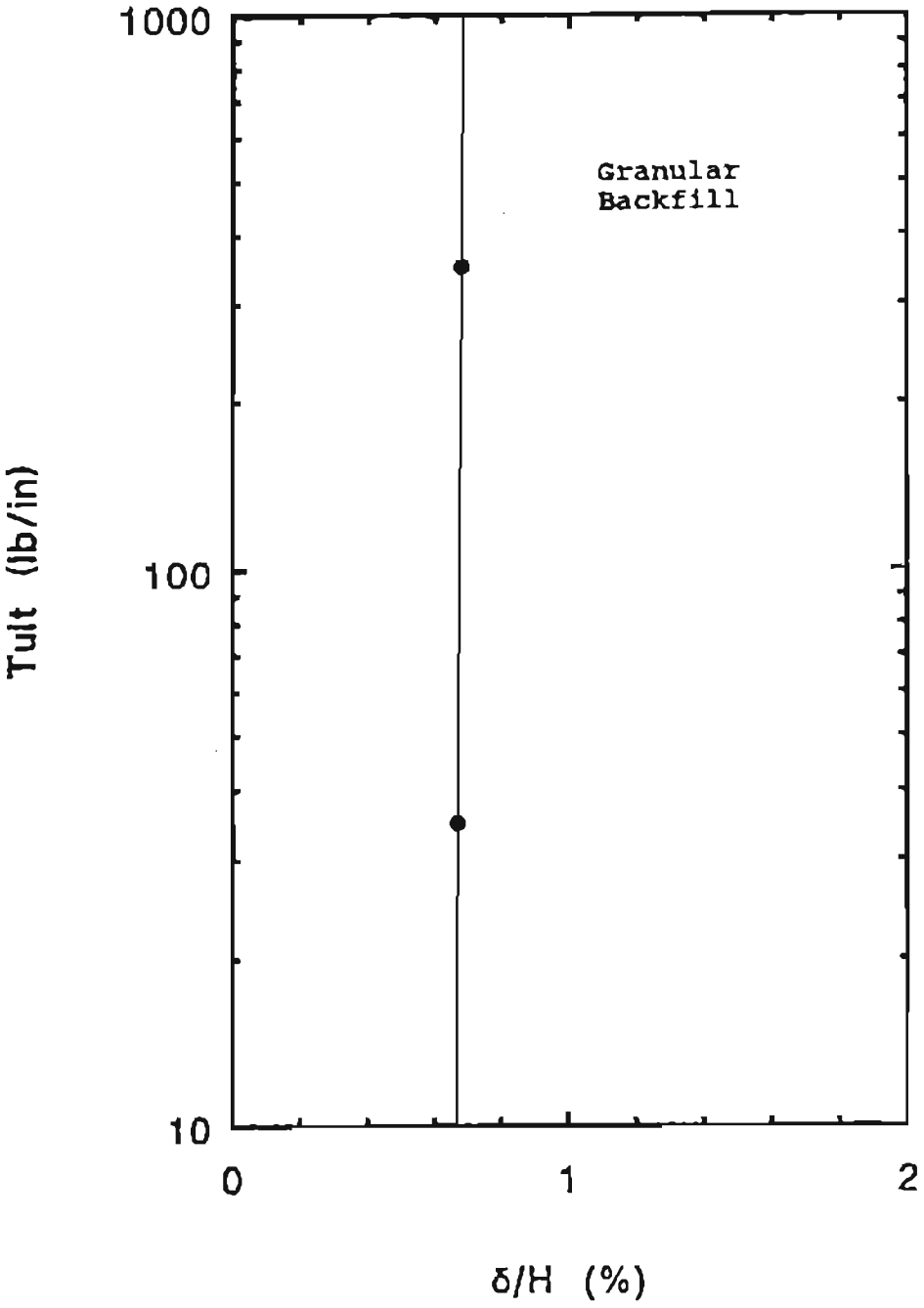

Figure 5.22: Effect of T_{ult} on Lateral Wall Displacement, Group 4 Properties

reinforcement, the increase of safety factor may be misleading as the wall performance is not improved.

5.7 Effect of Compaction & K_o

Duncan, et. al. (1991) developed a simple hand-calculation method to estimate the earth pressure induced by compaction. They used the FEM code SSCOMP which incorporated a hysteric loading-unloading model to obtain the compaction-induced stresses (see Section 3.2.1), and developed a series of earth pressure charts for various compaction equipment.

Using these charts and assuming that a vibratory plate is used for compaction, an as-compacted lateral earth pressure of 150 psf is obtained at a depth of 0.5 feet. Therefore, at the middle of a one-foot thick soil lift (with a density of 120 pcf), a K_o = 150/60 = 2.5 is calculated.

Sherif, Fang & Sherif (1984) recommended using the following equation for estimating K_o for a granular sand behind a rigid wall rotating at its base:

$$K_{od} = K_{oj} + K_{o1} \qquad (5.2)$$

and

$$K_{o1} = (\gamma_s / \gamma_t - 1) \times 5.5 \qquad (5.3)$$

where K_{od} = the coefficient of the at-rest pressure to be used in the design

K_{oj} = the Jaky coefficient of the at-rest earth pressure for a soil at its

loosest state and is equal to (1-sinϕ')

K_{o1} = the coefficient of locked-in at rest horizontal earth pressure due to soil prestressing or densification behind a rigid retaining wall

γ_s = in-place soil density

γ_l = loosest density of the soil

For the Ottawa sand used in the Denver Test Wall, the in-place unit weight was 107 pcf and the loosest unit weight was 97.5 pcf. With the frictional angle being 35 degrees, a K_{od} value of 0.97 was calculated.

The K_o value obtained from Sherif, et. al. method was much smaller than that from Duncan, et. al. method. To study the effect of K_o on the wall performance, the K_o values were varied as K_o= 2.5, 1.0 and 0.5. All other properties were kept the same as in the control wall.

It is seen from Figures 5.23 and 5.24 that the effects of K_o on lateral deformation of the wall and the tensile strains in the reinforcement are very significant. A higher K_o resulted in a much smaller wall displacement and much smaller strains in the reinforcement. It should be noted that the above analysis assumes that compaction only affects the backfill. The increase of lateral wall deformation, earth pressure (against the facing) and prestress in

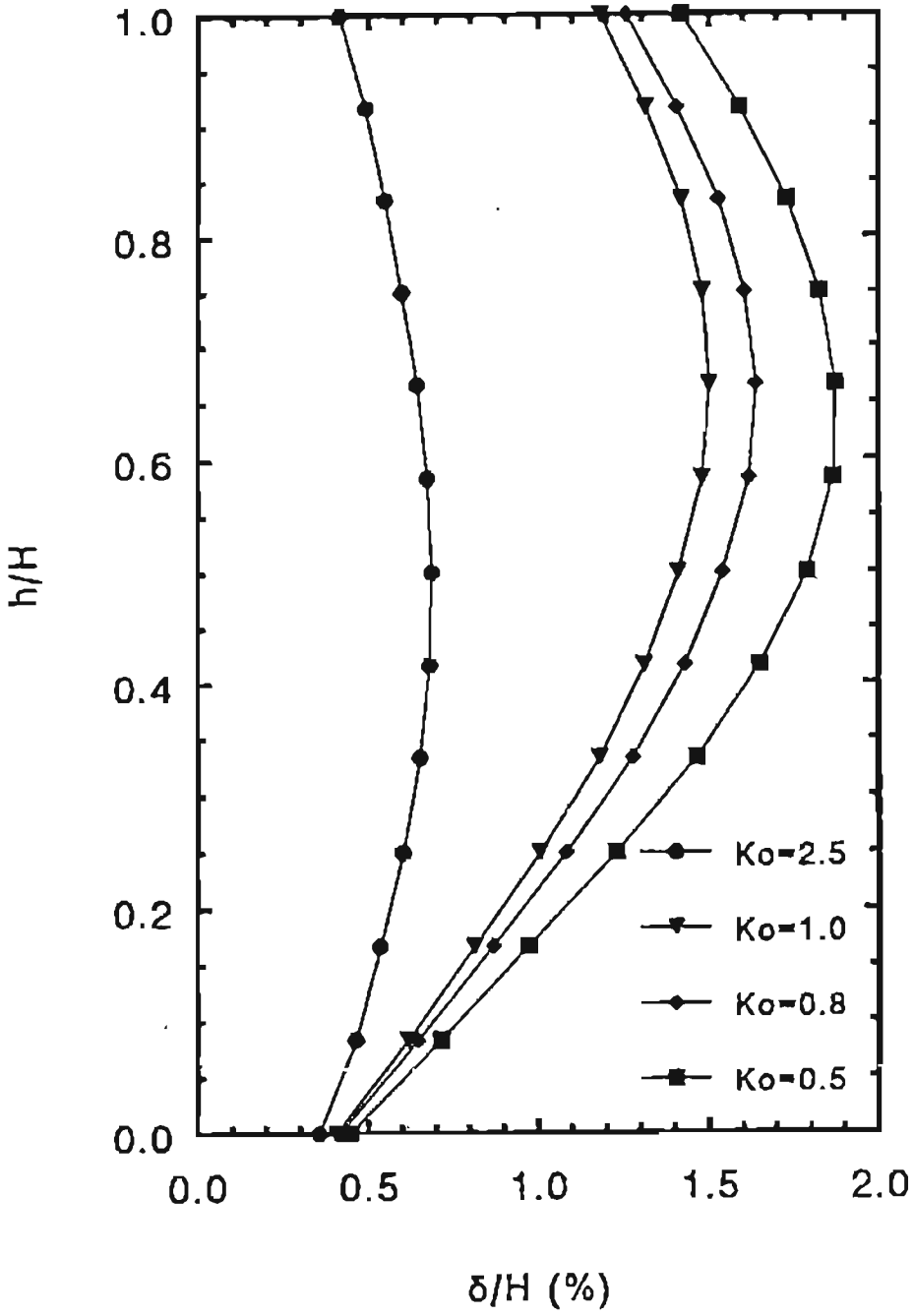

Figure 5.23: Effect of K_o on Lateral Wall Displacement

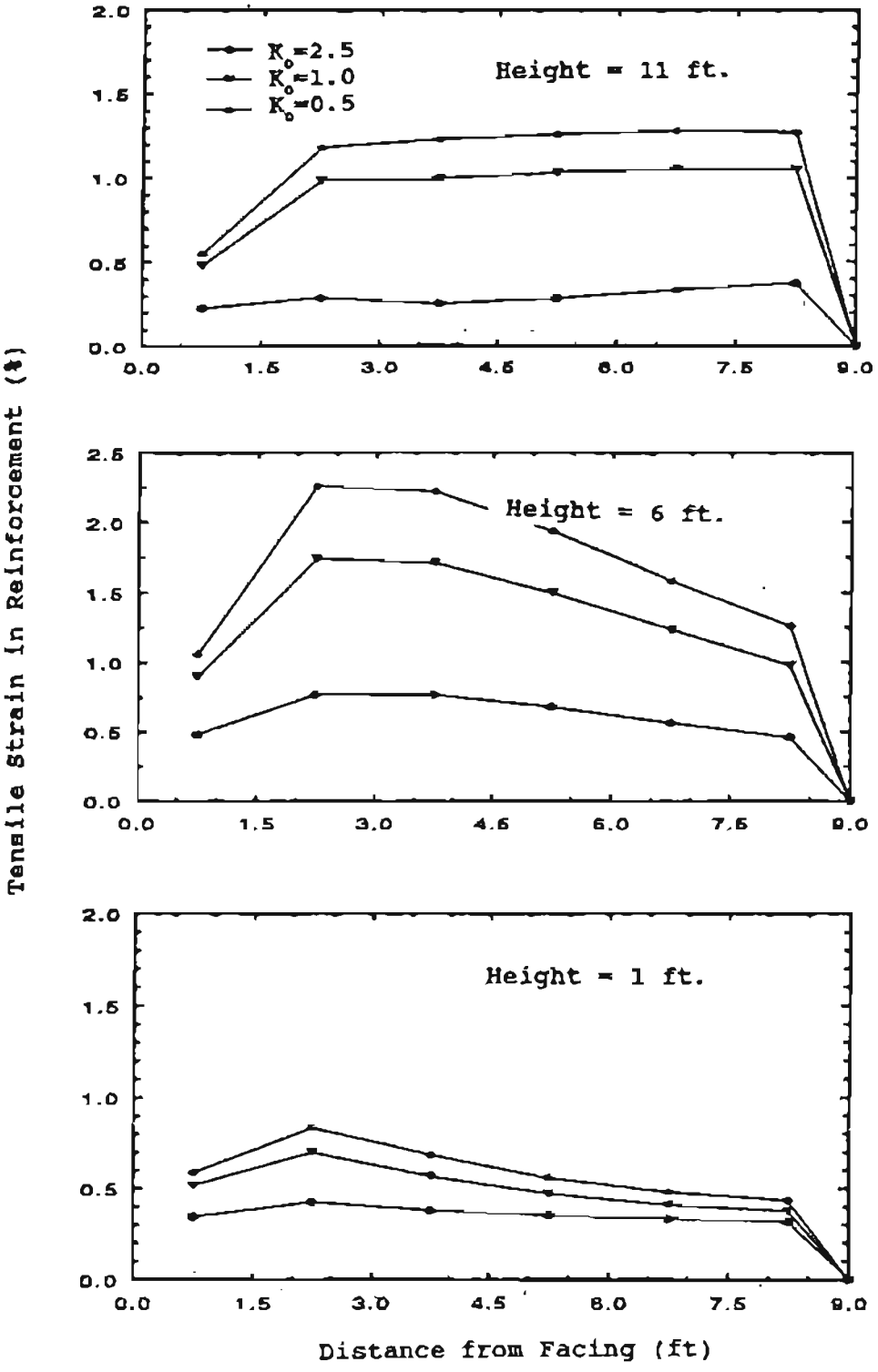

Figure 5.24: Effect of K_o on Reinforcement Tensile Strains

reinforcement due to compaction is not considered in the analyses. For GRS wall construction, it is recommended to limit the fill compaction to one foot from facing, so that the benefit of a high K_o can be gained, while the adverse effects of compaction may be minimized.

5.8 Effect of Wall Height

To study the influence of wall height on the performance of GRS walls, three different wall heights, i.e., 16, 12 and 8 feet, were analyzed. The spacing and the properties of reinforcement were kept the same as those of the control wall.

For the wall heights investigated, a larger wall height induces a larger wall displacement, in terms of wall height (see Figure 5.25), and higher tensile strains in the reinforcement (see Figure 5.26). For the three wall heights investigated, the wall displacements and reinforcement strain increase approximately linearly with the wall height.

5.9 Effect of Multiple Factors

The above parametric studies are limited to single-factor variations that deviate from the control wall. This section presents the behavior of the control wall under the influence of multiple-factor variations. Since the total number of combinations of all the factors considered is more than 1000, it is impractical to perform FEM analyses for all the cases.

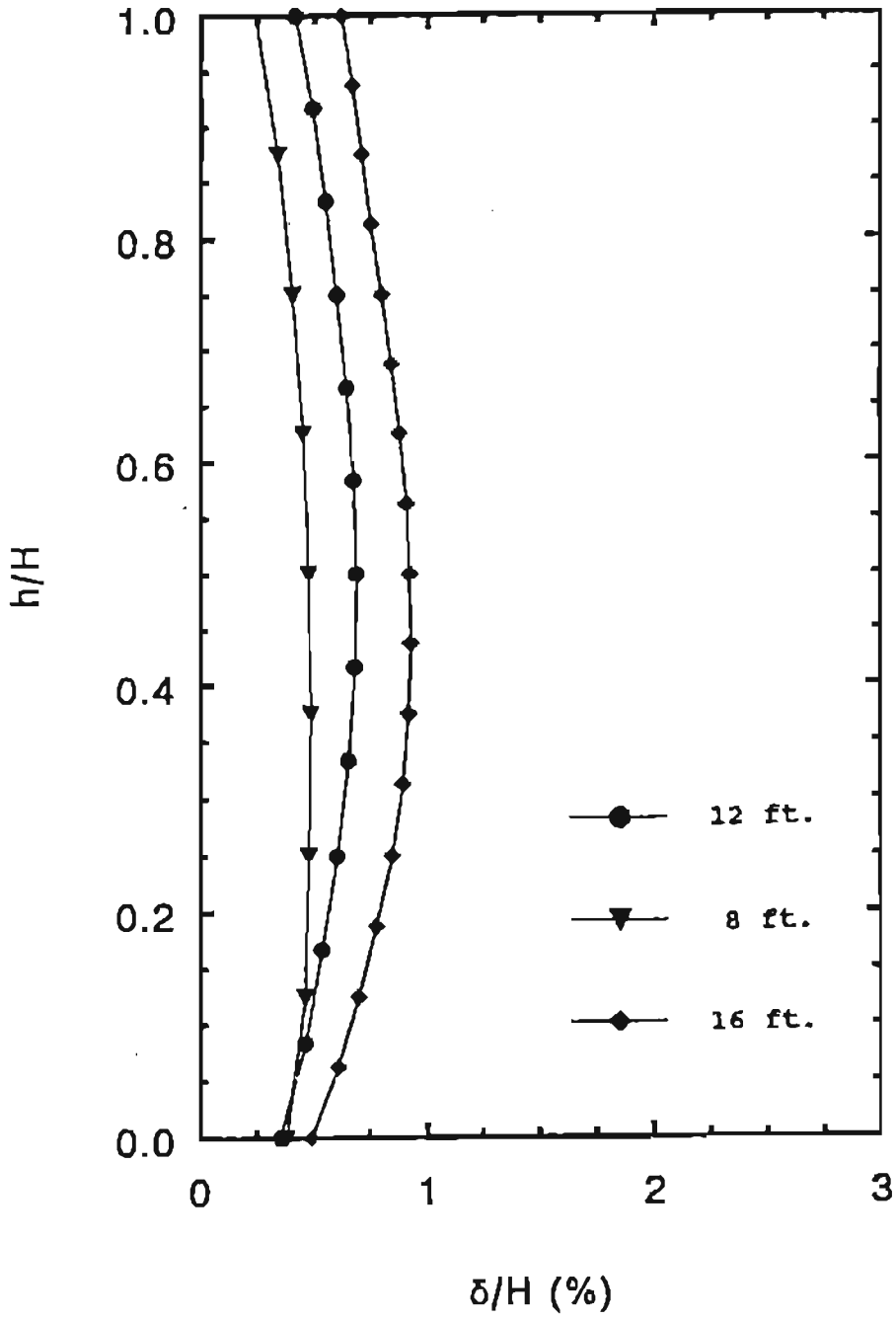

Figure 5.25: Effect of Wall Height on Lateral Wall Displacement

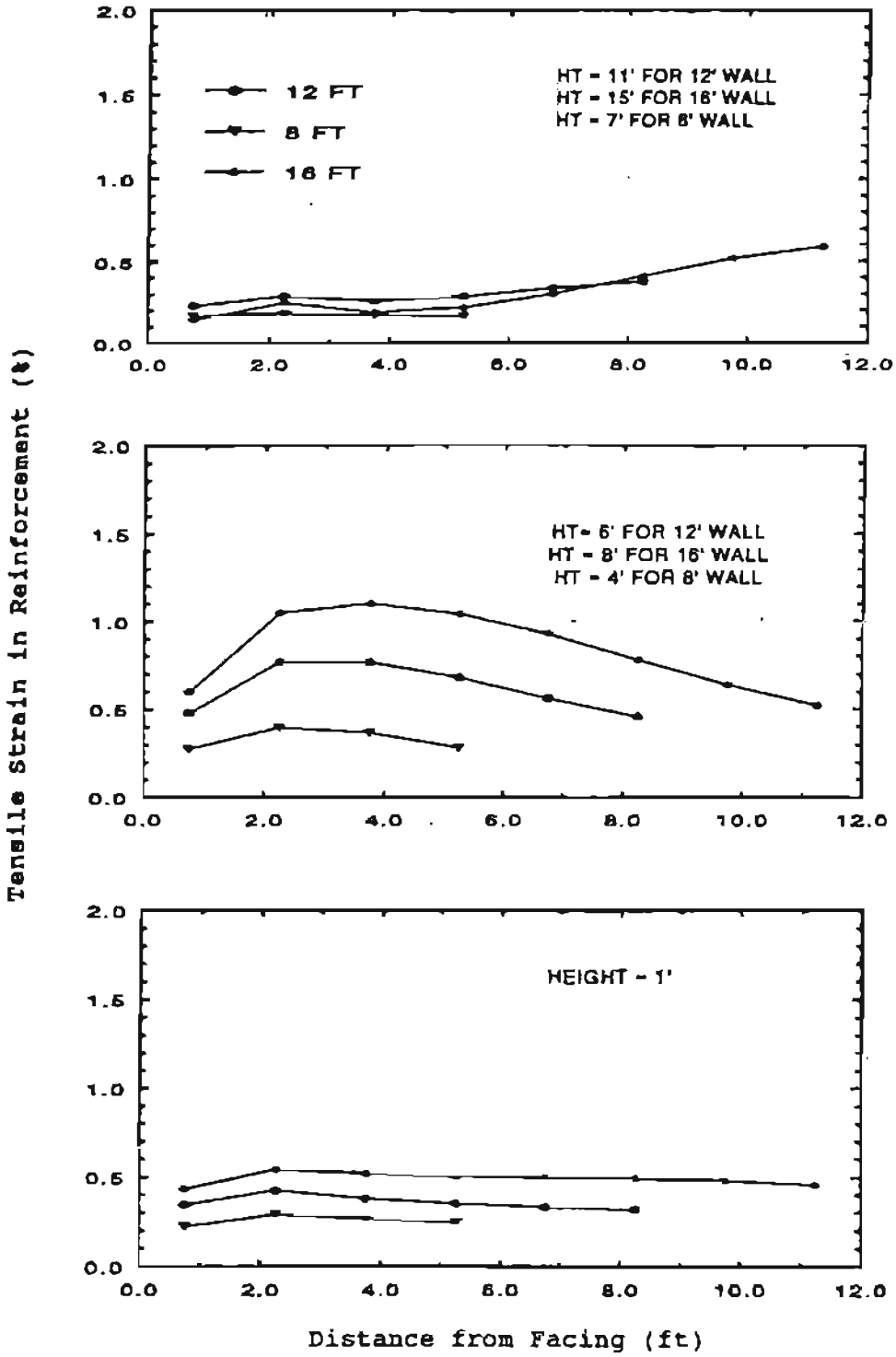

Figure 5.26: Effect of Wall Height on Reinforcement Tensile Strains

Therefore, it can be very useful to establish a simplified empirical method to account for multiple factor variations.

A total of 19 FEM analyses with multiple variations were performed in which the wall deformations and the maximum tensile strains in reinforcement were examined. For comparison purposes, the maximum lateral deformation of each analysis was normalized with respect to that of the control wall. The "Displacement Ratio" (DR) is defined as the ratio of a maximum lateral wall displacement (also in terms of wall height) of the particular analysis to the maximum lateral displacement (in terms of wall height) of the control wall. Hence, a DR of 1.5 means a 50% increase in the maximum lateral wall displacement from the control wall.

The maximum lateral wall displacements for the single factor and the combined factor cases are listed in Tables 5.8 and 5.9, respectively. In Table 5.8, the column "Factor Deviated From Baseline" corresponds to the factors listed on Table 5.4. For example, the factor "E-4" means the analysis is based on the same conditions as the control wall, except that the wall is situated on a rigid foundation. In this case, a lateral wall displacement of 0.465% of wall height was obtained, and the DR equals (0.465/0.688) = 0.676. Table 5.9 was prepared in a similar manner, except that

Table 5.8: Summary of Lateral Displacement of Walls with Single Variation

CASE NAME	FACTOR DEV. FROM BASELINE	δ_{max}/H (%)	DEFLECTION RATIO
PARA2X1	BASELINE	0.688	1.000
PARA2X2	F-3	0.608	0.884
PARA2X3	F-2	0.533	0.804
PARA1X1	E-3	0.722	1.089
PARA1X2	E-4	0.465	0.676
PARA1X3	E-2	3.014	4.381
PARA3X1	D-2	0.810	1.177
PARA3X2	D-3	0.550	0.799
PARA4X1	B-2	0.736	1.069
PARA5X1	A-4	0.499	0.725
PARA5X2*	A-3	0.781	1.135
PARA7X1	C-2	0.594	0.865
PARA7X2	C-3	7.430	10.799

* E_i = 1000 lb/in
  T_{ult} = 100 lb/in

TABLE 5.9
SUMMARY OF LATERAL DEFORMATION OF WALLS
WITH MULTIPLE VARIATIONS

FILE NAME	FACTORS DEV. FROM BASELINE	δ_{max}/H (%)	DR	(DR1x DR2x..)^n
CASE 1	C-2,E-2	2.979	4.330	3.78
CASE 2	C-2,E-4	0.729	1.059	0.941
CASE 3	C-2,E-5	0.446	0.648	0.584
CASE 5	C-3,E-4	106.25	154.43	--
CASE 6	C-3,E-5	25.139	36.539	--
CASE 7	B-2,E-2	8.472	12.314	--
CASE 8	B-2,E-4	0.715	1.039	1.164
CASE 9	B-2,E-5	0.493	0.717	0.722
CASE 10	B-2,C-2	0.665	0.967	0.924
CASE 11	B-2,C-2,E-2	2.722	3.956	4.051
CASE 12	B-2,C-2,E-4	0.736	1.069	1.006
CASE 13	B-2,C-2,E-5	0.448	0.651	06.25
CASE 14*	A-3,C-2	0.797	1.158	0.980
CASE 15*	A-3,B-2	0.922	1.340	1.227
CASE 16*	A-3,B-2,C-2	0.823	1.196	1.052
CASE 17	A-4,C-2	0.250	0.364	0.704
CASE 18	A-4,C-2,D-2	0.260	0.379	0.796
CASE 19*	A-3,D-3	0.589	0.856	0.901

* E_i = 1000 lb/in
  T_{ult} = 100 lb/in

multiple factors deviating from the control wall were analyzed. For example, the factors C-2 and E-4 (Case 2) imply that the wall was subjected to the same conditions as to the control wall, except that a cohesive-moist backfill was used and the wall was situated on a rigid foundation.

An attempt was made to find an empirical relationship between the maximum wall displacement due to a multiple-factor variation and the maximum wall displacement due to the corresponding single-factor variation. The following empirical equation is found to best fit the data (Figure 5.27).

$$DR = (DR1 \times DR2 \times DR3.....)^{n} \qquad (5.4)$$

where DR = the displacement ratio due to multiple-factor variation,

DR1, DR2... = the displacement ratio due to each single-factor variation considered and

n = 1.0 for 12-and 16-foot high walls, and

= 0.67 for 8-foot high walls

For example, if one desires to determine the maximum lateral wall deformation of a 12-foot high (n=1.0) timber facing wall with cohesive-moist backfill (DR1 = 1.069), a trapezoidal reinforcement layout (DR2

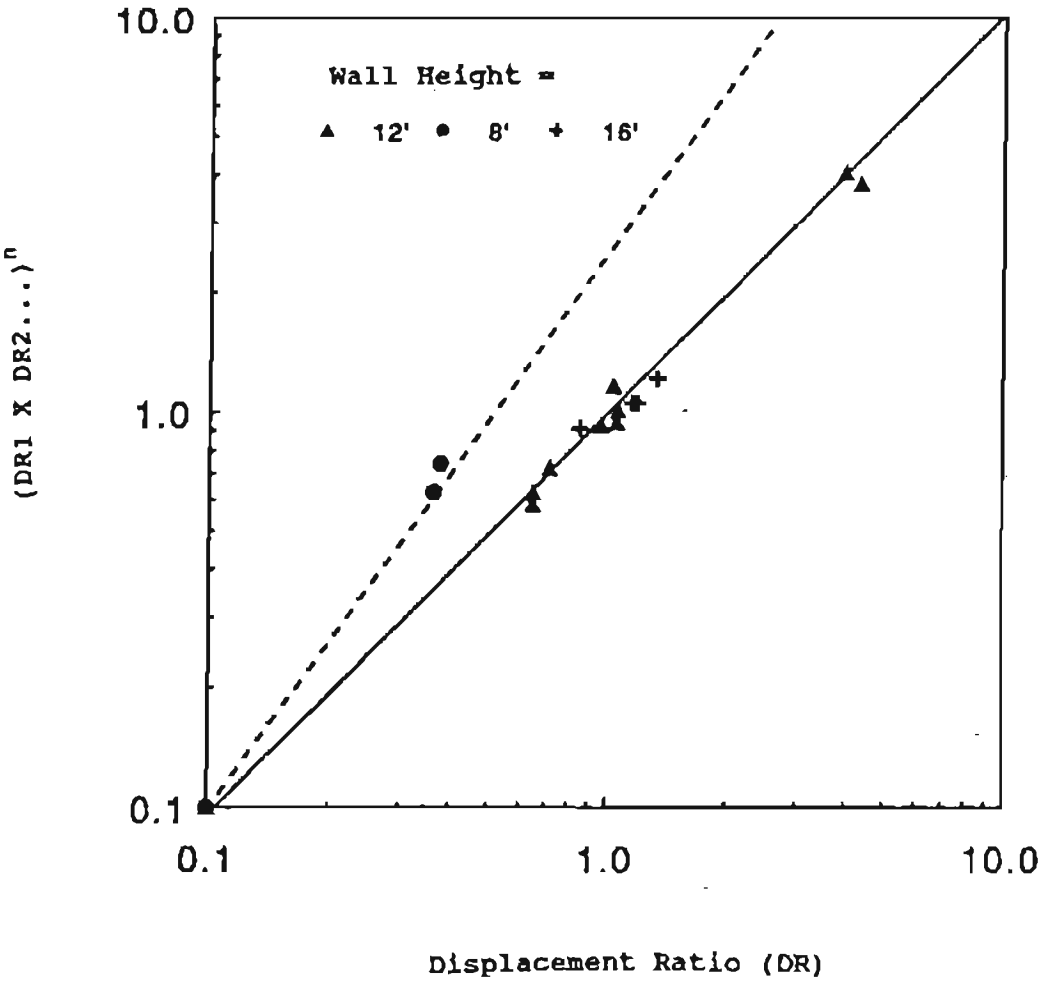

Figure 5.27: Relationships between the Deflection Ratios of Single-factor Variation and Multiple-factor Variations

= 0.865), situated on soft clay foundation (DR3 = 4.38), one may obtain DR of the multiple variations by using Equation 5.4 as DR=(1.069 x 0.865 x 4.38) = 4.05. This calculated DR is very close to the result obtained directly from the FEM analysis, which gives a DR of 3.956 (case 11 of Table 5.9). The maximum wall displacement, therefore, equals 4.05 x 0.688% x 12 ft. x 12 in., or 4.0 inches.

Although the empirical equation appears to work well in this instance, more research is needed to confirm the applicability of using Equation 5.4 in generalized cases.

The tensile strains induced in the reinforcement for the single and multiple variations are shown in Tables 5.10 and 5.11, respectively. The maximum strains for the top, middle and bottom layers of the reinforcement are presented. For comparison purposes, the maximum tensile strain for each analysis is also normalized with respect to the control wall. The "Strain Ratio" (ϵ ratio) is defined as the ratio of a maximum tensile strain of a particular analysis to the maximum tensile strain of the control wall, at the same layer of the reinforcement. The safety factor in rupture is defined as the ratio of T_{ult}/T, where T_{ult} is the rupture strength of reinforcement, and T is the maximum tensile force inducted in a layer of reinforcement. Tables 5.10 and 5.11 indicate that,

TABLE 5.10

MAXIMUM REINFORCEMENT TENSILE STRAINS FOR WALLS WITH SINGLE-FACTOR VARIATION

FACTORS DEVELOPED FROM BASELINE	ϵ_{max} AT TOP LAYER		ϵ_{max} AT MEDIUM LAYER		ϵ_{max} AT BOTTOM LAYER		F.S. (T_{ult}/T)
	ϵ(%)	ϵ RATIO	ϵ(%)	ϵ RATIO	ϵ(%)	ϵ RATIO	
Baseline	0.3	1.0	0.8	1.0	0.4	1.0	5.6
F-3	0.3	1.0	0.6	0.8	0.4	1.0	3.9
F-2	0.3	1.0	0.5	0.6	0.3	0.7	3.9
E-4	0.2	0.7	0.7	0.9	0.5	1.2	6.5
E-5	0.3	1.0	0.6	0.8	0.3	0.7	6.9
E-2	0.3	1.0	1.3	1.6	2.2	5.2	3.6
D-2	0.6	2.0	1.0	1.3	0.8	2.0	4.4
D-3	0.6	2.0	0.6	0.8	0.3	0.7	6.5
B-2	0.3	1.0	0.7	0.5	0.3	0.7	6.9
A-4	0.2	0.7	0.4	0.5	0.3	0.7	9.7
A-3	0.4	1.3	0.8	1.0	0.5	1.2	11.5
C-2	0.1	0.3	0.5	0.6	0.4	1.0	10.3
C-3	0.4	1.3	2.9	3.6	10.9	26	1.3

* E_f = 1000 lb/in
  T_{ult} = 100 lb/in

TABLE 5.11

MAXIMUM REINFORCEMENT TENSILE STRAINS
FOR WALLS WITH MULTIPLE-FACTOR VARIATIONS

CASE NAME	FACTORS DEV. FROM BASELINE	ε_{max} AT TOP LAYER		ε_{max} AT MEDIUM LAYER		ε_{max} AT BOTTOM LAYER		F.S. (T_{ult}/T)
		ε(%)	ε RATIO	ε(%)	ε RATIO	ε(%)	ε RATIO	
CASE 1	C-2,E-2	0.2	0.7	1.0	1.3	2.1	5.0	4.3
CASE 2	C-2,E-4	0.1	0.3	0.5	0.6	0.5	1.2	10.0
CASE 3	C-2,E-5	0.1	0.3	0.4	0.5	0.3	0.7	11.3
CASE 5	C-3,E-4	11.2	37.3	7.3	9.1	2.2	5.2	1.0
CASE 6	C-3,E-5	3.4	11.3	4.4	5.5	2.3	5.5	1.9
CASE 7	B-2,E-2	0.7	2.3	2.8	3.5	3.6	8.6	2.2
CASE 8	B-2,E-4	0.3	1.0	0.6	0.8	0.4	1.0	6.9
CASE 9	B-2,E-5	0.3	1.0	0.6	0.8	0.3	0.7	7.3
CASE 10	B-2,C-2	0.2	0.7	0.5	0.6	0.4	1.0	9.5
CASE 11	B-2,C-2,E-2	0.6	2.0	1.2	1.5	1.5	3.6	3.6
CASE 12	B-2,C-2,E-4	0.2	0.7	0.5	0.6	0.4	1.0	10.0
CASE 13	B-2,C-2,E-5	0.2	0.7	0.4	0.5	0.3	0.7	10.9
CASE 14*	A-3,C-2	0.1	0.3	0.6	0.8	0.5	1.2	13.2
CASE 15*	A-3,B-2	0.6	2.0	1.0	1.3	0.5	1.2	12.2
CASE 16*	A-3,B-2,C-2	0.2	0.7	0.6	0.8	0.6	1.4	11.8
CASE 17	A-4,C-2	0.01	0.03	0.1	0.1	0.1	0.2	31.8
CASE 18	A-4,C-2,D-2	0.05	0.2	0.1	0.1	0.2	0.5	16.7
CASE 19*	A-3,D-3	0.5	1.6	0.6	0.5	0.4	1.0	9.2

* E_{ℓ} = 1000 lb/in
  T_{ult} = 100 lb/in

except for the walls with the cohesive-wet backfill or on the soft foundation, all the analyses have adequate safety factors against rupture failure, although a relatively weak tensile strength (T_{ult}=35 lb/in) was chosen for the reinforcement. It should be reiterated that a high safety factor in rupture does not guarantee a satisfactory performance of the geosynthetic wall.

CHAPTER VI

PRELIMINARY DESIGN PROCEDURE AND CONSTRUCTION GUIDELINES

The results of the parametric study presented in Chapter 5 are the basis for proposing a preliminary design procedure and design guidelines for GRS walls. It is proposed that design of GRS walls for internal stability be based on allowable deformation. In addition, an appropriate safety factor (say 5) applied to the ultimate tensile strength of the reinforcement should be used to ensure long-term durability of the reinforcement. The proposed design method permits the use of cohesive-moist soils as backfill, provided that proper precautions are taken to avoid wetting of the backfill. Measures to prevent post-construction wetting of cohesive backfill will be discussed. Construction guidelines for GRS walls also will be presented.

6.1 Proposed Design Method

After the need of a wall is identified and a GRS wall has been selected as a potential wall type, the following step-by-step procedure may be used to obtain a detailed design.

Step 1: Determine wall geometry and the allowable wall movement

The wall geometry includes wall height, the extent of backfill and retained soil, and foundation conditions. The value of the allowable wall displacement should be determined based on the nature of the wall (i.e., whether temporary or permanent), tolerance of movement of the structures (i.e., high mast lights, signs, pavements, etc.) on the top of backfill, and its visibility (i.e., whether the wall face is visible). As a general rule, the allowable wall movement should be limited to 1 inch or 1% of the wall height for permanent and more visible walls; and between 2 to 6 inches for temporary or less visible walls.

Step 2: Select facing type and possible backfill types

The facing type may be one without any bending resistance (e.g., wrap-around geosynthetic), one with local bending resistance (e.g., an articulated facing), or one with global bending resistance (e.g., a continuous concrete panel or a timber/forming element facing). The selection of backfill depends mostly on availability. Both granular and unsaturated cohesive backfills are acceptable.

Step 3: Determine the material parameters of the foundation soil and the possible backfills

For soft to medium-soft clay foundations, the Sekiguchi-Ohta soil model is recommended. The Duncan-Chang soil model should be used for backfills and other foundation soils. Triaxial test results are needed to determinate the material parameters. Determination of the material parameters for the Sekiguchi-Ohta model and the Duncan-Chang model were presented by Iizuka & Ohta (1987) and Duncan et.al. (1980), respectively. If triaxial test results are not available, the parameter values summarized by Duncan et. al. (1980), or Table 3.2 & 3.3., may be used for estimating the Duncan-Chang model parameters.

Step 4: Select a trial design

The selection of a trial design involves selecting the reinforcement configuration, reinforcement stiffness and strength, and the most probable backfill. Recommended trial designs for various conditions are given in Table 6.1.

Step 5: Perform a finite element analysis on the trial design

It is recommended that DACSAR be used for analysis. If the maximum wall movement is smaller than the maximum allowable value, and the maximum tensile force in the reinforcement is considerably smaller than its ultimate strength (i.e., smaller than 0.2 T_{ult}), the trial design may be accepted. This step may be skipped if the conditions of the wall conform to those

Table 6.1 Recommended Trial Design for the Reinforcement

Wall Height (ft)	E_i (lb/in)	T_{ult} (lb/in)
less than 10	500	70
10 - 20	700	100
20 - 30	950	140
30 - 40	1,250	190

Note: The above-recommended values are based on the following conditions: uniform surcharge = 5 psi; reinforcement spacing = 1 ft; reinforcement length = 0.7 H (H = wall height); foundation soil has a blow count greater than 10; wall facing is either articulated panels or timber facing; backfill is either granular or cohesive-moist soil, with 95% Standard Proctor compaction and adequate drainage; wall shape is either rectangular or trapezoidal.

For walls with conditions different from the above, the following adjustments may be made for the trial design: (1) If the surcharge is greater than 5 psi, for each additional 1 psi, add 50 lb/in in E_i, and add 5 lb/in in T_{ult}; (2) If the reinforcement spacing is other than 1 ft, the E_i and T_{ult} values for the trial design should be increased in proportion to spacing (in ft), (3) If the foundation soil has blow counts between 5 and 10, the E_i and T_{ult} values should be increased by 50%; if the foundation soil has blow counts less than 5, the foundation soil should be improved (for example, using staged construction); (4) If wrap-around facing is used, the E_i and T_{ult} values may be increased by 50%; if articulated panel is used, the values should be increased by 20 %; if full height concrete facing is used, the values should be reduced by 40%; (5) If the potential for wetting of a cohesive backfill is high, the E_i and T_{ult} values should be increased by 5 times, and the reinforcement length should be increased to at least 1.0 H.

prescribed in Appendix A. In that case, the maximum wall movement (i.e., 1 inch) and the required E_i and T_{ult} in the reinforcement can be obtained from a table deduced from finite element analysis.

Step 6: If the trial design is found unsatisfactory, modify the design

If the maximum wall movement is considerably smaller than the allowable value, modifications to the trial design may be made by reducing the stiffness (E_i) of the reinforcement, and/or by increasing reinforcement spacing. A finite element analysis should be conducted on the modified design to ensure that the design is indeed acceptable.

If the maximum wall movement obtained from the trial design is greater than the allowable value, or if the maximum tensile force in the reinforcement is excessive (i.e., larger than 0.2 T_{ult}), modifications to the trial design should be made. The modifications may be in one or more of the following forms:

(a) Increase reinforcement stiffness/strength. If the reinforcement tension is excessive, increasing the strength usually will be most effective. Otherwise, reinforcement stiffness values that are larger than the trial design may be used in subsequent finite element analyses. An interpolation procedure

can be useful for selecting the optimum reinforcement stiffness.

(b) Increase reinforcement length, if space allowed; or decrease reinforcement spacing, but not less than 9-inch, especially in the lower portion of the wall.

(c) Use alternative backfills.

(d) Improve foundation soil if the foundation deformation is significant, or employ staged construction if soft clay foundation is present.

(e) Use continuous facings, such as full-height concrete panels.

The results of the parametric study (Chapter 5) can serve as guidelines for these modifications. Finite element analyses should be conducted on the modified designs to check their acceptability.

Step 7: Perform a cost comparison of acceptable modified designs, and select an optimum design

Step 8: Perform external stability analyses, and calculate settlement of the wall due to deformation of foundation

Conventional stability analysis methods in soil mechanics can be used for the external stability analyses. The external stability analyses include checking the overall slope stability, the sliding stability, bearing capacity, and overturning stability

(see Section 3.4.1.2). The reinforced wall may be considered as a rigid body in such analyses. Measures should be taken to ensure acceptable stability margins with respect to all possible modes of external instability, and to ensure that settlements are not excessive.

Step 9: Prepare specifications, and select a geosynthetic material

6.2 Proposed Design Guidelines

The following design guidelines are recommended:

(1) Wall shape: Based on the existing grade of the site, either a rectangular or trapezoidal shaped wall may be selected. For rectangular-shaped walls, a length/height (L/H) ratio of 0.7 is recommended. When constructing walls in constrained spaces, such as walls built to protect an existing slope, or to widen an existing highway, a trapezoidal-shaped wall (truncated base wall) is usually more cost-effective. For trapezoidal-shaped walls, a minimum length of 4 feet at the base and a L/H ratio of 1.0 at the top are recommended. It should be noted that external stability is generally the controlling factor for selecting a trapezoidal-shaped wall over a rectangular-shaped wall.

(2) Backfill: Using granular material as backfill is recommended, provided that it can be obtained at a reasonable cost. However, cohesive

backfill also may be substituted if all of the following criteria are met:

- Granular material is too costly;
- The construction site is located in an arid or a semi-arid area;
- The site grade is such that surface water is unlikely to infiltrate the backfill;
- Adequate drainage is provided (see Section 6.3).

(3) Facing: Any of the four types of facings discussed in Section 5.4 may be used. The timber/forming facing system developed by CDOT is easy to construct, aesthetically pleasing, cost-effective, and has demonstrated remarkable stability. It also provides moderate global bending rigidity.

Articulated panel facings (including modular blocks) are easy to construct and are aesthetic. They provide high local bending rigidity but little global bending rigidity. Due to the difficulties with connecting geotextiles to the facing, articulated panels have been used only with geogrid reinforcement. Wrap-around facings provide neither global nor local rigidity, and are not attractive in appearance. Their use should be limited to temporary walls, especially if no ultraviolet protection is provided.

Full-height continuous concrete facings provide the highest global rigidity, but they are more

expensive than other facing systems. Due to their high rigidity, full-height concrete facings generally are not suitable for soft foundations, unless a multiple-phase wall construction technique is adopted. The multiple-phase construction method uses a wrap-around facing (or gabions) as a temporary support. After the primary consolidation is essentially completed, full-height, cast-in-place or precast concrete panels may be added as facing.

(4) Foundation: GRS walls can be constructed on almost all types of foundation soils except soft clay (i.e., cohesion less than 500 psf). If a soft clay foundation is present and external stability appears to be a problem, the following remedial measures may be considered (Hausmann, 1990): (a) staged (or slow) construction with or without surcharge of the wall, (b) sub-excavation of the existing soft soil and replacement with compacted backfill, (c) lime or lime/fly ash treatment, (d) stone columns, (e) wick drains with or without surcharge, and (f) compaction grouting. If time is not a major concern, usually staged construction, perhaps with surcharge to accelerate consolidation, is the most cost-effective solution. When staged construction is not allowed due to time constraints, using wick drains to accelerate consolidation of the foundation soil should be considered.

(5) Reinforcement: The parametric study indicates that although a stiffer geosynthetic would reduce the lateral wall deformation, there is a limitation to the reduction. Increasing E_i generally does not reduce the portion of lateral wall deformations caused by foundation movement. Increasing E_i to reduce lateral wall deformation is usually more effective in granular backfill walls than in cohesive-moist backfill walls. However, if a cohesive-moist backfill becomes saturated, both the stiffness and the strength of the reinforcement may be crucial.

The wide-width tensile test is recommended for determining the stiffness and strength of the reinforcement that is insensitive to normal pressure (ASTM, 1987). For normal-pressure sensitive geosynthetics, the membrane-confinement test proposed by Wu (1991) is recommended (see Section 3.3.2.2).

6.3 Measures To Prevent Wetting of Cohesive Backfill

The presence of static or seeping water in cohesive backfill may cause the following adverse effects:

- A reduction in the shear strength of the backfill due to an increase of water content;
- An increase in the total weight of the backfill;
- Generation of seepage forces in the direction of seepage;

- An increase in the creep potential of the reinforcement and the soil due to an increase of the stress level.

The following measures are recommended to prevent post-construction wetting of the cohesive backfill:

(1) Surface drainage system: To reduce percolation of surface water into the backfill, the runoff should be directed away from the backfill. This is especially important in a half-cut, half-fill construction. For example, the author was involved in a highway embankment slide project along I-70 near Golden, Colorado. The slide resulted from surface runoff from a hillside that flowed toward the embankment fill; that created seepage forces, saturated and reduced the cohesion of the backfill, and caused a catastrophic failure. As a partial remedy, side ditches, paved shoulders, detention ponds, and culverts were provided to divert the surface runoff. They have proven successful since the correction was made in 1984.

(2) Subsurface drainage system: To prevent water from seeping into the cohesive backfill, the designer should consider using layers of filter or geocomposite around the top, back and bottom of the reinforced zone (see Figure 6.1). A perforated PVC pipe installed at the bottom of granular fill is necessary.

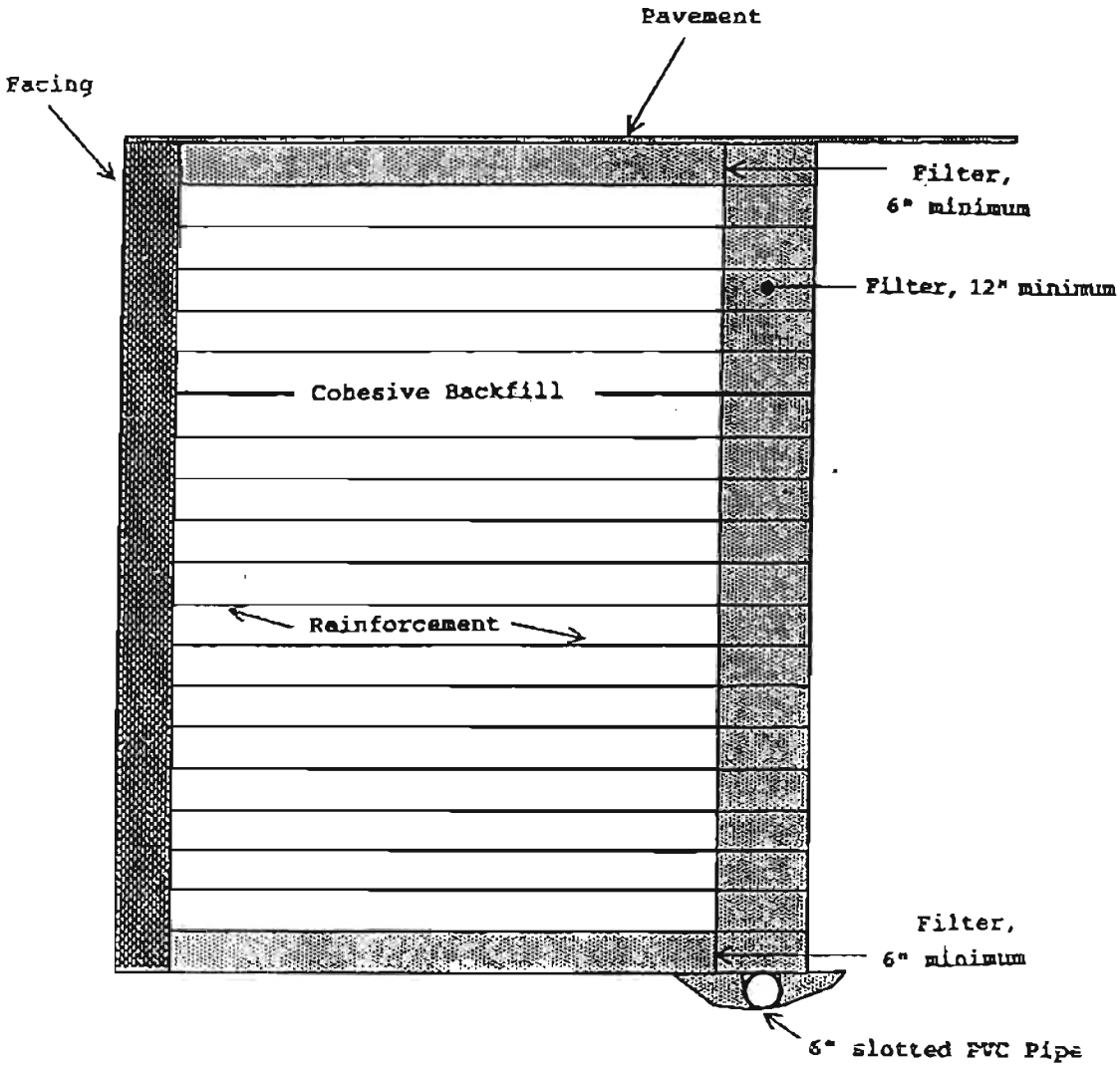

Figure 6.1: Recommended Subsurface Drainage Design for Cohesive Backfill Walls

An alternative to the above-described drainage system is to lay 6 inches of granular (free-draining) material at the bottom, then place 6 inches of compacted cohesive or on-site material on top of the granular material (see Figure 6.2). Repeat the process until the backfill reaches the top of the wall. By using only one-half of the granular material, the cost of backfill may be reduced significantly, and adequate drainage also is provided.

In Japan, non-woven/woven geotextile composites have been used for cohesive backfill walls (Tatsuoka et.al.,1992). The needle-punched nonwoven geotextile provides drainage, while the high stiffness, woven geotextile provides tension resistance. This dual-function geocomposite also may be a cost-effective alternative for walls constructed with cohesive backfill. It should be noted, however, that these two alternatives allow seeping water to flow toward the reinforced zone, which may reduce the shear strength of the cohesive backfill. The long-term performance needs to be evaluated.

The geotextile or granular filter used for drainage should meet established criteria for permeability and clogging. Details are described in the FHWA Geotextile Engineering Manual (Christopher and Holtz, 1985).

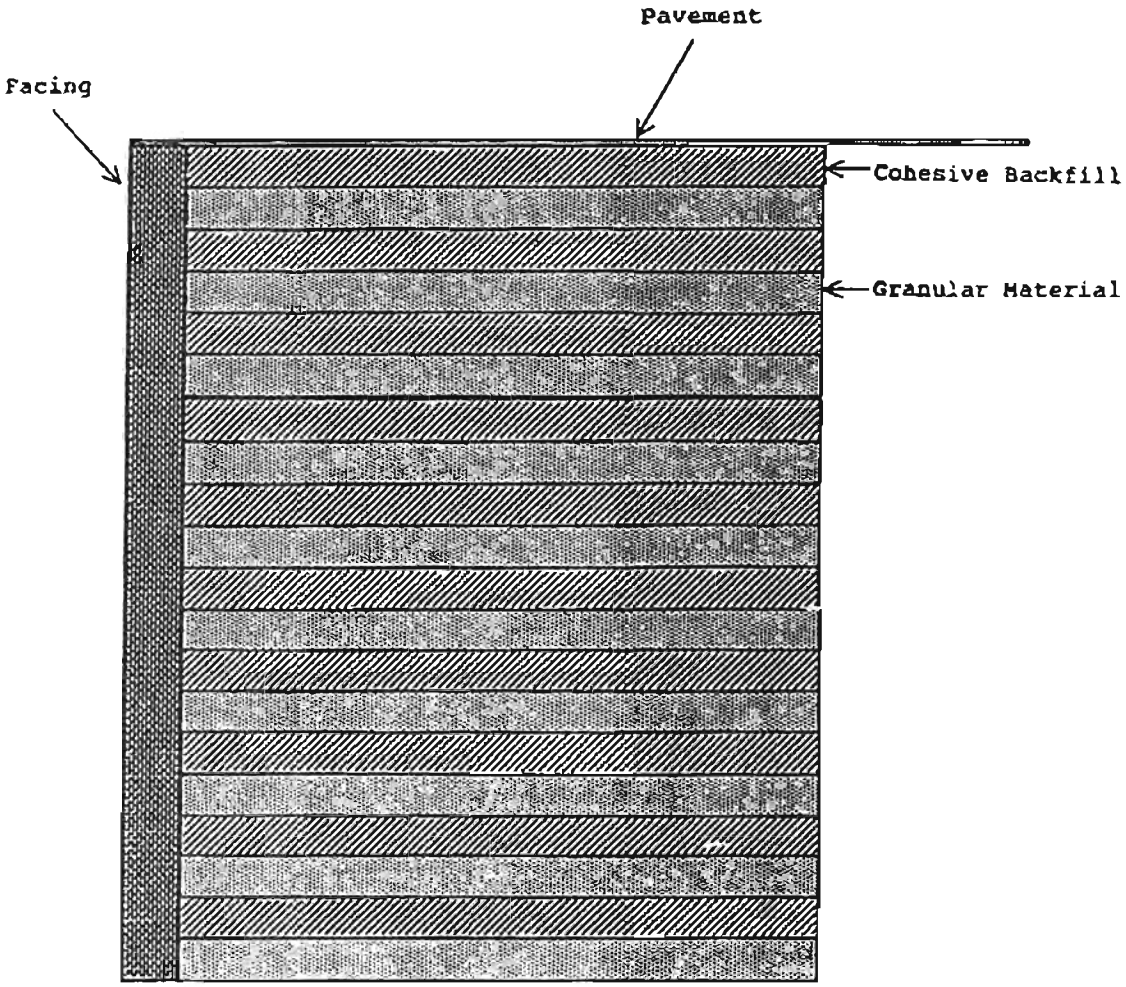

Figure 6.2: Alternate Drainage Design

6.4 Proposed Construction Guidelines

The construction methods for MSE walls have been presented by Wu, Chou & Yeh (1990), Christopher and Holtz (1985), and Jones (1985). The following guidelines are recommended for GRS wall construction.

Site Preparation

Before placing of a geosynthetic, grade the ground to provide a smooth, level surface. The surface should be clear of vegetation, large rocks, stumps, etc. It is not, however, necessary to routinely subexcavate the top 1 to 3 feet of soil, which is a common practice in the conventional concrete wall construction for embedment and/or for frost heave protection purposes. The site should be proof-rolled by at least two passes before placing the backfill. A nominal 4 inch granular leveling platform is recommended for the base of the wall. It also can be used as a drainage path for the backfill. For a GRS wall with cohesive backfill, a minimum 6 inch granular fill is required (see Figure 6.1).

Geosynthetic

The geosynthetic should be protected from exposure to sunlight and extreme temperatures. Any damaged or torn materials should be removed or repaired. In no case should construction equipment be allowed to operate directly on the geosynthetic before the fill is placed.

During placement of the geosynthetic, it should be unrolled transverse to the alignment of the wall, and wrinkles and folds should be minimized. Slight pretensioning by stretching the reinforcement in the field is preferred.

Overlaps of reinforcement should be at least 6 inches wide and should be perpendicular to the wall face. Sewing or connecting the overlaps is usually unnecessary for GRS wall construction.

The geosynthetic tail (i.e., the wrap-around portion) shall be at least 3 feet long on all lifts. The final lift tail should be extended to the full length of geosynthetic embedment.

Backfill Placement and Compaction

Backfill material should be compacted to at least 95% of the maximum dry density obtained from the Standard Proctor test, except within one foot of the wall face where only light compaction is allowed. The in-place moisture contents are recommended, as follows: within ± 2% of Optimum for granular backfill and within ± 2% of 2% wet of Optimum for cohesive backfill.

Backfill materials shall be placed in no more than 6 inch compacted lift thickness. Compaction should be done with equipment that will not damage the geosynthetic.

At the end of each day's backfilling operation, the last lift of fill should be sloped away from the

wall face to direct any possible runoff away from the face.

Facing

Most manufacturers of panel facings provide installation guidelines. Wrap-around facing construction procedures are outlined in the FHWA Geotextile Engineering Manual. Therefore, only the CDOT timber facing construction is presented in this section.

The step-by-step construction procedure for CDOT timber facing walls was presented in Section 4.8.1 (Figure 4.17). The timber may have 6" height x 6" width or 6" x 4" cross-sectional dimensions. For permanent construction, the timber shall be treated to an acceptable level with copper chromate preservative or an approved equivalent. The forming element may be timber, plywood (minimum 1 inch nominal thickness, treated by copper chromate or approved equivalent), fiberglass, plastic, or other approved material(s).

Nails or screws may be used to connect the timber facings with the forming elements. Nails should be 16d galvanized ring shank nails, or 4" deck screws; place at the top and bottom of the timbers at 1 foot intervals. Screws used in the Denver Test Walls (see Figure 4.17) are preferred to nails, and should be installed at the same locations as the nails. Screws

are usually preferred to nails for long-term performance.

Verticality shall be maintained to no more than 4 inches in 10 feet inward batter. No outward batter in the final wall is acceptable. Shimming of the timber to maintain verticality (or batter) is permissible. Heavy construction equipment should never be operated too closely to the face, otherwise undesirable bulging of the face may result.

CHAPTER VII

SUMMARY, CONCLUSIONS AND RECOMMENDATIONS

7.1 Summary

A review of current literature on existing design methods for Geosynthetic Reinforced Soil walls (GRS) reveals that these methods are deficient. Some of the drawbacks are: (1) Most of the methods fail to accommodate the interaction among soil, reinforcement, and facing in a GRS wall; (2) Most use arbitrarily assigned safety factors to ensure satisfactory performance; (3) None of the methods accounts for the effects of foundation stiffness and facing rigidity; and (4) None permits using cohesive soil as backfill.

The objectives of this research program were:

(1) To establish a reliable analytical model that is capable of simulating the performance of GRS walls under various conditions, such as soft clay foundation, cohesive backfill, and articulated facing.

(2) To investigate the effects of various factors on the performance of GRS walls, using the analytical model. Emphases were placed on studying the feasibility of using cohesive soil as backfill, and studying wall performance due to foundation settlement.

(3) To propose a preliminary design procedure and construction guidelines for GRS walls.

A comparative study of four finite element computer programs (SSCOMP, CRISP, CON2D86 and DACSAR) led to selecting DACSAR for this research, because:

- It is very well organized and appears to be "bug" free.

- It has all the element types needed for simulating the behavior of GRS walls. Namely, the program has bar (truss) element, beam element, and quadrilateral plane strain element.

- It contains both the viscid and inviscid versions of the Sekiguchi-Ohta soil model, which considers the effects of anisotropic consolidation, dilatancy, creep, shearing rate, and stress relaxation.

The following DACSAR modifications were made for analyzing the performance of GRS walls:

- The Duncan-Chang soil model was implemented to simulate the behavior of backfill.

- A nonlinear, stress-dependent hyperbolic model for the bar element was incorporated to simulate the load-deformation behavior of the reinforcement.

The analytical model was validated by comparing the analytical results with a closed-form solution; laboratory "element tests" of soil, reinforcement and facing; with another validated FEM program SSCOMP; and

with measurements from two full-scale test walls (the Denver test walls). The analytical results agreed well with those of the element tests. Similar analytical results for a GRS wall were obtained from SSCOMP and DACSAR. A class-A prediction on the Denver test walls, using DACSAR, was satisfactory for the cohesive backfill wall under service loads. Analyses, performed after the full-scale tests, showed that the behavior of both test walls could be properly simulated by the analytical model.

Using the validated analytical model, a parametric study was conducted to investigate the effects of various factors on the performance of GRS walls. A 12-foot high rectangular wall, with granular backfill and timber/plywood facing, situated on a medium-stiff clayey foundation soil, was selected as the control wall for this study.

Specifically, the following factors were examined:

(1) Wall height: 16, 12 and 8 feet.

(2) Wall shape: rectangular and trapezoidal.

(3) Backfill: granular, cohesive-moist (unsaturated), and cohesive-wet (saturated) soils.

(4) Foundation: granular, cohesive-low plasticity, cohesive-high plasticity, and rigid foundations.

(5) Facing: timber, wrap-around, articulated (modular block), and continuous concrete facings.

(6) Reinforcement: various values of stiffness and ultimate strength.

(7) Compaction effect: K_o=0.5, 1.0 and 2.5.

The effects of single as well as multiple-factor variations (deviating from the control wall) were examined. From the results of the parametric study, combined with experiences gained from actual construction of GRS walls, a preliminary design procedure and construction guidelines were proposed. The design procedure is based on the concepts of allowable facing deformation and limited reinforcement strain.

7.2 Conclusions

The following conclusions are derived from the study:

(1) The literature review clearly demonstrates the need to develop a design method based on the lateral wall deformation of GRS walls.

(2) A comparative study on finite element computer programs (CRISP, CON2D, SSCOMP and DACSAR) indicate that DACSAR is the best among four finite element programs for analysis of GRS walls.

(3) The analytical model is reliable for simulating the behavior of GRS walls. The analytical model has been validated through comparing analytical results with a closed-form solution, laboratory "element" tests (for soils, geosynthetic, and timber facing), a different FEM program, and two full-scale test walls.

(4) The parametric study indicates that:

A. The earth pressures evaluated at the following three locations are very different: (a) earth pressure against the facing, (b) earth pressure against the reinforced soil mass, and (c) earth pressure along the plane of maximum tensile force in the reinforcement. The analytical results indicated that a is the smallest, b is slightly larger than a K_a condition, and c lies between a and b.

B. The soil reaction distribution obtained from the analytical model is quite different from the trapezoidal profile commonly assumed in the design of GRS walls.

C. A GRS wall with a trapezoidal shaped reinforcement configuration (as shown in Figure 5.9) performs as well as a rectangular wall (see Figure 5.1) under service loads.

D. When kept near optimum moisture, cohesive backfill walls perform at least as well as those with

granular backfill, provided that wetting of backfill is prevented. The triaxial CD tests on a cohesive-wet clay indicate that the cohesion is lost completely by wetting, and the soil behaves as a loose granular material. The one-dimensional consolidation test also shows that the saturated clay is highly compressible. For the wall with a wet (saturated) cohesive backfill investigated in this study, the bottom portion of the wall deforms more than 7% of the wall height; the tensile strains at the middle and bottom layers of reinforcement are as high as 11%, indicting a high potential for wall instability. However, it is believed that, with proper surface and subsurface drainage, cohesive soils may be used as backfill for GRS walls constructed in semi-arid areas.

E. The wall facing affects lateral movement of GRS walls. Among all the facings examined in this study, continuous concrete facing exhibits the smallest wall movement and tensile strains in the reinforcement. The timber/plywood and the articulated (modular block) facings show about equal lateral wall movement, while the wrap-around facing yield the largest wall displacement. For the walls investigated, the continuous concrete facing move about 0.50% H (H = wall height), the timber/plywood move 0.67% H, the articular

block move 0.70% H, and the wrap-around facing move 0.80% H under a uniform pressure of 5 psi.

F. Foundation soil has a significant influence on the wall performance. The wall investigated in this study has maximum lateral wall displacements of: 0.45%, 0.67%, 0.75% and 3.0% of the wall height for the rigid, stiff clay, loose sand, and soft clay foundations, respectively, under a service load of 5 psi. The wall constructed on a rigid foundation rotates about its toe. The wall with soft clay rotates about the top of the wall, due to the significant movement of the foundation.

The analytical results indicates that, with a soft clay foundation, the tensile strains induced in the reinforcement are much larger near the bottom portion of the wall, due to large lateral deformation of the foundation. The wall with a rigid foundation exhibits the lowest tensile strain, and the walls with the loose sand and medium stiff clay foundations exhibit about equal tensile strains in the reinforcement.

G. For a GRS wall with granular backfill, increasing the reinforcement stiffness may reduce wall deformation and decrease tensile strains in the reinforcement. However, for a cohesive backfill wall and for a wall constructed on a soft foundation, increasing reinforcement stiffness may not be

effective. Under service loads, increasing the ultimate strength of the reinforcement may not improve the performance of the wall.

H. The at-rest earth pressure due to compaction, as reflected by the K_o value of backfill, significantly affects the lateral deformation of the wall. The higher the K_o value is, the smaller the wall will deform.

I. For the three wall heights investigated (i.e., 8 to 16 feet), the wall movement (normalized by the wall height) and reinforcement strains increases approximately linearly with the wall height.

J. To estimate the maximum displacement of a wall with multiple-factor variation, i.e., with a combination of factors deviating from the control wall (for example, a wall with cohesive-wet backfill and constructed on a soft foundation) the following empirical equation may be used:

$$DR = (DR1 \times DR2 \times .....)^n$$

where DR = the displacement ratio with multiple-factor deviation; the displacement ratio is ratio of the maximum wall movements for a wall and for the control wall,

DR1, DR2 ... = the displacement ratios with single-factor deviation,

n = correlation constant

= 1.0 for 12 and 16 ft high walls;

= 2/3 for 8 ft high walls

(5) From the results of the parametric study, a preliminary design procedure, based on an allowable lateral wall deformation, was proposed. To ensure long-term durability of the geosynthetic reinforcement, an appropriate safety factor for reinforcement strength may be employed. The proposed design procedure overcomes the three major drawbacks of the current design methods; namely: (1) The proposed design procedure accommodates the interaction among soil, reinforcement and facing. (2) The proposed design method does not use arbitrarily assigned safety factors to ensure satisfactory performance of a GRS wall. (3) The proposed design method accounts for the effects of foundation deformation and facing rigidity and permits judicious use of cohesive backfill.

7.3 Recommendations for Future Research

It is recommended that further research is needed in the following areas:

(1) More well-controlled, well instrumented full-scale tests are needed to gain a better understanding of the performance of GRS walls under different

conditions and to further validate the analytical model established in this study.

(2) Long-term effect due to creep, construction damage, and chemical aging needs to be investigated.

(3) Further studies are needed on the performance of GRS walls with other backfills, such as silt, swelling clay, recycled asphalt aggregate, shredded tires, and landfill.

(4) Further parametric studies are recommended for different reinforcement spacings and for foundations with multiple layers of subsoil. In addition, the effects of differential settlements in both alignment and cross-section directions are of interest to designers.

(5) Additional research is needed to verify the empirical relationship of displacement ratio of single and multiple variations under different conditions.

(6) Special wall geometries, such as rigid facing with short reinforcement length, double facings (side-by-side) with relatively short reinforcement, stacked walls, and reinforced steep slope need to be investigated.

(7) The GRS walls may be used to support the bridge abutments (i.e., placing the girder directly on the backfill) to eliminate the use of deep foundations. This could be a very cost-effective alternative to

conventional abutments, and full-scale tests are needed for this application.

(8) Additional research is needed to study special wall construction sequences, such as a wall constructed with temporary support (i.e., the Calgary geogrid wall) and a wall constructed by multi-phases.

(9) Additional research is needed to study the effect of "directional instability" of the geogrids and woven geotextiles lacking junction stiffness. For example, the stiffness and strength of these geosynthetics may be quite weaker along the diagonal direction than the machine or cross-machine directions. This may cause adverse effects on wall performance when a wall is built along a curved alignment.

BIBLIOGRAPHY

Adachi, T. Mimura, M. & Oka, F. (1985), "Descriptive Accuracy of Several Existing Constitutive Models for Normally Consolidated Clays," 5th International Conference on Numerical Methods in Geomechanics, Nagoya, 1985, pp. 259-266.

Adib, M.E. (1988), "Internal Lateral Earth Pressures in Earth Walls," Dissertation submitted in partial satisfaction of the requirements of the degree of Doctor of Philosophy in Engineering, University of California at Berkeley.

Adib, M., Mitchell, J. & Christopher, B. (1990), "Finite Element Modeling of Reinforced Soil Walls and Embankment," Proceedings, Design and Performance of Earth Retaining Structures, ASCE, Cornell University, June 18-21. pp. 409-423.

Akai, K. and Tamura, T. (1976), "An Application of Nonlinear Stress-Strain Relations to Multi-Dimensional Consolidation Problem," Annuals, Disaster Prevention Research Institute, Kyoto University, No. 19, B-2, pp. 15-29 (in Japanese).

Allen, T.M., Christopher, B.R., and Holtz, R.D (1992), "Performance of a 12.6 M High Geotextile Wall in Seattle, Washington," Proceedings of the International Symposium on Geosynthetic-Reinforced Soil Retaining Walls, August 8-9, 1991, Denver, Colorado

ASTM D-4595-86, (1987), "Standard Test Method for Tensile Properties of Geotextiles by the Wide-Width Strip Method," Annual Book of ASTM Standards, Vol. 04.08, pp. 1041-1055.

Balasubramaniam, A.S. (1991), "Contributions in Geotechnical Engineering--Soil Mechanics and Foundation Engineering," An Inaugural Lecture, March 14, AIT, Bangkok, Thailand.

Barrett, R., (1992), "Can You Build a Retaining Wall for Less Cost?", Geotechnical Fabric Report, Vol. 10, No.2.

Bassett, R.H. and Last, H.C. (1978), "Reinforced Earth Below Footings and Embankments," Proceeding, Symposium on Reinforced Earth, ASCE, Pittsburgh, pp. 222-231.

Bathurst, R. & Benjamin, D. (1990), "Failure of a Geogrid Reinforced Soil Wall," Presented at the 69th Annual Meeting of the Transportation Research Board. Jan. 7-11, Washington, D.C.

Bell, J.R., Stilley, A.M., and Vandre, B., (1975), "Fabric Retained Earth Walls," Proceedings of the 13th Annual Engineering Geology and Soils Engineering Symposium, Boise, Idaho.

Bell, J.R., Barrett, R.K, and Ruckman, A.C. (1983), "Geotextile Earth Reinforced Retaining Wall Test, Glenwood Canyon, Colorado," Presented at the Annual Meeting, Transportation Research Board, Washington, D.C.

Billiard, J.W. (1989), "Performance of a Large Scale Fabric Wall During Load Test," Master's Thesis, University of Colorado at Denver, Denver, Colorado.

Billiard J.W. and Wu, J.T.H. (1991), "Load Test of a Large-Scale Geotextile-Reinforced Retaining Wall," Proceedings, Geosynthetics '91 Conference, Feb. 26-28, Atlanta, Georgia.

Bonaparte, R , Holtz, R.D., and Giroud, J.P. (1985), "Soil Reinforcement Design Using Geotextiles and Geogrids," ASTM Symposium, Geotextile Testing and the Design Engineer, ASTM SPT 952. June, Los Angeles, pp. 69-116.

Boscardin, M.D. Selig, E.T., Lin, R.S., and Zong, R.R. (1990), "Hyperbolic Parameters For Compacted Soils," Journal of Geotechnical Engineering, January, Vol. 116, No. 1, pp. 88-103.

Brakel, J., Coppens, M., Maagdenberg, A.C., Risseeuw, (1982), "Stability of Slopes Constructed with Polyester Reinforcing Fabric, Test Section at Almere-Holland, '79," 2nd International Conference on Geotextiles, Las Vegas.

Britto, A.M., Gunn, M.J., (1987), "Critical State Soil Mechanics Via Finite Elements," Ellis Horwood Limited, Great Britain.

Broms, B.B. (1978), "Design of Fabric Reinforced Retaining Structures," Proceedings of the Symposium on Earth Reinforcement, ASCE, Pittsburgh.

Burwash, W.J. and Frost, J.D. (1991), "Case History of a 9 Meter High Geogrid Reinforced Retaining Wall

Backfilled with Cohesive Soil," Proceedings Geosynthetics '91, NAGS and IFAI, Feb. 26-28, Atlanta, pp. 485-494.

Chandrasekaran, B. (1988), "An Experimental Evaluation of Fabric Strength Reinforced Soil," M.S. Thesis, National University of Singapore.

Chang, C.S. and Duncan, J.M. (1977), "Analysis of Consolidation of Earth and Rockfill Dams," Report No. TE77-3, Dept. of Civil Engineering, University of California at Berkeley.

Chang, D.T.T, Chen, T.C., and Su, K.H. (1991), "Utilization of Geotextile-Reinforced Retaining Wall for Stabilizing Weathered Mudstone Slope," Geosynthetics '91, Feb. 26-28, Atlanta, pp. 739-774.

Chassie, R.G. (1988), "Basic Primer on Retaining Wall Alternates," Alaska Department of Transportation, Retaining Wall Seminar, p. 21.

Chirapuntu, S. and Duncan, J.M. (1975), "The Role of Fill Strength in the Stability of Embankment on Soft Clay Foundations," Geotechnical Engineering Research Report, Department of Civil Engineering, University of California, Berkeley.

Chou, N.N.S., Chou, K.T., Lee, C.C. and Tsai, K.W. (1980), "Preloading by Water Testing Eliminated Sand Drains for a 65,000 Ton Raw Water Tank in Taiwan," Proceedings of the 6th Southeast Asian Conference on Soil Engineering.

Chou, N.N.S., Wu, J.T.H. and Siel, B.D. (1987) "The Effectiveness of Tensile Reinforcement in Strengthening an Embankment Over Soft Foundation," Geosynthetics 87, New Orleans, pp. 332-340.

Chou, N.N.S., Su, C.K. (1990), "External Stability of a Reinforced Earth Wall Constructed Over Soft Clay," Proceedings, Conference on Design and Performance of Earth Retaining Structures, ASCE, June 18-21, Ithaca, N.Y.

Chou, N.N.S., Chao, S.J., Chang, C.S. and Ni, J. (1991) "FEM Analysis of Staged Construction For A Reinforced Earth Wall," ASCE Geotechnical Congress, Boulder, Colorado.

Chou, N.N.S. (1992), "Performance Predictions of the Colorado Geotextile Test Walls," Pre-Symposium

Proceedings, International Symposium on Geosynthetic-Reinforced Soil Retaining Walls, Aug. 5-9, Denver, Balkama Publisher, pp. 184-205.

Christopher, B.R. and Holtz, R.D. (1985), "Geotextile Engineering Manual", FHWA

Christopher, B.R., Holtz, R.D. and Allen, T.M. (1990), "Instrumentation for a 12.6 M High Geotextile Reinforced Wall," Proceeding of the International Reinforced Soil Conference, Performance of Reinforced Soil Structures, Sept. 10-12, Glasgow, England.

Christopher, B.R., Gill, S.A., Giroud, J.P., Juran, I., Schlosser, F., Mitchell, J.K and Dunnicliff, J. (1989), "Reinforced Soil Structures," FHWA-RD 89-043

Claybourn, A.F. (1989), "A Comparison of Designing Methods for Geosynthetic-Reinforced Earth Walls," M.S. Thesis, University of Colorado.

Claybourn A.F. and Wu, J.T.H. (1991) "Case History Comparison of Geosynthetic Reinforced Soil Walls," Geosynthetics '91 Conference Proceeding, Feb. 26-28, Atlanta, pp. 485-494.

Collin, J.G. (1986), "Earth Wall Design," Dissertation submitted in partial satisfaction of the requirements for the degree of Doctor of Philosophy in Engineering, University of California at Berkeley.

Colorado Department of Transportation (1991), "Retaining Wall Selection Memorandum."

Colorado Department of Transportation (1991), Cost Book 1990.

Colorado Department of Transportation (1991), Standard Design of Geotextile Reinforced Earth Walls.

Douglas, G.E. (1981), "Design and Construction of Fabric-reinforced Retaining Walls by New York State," TRB 872, p. 32.

Drucker, D.C., Gibson, R.E. and Henkel, D.J. (1957), "Soil Mechanics and Work Hardening Theories of Plasticity," Transportation ASCE, Vol. 122, pp. 338-346.

Drucker, D.C. (1975): "A More Fundamental Approach to Stress-Strain Relations," Proceedings 1st U.S. National Congress Appl. Mech., ASME, pp. 487-491.

Duncan, J.M., Byrne, P., Wong, K.S. and Mabry, P. (1980), "Strength, Stress-Strain and Buck Modulus Parameters for Finite Element Analyses of Stresses and Movements in Soil Masses," Report No. VCB/GT/80-01, Department of Civil Engineering, University of California at Berkeley, August, p. 77.

Duncan, J.M., D'Orazio, J.B., Chang, C.S., Wong, K.S., and Namiq, L. (1981), "CON2D: A finite Element Computer Program for Analysis of Consolidation," Report No. UCB/GT/81-01, College of Engineering, University of California at Berkeley.

Duncan, J.M., Schaefer, V.R., Franks, L.W., and Collins, S.A. (1989), "Design and Performance of a Reinforced Embankment for Mohicanville Dike No. 2 in Ohio," Transportation Record 1153, pp. 15-25.

Duncan, J.M., Williams, G.W., Sehn, A.L. and Seed, R.B. (1991), "Estimation Earth Pressures Due to Compaction," Journal of Geotechnical Engineering ASCE, Vol. 117, No. 12, December, pp. 1833-1847.

El-Fermaoui, A. and Nowatzki, E. (1982), "Effect of Confining Pressure on Performance of Geotextiles in Soil," Proceedings of the Second International Conference on Geotextiles, Las Vegas, pp. 799-804.

Fabian, K.J. and Fourie, A.B. (1988), "Clay-Geotextile Interaction in Large Retaining Wall Models," Geotextiles and Geomembranes Journal, Vol. 7, pp. 179-201.

Fukuda, N., Yamanouchi, T. and Miura, N. (1986), "Comparative Studies of Design and Construction of a Steep Reinforced Embankment," Geotextiles and Geomembranes, Vol. 4, pp. 269-284.

Gibson, R.E., and Lo, K.Y. (1961), "A Theory of Consolidation for Soils Exhibiting Secondary Compression," Publication No. 41, Norwegian Geotechnical Institute, Oslo, Norway.

Goodman, R.E., Taylor, R.L. and Brekker, T.L. (1968), "A Model for the Mechanics of Jointed Rock," Journal of Soil Mechanics and Foundations, ASCE, Vol. 94, SM3, pp. 637-659.

Gourc, J.P., Ratel A., Delmas P., (1986), "Design of Fabric Retaining Walls: the Displacement Method," 3rd International Conference on Geotextiles and Geomembranes, Vienne.

Gourc, J.P., Gotteland, Ph., Delmas, Ph. (1988), "Design of Geosynthetic Retaining Walls: Displacement Method and Two Blocks Method-Comparison and Charts," Proceedings of the International Geotechnical Symposium on Theory and Practice of Earth Reinforcement, Fukuoka, Japan, Oct. 5-7, pp. 517-522.

Gourc, J-P and Matichard, Y. (1992), "Development of Geotextile Reinforcement Techniques in France - Application to Retaining Structures," Proceedings of the International Symposium on Geosynthetic-Reinforced Soil Retaining Walls, August 8-9, 1991, Denver, Colorado.

Hausmann, M.R. (1990), "Engineering Principles of Ground Modification," McGraw-Hill Publishing Company.

Herrmann, L.R. and Al-Yassin, Z. (1978), "Numerical Analysis of Reinforced Earth Systems," Proceeding Symposium of Reinforced Earth, ASCE, April, Pittsburgh.

Hilf, J.W. (1975), "Compacted Fill," Chapter 7, Foundation Engineering Handbook, Van Nostrand Reinhold Company

Holtz, R.D. and Broms, B.B. (1977), "Walls Reinforced By Fabrics: Results of Model Tests," Proceedings of the International Conference on the Use of Fabrics in Geotechnics, Paris, Vol. 1, pp. 113-117.

Iizuka, A. and Ohta, H. (1987), "A Determination Procedure of Input Parameters in Elasto-Viscoplastic Finite Element Analysis," Soils & Foundation, Vol. 27, No. 3, pp. 71-87.

Iizuka, A. (1987), "Deformation and Stability Analyses on Soft Ground," Ph.D Dissertation, Kyoto University, Japan (in Japanese).

Iizuka A. and Ohta, H. (1987), "A Determination Procedure of Input Parameters in elasto-viscoplastic finite Element Analysis," Soils and Foundations, Vol. 27, No. 3, September, pp. 71-87.

Iizuka, A. (1991), personal communication.

Jaber, M., Collin, J.G. and Schmertmann, G.R. (1991), "Prediction of Geosynthetic Reinforced Wall Performance Using Finite Element Analyses," Pre-Symposium Proceedings, International Symposium on

Geosynthetic Reinforced Soil Retaining Walls, Aug. 5-9, Denver, pp. 175-183.

Jewell, R.A. (1985), "Limited Equilibrium Analysis of Reinforced Soil Walls," 11th ICSMFE, San Francisco, Vol. 3, pp. 1705-1708.

Jewell, R.A. (1988), "Compatibility, Serviceability and Design Factors for Reinforced Soil Walls," Proceedings of International Symposium on Theory and Practice of Earth Reinforcement, Kyushu, Japan, pp. 611-616.

Jewell, R.A. (1988), "Reinforced Soil Wall Analysis and Behavior," The Application of Polymeric Reinforcement in Soil Retaining Structures, Kluwer Academic Publishers, pp. 365-408.

Jewell, R.A. & Milligan, G.W.E. (1989), "Deformation Calculations for Reinforced Soil Walls," Proceedings 12th ICSMIE, Rio de Janeiro, Vol. 2, pp. 1257-1162.

Jones, C.J.F.P. (1985), "Earth Reinforcement and Soil Structures," Butterworths.

Juran, I. and Christopher, B. (1989), "Laboratory Model Study on Geosynthetic Reinforced Soil Retaining Walls," Journal of Geotechnical Engineering, July, Vol. 115, No. 7.

Juran, I., Ider, M.M and Farrang, K. (1990), "Strain Compatibility Analysis for Geosynthetics Reinforced Soil Walls," Journal of Geotechnical Engineering. ASCE, Vol. 116, No. 2, pp. 312-329.

Katona, M.G., et al., (1976) "CANDE - A Modern Approach for the Structural Design and Analysis of Buried Culverts," Report No. FHWA-RD-77-5, Federal Highway Administration, Washington, D.C.

Koerner, R. (1986), "Designing with Geosynthetics," Prentice Hall.

Lambe, T.W., and Whitman, R.V. (1969), "Soil Mechanics," John Wiley & Sons, Inc., New York

Lee, K.L., Adams, B.D. and Vagneron, J.J. (1973), "Reinforced Earth Retaining Walls," Journal of the Soil Mechanics and Foundation Division, ASCE, Vol. 99, No. SM10, p. 745.

Leshchinsky, D. and Field, D.A. (1987), "In-Soil Load Elongation, Tensile Strength and Interface Friction of Nonwoven Geotextiles," Proceedings, Geosynthetics '87, New Orleans, pp. 238-249.

Leshchinsky, D. and Perry, E.B. (1987), "A Design Procedure for Geotextile-Reinforced Walls," Proceedings of the Geosynthetics '87 Conference, New Orleans, Vol 1, pp.95-107.

Leshchinsky, D. (1992), "Discussion: Strain Compatibility Analysis for Geosynthetics Reinforced Soil Walls", Journal of Geotechnical Engineering, ASCE, Vol. 118, No. 5, pp. 816-819.

Lin, R.S. (1987), "Direct Determination of Bulk Modulus of Partially Saturated Soils," M.S. Thesis, University of Massachusetts.

Lin, J.C., Macklin, P., Chou, N.N.S., Wu, J.T.H. (1991), A PC Program for Geosynthetic Wall Design by the GeoService Method.

Ling, H.I., Wu, J.T.H. and Tatsuoka, F. (1991), "Effectiveness of In-Membrane Test in Simulating Strength and Deformation Characteristics of a Nonwoven Geotextile Under Operational Conditions," Proceedings of Geosynthetic '91 Conference, Atlanta, pp. 601-614.

Ling, H.I. and Tatsuoka, F. (1991), "Nonlinear Analysis of Reinforced Soil Structures by Modified CANDE (M-CANDE)," International Symposium of Geosynthetic-Reinforced Soil Retaining Walls, August 5-9, Denver.

Ling, H.I., Wu, J.T.H., and Tatsuoka, F. (1992), "Short-Term Strength and Deformation Characteristics of Geotextiles Under Typical Operational Conditions, Geotextiles and Geomembranes, Vol. 10, No. 2.

McGown, A., Andrawes, K.Z., and Kabir, M.H. (1982), "Load-Extension Testing of Geotextiles Confined in Soil," Proceedings of the Second International Conference on Geotextiles, Las Vegas, pp. 793-798.

McGown, A. (1989), "General Report for the Session on Soil Reinforcement," Proceedings, 12th ICSMFE, Vol. 4, Rio de Janeiro.

Mitchell, J.K. and Villet, W.C.B. (1987), "Reinforcement of Earth Slopes and Embankment," NCHRP Report 290, TRB, Washington, D.C.

Mitchell, J.K. and Christopher, B.R. (1990), "North American Practice in Reinforced Soil Systems," Proceedings of Conference on Design and Performance of Earth Retaining Structures, ASCE, June 18-21, Ithaca, New York.

Murray, R. (1988), "Fabric Reinforcement of Embankments and Cuttings," Proceedings, 2nd International Conference on Geotextiles, Las Vegas, pp. 707-713.

National Highway Institute (1989), "Geotextile Engineering Workshop - Design Examples," NHI Courses No. 13213.

Ng, H.Y., Mak, C.H. (1988), "A 14 Metre High Reinforced Soil Embankment as the Abutment of a Steel Bridge in Tuen Mun, Hong Kong," International Geotechnical Symposium on Theory and Practice of Earth Reinforcement, Oct. 5-7, Fukuoka, Japan, pp. 449-454.

Ohta, H., Yoshitani, Susumu & Hata, S. (1975), "Anisotropic Stress-Strain Relationship of Clay and Its Application to Finite Element Analysis," Soil and Foundations, December, Vol. 15, No. 4.

Ohta H. and Sekguchi, H. (1979), "Constitutive Equations Considering Anisotropy and Stress Reorientation in Clay," Third International Conference on Numerical Methods in Geomechanics, April 2-6, Aachen.

Ohta, H. and Iizuka, A. (1986), Manual of DACSAR FEM Program, Kanazawa University.

Ouyang, Z. (1988), "Twenty-six Meter Height Reinforced Soil Quaywall: Design and Full-Scale Test," International Geotechnical Symposium on Theory and Practice of Earth Reinforcement, Oct. 5-7, Fukuoka, Japan, pp. 599-604.

Parry (1982), Personal Communication with Britto and Gunn (1987).

Peck, R.B., Hanson, W.E. and Thornburn, T.H. (1974), Foundation Engineering, 2nd ed., John Wiley & Sons, Inc.

Pueg, J., Blivet, J.C. and Pasquet, (1977), "Remblai Arme avec un Textile Synthetique," Proceedings of the International Conference on the Use of Fabric in Geotechnic, Paris, Vol. I, p. 85.

Richardson, G.N. and Bove, J. (1988), "The Use of Construction Fabrics in Retaining Walls and Steep Embankments," Report submitted to Amoco Fabrics and Fibers Company.

Romstad, K.M., Herrmann, L.R. and Shen, C.K. (1976), "Integrated Study of Reinforced Earth - 1: Theoretical Formulation," Journal of Geotechnical Engineering Division, ASCE, May, Vol. 102, No. GTS.

Roscoe, K.h., Schofield, A.N. and Thurairajah, A. (1963), "Yielding of Clays in States Wetter Than Critical", Geotechnique, Vol. 13, pp.211-240.

Schaefer, V.R. and Duncan, J.M. (1987), "Analysis of Reinforced Embankments and Foundations Overlying Soft Soil," VPI and State University, Blacksburg, VA.

Schlosser, F. and Long, N.T. (1972), "Comportement de la Terra Armee dans les Ouvrages de Soutenement," Proceedings of 5th E.C.S.M.F.E., Madrid, Vol. 1, pp. 299-306.

Schlosser, F. and Buhan, P.D. (1990), "Theory and Design Related to the Performance of Reinforced Soil Structures," State-of-the-art Report, Proceedings of the International Reinforced Soil Conference, Sept. 10-12, Glasgow, England.

Schlosser, F. (1990), "Mechanically Stabilized Earth Structures in Europe," Proceedings, Design and Performance of Earth Retaining Structures ASCE, Cornell University.

Seed, H.B. and Duncan, J.M. (1983), "Soil-Structure Interaction Effects of Compaction-Induced Stresses and Deflection," Dept. of Civil Engineering, University of California, Berkeley.

Sekiguchi, H. and Ohta, H. (1977), "Induced Anisotropy and Time Dependency in Clays," 9th International Conference on Soil Mechanics & Foundation Engineer, Tokyo.

Sekiguchi, K. (1991), "On The Choice of Finite Elements in Elasto-Viscoplastic Consolidation Analysis," 26th Japanese Geotechnical Engineering Conference, pp. 1167-1170.

Sherif, M.A., Fang Y.S. and Sherif R.I. (1984), "Ka and Ko Behind Rotating and Non-yielding Walls,"

Journal of Geotechnical Engineering, ASCE, January, Vol. 110, No. 1, pp. 41-56.

Shibata, T. (1963), "On the Volume Changes of Normally Consolidated Clays," Annuals, Disaster Prevention Research Institute, Kyoto University, No. 6, pp. 128-134 (in Japanese).

Siel, B. (1986), "An Investigation of the Effectiveness of Tensile Reinforcement in Strengthening an Embankment Over Soft Foundation," M.S. Thesis, Department of Civil Engineering, University of Colorado at Denver.

Siel, B.D., Wu, J.T.H., and Chou, N.N.S. (1987), "In-Soil Stress-Strain Behavior of Geotextile,", Proceedings, Geosynthetics '87 Conference, Feb 24-25, New Orleans. LA.

Skempton, A.W. (1957), "Discussion on The Planning and Design of New Hong Kong Airport," Proc. Inst. Civil Engineering, Vol. 7.

Stewart, J.E., Williamson, R., and Mohney, J. (1977), "Guidelines for Use of Fabrics in Construction and Maintenance of low-Volume Roads," National Technical Information Service, Revised (1983).

Stewart, J.E. and Mohney, J. (1982), "Trial Use Results and Experience for Low-Volume Forest Roads," Proceedings of the Second International Conference on Geotextiles, Las Vegas, Vol. 2, p. 335.

Task Force 27 (1986), AASHTO-AGC-ARTBA, Draft Copy, July.

Tatsuoka, F. and Yamauchi, H. (1986), "A Reinforcing Method for Steep Clay Slopes Using a Non-woven Geotextile," Geotextiles and Geomembranes Journal, Vol. 4, pp. 241-268.

Tatsuoka, F. Murata, O. and Tateyama, M. (1992), "Permanent Geosynthetic-Reinforced Soil Retaining Walls for Railway Embankment in Japan," Proceedings of the International Symposium on Geosynthetic-Reinforced Soil Retaining Walls, August 8-9, 1991, Denver, Colorado

Vidal, H. (1978), "Keynote Address- The Development and Future of Reinforced Earth," Proceedings of a Symposium on Earth Reinforcement, ASCE Annual Convention, April 27, Pittsburgh.

Wichter, L., Risseeuw, P. and Gay, G. (1986), "Large-Scale Test on the Bearing Behavior of a Woven-Reinforced Earth Wall," 3rd International Conference on Geotextiles, Vienna, Austria, pp. 1073-1078.

Wroth, C.P. and Wood, D.M. (1978), "The Correlation of Index Properties With Some Basic Engineering Properties of Soils," Canadian Geotechnical Journal, May, Vol. 15, No. 2.

Wu, J.T.H. (1980), "Predicting Performance of Buried Conduits," Doctoral Dissertation, Department of Civil Engineering, Purdue University.

Wu, J.T.H., Chou, N.N.S. and Yeh, S.T. (1990), "Earthwork for Retaining Structures and Abutments," Chapter 7, Guide to Earthwork Construction, State of the Art Report 8, TRB.

Wu, J.T.H and Lin, J.C. (1991), "Analysis and Design of Geotextile-Reinforced Earth Walls, Vol. 3, Parametric Study and Preliminary Design Method," Final Report to Colorado Department of Highways, Department of Civil Engineering, University of Colorado at Denver, March

Wu, J.T.H. (1991), "Measuring Inherent Load-Extension Properties of Geotextiles for Design of Reinforced Structures," Geotechnical Testing Journal, June, Vol. 14, No. 2, pp. 157-165.

Wu, J.T.H., Siel, B.D., Chou, N.N.S. and Helwany, H.B. (1992), "The Effectiveness of Geosynthetic Reinforced Embankments Constructed Over Weak Foundations," Journal of Geotextile and Geomembranes, Vol. 11, Elsevier Science Publishers Ltd., England.

Wu, J.T.H. (1992a), "Predicting Performance of the Denver Walls: General Report," Proceedings of the International Symposium on Geosynthetic-Reinforced Soil Retaining Walls, August 8-9, 1991, Denver, Colorado.

Wu, J.T.H. (1992b), "Construction and Instrumentation of the Denver Walls," Proceedings of the International Symposium on Geosynthetic-Reinforced Soil Retaining Walls, August 8-9, 1991, Denver, Colorado.

Wu, J.T.H. (1992c), "Measured Behavior of the Denver Walls," Proceedings of the International Symposium on Geosynthetic-Reinforced Soil Retaining Walls, August 8-9, 1991, Denver, Colorado.

Wu, J.T.H., Qi, X., Chou, N.N.S., Ksouri, I., Helwany, M.B., Huang, C.C. (1992d), "Comparisons of Predictions for the Denver Walls," Proceedings of the International Symposium on Geosynthetic-Reinforced Soil Retaining Walls, August 8-9, 1991, Denver, Colorado.

Yang, Z. (1972), "Strength and Deformation Characteristics of Reinforced Sand", Ph.D Dissertation, University of California at Los Angeles.

Zanten, R.V.V. (1986), "Geotextiles and Geomembranes in Civil Engineering," John Wiley & Sons.

APPENDIX A

A DESIGN TABLE FOR 12 FOOT HEIGHT GRS WALLS

A design table for 12-foot high walls is presented in Table A.1. The assumptions made in establishing this table include:

(1) The wall height is 12 ft.

(2) The allowable lateral wall movement is 1 inch.

(3) The safety factor against rupture of the reinforcement is 10.

(3) A uniform surcharge of 5 psi is applied at the top of the backfill. No seismic force is considered.

(4) The spacing between the geosynthetic reinforcement is 1 ft.

(5) The stiffness and strength of the reinforcement are assumed to be confining pressure independent.

(6) The CDOT construction method (Barrett, 1992) with the timber/plywood facing is used.

(7) The wall facing is vertical.

(8) The top of backfill (crest) is horizontal.

The proposed design procedure (see Chapter 6) and the empirical equation of single- and multiple-factor variations (Equation 5.4) were used to generate this

design table. Interpolation method was used to obtain values of the required E_i and T_{ult} of the reinforcement in this table.

The following example illustrates how the table can be used. For instance, the E_i and T_{ult} are required for design a wall with the following conditions (see Table 5.1): A-1 (12' high wall), B-1 (rectangular shape), C-3 (cohesive-wet backfill), D-1 (timber facing) and E-1 (stiff clay foundation). With an allowable lateral deformation of 1.0 inch, a designed E_i of 10,000 lb/in. and a designed T_{ult} of 360 lb/in can be obtained (case #9 of Table A.1).

Other tables for different wall heights and different allowable deformations also can be established in a similar manner.

Table A.1: Preliminary Design Chart for 12-ft Walls

CASE	CONDITION (See Table 5.4)	MIN E_t (lb/in)	MIN T_{ult} (lb/in)	REMARKS
1	A-1,B-1,C-1,D-1,E-1	500	70	Baseline (control wall)
2	A-1,B-1,C-1,D-1,E-2	N/A	N/A	Need to improve foundation, or use staged construction
3	A-1,B-1,C-1,D-1,E-3	500	70	
4	A-1,B-1,C-1,D-1,E-4	400	70	
5	A-1,B-1,C-2,D-1,E-1	500	70	
6	A-1,B-1,C-2,D-1,E-2	N/A	N/A	See remarks Case 2
7	A-1,B-1,C-2,D-1,E-3	500	70	
8	A-1,B-1,C-2,D-1,E-4	400	70	
9	A-1,B-1,C-3,D-1,E-1	10,000	360	May consider using granular backfill or providing surface and subsurface drainage
10	A-1,B-1,C-3,D-1,E-2	N/A	N/A	(1) Use granular backfill or provide drainage (2) See remarks Case 2
11	A-1,B-1,C-3,D-1,E-3	10,000	360	See remarks Case 9
12	A-1,B-1,C-3,D-1,E-4	10,000	320	See remarks Case 9
13	A-1,B-2,C-1,D-1,E-1	500	70	
14	A-1,B-2,C-1,D-1,E-2	N/A	N/A	See remarks Case 2
15	A-1,B-2,C-1,D-1,E-3	500	70	
16	A-1,B-2,C-1,D-1,E-4	400	70	
17	A-1,B-2,C-2,D-1,E-1	500	70	
18	A-1,B-2,C-2,D-1,E-2	N/A	N/A	See remarks Case 2
19	A-1,B-2,C-2,D-1,E-3	500	70	
20	A-1,B-2,C-2,D-1,E-4	400	70	
21	A-1,B-2,C-3,D-1,E-1	N/A	N/A	See remarks Case 9
22	A-1,B-2,C-3,D-1,E-2	N/A	N/A	See remarks Case 9
23	A-1,B-2,C-3,D-1,E-3	N/A	N/A	See remarks Case 9
24	A-1,B-2,C-3,D-1,E-4	N/A	N/A	See remarks Case 9

NOTE: This table is prepared for a 12 ft. high wall with timber facing. When other types of facing are used, the E_t and T_{ult} values listed above should be adjusted by multiplying the following coefficient: Wrap around :1.5; articulated panels :1.2; full height concrete :0.6.

APPENDIX B:

Extended Anisotropic Cam-Clay Model

The original soil model adopted in DACSAR is the Sekiguchi & Ohta (1977) model. This is an elasto-viscoplastic model which is able to describe the anisotropic behavior of clay. This model can be reduced to the original Cam-clay model (Roscoe, Schofield and Thurairajah, 1963) under conditions of isotropic initial stress state.

Inviscid Formulation

The constitutive equation proposed by Sekiguchi and Ohta can be characterized by the plastic volumetric strain hardening and the associated flow rules. The yield condition is associated with plastic volumetric strain as the hardening parameter as follows:

$$f(\sigma_{ij}) - F(v^p) = 0 \qquad (3.6)$$

where f is the yield function, F is the hardening functions, σ_{ij} is effective stress tensor and v^p is the plastic volumetric strain.

The critical state lines and yield loci for the normally consolidated soils (wetter than critical) and over- consolidated soils (drier than critical) are shown

in Figure 3.1.a and 3.1.b, respectively. These loci are similar to those obtained from the Cam-clay model, except that the anisotropic consolidation is taken into account, and the stress paths start from the normal consolidation lines.

The Sekiguchi-Ohta model assumed that the volume changes of soil are due to two components, volumetric strain due to consolidation (v_c) and that due to dilatancy (v_d), as shown in Figure 3.2. Dilatancy is defined as volume change under the loading system keeping the effective mean principal stress σ_m, or P, constant (Ohta, Yoshitani & Hatta, 1975). The dilatancy of anisotropically, normally consolidated clay is expressed in terms of η^* as follows:

$$v_d = D \cdot \eta^* \tag{A.1}$$

where D = coefficient of dilatancy (see Figure 3.2), and

$$\eta^* = \sqrt{\frac{3}{2}(\eta_{ij} - \eta_{ij_o})(\eta_{ij} - \eta_{ij_o})} \tag{A.2}$$

in which

$$\eta_{ij} = \frac{S_{ij}}{P} \ , \ \eta_{ij_o} = \frac{S_{ij_o}}{P_o} \tag{A.3}$$

where η_{ij} is the (i,j) component of "pressure-normalized

deviatoric stress tensor" ; η_{ij_o} is the value of η_{ij} at the end of anisotropic consolidation; P is the mean effective stress and P_o is the mean effective stress at the end of Ko consolidation. This equation indicates that dilatancy is caused by a change of deviatoric stress. Further, it is assumed that total volume changes are the sum of those resulting from consolidation and dilatancy:

$$v = \frac{\lambda}{1+e_o} \ln\left(\frac{P}{P_o}\right) + D\,\eta^* \qquad (A.4)$$

where v = total volumetric strain

λ = 0.434 x Cc

e_o = void ratio at the end of Ko consolidation

The elastic component of volumetric strain can be expressed in the form:

$$v^e = \frac{\kappa}{1+e_o} \ln\left(\frac{P}{P_o}\right) \qquad (A.5)$$

where κ = 0.434 x Cs

Subtracting Equation A.5 from Equation A.4, one can obtain the plastic component of volumetric strain v^p in the form:

$$v^p = \frac{\lambda-\kappa}{1+e_o} \ln\left(\frac{P}{P_o}\right) + D \cdot \eta^* \qquad (A.6)$$

Sekiguchi and Ohta introduced a plastic potential function, f, and assumed it to be given by:

$$f = \frac{\lambda-\kappa}{1+e_o} \ln\left(\frac{P}{P_o}\right) + D \cdot \eta^* \qquad (A.7)$$

and therefore:

$$f = v^p \qquad (A.8)$$

When $f = V^p = o$, it means that the soil at the end of anisotropic consolidation is also in a state of yielding (see Figure 3.1).

According to the associated flow rule (Drunker 1951), it follows that:

$$\delta\varepsilon^p_{ij} = \psi \frac{\partial f}{\partial \sigma_{ij}} \qquad (3.7)$$

where $\delta\varepsilon^p_{ij}$ is the (i,j) component of plastic strain increment tensor, and ψ is the proportional constant and σ_{ij} is the (i,j) component of effective stress tensor. The magnitude of plastic strain increment can be obtained by Equation (3.7), and its direction can be illustrated from Figure 3.3.

For elastic strain increments, the cam-clay model results in:

$$\delta\varepsilon^{e}_{ij} = \frac{\kappa}{3(1+e_o)} \frac{\delta p}{p} \delta_{ij} \qquad (A.9)$$

where $\delta\varepsilon^{e}_{ij}$ is the (i,j) component of elastic strain increment tensor, and δ_{ij} is the Kronecker delta.

Finally, the total strain increment is the sum of the plastic and elastic components, that is:

$$\delta\varepsilon_{ij} = \delta\varepsilon^{p}_{ij} + \delta\varepsilon^{e}_{ij} \qquad (3.8)$$

Viscid Formulation

Sekiguchi and Ohta (1977) developed the following equation in consideration of soil viscosity:

$$v = \frac{\lambda}{1+e_o} \ln\left(\frac{p}{p_o}\right) + D \cdot \eta^{*} - \alpha \ln\left(\frac{\dot{v}}{\dot{v}_0}\right) \qquad (A.10)$$

where $\dot{v}$ = volumetric strain rate (with respect to time)

$\dot{v}_0$ = initial value of $\dot{v}$ at the state immediately before the change of loading.

Other terms were defined previously.

To solve the differential Equation A.10, it is assumed that the volumetric strain immediately after the change of loading is elastic. Subtracting this elastic volumetric strain component form the total one (Equation A.10), we get,

$$F \equiv \alpha \cdot \ln\left\{\left(1+\frac{\dot{v}t}{\alpha}\right) \exp\left(\frac{f}{\alpha}\right)\right\} = v^{p} \qquad (A.11)$$

where F is a scalar function referred to as the viscoplastic potential, t is the elapsed time since the change of loading, and f is a scalar function defined by Equation 3.19, and V^p in the visco-plastic component of volumetric strain.

Sekiguchi and Ohta regarded the function F as the viscoplastic potential. Derivatives of F with respect to any effective stress component defined the directions of viscoplastic deformation. It was thus further assumed that:

$$\dot{\varepsilon}^{P}_{ij} = \varphi \frac{\partial F}{\partial \sigma_{ij}} \tag{A.12}$$

where $\dot{\varepsilon}^{P}_{ij}$ is the (i, j) component of visco-plastic strain rate tensor and φ is the viscoplastic proportional constant.

By assuming the condition for continuing viscoplastic deformation in the form: $\dot{F} = \dot{v}^p$, one may derive:

$$\dot{\varepsilon}^{p}_{ij} = \dot{v}^p \cdot \frac{\partial f}{\partial \sigma_{ij}} \Big/ \frac{\partial f}{\partial p} \tag{A.15}$$

where $\dot{v}^p$ is given by

$$\dot{v}^p = \left(1-\exp\left(-\frac{v^p}{\alpha}\right)\right) \cdot \left(\frac{\lambda-K}{1-e_o}\frac{\dot{P}}{P} + D \cdot \dot{\eta}^*\right) + \dot{v}_o \exp\left((f-v^p)/\alpha\right) \tag{A.16}$$

The elastic strain rates can be expressed in the

following form:

$$\dot{\varepsilon}^{e}_{ij} = \frac{\kappa \dot{P}}{3(1+e_o)P}\,\delta_{ij} + \frac{1}{2G}\,\dot{\delta}_{ij} \qquad (A.17)$$

where $\dot{\varepsilon}^{e}_{ij}$ is the (i,j) component of elastic strain rate tensor, and G is the modulus of rigidity.

The total strain rates are finally obtained as:

$$\dot{\varepsilon}_{ij} = \dot{\varepsilon}^{p}_{ij} + \dot{\varepsilon}^{e}_{ij} \qquad (A.18)$$

By using this rheological model, creep (ie, a soil under a constant stress) and stress relaxation (ie, a soil under a constant deformation) can be incorporated in the FEM analyses. The stress paths for a soil subjected to creep and stress relaxation in a P (mean effective stress)-Q (deviatoric stress) diagram are shown in Figure 3.4.